Wave-induced Responses of Stepped Revetments

Von der Fakultät für Bauingenieurwesen und Geodäsie
der Gottfried Wilhelm Leibniz Universität Hannover

zur Erlangung des Grades

DOKTOR-INGENIEUR
Dr.-Ing.

genehmigte Dissertation

von

Dipl.-Ing. Nils Bernhard Kerpen

geboren am 23. August 1983

in Gronau (Westf.)

2017

Preface

With climate change and sea level rise, urban development and economic growth, in particular in the coastal zone, more assets and infrastructures will be exposed to coastal erosion and potential flooding. These apparent trends implicate an ever increasing risk of damages and losses, requiring coastal authorities worldwide to regularly reassess and potentially redirect their adaption concepts for the related coastline, i.e. rethinking coastal protection strategies and infrastructure.

The underling physical processes and the daring question of adequate responses under deep uncertainty, either from a strategic or infrastructure point of view, are rendered multifaceted. It is the Coastal Engineer who innovates applicable solutions that suits the protection of a portfolio of assets in the coastal zone while trying to help avoiding any further deterioration of the environment as well as minimizing financial investments and mitigating maintenance costs for coastal infrastructure.

The present PhD thesis by Dr. Nils Bernhard Kerpen proposes and thoroughly investigates the wave-induced responses of an innovative coastal protection infrastructure, i.e. stepped revetment, that is supposed to represent one of those ideal candidates meeting the above listed demands and requirements for a sustainable development of our coasts. Stepped revetments are aesthetically pleasing coastal protection infrastructures (at least from an Engineering point of view) that recently gained attraction of coastal authorities mainly due to the beneficial side-effects in comparison to conventional coastal structures, i.e. in the dimensions of effectiveness, accessibility, maintenance and durability. At present, neither comprehensive studies of the inherent physical processes nor consensus about the functioning or the overall efficiency of stepped revetments are given in literature; evidently leading to a profound lack of knowledge of design guidelines and practical recommendations for construction.

Nils Kerpen facilitates closing these knowledge gaps with presenting and discussing his research findings conducted over the last three years. Stepped revetments effectively reflect incoming wave energy and induce additional turbulence during wave run-up which accordingly leads to increased energy dissipation induced by the actual macro roughness feature of the step faces. In consequence, the run-up process is mitigated which finally leads to reduced wave overtopping rates in contrast to smooth sloping structures. While other features of stepped revetments are addressed additionally, i.e. wave reflection and dissipation as well as induced loads and pressures from wave breaking, the author recalls to provide valuable recommendation on design and construction of stepped revetments so that the responsible Coastal Engineering can start using the depicted design formulae for any practical application from scratch.

I hope you enjoy reading the PhD thesis that has been successfully defended by Dr. Nils Kerpen in May 2017 and we are looking forward to your comments!

Yours faithfully,
T. Schlurmann

Danksagung

Abstract

Hard coastal structures represent a crucial element in current coastal defense strategies. The surface roughness of coastal structures, often impermeable and sloped, causes an increase in turbulence during the wave run-up. The increased turbulence results in a reduction of wave reflection, wave run-up and wave overtopping in a range of $10 - 50\%$ compared to smooth slopes which are normally asphalt- or grass-covered. Stepped revetments naturally exhibit surface roughness which acts as an obstacle to the interacting flow. In cases where the steps are specifically designed to walk over or sit on, stepped revetments enable save and easy access to the beach or the water. Then, the dimensions of the steps will inevitably have a significant influence on the energy dissipation of the waves. For the first time, the processes of the energy dissipation over a stepped revetment are examined in this study in a comprehensive manner.

Based on an in-depth literature review 60 years of research on stepped revetments are summarized. As a result of the literature review, it was found that the most significant relationship between the step height of stepped revetments and the wave height of the incoming waves on the overall energy dissipation has never been studied in a broader framework; this knowledge gap has thus been addressed in this work. Therefore, physical model tests were conducted in a $100\,m$ long wave flume. Wave impacts on a stepped revetment by plunging and surging wave breaking were evaluated for 34 varying sea states. Three slopes were tested for three different step heights. Additional tests with regular waves focused on the vorticity induced at the step edges. Further analysis concentrated on the energy dissipation of waves interacting with a stepped revetment which was thoroughly discussed in analytical terms.

Previously derived methods which consider the energy dissipation at a stepped revetment result in significant scatter in their range of applicability. This is a result of the large inhomogeneity of the underlying data they are derived from. Published reduction coefficients, describing the reducing impact of stepped revetments relative to a smooth revetment, range from $0.35 - 0.9$. For cases where the step heights are larger than the wave height, it was detected that the wave reflection and run-up over a stepped revetment can be reduced by $10 - 30\%$ compared to a smooth slope. The efficiency of stepped revetments in reducing the wave run-up increases if the wave height is larger than the step height ($30 - 60\%$). If the wave height is two times larger than the step height, the energy dissipation is most effective. If the step height is two times larger than the wave height, the revetment is highly reflective and the wave overtopping cannot be reduced significantly ($2 - 10\%$). Due to the macro-roughness of a stepped revetment, the overtopping volume of plunging waves is reduced most effectively ($40 - 60\%$). For surging waves, $10 - 30\%$ reduction is detected. The importance of the still water level with respect to the step edge on the wave overtopping is derived for step heights equal to the wave height. Changes in the reduction of approximately $\pm 20\%$ are possible for this case. The highest energy dissipation can be achieved if the still water level is close to the step edge. The maximum pressures are measured at the still water level. All dynamic pressures decrease significantly with increasing

water depth ($< 20\,\%$ for depths two times larger the wave height). Above the still water level the pressure distribution is comparable with a plain vertical wall.

In this study, four formulae, valid for a wide range of applications, are derived empirically to predict (1) the wave reflection coefficient, (2) the reduction coefficient for wave run-up and (3) wave overtopping to be used in the context of the widely known Eurotop (2016) equations and (4) the pressure loading for stepped revetments. For the first time, a holistic prediction of the reduction coefficient correlated to the wave run-up and overtopping considers the wave steepness, the slope and the step ratio coincidently.

In many places coastal protection structures are located in urban areas. Consequently, it often leads to conflicts between touristic interests and the protective function. Ideal coastal protection structures should provide access to coastal waterfronts and simultaneously provide an optimized protection level against storm surges. In this regard, stepped revetments promise an architecturally pleasing synthesis of both demands allowing the access to the waterfront easily and assuring designed safety margins for coastal protection. As a key characteristic, stepped revetments create higher surface roughness in comparison to conventional revetment surfaces, e.g. grass, asphalt or block revetments. Consequently, the principle of placing roughness elements on revetment slopes in the wave run-up area has proven to be a most effective measure to reduce the wave run-up and wave overtopping.

Keywords: Stepped revetment, energy dissipation, wave run-up, wave overtopping, physical model test

Kurzfassung

Harte Küstenschutzbauwerke stellen nach wie vor ein wesentliches Element in Küsten-schutzstrategien dar. Die Oberflächenrauheit dieser oftmals undurchlässigen und geneigten Bauwerke beeinflusst die Turbulenz während des Wellenauflaufs. Durch eine erhöhte Turbulenz werden die Wellenreflexion, der Wellenauflauf und der Wellenüberlauf um $10-15\,\%$ gegenüber glatten Böschungen, welche standardmäßig mit Gras oder Asphalt bedeckt sind, reduziert. Treppenstufen stellen ein Hindernis auf der Oberfläche eines Deckwerks dar und erhöhen dadurch die Oberflächenrauheit. Gleichzeitig kann ein Strandabschnitt über Treppenstufen von einer erhöhten Position durch den Menschen einfach und sicher erreicht werden. Die Dimensionen der Treppenstufen beeinflussen die Energiedissipation dabei erheblich. Die vorliegende Studie untersucht die Energiedissipation über gestuften Deckwerken erstmalig in einem ganzheitlichen Ansatz.

Erkenntnisse aus über 60 Jahren Forschung in Bezug auf gestufte Deckwerke werden zusammengefasst. Diese Literaturstudie zeigte, dass das Verhältnis der Stufenhöhe zur Wellenhöhe die Energiedissipation maßgeblich beeinflusst. Zu Grunde liegende Prozesse sind bis heute nicht hinreichend untersucht und daher unverstanden. Diese Studie liefert einen Erkenntnisgewinn mit Bezug auf diese Wissenslücke. Hierzu wurden physikalische Modellversuche in einem $100\,m$ langen Wellenkanal durchgeführt. Belastungen gestufter Deckwerke durch Sturz- und Reflexionsbrecher wurden für 102 Einzelversuche mit Wellen-spektren bestimmt. Zusätzlich wurden Versuche zum Prozessverständnis der Wirbelbildung an Stufenkanten mit regelmäßigen Wellen durchgeführt. Die Analyse der Daten konzentrierte sich auf die Energiedissipation von Wellen an gestuften Deckwerken und wurde mit Bezug auf das analytische Systemverhalten sorgfältig diskutiert.

Bislang entwickelte Ansätze zur Beschreibung der Energiedissipation an gestuften Deck-werken streuen, aufgrund der zumeist inhomogenen Datengrundlage, deutlich in Bezug auf die Gültigkeits- und Anwendungsbereiche. In der Literatur angegebene Beiwerte, die die Energiedissipation an rauen Böschungen gegenüber Böschungen mit glatter Oberfläche beschreiben, liegen in Bereichen von $0.35-0.9$. Für Stufenhöhen, die größer waren als die Wellenhöhe, veringerten sich die Reflexion von Wellen sowie deren Auflauf im Vergleich zu glatten Böschungen um $10-30\,\%$. Für Fälle, in denen die Wellenhöhe größer war als die Stufenhöhe, wurde der Wellenauflauf um $30-60\,\%$ verringert. Stufen, deren Höhe genau einer halben Wellenhöhe entsprach, zeigten den besten Wirkungsgrad mit Bezug auf die Energiedissipation. Stufen mit einer Höhe größer als die doppelte Wellenhöhe reflektierten die Wellenenergie stark und konnten den Wellenüberlauf daher im Vergleich zu glatten Böschungen nur um $2-10\,\%$ verringern. Durch die Macro-Rauheit von gestuften Deck-werken wurde der Wellenüberlauf von Sturzbrechern gegenüber glatten Böschungen effek-tiv verringert ($40-60\,\%$); der Wellenüberlauf von Reflexionsbrechern verringerte sich nur zu $10-30\,\%$. Für Stufen mit einer Höhe vergleichbar zur Wellenhöhe zeigte sich, dass die Lage des Ruhewasserspiegels am Deckwerk von enormer Bedeutung ist. Diese beeinflusste die Energiedissipation um bis zu $\pm 20\,\%$ mit einem Maximum für Ruhewasserspiegella-gen nahe der Stufenkante. Die höchste Druckschlagbelastung, induziert durch brechende Wellen, wurde in Ruhewasserspiegellage gemessen. Alle dynamischen Drücke nahmen mit

zunehmender Wassertiefe überproportional stark ab ($< 20\,\%$ für Wassertiefen größer der doppelten Wellenhöhe). Oberhalb des Ruhewasserspiegels nahm die Druckschlagbelastung ebenfalls ab und war quantitativ vergleichbar mit der Belastung einer senkrechten Wand.

Es wurden vier Formeln mit umfassendem Geltungsbereich zur Vorhersage der Verringerung der (1) Wellenreflexion, (2) Wellenauflaufhöhe, (3) Wellenüberlaufmenge und (4) Druckschlagbelastung durch Wellen an gestuften Deckwerken im Vergleich zu glatten Böschungen empirisch ermittelt. Die ermittelten Koeffizienten zur Berücksichtigung der Energiedissipation an gestuften Deckwerken können nun mit den im Allgemeinen bekannten Formeln des Eurotop (2016) zur Bestimmung des Wellenauf- und -überlaufs verwendet werden. Erstmalig können die Koeffizienten zur Berücksichtigung der Energiedissipation an gestuften Deckwerken unter Berücksichtigung der Bauwerksneigung, der Wellensteilheit und der Stufenhöhe in Relation zur Wellenhöhe für verschiedene Formen des Wellenbrechens in einem ganzheitlichen Ansatz bestimmt werden.

Da Küstenschutzmaßnahmen häufig in urbanen Arealen durchgeführt werden müssen, kann dies zu Interessenskonflikten in Bezug auf die Flächennutzung führen (Schutzfunktion vs. touristische Nutzung). Ein idealer Küstenschutz sollte daher in urbanen Arealen neben einem optimierten Schutzgrad gegen Sturmfluten auch einen sicheren Zugang zum Ufer ermöglichen. Vor diesem Hintergrund können gestufte Deckwerke eine architektonisch ansprechende Vereinbarkeit zwischen Zugänglichkeit und Schutzfunktion gewährleisten. Die Schlüsseleigenschaft der gestuften Deckwerke liegt dabei in der Oberflächenrauheit, welche im Vergleich zu konventionellen Deckwerken aus Gras, Asphalt oder Betonblöcken deutlich erhöht ist und somit eine effektive Maßnahme zur Reduzierung des Wellenauf- und -überlaufs darstellen kann.

Schlüsselwörter: getreppte Deckwerke, Energiedissipation, Wellenauflauf, Wellenüberlauf, physikalischer Modellversuch

Contents

Nomenclature

SWL	Still Water Level
ADV	acoustic Doppler velocimeter
AVI	Audio Video Interleave video container format
BNC	Bayonet Neill Concelman connection
Ca	Cauchy Number
Eu	Euler Number
Fr	Froude Number
GWK	large wave flume in Hannover
IQR	interquantile range
JS	North Sea spectrum (Jonswap)
Ma	Mach Number
PM	fully developed wave spectrum (Pierson-Moskowitz)
px	pixel, physical point in a raster image
Re	Reynolds Number
Ri	Richardson Number
RW	regular waves
SP	wave spectrum
St	Strouhal Number
TMA	shallow water spectrum (Texel, Marsen and Arsloe)
US	ultrasonic sensor
We	Weber Number
WKS	Wave Flume Schneiderberg

Greek Symbols

Symbol	Description	Dimensions	Units
α	slope angle	$-$	°

η_c	wave crest amplitude	L	m
Γ	circulation or flow of vorticity	$L^2 T^{-1}$	m²/s
γ_β	influence factor for oblique wave attack	–	1
γ_b	influence factor for a berm	–	1
γ_E	reduction factor for the wave energy	–	
γ_f	influence factor for roughness elements on a slope	–	1
γ_q	reduction factor for the wave overtopping	-	1
γ_v	influence factor for a vertical wall	–	1
$\gamma_{f_{R_{u,2\%}}}$	reduction factor for the wave run-up	–	
μ	dynamic viscosity	$M\,L^{-1}\,T^{-1}$	kg/(m s)
ν, ν_k	kinematic viscosity	$L^2\,T^{-1}$	m²/s
Ω	vorticity	$T^{-}1$	s⁻¹
ω	angular velocity	$T^{-}1$	s⁻¹
ρ	density	$M\,L^{-3}$	kg/m³
σ	surface tension	$L^{-}1\,T^{-2}\,M^1$	kg/(s²m
$\xi,\ \xi_0,\ \xi_{m-1,0}$	Iribarren Number	–	1

Roman Symbols

Symbol	Description	Dimensions	Units
B	concreted revetment width	L	m
B_r	width of a toe berm	L	m
C_r	reflection coefficient	–	1
C_v	speed of sound in a vertical wall	LT^{-1}	m/s
C_w	speed of sound in water	LT^{-1}	m/s
D	mean initial thickness of an air cushion	L	m
d	water depth at the toe of the structure	L	m
D_n	nominal diameter of an armour unit	L	m
d_{st}	water depth over the step closest to the SWL	L	m

E_v	lost energy	ML^2T^{-2}	Nm
f_b	width of block or rib	L	m
f_h	height of block or rib	L	m
f_L	distance between two blocks or ribs	L	m
g	gravitational acceleration ($g = 9.81\,m/s^2$)	L T^{-2}	m/s^2
H	wave height	L	m
H_I	incident wave height	L	m
H_R	reflected wave height	L	m
h_s	water depth in the far field	L	m
H_{br}	height of a breaking wave	L	m
H_{m0}	spectral wave height ($= 4 \cdot \sqrt{m_0}$)	L	m
K	vertical length of a water column	L	m
k_h	step diameter ($= cos\alpha \cdot S_h$)	L	m
k_r	characteristic diameter	L	m
L	length	L	m
M	mass	M	kg
m_0	zeroth–moment of the variance spectrum	L^2	m^2
m_0	zeroth-moment of the variance spectrum	L^2	m^2
n	slope ($n = 1/tan(\alpha)$)	L	m
N, N_w	number of waves	$-$	
$P_{2\%}$	mean of the 2% highest pressures	$ML^{-1}T^{-2}$	kg/(ms)
$p_{2\%}$	pressure exceeded by only 2 % of all waves	$ML^{-1}T^{-2}$	kg/(ms)
P_{IQR}	interquantile range of $P_{2\%}$	$ML^{-1}T^{-2}$	kg/(ms)
P_{max}	maximum pressure	$ML^{-1}T^{-2}$	kg/(ms)
P_{range}	bandwidth of $P_{2\%}$	$ML^{-1}T^{-2}$	kg/(ms)
q	average wave overtopping discharge	L^2 T^{-1}	m^{2}s^{-1}
r	reduction factor	$-$	1
R_c	vertical elevation of the crest over SWL	L	m

r_k	vortex radius	L	m
R_p	vertical elevation of a promenade over SWL	L	m
R_u	wave run-up height	L	m
$R_{u,2\%}$	wave run-up height exceeded by 2% of all run-ups	L	m
S_η	surface elevation's energy density spectra	$L^2\,T$	m^2s
S_h	step height	L	m
S_w	step width	L	m
T	wave period	T	s
t	time step	T	s
T_p	peak wave period	T	s
$T_{m-1,0}$	spectral or mean energy wave period	T	s
U	velocity of the water column	LT^{-1}	m/s
v	velocity	$L\,T^{-1}$	m/s
V_w	velocity of a wave front impacting a wall	LT^{-1}	m/s
v_{phi}	circumferential velocity	LT^{-1}	m/s
x_{br}	horizontal distance from the wall to the breaking point	L	m

List of Figures

List of Tables

1   Introduction

Urban settlement close to the sea develops new demands with regard to environmental and touristic compatibility of coastal protection structures. As architecturally pleasing solutions to coastal defense gains increasing interest, accessible revetments like e.g. stepped surfaces have recently entered the stage of outer surface slopes of coastal structures. National examples are the recently installed revetments on the East Frisian Islands Norderney and Baltrum or the intensive refurbishments in the 'HafenCity' in Hamburg. International examples are the intensive refurbishment projects of the coastal protection schemes in Blackpool, UK (Fig. 1.1, left), the Sea Organ[1] in Zadar, Croatia or the shore line revetment in Chicago, US. Additionally, simple breakwaters are sometimes shaped like a stepped slope (Fig. 1.1, right).

Increased surface roughness of a revetment as compared to smooth slopes (e.g. grass- or asphalt-cover) is the reason for implementing steps to a sloping coastal protection structure. A rough surface induces additional turbulence in the flow which leads to increased energy dissipation. Consequently, wave energy available as kinetic energy for the wave run-up process is reduced. The intensity of the turbulence is dependent on the roughness elements (shape and dimensions) and the flow velocity (Kármán, 1930). Hence, a coastal protection system with a rough surface can be built either with a reduced freeboard height or a higher safety-factor in comparison to a system with a smooth surface. In parallel, a quick, accurate and aesthetic construction with pre-fabricated components, coincidentally allowing an easy access to the water for residents and tourists beyond the storm season, is enabled.

Different construction approaches are possible in order to form a stepped revetment (Fig. 1.2). According to McCartney (1976), stacked gabions (a) are utilized as shore protection measure at Lake Erie and Sheffield Lake in Ohio. A stepped revetment from

---

[1]A stepped revetment including organ pipes encouraged and played by the incident waves. In 2006 the *Sea-Organ* was awarded by six international architecture associations with the *European Prize for Urban Public Space.*

Figure 1.1: Examples of stepped revetments. Left: Shoreline revetment in Blackpool, UK (photo taken by M. Beckwith in 2011). Right: Stepped breakwater in Varna, Bulgaria in 2014.

prefabricated components (b) is built up at Lake Michigan in Chicago, US, in Scarborough, UK (Rowe, 2012b) in Cleveleys, UK and in Hamburg, Germany. A geo-bag revetment (c) is installed at Lake Erie in Ohio. A soil-cement[2] revetment with stepped face (d) is applied at Bonny Dam in Colorado, Ute Dam in New Mexico, Merritt Dam in Nebraska or Castaic Dam in California, US.

1.1   Motivations

The motivation for a more comprehensive study of the influence of a stepped revetment on the wave run-up has been given by a commission of Franzius-Institute in 2012 to conduct hydraulic model tests with the focus on the freeboard prediction for a stepped revetment. For the design of the stepped revetment 'Strandkai' in the 'HafenCity' in Hamburg, Germany, a reduction in the required freeboard height was assumed as the rough surface of a stepped revetment must reduce the wave run-up compared to a smooth slope. As no generally valid approaches for the assumption of the run-up reduction were available these days, small scale model tests had been conducted in a preliminary study[3] with a limited range of hydraulic and geometrical boundary parameters. The tests initially confirmed a run-up reduction in a range of $30-40\,\%$ compared to a smooth slope. In 2015, a survey[4] was conducted to identify national and international sites with stepped revetments as coastal protection. Relevant authorities and engineering companies in Germany were interviewed to identify the current basis of decision-making in the context of designing a stepped revetment. As a result, no generally valid design guidelines are established for stepped revetments to date. The advantages of stepped revetments with respect to energy dissipation were not considered at all in the design of present building measures, and it was conjectured that this was mainly due to missing appropriate design guidelines. However, the benefits of a valid design approach were heightened with the research that was conducted based on the initial motivation.

Based on the research conducted following the motivational input from practitioners, it was clearly revealed that a structured, considerable examination of the energy dissipation over stepped revetments is needed in order to enable reliable designs. Fundamental knowledge of the processes underlying the energy dissipation of stepped revetments is required.

1.2   Objective and scope

The objective of this study is to gain knowledge about the hydraulic processes which take place when waves interact with stepped revetments. The structure of the study is given in Fig. 1.3. The findings of the study contribute to the identification stage of future projects related to coastal and flood protection. The benefits of stepped revetments as enhanced

---

[2]A mixture of pulverized natural soil with a small amount of cement and water to improve the slope protection.

[3]Diploma thesis by Kornelius Müller entitled *Run-up of waves on stepped embankments: Experimental investigation*, Franzius-Institute, 2014.

[4]Paper by Mathias Wien and Nico Ommen entitled *Treppenstrukturen als Hochwasserschutz an der deutschen Küste und den tidebeeinflussten Gewässern*, Franzius-Institute, 2015.
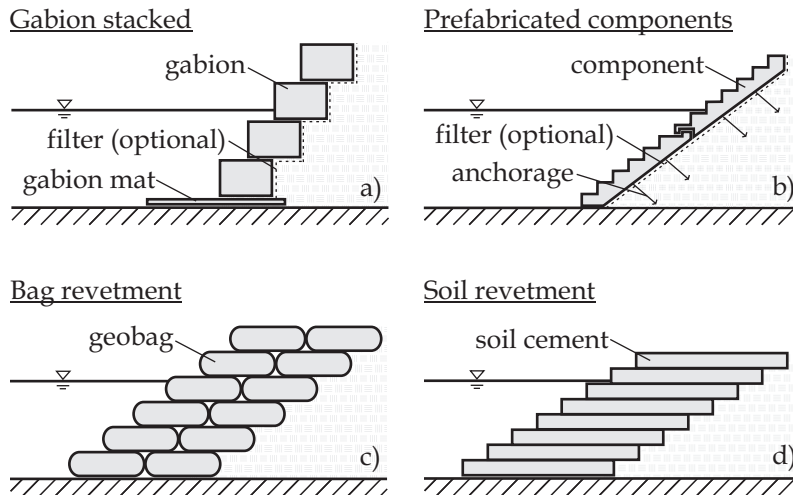
Figure 1.2: Stepped revetment types: a) gabion stacked, b) prefabricated components, c) geo bags stacked, d) soil cement layers.

coastal protection system – by increasing energy dissipation and gentrifying urban public space – can be utilized by the design approach provided after thoroughly outlining the effects and impacts of stepped revetments on the dynamic wave run-up and run-down process.

A method to determine the hydraulic impacts (wave reflection, wave run-up, overtopping, wave loads) on a revetment with stepped face is derived. The key parameter in this consideration is the turbulence induced energy dissipation over a stepped revetment. It is necessary to understand the influence of hydraulic- and geometry-related boundary conditions on the energy dissipation at stepped revetments. The energy dissipation in the flow in interaction with small (micro roughness) and large (macro roughness) steps has to be quantified. The aim of this procedure is the definition of roughness coefficients for the prediction of wave run-up and overtopping at revetments with stepped surfaces. The research assignment is addressed to:

- Identification and description of functional and active principles governing the energy dissipation of the wave run-up and wave overtopping process at stepped revetments.

- Implementation of the findings to the present design assessment.

To identify knowledge gaps on the wave interaction with stepped slopes, a comprehensive literature review is conducted. This review describes more than 60 years of research history. As referred to in the permanent literature, numerous terms like stepped wall, stepped-face wall, stepped face seawall, soil-cement, stepped slope, stepped face slope, stepped surface and stepped shapes have been used to name a revetment surface formed by a number of steps. All these terms describe a stepped revetment which is henceforth used in this work.

Based on the literature review and an identification of key parameters affecting the hydraulic- and geometry-related boundary conditions of stepped revetments, the state-

of-the-art regarding the influence of the surface roughness on the wave run-up and wave overtopping is presented firstly and this in turn defines the scope of this work. This scope is meant to derive approaches and methods to parameterize the surface roughness of a stepped revetment in a more general manner. A quantification of the influence of these parameters on the wave run-up and wave overtopping has to be enabled.

This is achieved by analyzing additional data-sets derived from hydraulic model tests. Hydraulic processes, driving the energy dissipation over stepped revetments, are described in detail. With these additional tests, asymptotic properties for extreme values and limitations of hydraulic processes can be discussed.

The extension of an analytical approach by Pereira (1996), that derives the energy dissipation over a single submerged step under waves, to be applicable for a number of consecutive steps, complements the findings from the hydraulic model tests in order to draw the final results on the energy dissipation at stepped revetments.

As a result, a profound design approach for stepped revetments valid for a wide range of hydraulic- and geometry-related boundary conditions is developed. It is the objective to integrate the determined influence of the surface roughness at stepped revetments in common design formulae. This enables a save assessment of required freeboard heights at stepped revetments.

1.3   Outline

In Chapt. 2 a general overview of state-of-the-art prediction methods for the wave reflection, wave run-up, wave overtopping and wave impact on coastal defense structures is given. A focus is placed on special prediction methods for stepped revetments in Chapt. 2.4. The findings are evaluated regarding their applicability for stepped revetments. In Chapt. 3, the conducted hydraulic model tests are described in detail with focus on requirements, the facility, the model set-up, the instrumentation, the test program and the data post-processing. The results of the conducted model tests are presented and discussed in Chapt. 4. A theoretical approach to derive the energy dissipation at stepped revetments is presented in Chapt. 5. A summary of conclusions is given Chapt. 6.

Objective
Gain knowledge about hydraulic processes present during the interaction of waves with stepped revetments to develop an optimized and reliable design guidance for coastal engineers.

State of the Art
Summary of knowledge to date and identification of persistent knowledge gaps on the wave interaction with rough slopes, particularly stepped revetments. (*Chapt. 2*)

Identification of Key Parameters
affecting the hydraulic- and geometry-related boundary conditions of stepped revetments. (*Chapt. 3.1*)

Scope   of   Work
Analysis and discussion of hydraulic- and geometry-related parameters which define the roughness of a stepped revetment. Quantification of the influence of these parameters on wave run-up and wave overtopping.

Hydraulic Model Tests
are conducted for a direct measurement of the target processes with respect to hydraulic- and geometry-related key parameters. (*Chapt. 3*)

Description of Hydraulic Processes
driving the energy dissipation over stepped revetments based on results from literature and hydraulic model tests. (*Chapt. 4*)

Theoretical Approach
to describe the energy dissipation at stepped revetments by an analytical determination of the energy dissipation. (*Chapt. 5*)

evaluation

Result
Profound design approach which is valid for a wide range of step heights to define the energy dissipation at a stepped revetment. Empirically derived and analytically proven roughness coefficients are determined to be integrated in common design formulae leading to a save assessment of freeboard heights at coastal structures.

Figure 1.3: Overview of objective and scope of work

2 State of the art

According to Goda (2010) waves have the greatest influence on maritime structures among the environmental conditions (wind, wave, tidal currents, earthquakes, etc.). This large influence is based on the fact that waves exert the most dominant load on the structure and are very complex and dynamic phenomena in nature. Many of these phenomena are not fully understood to date. Waves are generated by wind and propagate in a most irregular way in many directions. While waves are propagating towards the shore they are transformed and deformed in many ways (changes in direction due to wind, global streams and long-shore currents, diffraction, reflection, transmission and dissipation at islands and coastal structures, refraction and shoaling with decreasing water level and wave breaking). All these factors are widely discussed in literature and will not be the focus of the present study. The present study merely focuses on the direct wave interaction with stepped revetments as well as the influence of the structure geometry and surface. This chapter will summarize the state of the art of relevant boundary conditions concerning wave run-up, wave overtopping, wave reflection and wave loads on sloping structures with special focus on stepped revetments. The present knowledge about stepped revetments in the use of coastal protection structures are elaborated. To conclude, the main findings are evaluated and available data are re-analyzed and critically discussed.

2.1 Wave reflection

As an incident wave reaches a coastal protection structure, some wave energy is dissipated by turbulence, other parts may transmit or overtop the structure. The remaining wave energy is reflected. The intensity of reflection is dependent on hydraulic parameters (e.g. wave steepness, obliqueness of incoming waves) and geometry-related parameters (e.g. bathymetry and slope of the structure face, permeability). A summary of recent literature regarding wave reflection is given by Hughes (1993), Neelamani and Sandhya (2005) or Goda (2010). Knowledge about the reflected wave energy is important because these waves cause increased agitation of the water in front of the structure. Furthermore, reflected waves may propagate in areas that would otherwise be calm. Also the formation of partially standing waves with relatively high amplitudes is possible. For most structures the reflection coefficients are estimated empirically by means of hydraulic model tests. The reflection coefficient can be calculated in its easiest form for regular waves by

$$C_r = \frac{H_R}{H_I} \tag{2.1}$$

with H_R representing the reflected and H_I the incident wave height (Goda, 2010). According to EAK (2007) the significant wave height H_s directly at the toe of a structure is subject to phase coupling and can be calculated by

$$H_s = H_{s,I} + H_{s,R}. \tag{2.2}$$

At some distance from the reflecting structure the incident wave height has to be calculated by

$$H_s = \sqrt{H_{s,I}^2 + H_{s,R}^2}. \tag{2.3}$$

Eq. (2.3) has to be used since the period of the incident and reflected wave differs and therefore a phase coupling is highly improbable. Wave reflection caused by wave attack at an angle induces an amplification due to superposition with partly diffracted waves in front of the structure in some distance to the beginning – the so-called $Mach$-reflection – which is not focused on in this study. For the analysis of measured irregular waves, multi-gauge routines are used based on frequency domain methods as developed by Goda and Kishira (1976). Mansard and Funke (1980) improved the method by using the least square method for a time domain approache as provided by Frigaard and Brorsen (1995) with real time separation improved by Baldock and Simmonds (1999) for sloping bathymetries following Eq. (2.1) whereas H_I and H_R are calculated from the surface elevations at position x_1 and x_2 and the corresponding energy density spectra (with m_0 as zeroth-moment of the variance spectrum and as the energy density spectra of the surface elevation) to

$$C_r = \frac{\sqrt{m_{0,R}}}{\sqrt{m_{0,I}}} \text{ or } C_r(f) = \sqrt{\frac{S_{\eta,R}(f)}{S_{\eta,I}(f)}}. \tag{2.4}$$

Goda (2010) provides approximate values for reflection coefficients. Reflection coefficients are dependent on the wave steepness H/L and the structure slope n. Additionally, Goda and Kishira (1976) propose reflection coefficients for stepped revetments. Tab. 2.1 summarizes above mentioned coefficients.

Table 2.1: Approximate values for reflection coefficients (after Goda and Kishira (1976) and Goda (2010)).

Structure type	Reflection coefficient
Vertical wall with crest above water	$0.7 \sim 1.0$
Vertical wall with submerged crest	$0.5 \sim 0.7$
Slope of rubble stones ($n = 2$ to 3)	$0.3 \sim 0.6$
Slope of energy dissipating concrete armor units	$0.3 \sim 0.5$
Vertical structure (partly perforated)	$0.3 \sim 0.8$
Stepped revetment ($n = 2$, $i = 10$)	$0.2 \sim 0.3$
Stepped revetment ($n = 2$, $i = 30$)	0.1
Natural beach	$0.05 \sim 0.2$

n: slope, i: foreshore slope

Several empirically derived formulae allow to predict the reflection coefficient with respect to the Iribarren number $\xi = \frac{tan\alpha}{\sqrt{H_{m0}/L_0}}$. According to Battjes (1974a) the reflection coefficient for periodic waves over a plain slope can be predicted by

$$C_r \approx 0.1\xi^2. \tag{2.5}$$

Seelig and Ahrens (1981) provide the following equation to predict reflection coefficients under irregular waves for slopes with $n \leq 6$ to

$$C_r = \frac{a\xi^2}{\xi^2 + b}$$ (2.6)

where $a = 1$ and $b = 5.5$ for revetments. These values provide a conservative estimate.

Postama (1989) provides a simple formula to predict wave reflection from rock slopes under random wave attack. The formula is empirically derived from almost 200 random wave tests and takes into account the deep water Iribarren number ξ_0. The developed formula is

$$C_r = 0.14\xi_0^{0.73}(\sigma = 0.055).$$ (2.7)

Based on a data base with more than 4,000 tests, Zanuttigh and Van der Meer (2008) analyzed the wave reflection for various types of coastal structures. From the analysis a formula which is applicable for a wide range of slopes and revetments was determined to

$$C_r = tanh(a\xi_0^b)$$ (2.8)

where the calibrated values of the coefficients a and b are given together with the reduction coefficient γ_f in Tab. 2.2.

Table 2.2: Coefficients a, b to be included in Eq. (2.8).

	a	b	γ_f
rock (permeable)	0.12	0.87	0.40
armor units	0.12	0.87	various
rock (impermeable)	0.14	0.90	0.55
smooth	0.16	1.43	1.00

Conclusions

The wave reflection has been analyzed for a wealth of coastal protection structures and a wide range of reflection coefficients ($0.05 < C_r < 1$) are possible with respect to the structure's geometry and underlying hydraulic boundary conditions. Nevertheless, very few investigations have been conducted for stepped revetments. These investigations are conducted under very idealized boundary conditions with a limited number of tests. The currently available research does not allow a general valid statement regarding the reflectiveness of a stepped revetment.

2.2 Wave run-up and overtopping

This section summarizes approved state of the art prediction methods for the calculation of the wave run-up heights and wave overtopping volumes. Additionally, related approaches to predict the influence of the surface roughness are given. Literature and prediction approaches focusing on stepped revetments are discussed independently in section 2.4.

2.2.1 Wave run-up

Wave run-up occurs when waves reach the coast. Dependent on the slope the water is forced upwards until the energy content in the wave is dissipated. The wave run-up of a single wave is defined as the vertical distance between the still water level (SWL) and the highest point the water reaches. The present knowledge of wave run-up on coastal structures is obtained by prototype measurements and scaled model tests. Research on this topic has more than 100 years of history. In the design process of a coastal protection system the decision of the crest height is most important for the limitation of overtopping water volumes. European design guidelines (e.g. TAW (2002) and EAK (2007), replaced by Eurotop (2007) replaced by Eurotop (2016)) itemize a number of factors which have to be considered when designing the crest height of a dike:

1. the reference water level with a certain probability of exceedance

2. the sea level rise during design period

3. the expected local ground subsidence during design period

4. the influence of local wind conditions (seiches, squalls, gusts)

5. the expected decrease in crest height due to settlement of the dike body and the foundation soils during the design period

6. the wave run-up height

An active short-term influence on the processes described in 1-4 is not possible. The local ground subsidence (5) can be limited by special soil stabilization. The most dominant factor to determine the required crest height is the wave run-up (6). As a result the wave run-up is also the factor that can most significantly limit the crest height. This factor can be substantially reduced by an ingenious adaptation of certain geometry parameters (e.g. slope angle, micro and macro surface roughness due to different materials, berms or crown walls).

According to its own admission, Eurotop (2007) is the latest design guideline throughout Europe including the three former standard design guidelines *EA Overtopping Manual* by Besley (1999), TAW (2002) *Technical Report on wave run-up and wave overtopping at dikes* (The Netherlands), and EAK (2007) *Die Küste – Empfehlungen für Küstenschutzbauwerke* (Germany). Today, the Eurotop (2007) is replaced by the Eurotop (2016). The *Coastal*

Engineering Manual (CEM, 2002) replaced the *Shore Protection Manual* (SPM, 1984) as basis for coastal engineering practices in the U.S. Army Corps of Engineers.

Generally, the wave run-up R_u of a single wave is defined as the vertical distance between the still water level (SWL) and the maximum wave run-up-elevation over an inclined slope or at a vertical wall (Van der Meer and Janssen, 1994). In irregular waves, the wave run-up R_u is described as the wave run-up which is exceeded by only 2% of all waves as $R_{u,2\%}$ (Van der Meer and Stam, 1992). A wide range of design formulae have been derived in the past 50 years. It is not the object of this study to give a complete list of all these formulae and authors. A comprehensive overview is given in Hunt (2003). Subsequent authors have set some milestones in the development of design formulae regarding wave run-up (e.g. Hunt (1959), Battjes (1974a), Ahrens and Titus (1985), Mase (1989), Van der Meer and Stam (1992), Schüttrumpf (2001)). Today, the 2% run-up height $R_{u,2\%}$ is defined as the required crest height of a dike since these 2% of waves cause reasonable loads on the crest – and in case of a simultaneously wave overtopping also on the onshore directed slope of the structure. (Eurotop, 2016)

Eurotop (2016) gives empirically derived design formulae for the calculation of the dimensionless wave run-up. The mean value approach[5] is provided for three specified boundary conditions:

- relatively gentle slopes ($cot\alpha \geq 2$)

$$\frac{R_{u2\%}}{H_{m0}} = 1.65 \cdot \gamma_b \cdot \gamma_f \cdot \gamma_\beta \cdot \xi_{m-1,0} \tag{2.9}$$

  with a maximum of:

$$\frac{R_{u2\%}}{H_{m0}} = 1.0 \cdot \gamma_f \cdot \gamma_\beta \left(4 - \frac{1.5}{\sqrt{\gamma_b \cdot \xi_{m-1,0}}} \right) \tag{2.10}$$

  where H_{m0} is the spectral wave height, γ_b depicts the influence factor for a berm, γ_f is the influence factor for roughness elements on a slope, γ_β is the influence factor for oblique wave attack and $\xi_{m-1,0}$ the spectral Iribarren number derived from the spectral wave period $T_{m-1,0}$. These factors were derived empirically, too.

- steep slopes up to vertical walls ($cot\alpha < 2$)

$$\frac{R_{u2\%}}{H_{m0}} = 0.8cot\alpha + 1.6 \quad (\text{min.: } 1.8, \text{max.: } 3.0) \quad \text{for: } 0.01 \leq s_{m-1,0} \leq 0.06 \tag{2.11}$$

  with $s_{m-1,0} = H_{m0}/L_{m-1,0}$ as spectral wave steepness .

- very shallow foreshore
  $4.0 < \xi_{m-1,0} < 14$: Eq. (2.10)
  $\xi_{m-1,0} > 15 : \quad \frac{R_{u2\%}}{H_{m0}} = 3.6.$

[5]A definition in Eurotop (2016) to 'use the formula as given with the mean value of the stochastic parameter(s). This should be done to predict or compare with test data. [...]' Parallel, a design or assessment approach was defined as 'an easy semi-probabilistic approach with a partial safety factor; this is the mean value approach above, but now with the inclusion of the uncertainty of the prediction. [...]'.

2.2.2   Wave overtopping

Along with investigations on the wave run-up, investigations on the prediction of wave overtopping discharges also have a long history as research field in coastal engineering. During a storm event a coastal protection system is subjected to wave attack for several hours. Small waves do not lead to wave overtopping whereas the highest waves are responsible for a high percentage of the total overtopping volume within a storm event. Therefore, the process of wave overtopping is highly random in time and volume (Eurotop, 2016).

The wave overtopping discharge q is defined as the volume of water that flows over the crest of a coastal protection system when the wave run-up height R_u is larger than the wave crest height R_c. This disscharge can be idealized defined as the mean overtopping volume measured during a storm normalized for a time interval of one second and one meter crest width with the unit $[m^3 s^{-1} m^{-1}]$. On the other hand the volume can be defined as an overtopping volume per wave. According to Eurotop (2016) these overtopping volumes measured within a storm event with a number of waves N in the duration t underlay a Weibull distribution so that each overtopping volume has a certain exceedance probability.

The prediction of wave overtopping has a long history. Prediction approaches are gathered in recent literature (e.g. Schüttrumpf (2001), Van der Meer and Bruce (2014)). Schüttrumpf (2001) investigated wave overtopping for regular and irregular waves on sloping structures and summarized the significant literature (11 authors) on overtopping investigations starting back in the 1950s. Van der Meer and Bruce (2014) discussed the literature leading to the design formulae gathered in Eurotop (2007) and improved the existing approach for low and zero freeboard heights. Today, the principle correlation between the wave overtopping volume q, the spectral wave height H_{m0} and the corresponding freeboard height R_c can be generally described with empirically derived parameters a, b, and c by the semi-empirical equation

$$\frac{q}{\sqrt{g \cdot H_{m0}^3}} = a \cdot exp\left[-\left(b\frac{R_c}{H_{m0}}\right)^c\right]. \tag{2.12}$$

Eurotop (2007) provides empirical derived state-of-the-art formulae to predict the average wave overtopping discharge q by the probabilistic formulation

$$\frac{q}{\sqrt{g \cdot H_{m0}^3}} = \frac{0.067}{\sqrt{tan\alpha}}\gamma_b \cdot \xi_{m-1,0} \cdot exp\left(-4.75\frac{R_c}{\xi_{m-1,0} \cdot H_{m0} \cdot \gamma_b \cdot \gamma_f \cdot \gamma_\beta \cdot \gamma_v}\right). \tag{2.13}$$

This formula was improved in Eurotop (2016) by the approach by Van der Meer and Bruce (2014) in order to increase the applicability for low and zero freeboard heights. Today, the prediction approaches as presented in Eurotop (2016) differ for the following boundary conditions:

- relatively gentle slopes ($cot\alpha \geq 2$)

$$\frac{q}{\sqrt{g \cdot H_{m0}^3}} = \frac{0.023}{\sqrt{tan\alpha}} \gamma_b \cdot \xi_{m-1,0} \cdot exp\left[-\left(2.7 \frac{R_c}{\xi_{m-1,0} \cdot H_{m0} \cdot \gamma_b \cdot \gamma_f \cdot \gamma_\beta \cdot \gamma_v}\right)^{1.3}\right]$$

with q :   overtopping disscharge $[m^3/(sm)]$

H_{m0} :   significant wave height [m]

α :   structure slope angle [°]

$\xi_{m-1,0}$:   Iribarren number [–]

R_C :   freeboard height [m]

γ_b :   influence factor for a berm [–]

γ_f :   influence factor for slope roughness [–]

γ_β :   influence factor for oblique wave attack [–]

γ_v :   influence factor for a vertical crest wall [–]

(2.14)

with a maximum of

$$\frac{q}{\sqrt{g \cdot H_{m0}^3}} = 0.09 \cdot exp\left[-\left(1.5 \frac{R_c}{H_{m0} \cdot \gamma_f \cdot \gamma_\beta \cdot \gamma^*}\right)^{1.3}\right] .$$

(2.15)

with γ^* :   influence factor for a crest wall for non-breaking waves [–]

The reliability of Eq. (2.13) is given with the normally distributed stochastic coefficient 4.75 with a responsible standard deviation of 0.5.

- steep slopes up to vertical walls ($cot\alpha < 2$)

$$\frac{q}{\sqrt{g \cdot H_{m0}^3}} = a \cdot exp\left[-\left(b \frac{R_c}{H_{m0} \cdot \gamma_\beta}\right)^{1.3}\right] .$$

for $cot\alpha <2$

$$a = 0.09 - 0.1(2 - cot\alpha)^{2.1}$$

$$b = 1.5 + 0.42(2 - cot\alpha)^{1.5} \quad (max.: 2.35)$$

for $cot\alpha \geq 2$

$$a = 0.09$$

$$b = 1.5$$

(2.16)

- very shallow foreshore (with $\xi_{m-1,0} > 7$ and $s_{m-1,0} < 0.01$)

$$\frac{q}{\sqrt{g \cdot H_{m0}^3}} = 0.162 \cdot exp\left(\frac{R_c}{H_{m0} \cdot \gamma_f \cdot \gamma_\beta \cdot (0.33 + 0.022 \cdot \xi_{m-1,0})}\right) .$$

(2.17)

- negative freeboard height $(R_c < 0)$

$$
\begin{aligned}
&\text{for } R_c/H_{m0} < -0.3 \\
&q_{overflow} = 0.54 \cdot \sqrt{g \cdot |-R_c^3|} \\
&\text{for } 0 > R_c/H_{m0} \geq -0.3 \\
&Eq.(2.14) \quad \text{with } R_c = 0
\end{aligned}
\tag{2.18}
$$

Especially the influence factor for the slope roughness γ_f is of special interest for the analysis of stepped revetments since it quantifies the influence of a stepped revetment on wave overtopping when compared to a plain slope. The factor can be empirically derived (i.e. for plain and stepped slopes) by

$$
\gamma_f = \frac{ln\left(q_{\text{plain slope}}\right)}{ln\left(q_{\text{stepped slope}}\right)}.
\tag{2.19}
$$

If the wave conditions in both underlying test series are not exactly the same, Eurotop (2016) recommends to compare fitting curves through one or more test results.

In the case where the step height S_h of a stepped revetment and wave height H_{m0} are equal, the conditions are comparable to a composite wall[6]. Eurotop (2016) recommends to predict the wave overtopping according to composite wall conditions if the relative water depth directly in front of the vertical wall becomes smaller than $d/h_s \leq 0.6$. To take the possibility of wave breaking into account two different prediction methods are recommended:

$$
\begin{aligned}
&\text{for } \frac{h \cdot d}{H_{m0} \cdot L_{m-1,0}} \geq 0.65 : \\
&\frac{q}{\sqrt{g \cdot H_{m0}^3}} = 0.05 \cdot exp\left(-2.78 \frac{R_c}{H_{m0}}\right) \\[2em]
&\text{for } \frac{h \cdot d}{H_{m0} \cdot L_{m-1,0}} < 0.65 : \\
&R_c/H_{m0} \geq 1.35 : \\
&\frac{q}{\sqrt{g \cdot H_{m0}^3}} = 1.3 \left(\frac{d}{h}\right)^{0.5} \cdot 0.0014 \left(\frac{H_{m0}}{h_s \cdot s_{m-1,0}}\right)^{0.5} \left(\frac{R_c}{H_{m0}}\right)^{-3}. \\
&R_c/H_{m0} < 1.35 : \\
&\frac{q}{\sqrt{g \cdot H_{m0}^3}} = 1.3 \left(\frac{d}{h}\right)^{0.5} \cdot 0.0011 \left(\frac{H_{m0}}{h_s \cdot s_{m-1,0}}\right)^{0.5} \cdot exp\left(-2.2 \frac{R_c}{H_{m0}}\right)^{-3}.
\end{aligned}
\tag{2.20}
$$

---

[6]Presence of a toe mound in front of a vertical wall affecting the wave breaking.

Conclusion: Available prediction methods for the wave run-up and wave overtopping consider the influence of friction by a reduction coefficient γ_f. Hence, it is possible to implement the influence of stepped revetments in the available prediction methods as a stepped surface influenced friction.

2.2.3 Surface roughness

Surface roughness can be defined as a homogeneous or heterogeneous deviation from the mean alignment of a surface. Thus, an ideal smooth surface could physically not exist. But, in relation to the surrounding dimensions, a more or less ideal smooth surface can be achieved if the deviations from the mean alignment of the surface are much smaller than the dominating parameters that are involved in the adjacent processes. When considering waves (prototype and *Froude* scaled) a flat glass surface can be denoted as a smooth surface since the surface roughness of $k_s = 0.2\,nm$ can be considered as negligible. Dominating parameters of a wave are the wave height, its length and the local water depth whereas the wave velocity and orbital velocities of the wave can be derived by these parameters. Thus, any kind of revetment has its own surface roughness coefficient and therefore a distinct influence on the wave impact. A general overview of a variation of revetments including overall description, technical drawings, images and design factors is given in detail by McCartney (1976) and USACE (1995) and will not be repeated in this study.

In common design guidelines, the surface roughness is considered by empirical influence parameters representing the reduction of wave run-up or wave overtopping on a revetment with rough surface relative to a revetment with smooth surface. The influence of the surface roughness on the wave run-up was widely tested, e.g. by Saville (1955), Wassing (1957), Franzius (1965), Szmytkiewicz et al. (1994), Capel (2014). Eurotop (2016) provides surface roughness factors for different types of revetments (Tab. 2.3).

Table 2.3: Surface roughness factors γ_f for typical elements (Eurotop, 2016).

Revetment type	γ_f
Concrete	1.0
Asphalt	1.0
Closed concrete blocks	1.0
Grass	for $H_s < 0.75$: $1.15\sqrt{H_s}$
	for $H_s \geq 0.75$: 1.0
Basalt	0.9
Placed revetment blocks	0.9
Small blocks over $\frac{1}{25}$ of surface	0.85
Small blocks over $\frac{1}{9}$ of surface	0.80
$\frac{1}{4}$ of stone setting 10 cm higher	0.90
Ribs (optimum dimension)	0.75

Roughness elements are implemented on revetments in order to influence the wave run-up or run-down by increased turbulence over the surface. A suitable relation between width of the element f_b, height of the element f_h and distance between the elements f_L is important for the effectiveness of roughness elements. An optimum design was derived by Van der Meer (1998) from a re-analysis of data by Szmytkiewicz et al. (1994). He suggests the optimum relations are $\frac{f_h}{f_b} = 5$ to 8 and $\frac{f_L}{f_b} = 7$. Tab. 2.3 presents a roughness factor of 0.75 for ribs with optimum dimensions. This roughness factor is applicable for an entirely covered surface with blocks of a height of at least $\frac{f_h}{H_{m0}} = 0.15$. Greater elements ($\frac{f_h}{H_{m0}} > 0.15$) do not offer any additional reduction. For $\frac{f_h}{H_{m0}} < 0.15$ the reduction factor can be calculated with an interpolation to

$$\gamma_f = 1 - (1 - \gamma_{f,min}) \cdot \left(\frac{f_h}{0.15 \cdot H_{m0}} \right) \text{ for } \frac{f_h}{H_{m0}} < 0.15. \tag{2.21}$$

Furthermore, Eurotop (2016) concludes that roughness elements located on a slope are not or only slightly effective at a distance of $0.25 \cdot R_{u2\%,smooth}$ below SWL or $0.5 \cdot R_{u2\%,smooth}$ above SWL. Within these boundary conditions the reduction factor can be calculated for the length of the installation L_i with a weighting function by

$$\gamma_f = \frac{\sum \gamma_{f,i} \cdot L_i}{\sum L_i}. \tag{2.22}$$

Block-type revetments are separately discussed in Eurotop (2016). Two types of block revetments that can be implemented to increase the roughness of a slope to thereby reduce the run-up height. The block revetments are on the one hand a partly open and therefore porous systems. On the other hand the revetments are roughened by chessboard or rib pattern.

The reduction coefficient for block type revetments have been derived by large scale tests by Van Steeg et al. (2016) and can be calculated by

$$\gamma_f = 0.0028 \cdot \frac{H_{m0}}{d_{channel}} + f$$

$$\text{with: } d_{channel}: \quad \text{open volume per squaremeter } [m^3/m^2]$$
$$f = 0.69 \quad \text{for } Hillblock\text{\textregistered}$$
$$f = 0.72 \quad \text{for } Rona\text{\textregistered}Taille$$
$$f = 0.75 \quad \text{for } Verkalit\text{\textregistered}GOR$$

$$\tag{2.23}$$

Capel (2014) provides formulae for the prediction of wave reflection, wave run-up, wave overtopping and the corresponding roughness coefficient for block type revetments. The

roughness coefficient can be calculated with the following equation:

$$\gamma_f = 1 - \left(0.585 \cdot \sqrt{0.075 - s'_{m-1,0}} \cdot \rho_{\gamma_f}^{0.5} \cdot \left[6.5 \frac{R_c}{R_{u,2\%}} - ln \left(\frac{0.027}{\sqrt{tan\alpha}} \cdot \xi_{m-1,0} \right) \right] \right)$$

with: $s'_{m-1,0}$:   shallow water wave steepness $[-]$

$$\rho_{\gamma_f} = \frac{\gamma_{f,w} \cdot sin\alpha \cdot h_{prot}}{R_c}$$

h_{prot} :   protrusion height $[m]$

$$R_{u,2\%} = 3.45 \cdot tanh(0.65\xi_{m-1,0}) \cdot \gamma_f \cdot H_{m0}$$

$$(2.24)$$

Available prediction methods to quantify the surface roughness of a stepped revetment are extensively discussed in section 2.4. Provided reduction coefficients γ_f considering the roughness of a stepped revetment are listed for completeness without further interpretation in Tab. 2.4. For now, only the scatter of the average reduction coefficients γ_f based on varying hydraulic- and geometry-related boundary conditions is pointed out.

Conclusions

The influence of the surface roughness on the wave run-up is known for a wide range of materials and revetment types. Reduction coefficients are available for stepped revetments, too. But, the factors differ significantly ($0.35 < \gamma_f < 0.9$) with changes of the hydraulic- and geometry-related boundary conditions. A reliable choice of the right value for a prediction is not possible based on existing data. It should be considered that roughness elements reduce the wave run-up significantly if they are placed close to the SWL ($SWL - 0.25 \cdot R_{u,2\%,smooth}$ to $SWL + 0.5 \cdot R_{u,2\%,smooth}$).

2.3   Wave loads

Knowledge about impact loads on coastal protection systems is important to determine the final design. The purpose of prediction methods is to enable an estimation of expected loads for a certain type of geometry under hydraulic load. Subsequent, a brief overview of load cases on coastal structures is given.

2.3.1   Static loads

A dike separates the shore area from the onshore region. In case of a storm the offshore water level increases due to surge water levels and the wave set-up. The higher water level increases the hydro-static load on the dike. An increased static load increases the probability of penetration of water through the several revetment and filter layers into the dike body. The dike has to be designed to be stable, well founded and with adequate filter layers to withstand these increased hydro-static loads for adequate storm periods (2-3 days). A permeable revetment layer drains more water than an impermeable layer

Table 2.4: Summary of the roughness factors for stepped revetments as presented in several sources. Further boundary conditions related to the conducted tests are summarized in the appendices C and **??**.

source	step type	n	d	$\frac{d}{H}$	$\frac{H}{S_h}$	γ_f
		[$-$]	[m]	[$-$]	[$-$]	(avg.)
Saville (1955)	vertical	1.5		0.38	12.0	0.56
				0.75	6.0, 12.0	0.74
				1.5	3.0, 6.0	0.80
				3.0	3.0	0.76
Wassing (1957)	vertical	3.5	0.32			0.77
Jachowski (1964)	vertical	2	0.38	4.0	5.0	0.74
				8.0	2.5	0.75
				15.0	1.3	0.76
		3	0.38	4.0	5.0	0.64
				8.0	2.5	0.64
				15.0	1.3	0.68
Nussbaum and Colley (1971)	vertical (sharp edge)	3	0.46	2.5	7.2	0.73
				3.0	6.0	0.67
				5.0	3.6	0.66
				8.0	2.3	0.67
	vertical (round edge)	3	0.53	3.0	7.0	0.90
				5.0	4.2	0.82
				8.0	2.6	0.82
Goda and Kishira (1976)	vertical	2			20-30	0.8-0.9
Takayama et al. (1982)	vertical	2, 3, 4	0.0-0.12		16-40	0.7-0.9
Van Steeg et al. (2012)	vertical, inclined	2, 3	0.7-0.9		1.6-6.7	0.6-0.9
Xiaomin et al. (2013)	vertical	2.5	0.73	9-15	0.2-8.0	0.35-0.77
Chuenchai et al. (2014)	vertical	2.5	0.35	2.7-12	0.6-6.5	0.64

like for instance a stepped revetment. The principle of hydro-static loads on dikes and revetments is briefly discussed for the sake of completeness. Hydro-static loads are not in the focus of the present research and will therefore not be discussed in greater depth.

2.3.2   Dynamic pressure loads/shocks

Dynamic pressure loads occur as wave impact on a structure. The progress of a single impact is dependent on the hydraulic- and geometry-related boundary conditions described in this chapter. A stepped revetment has horizontally and vertically aligned faces relative to gravity. Due to asymmetric orbital velocities in shallow waters and the asymmetric geometry of a wave ($H \ll L$) the loads on these two faces are different. Furthermore, the effect of wave loads is dependent on the overall slope n of a structure. One extreme case is a plain vertical wall without horizontal planes where breaking waves are slamming undamped against the wall. The other extreme case is an approximate gentle slope where plunging and spilling breakers appear (dependent on the Iribarren number $\xi = tan\alpha/(H/L)^{0.5}$). In this case the load on a nearly horizontal face is often damped by previous waves.

On a structure with horizontal and vertical faces waves can be redirected upwards and form an up-rushing jet of water. This jet of water will fall back down and in turn induces pressure loads on the horizontal faces. It is evident that the pressure loads on a horizontally aligned face is smaller than on a vertical face. For vertical walls 'the shock pressure exerted by a breaking wave is due to the violent simultaneous retardation of a certain limited mass of water which is brought to rest by the action of a thin cushion of air, which in the process becomes compressed by the advancing wave front' (Bagnold, 1939). SPM (1984) indicates that the wave forces are reduced for an inclined impact of the wave on a structure. A horizontal inclination of the impact is induced by oblique wave attack ($\beta \neq 90°$), a vertical inclination by a sloping structure (slope angle α). The reduced impact force for oblique wave attack on a sloped structure can therefore be calculated by

$$
\begin{aligned}
F_{oblique} &= F_{vertical} \cdot sin^2\beta \\
F_{sloped} &= F_{oblique} \cdot sin^2\alpha.
\end{aligned}
\tag{2.25}
$$

It is recommended for design purposes to calculate the forces on stepped structures following the same approach as for vertical walls. Therefore, the reduction of the inclined slope can be neglected since the dynamic pressures for stepped slopes and vertical walls are in a comparable range.

Pressure loads on vertical structures such as breakwaters are analyzed by many authors. This report will not discuss pressure loads on vertical structures in depth. However, some milestones will be highlighted. Sainflou (1928) derived an analytic approach to determine the wave loads on caisson breakwaters. Bagnold (1939) conducted hydraulic model test with the aim to analyze the nature of shock pressures exerted on the face of a vertical sea-wall by incident waves. Shock pressures up to 10 times greater than the ordinary hydro-static wave-pressure were measured. A formula for calculating the maximum pressure $\pm 10\,\%$ was derived to

$$(P_{max} - p_0) = 2.7\rho U^2 \frac{K}{D} \tag{2.26}$$

where U is the initial velocity of the water column, K is the length and D the mean initial thickness of an air cushion. The related pressure duration was derived to

$$T = a\frac{D}{U}. \tag{2.27}$$

with a as coefficient representing the influence of different peak pressures (1.1 for 4.1 bar, 1.7 for 1.4 bar and 3 for 0.5 bar). The main pressure-zone could be identified over the area covered by the air cushion. Below this area the pressures decrease rapidly. The high shock pressure area could be located between the top of the wave height ($2\,H$ at a vertical wall and extreme shallow water) and $1.2\,H$ above the wave trough. The author theorized that the short duration shock pressures result from a rapid compression of an air pocket trapped between the face of a breaking wave and the wall. Minikin (1963) refined Bagnold's model to estimate impact pressures caused by waves breaking directly onto a wall, and therefore addressed the problems of impact pressures. Kamel (1968) provided diagrams for the selection of the design wave that is reflecting at or breaking on a structure. The height of the design wave therefore is a function of the deep water wave, the wave reflection coefficient of the structure, the water depth in front of the structure and the bottom slope seawards. Design formulae were derived from results of experimental investigations. Hughes (1993) summarized Kamel's so called Hammer Shock as the theoretical maximum pressure:

$$P_{max} = \frac{\rho_v C_v}{\rho_w C_w + \rho_v C_v}\rho_w C_w V_w \tag{2.28}$$

where C_v represents the speed of sound in the vertical wall, C_w the speed of sound in water and V_w the velocity of the wave front impacting the wall. Much research took place to investigate the first pressure impact of a wave – the so called peak pressure impact. Kirkgöz (1983) additionally analyzed the secondary pressure impact and found it to be less intensive (in the order of the hydro-static pressure). However, the secondary pressure impact is present for a longer duration. The vertical distribution of the second peak can thereby be expressed by

$$\frac{P_s}{\rho_w/\rho_a} = K\eta_b - y \tag{2.29}$$

in which K represents a coefficient as function of H_0/L_0 for related bottom slopes, η_b the maximum water surface elevation at the breaking point and y the elevation relative to SWL. The second peak is significantly influenced by the wave steepness H_0/L_0 whereas variations in the bottom slope i have minor influence. Grilli et al. (1993) presented experimental and numerical results regarding the creation of large wave impact pressures on a vertical wall with an adjacent submerged horizontal toe step. Within their results, peak pressures on a vertical wall could be linked to a converging flow and to a formation of a small scale jet with large vertical velocity and acceleration. Peak impact pressures of 9 and 15 times larger than the hydro-static values could be recorded. Hughes (1993) lists five

important physical factors, namely (1) wave characteristics including wave dimensions, (2) the concentration of entrained air, (3) pressures in air pockets trapped between a structure and (4) the wave front and finally (5) the pressure in air cushions that contribute to shock pressures.

Oumeraci et al. (1993) developed criteria for wave breaking and breaker-type classification in the presence of vertical structures such as caisson breakwaters. A summary of the four major occurring load cases for wave impacts on vertical walls including breaker type classification and qualitative temporal and spacial pressure distribution is given in Fig. 2.1. Four main breaker types – (1) turbulent bore with foamy front, (2) well-developed plunging breaker with large air cushion, (3) plunging breaker with small air cushion and (4) upward deflected breaker with nearly no air entrapped – were classified. Impact loads may be considerably reduced by providing a proper shape of the structure front e.g. cylindrical shells where the total forces are reduced due to a delay in the pressure development along the cylinder. Impact forces cannot be described by a single formula. The most critical impact loading case is induced by plunging breakers and should be investigated more extensively. The breaking criteria commonly given in the literature for regular waves on unobstructed flat sea bottoms cannot be applied for incident random waves on vertical structures. For this case, much smaller values of the limiting wave steepness are obtained, due to the incident and reflected wave interference and shallow water wave breaking.

Allsop and Vicinanza (1996) investigated a 2D-study on the influence of normal wave attack on pressures at vertical breakwaters followed by Allsop and Calabrese (1999) with a 3D-study focused on effects induced by oblique or short-crested waves. Obviously, wave impacts reduced under oblique long-crested waves. Over a representative horizontal distance (about 20 m) variations of peak forces were relatively small ($\pm 20\,\%$) for oblique and short-crested waves. Design formula are given to calculate the horizontal forces on a vertical structure for transition or impact conditions.

Within the research project *PROVERBS – Probabilistic Design Tools for Vertical Breakwaters*, founded by the European Union – the complex phenomena of wave breaking at vertical walls have been investigated intensively in 1999. An empirically derived formulae to calculate the impact loading as combination of horizontal and uplift forces are given with an initial force calculation, statistics for relative forces, a calculation of the force history and the reduction by aeration.

Beside a comprehensive literature review on exisiting prediction methods for pressure loads on vertical structures Cuomo et al. (2010) conducted large scale model tests. They measured pressures of breaking waves on a battered seawall in order to quantify the contribution of wave activity to pulsating and impacting loads. A prediction formula for impacting forces

$$F_{h,imp(1/250)} = C_r^{1.65} \rho g H_{m0} L(h_s) \left(1 - \frac{|h_b - d|}{d}\right) \qquad (2.30)$$

and quasi-static forces

$$F_{h,qs(1/250)} = 4.8 \rho g H_{m0}^2 \qquad (2.31)$$
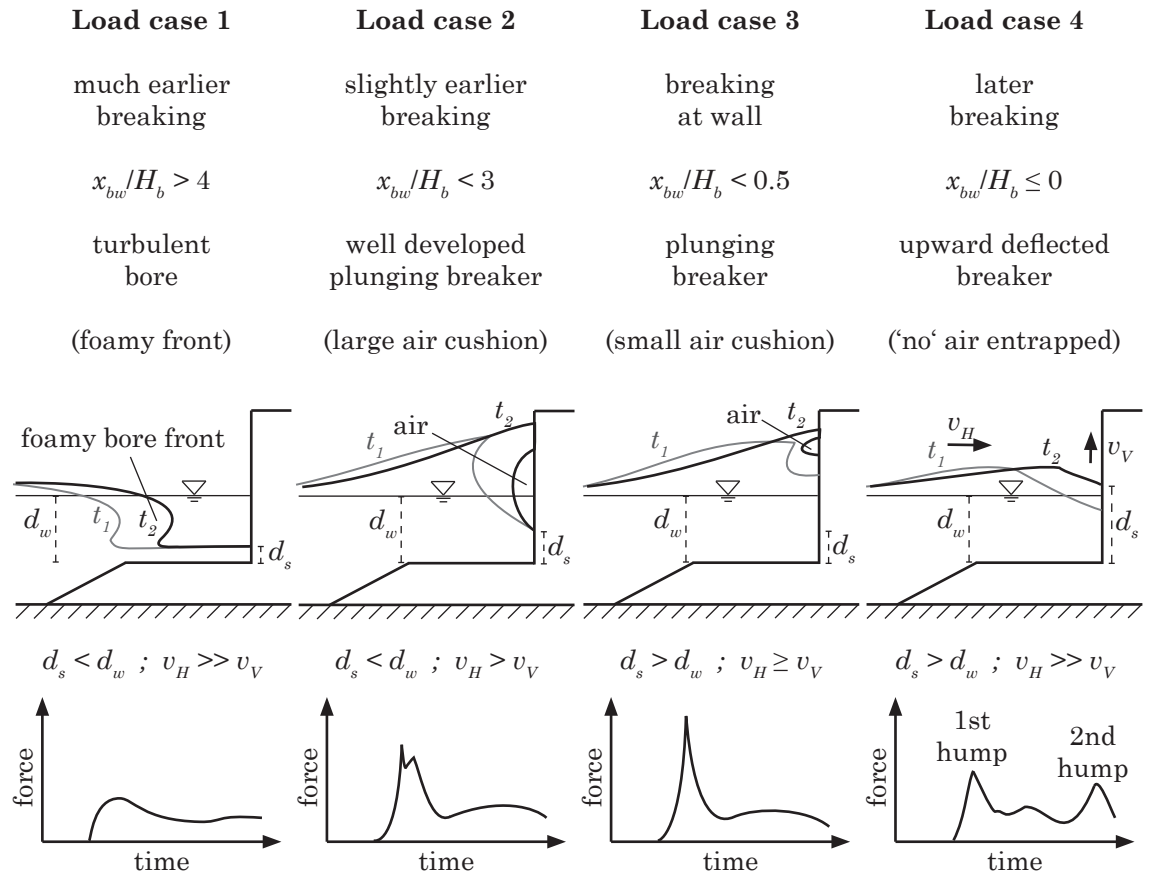
Figure 2.1: Definition of the four major occuring load cases for wave impact on vertical walls including breaker type classification and qualitative temporal and spacial pressure distribution (redrawing from Oumeraci et al. (1993)).

was derived. The normalized quasi-static pressure distribution is given as an interpolation function over the relative water depth by

$$P_{qs+(1/250)} = \frac{-0.054 \left(\frac{z-d}{H_{m0}}\right)^3 + 0.43 \left(\frac{z-d}{H_{m0}}\right)^2 - 1.4 \left(\frac{z-d}{H_{m0}}\right) + 2.7}{\left(\frac{z-d}{H_{m0}}\right)^3 - 0.68 \left(\frac{z-d}{H_{m0}}\right) + 1.6}. \tag{2.32}$$

Loads on sloping structures have been slightly less researched in the past. Selivanov (1972) measured 30% greater wave pressures on a slope with $n = 3.5$ in comparison to normative design pressures[7]. For mean wave heights of $0.4 - 0.85\,m$ the duration of the wave impact is in the range of $0.002 - 0.05\,s$. The highest wave impacts were recorded after a very large wave run-down. For slopes $n = 3.5$, the probability of occurrence for the case where the slope is exposed to maximum wave loads below one half the maximum wave height does not exceed 0.01 (recordings for 50 waves).

Bruun and Günbak (1977) discussed the importance of the wave period for the stability of permeable and impermeable sloping-faced wave protection structures. Maximum impact pressures on smooth slopes occur for a range of Iribarren numbers $(2.0 < \xi < 3.0)$ when the breaking wave hits the bare slope. The hydro-static pressure builds up due to wave run-up and increases with decreasing permeability and for increasing Iribarren numbers ξ for $\xi < 4.0$. Forces on a revetment are at a maximum when the wave run-down is located far under the *SWL* followed by collapsing and plunging wave breaking. Grüne and Bergmann (1994) conducted large scale hydraulic model tests regarding loads from wave-induced (regular waves, Pierson Moscowitz spectra, field spectra) shock pressures on sea dikes with composite slopes and berms. The study observed strong influences of the wave characteristics on the initial wave loads. Regular wave heights H always lead to smaller related pressure values (P_{max}/H) compared with irregular wave heights $H_{1/3}$. An increasing peak pressure could be observed for a slope with a berm in front due to the shoaling effect. A decreasing peak pressure was detected for the same geometry due to wave breaking in front of the slope. The decrease or increase of the peak pressure is therefore dependent on the water depth d on the berm. A broad overview of knowledge in the field of wave forces on inclined and vertical wall structures is summarized in ASCE (1995).

Loads on stepped structures were analyzed by Heimbaugh (1988) for Iribarren numbers of $2.8 < \xi < 6.3$ and step ratios in a range of $2.0 < H_{ms}/S_h < 3.9$. The importance of the short duration shock pressures resulting from the rapid compression of an air pocket trapped between the face of a breaking wave and the wall is discussed. The position of the highest measured pressures was dependent on the initial *SWL*. According to the analysis of pressure distributions, the maximum pressures at different wall elevations rarely occur simultaneously. Especially in the case of a non-vertical wall such as the stepped wall studied here, on which some wave energy is dissipated through turbulence. In some cases a negative pressure duration was measured. The negative pressure duration is interpreted as a characteristic of turbulence and air entrainment occurring at the base of each seawall

---

[7]In these days the Russian norm SN 92-60 from Gosstroiizdat (1960) recommended that wave loads on sloping structures should be treated as static loads.

step. Finally, Heimbaugh (1988) summarizes a discussion about the importance of shock pressures for the actual design of a stepped seawall. Hereafter, pressures of such short duration should not be used for establishing the design load case. It is recommended to rather consider the smaller surge pressures of longer duration are more suitable indicators of the critical dynamic loading.

Conclusions

Pressure loads are dependent on the wave characteristics, the concentration of entrained air in the wave, the shape of the wave front at the impact and the geometry of the stressed structure. Plunging breakers forming a small air-cushion between wave and structure slightly before the impact induce the highest impact loads. These impact loads are short-duration loads ([ms]) and up to $10-15$ times larger than the ordinary hydro-static pressure. Impacts on a revetment are at a maximum when the run-down is located far under the SWL followed by collapsing and plunging wave breaking. A reduced water depth d by the presence of a submerged berm can decrease (early wave breaking) or increase (shoaling) the impact loads on the revetment. At stepped revetments, short duration pressures were detected. It is recommended to consider surge pressures of longer duration for design loads instead.

2.3.3 Aging and durability

Reinforced concrete structures need a sufficient cover to prevent corrosion. If a stepped revetment is constructed from concrete, it is necessary that the structure has an adequate finish of the surface in order to resist corrosion by saline water as well as abrasion from debris transported by waves (Bradbury et al., 2012). Rowe (2012a) documents the degradation of the Blackpool-Revetment after two years due to abrasion from the sediment load (large cobble and shingle beach deposit). As a result maintenance was required. Blackpool is a purely sandy beach with no rocks and abrasion is minimal. Some concrete surfaces might be polished by regular aeolian sand transported. Photos document the abrasion of the step units fabricated by C70 micro silica grey concrete with granite aggregate. The degree of abrasion increases for steps on a lower level (Fig. 2.4). Algae had built up in the tidal zone (Fig. 2.3). Within a survey in Southampton, UK, West (2016) documented spalling of step edges over the whole length of a stepped revetment. As against Blackpool a shingle beach was located in front of this revetment.

Bradbury et al. (2012) reviewed several toe structures and recommended regular inspections of the sediment bed beneath the toe of the stepped revetment in order to assess scour of the fill material. At Teignmouth promenade, UK, overtopped water increased the pore water pressure on the landside of the revetment and drained behind the seawall under the revetment toe with each high tide. An additional loss of beach material led to the undermining of the toe. An installation of a cut-off wall[8] or beach nourishment as recommended by McCartney (1976) could have prevented this failure.

---

[8]Toe stabilization measure e.g. by sheet-piling.

Figure 2.2: Significant algae growth on the Blackpool revetment visible at low tide (photo taken from Rowe (2012a)).

Figure 2.3: Blackpool revetment during high tide point to the fact of algae growth for areas with wet and dry cycles (photo taken from M. Beckwith in 2011).
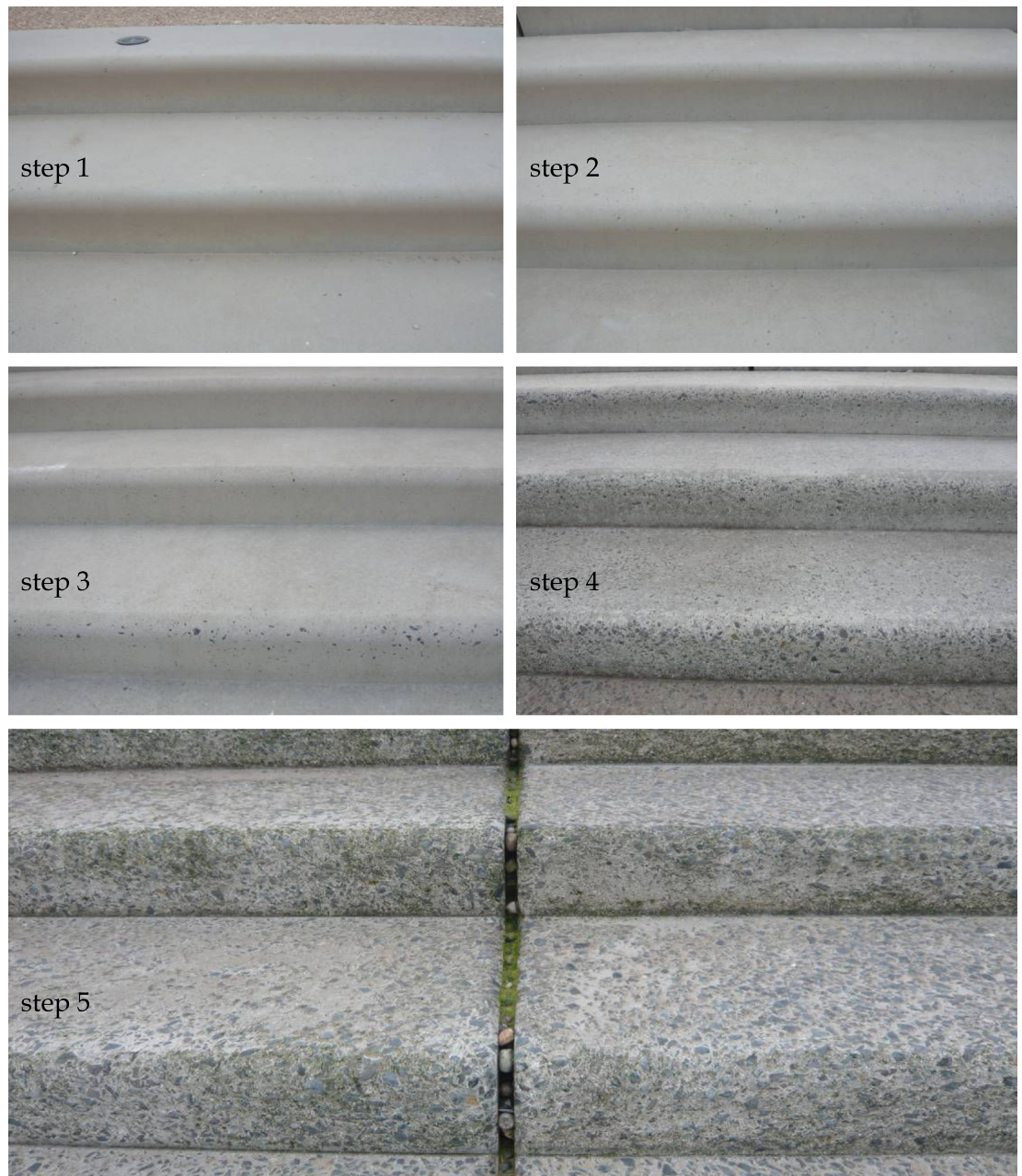
Figure 2.4: Degradation of precast step units constructed from C70 micros silica grey concrete with granite aggregate after two years in extremely aggressive environment with large cobble and shingle beach deposit (although the beach is purely sandy). step1: still in original condition as constructed, step 2: negligible wear, step 3: minor wear of vertical faces and start of aggregate exposure, step 4: aggregate exposed, step 5: significant wear and full aggregate exposure to vertical and horizontal faces (photos taken from Rowe (2012a)).

Conclusion

Stepped revetments constructed from concrete have to resist corrosion. Abrasion has been
detected at stepped revetments – mainly at shingle beaches. The swash zones are prone
to flora- and fauna-growth. An insufficient design of a filter-layer can lead to increased
pore pressures, a drainage of core material and finally a failure of the revetment.

2.4   Stepped revetments

This section summarizes present knowledge on stepped revetments implemented in present
coastal protection structures. A critical reflection of the findings is presented in sec-
tion 2.5.1. Published and unpublished results of experimental investigations on wave re-
flection, wave run-up, wave overtopping, wave loads and scouring on stepped revetments
are re-analyzed. Persistent knowledge gaps are addressed in section 2.6. Many data from
small scale tests have been identified, some data from larger scales and in some cases data
from in-situ observations. A chronological review on the history of stepped revetments as
coastal protection structure is given in order to show the consecutive increase of knowledge
in this field of research (Fig. 2.5). Where possible, model set-ups and configurations are
described in detail to enable a later discussion with the focus on model- and scale effects
related to these findings. A subject related summary of the major findings and improve-
ments is given at the end of the chapter (page 41). Summary sheets are provided in the
appendices C and **??**.

The first document of stepped revetments has been published by O'Shaughnessy et al.
(1924). The document presents the design and construction of the ocean beach esplanade
sea-wall along the great highway on San Francisco's ocean beach. The seawall was installed
to prevent beach erosion. It consists of a stepped section founded on concrete piles topped
by a re-curved reinforced concrete section. After construction of the seawall, the beach in
front of it remained relatively stable. Furthermore, the document includes a discussion on
erosion and sea-walls at other places.

First published investigations on stepped revetments have been carried out by Saville
(1955), analyzing the wave run-up and overtopping on composite slope. Revetments of
smooth surfaces, riprap and vertical walls are analyzed. Parallel, a slope ($n = 1.5$) cov-
ered with a stepped revetment (here called 'Step - Faced Wall') was analyzed regarding
wave run-up (25 tests) and wave overtopping (88 tests) (Fig. 2.6). The model tests were
conducted in a $36.5\,m$ long wave flume with a width of $1.5\,m$ and a maximum water depth
of $1.5\,m$. The flume is equipped with a plunger type wave maker for regular waves. The
model was built to a *Froude* scale of 1:17. The step ratio was in a range of $2 < H/S_h < 10$
for Iribarren numbers of $1.4 < \xi < 13$. The mean overtopping discharge q was calculated
from 6–7 single waves. Each single test configuration was repeated 2–3 times. Thereby,
deviations in q of $8 - 10\,\%$ occurred from test to test. The wave run-up R_u was defined as
the maximum run-up height of the 6–7 analyzed waves. Each single test configuration was
repeated 6-7 times and R_u represents the mean of these tests. Saville (1955) concluded
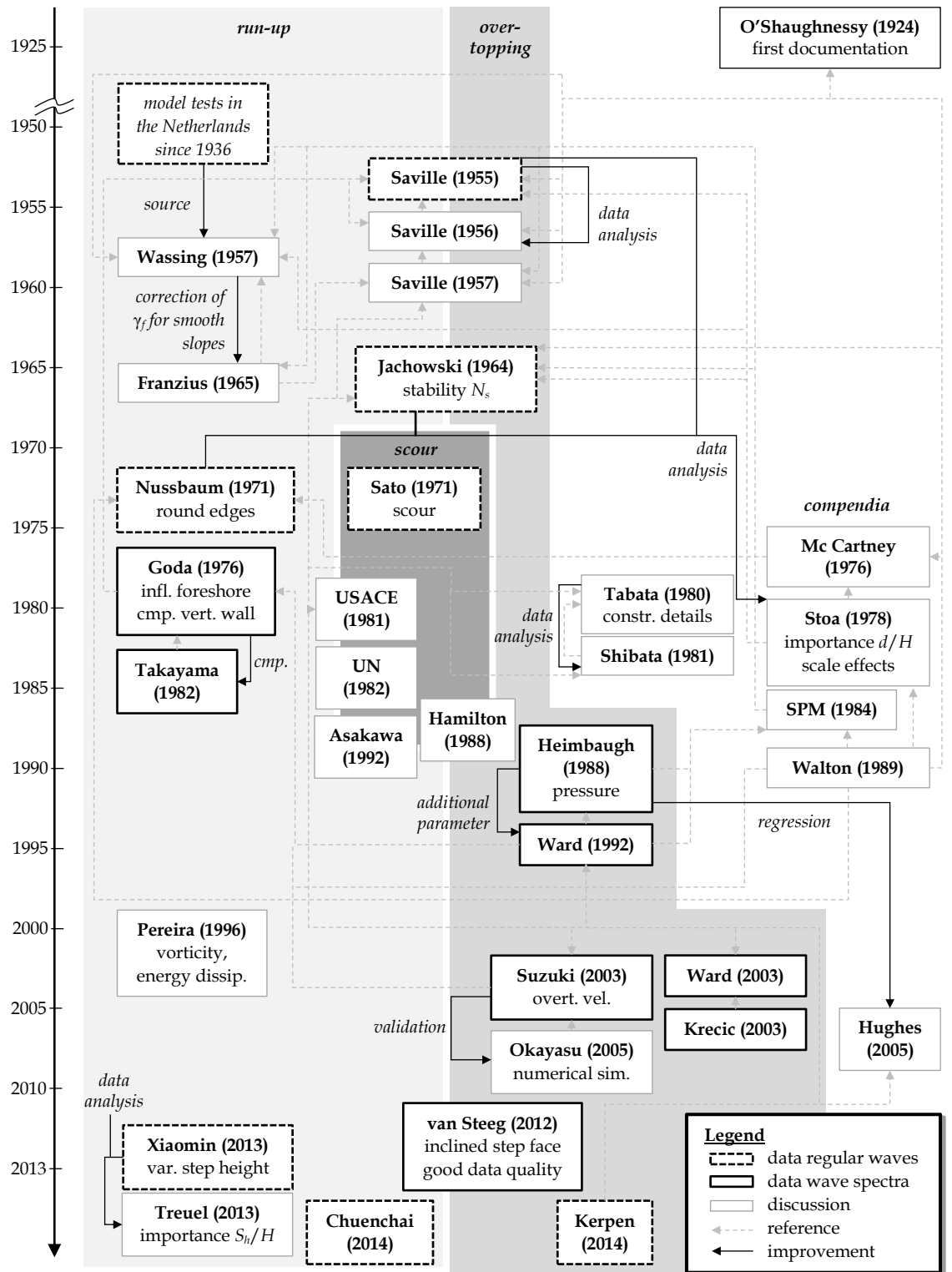
Figure 2.5: Flowchart of literature providing data and discussions with respect to wave run-up, wave overtopping, scour and wave loads on stepped revetments.

that the wave run-up R_u and wave overtopping volume q of stepped revetments increased with increasing wave height, increasing wave period or increasing Iribarren number and decreasing wave steepness. The reduction of wave run-up and overtopping of a stepped

revetment in comparison to a smooth surface was determined as $0.65 < \gamma_f < 0.85$ for $\xi > 3.3$ and $0.35 < \gamma_f < 0.7$ for $1.0 < \xi < 3.3$, with γ_f depicting the reduction factor. An own re-analysis of data (Fig. 2.6) shows that this reduction factor increases disproportional to an increasing overtopping volume q. The range of reduction factors derived in the tests for wave run-up is $0.33 < \gamma_f < 0.85$ and for wave overtopping $0.06 < \gamma_f < 0.99$. From the data described in Saville (1955), together with further investigations, Saville (1957) presents run-up dependencies for composite slopes.

Wassing (1957) summarized results of physical model tests on wave run-up carried out in the Netherlands since 1936. These tests include two test series on the influence of 'steps' on a 1:3.5 inclined slope. Small steps ($S_h = 0.14\,m$) reveal a reduction factor of $\gamma_f = 0.78$ and large steps ($S_h = 0.35\,m$) a reduction factor of $\gamma_f = 0.77$. Hydraulic parameters are not given in the paper, thus the step height 'small' and 'large' cannot be seen in proportion to other parameters like e.g. the wave height. As tests for two wave steepnesses ($H/L\ \{0.05, 0.07\}$) are given, the Iribarren number is assumed to be in a range of $1.08 \leq \xi \leq 1.27$. According to Wassing (1957) the wave run-up can be calculated by the equation

$$\frac{R_u}{H} = A \cdot \gamma_f \cdot sin2\alpha. \tag{2.33}$$

A is defined with regard to the probability of exceedance of the run-up value. The roughness factor γ_f represents the characteristic of the dike facing roughness. In this case, the run-up over the stepped revetment was compared with the run-up of a revetment of neatly-set stones (large steps: $\gamma_f = 0.89$, small steps: $\gamma_f = 0.90$). Hence, the reduction factor has to be corrected directly for a smooth protective layer (large steps: $\gamma_f = 0.77$, small steps: $\gamma_f = 0.78$) as also mentioned in Franzius (1965). It was concluded that roughness elements can reduce the wave run-up and have to be placed above SWL to be effective.

Table 2.5: Regression parameter A for wave run-up prediction according to the probability of exceedance (Wassing, 1957).

run-up	$H/L = 0.05$	$H/L = 0.07$
$R_{u,0.1\%}$	$A_{0.1} = 4.90$	$A_{0.1} = 4.75$
$R_{u,1\%}$	$A_1 = 4.50$	$A_1 = 4.30$
$R_{u,2\%}$	$A_2 = 4.30$	$A_2 = 4.10$
$R_{u,5\%}$	$A_5 = 4.10$	$A_5 = 3.85$
$R_{u,10\%}$	$A_{10} = 3.90$	$A_{10} = 3.60$
$R_{u,30\%}$	$A_{30} = 3.50$	$A_{30} = 3.10$
$R_{u,50\%}$	$A_{50} = 3.25$	$A_{50} = 2.80$

Jachowski (1964) tested a stepped revetment build up by interlocking concrete blocks[9].

---

[9]'Typical blocks used in Europe and the United States are generally square slabs with ship-lap type interlocking joints' in order to benefit from wave energy absorption and reduced wave run-up known from rubble mound revetments and parallel avoid the undesirable features of rubble mound revetments named by the author as 'limited access to the beach, [...] a safety hazard to people who cross the rubble slope to the beach and the unattractive or non-aesthetic appearance'. Jachowski (1964)
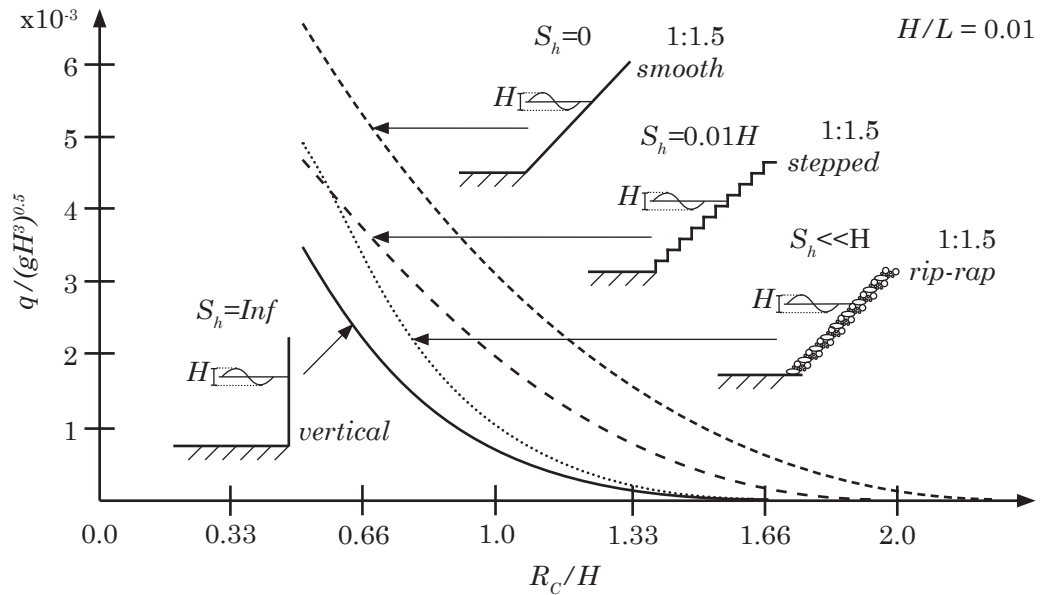
Figure 2.6: Comparison of the wave overtopping with respect to the relative freeboard height at a vertical wall, a 1:1.5 inclined plain-, stepped- and rip-rap slope (modified after Saville (1955)).

Therefore, Jachowski (1964) performed stability (*Froude* scale 1:10) and run-up (*Froude* scale 1:16) tests in a physical model focusing on the interlocking of a precast concrete block seawall with a stepped slope ($n = 2$ and $n = 3$). The tests were conducted in a $21.9\,m$ long wave flume with regular waves. The step ratio was in a range of $0.04 < H/S_h < 1.9$ with step heights of $0.016\,m$. The main design criteria were a heavy weight of blocks to withstand design wave conditions and a preferably ample surface roughness to be most efficient in reducing ware run-up, overtopping, backwash and reflection. Three types of blocks were tested – a waffle type block with vertical face, and two interlocking precast concrete blocks with vertical and offshore-inclined face (Fig. 2.7). Jachowski (1964) concluded that a stepped-face seawall is the most effective in reducing the wave run-up. Test results indicate that inclined-face steps have little to no additional benefit compared to vertical-faced steps since the inclined-face steps slightly reduce the wave run-up in comparison to vertical-faced steps. The run-up height is influenced by the Iribarren number ("run-up and overtopping were larger for surging waves, as differentiated from plunging waves, at the time of breaking") and reduced with increasing relative water depth at the toe of the structure (d/H_{m0}). Reduction factors γ_f are not given in the paper. Tests on the stability of the vertical-face stepped revetment revealed a stability number $N_s > 12.8$ (derived with the approach by Hudson (1959)). This large stability-value can be attributed to excellent mechanical interlocking of the ship-lap joints. For large freeboard heights R_c the revetment failed at or slightly above the *SWL* due to single blocks that are forced up the slope by incident breaking waves followed by a gradual dislodging of the blocks in the area of *SWL*. At set-ups with low freeboard heights, wave overtopping occurs and the stepped revetment fails due to the uplift and displacement of the top row (an adequate anchorage of the top row is required and feasible). The prime importance of a properly

designed filter layer beneath the block-layer was mentioned in order to avoid sand losses through joints between the blocks.

Nussbaum and Colley (1971) conducted physical model tests to determine the wave run-up on a smooth and stepped revetment constructed by soil cement[10]. The main findings are redrawn in Fig. 2.8. The study concluded that the wave run-up will be reduced by a stepped configuration in comparison to a smooth slope and that an increasing slope steepness $1/n$ results in higher run-up heights. Larger steps are not as efficient in reducing the wave run-up as smaller steps. An unexpected finding – pointed out with the redraw of the data in Fig. 2.8 – is that a 1 in 2 slope with rounded steps results in higher relative run-up heights than a smooth slope. This seems to be impossible since the turbulence induced by round steps should also reduce the run-up in comparison to a smooth slope.

Sato et al. (1971) investigated on scour prevention works at the toe of sea walls. In the physical model tests (*Froude* scaling 1:10) in a $31.65\,m$ long and $0.17\,m$ wide wave flume, the scour development at the toe of a 1:3 slope with a smooth and stepped surface, among others, were compared (Fig. 2.9). A fine sand ($D_{50} = 0.2\,mm$) was used to set up a 1:10 inclined fore slope. The bathymetry profile was measured in $0.05\,m$ sections before the start of the tests, after 10 minutes (400 waves), 120 minutes (4,700 waves) and 300 minutes (11,800 waves) to represent the equilibrium state condition. The results indicate a very similar scour development in front of the plain and the stepped slope. The scour depth in front of the toe increases with the increasing number of attacking waves. After 300 minutes the maximum scour depth in front of the stepped slope is approximately 11 % deeper in comparison to the smooth slope. For both revetment geometries the maximum scour depth is in a distance of $L/3$ from the toe and the maximum scour is one wave length L from the toe.

Goda and Kishira (1976) published results of experiments on irregular wave overtopping characteristics of seawalls for five low crest types ($n = 2$). The overtopping volumes for three wave heights and a fixed wave period with two different step heights were compared (9 tests, Fig. 2.10). The physical model tests were conducted in a wave flume at the *Port and Harbour Research Institute* in Japan with *Froude* scaling (1:33). Goda and Kishira

---

[10]A mixture of pulverized natural soil with a small amount of cement and water to improve the slope protection.
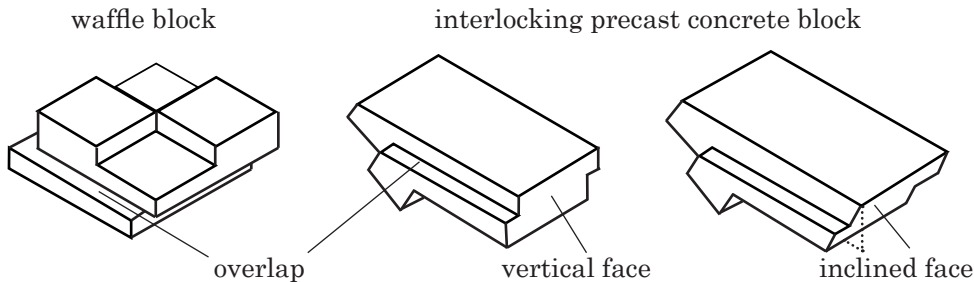
Figure 2.7: Precast interlocking concrete blocks with stepped surface (waffle block) or vertical and inclined face (Jachowski, 1964).
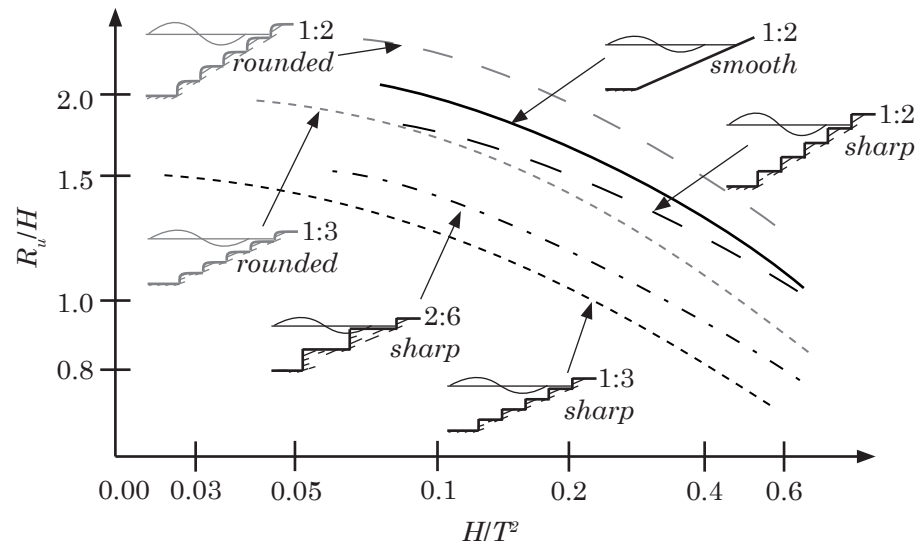
Figure 2.8: The effect of slope steepness and step-edge geometry on the wave run-up (modified after Nussbaum and Colley (1971)).
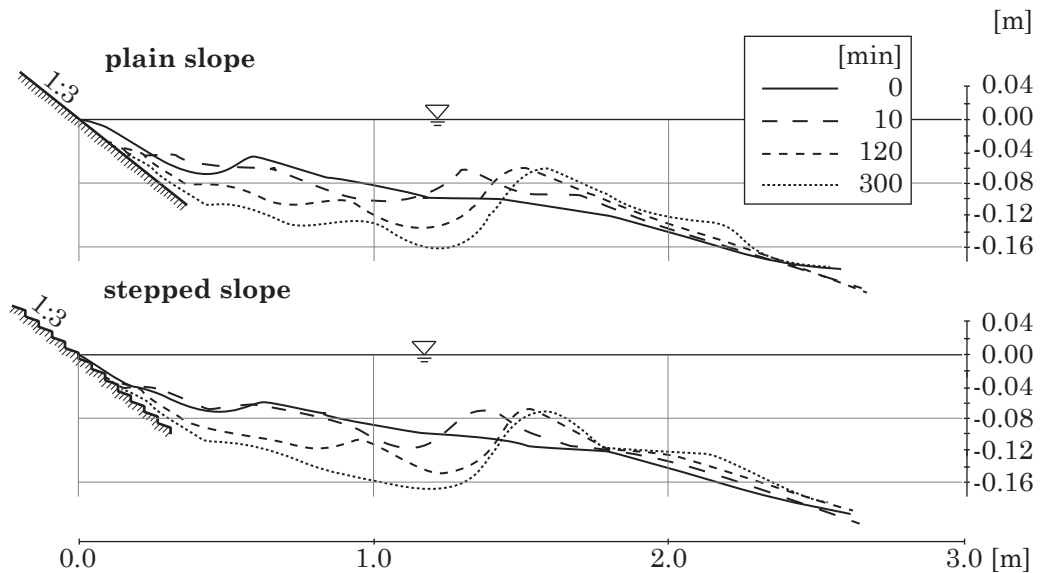
Figure 2.9: Scour evolution at a 1:3 slope with plain and stepped face (modified after Sato et al. (1971)).

(1976) concluded that lower crest heights are required for 'stepped slopes' in comparison to smooth slopes. Furthermore, the stepped slope requires a $10 - 20\,\%$ higher freeboard height in comparison to a vertical wall. Goda and Kishira (1976) analyzed the influence of an inclined foreshore in front of the stepped revetment. It was found that the overtopping volumes are about 30 times smaller for a 1:30 foreshore in comparison to a 1:10 foreshore. The reduction of the overtopping volume for a plain slope adjacent to the inclined foreshore was only 20 times smaller.

McCartney (1976) published a study of 25 coastal revetment types. Idealized geometries representing a stepped face are given in Fig. 1.2. Among the revetment types a 'gabion-stacked' revetment and a 'soil cement' revetment are presented. These two represent geometries similar to a stepped revetment. For 'gabion-stacked' revetments McCartney (1976) estimated a reduced wave run-up in comparison to a smooth slope. The 'gabion-stacked' revetment has a roughness coefficient between $0.5 < \gamma_f < 0.6$ and a low reflection coefficient. The author suggests that gabions should be stacked as steps. A gabion mat[11] is placed as a foundation for the steps and serve as toe protection. For 'soil cement' revetments the author refers to small-scale tests by Nussbaum and Colley (1971). The roughness factor for 'soil cement' was found to be between $0.7 < \gamma_f < 0.8$ with a moderate wave reflection coefficient. In order to prevent scour, it is suggested to install a 'soil cement' revetment from SWL upwards and with cutoff wall or beach nourishment.

Stoa (1978) reanalyzed data from previous studies on wave run-up at 'stepped-slope' configurations (Saville (1955), Jachowski (1964) and Nussbaum and Colley (1971)). The study summarized r-values, which is the reduction factor γ_f for wave run-up (Fig. 2.11). Stoa (1978) concluded that the relative water depth (d_s/H) has a significant influence on the wave run-up even when the water depth at the toe of the structure is zero. The reduction factor γ_f is not significantly influenced by varying wave steepness values if the foreshore is flat. Due to the high variation of γ_f for nearly every revetment type, the factor proves to be highly dependent on the wave and structure conditions. As the author states: *'any one value of γ_f does not seem applicable for all wave conditions for a given armor unit'*. Furthermore, scale effects in model tests on the wave run-up at smooth and rough slopes are discussed. As Stoa (1978) suggests, the wave run-up therefore has to be adjusted with a correction factor for scale effects. The scale effect correction factor has to be applied to the data from which γ_f is derived. Correction curves are given but are based on a limited number of large-scale tests. Therefore, care should be taken when applying the correction curves.

Tabata et al. (1980) give a comprehensive summary of previous studies in Japan. As part of the summary, designs of 105 so-called 'stepped face seawalls' are presented. In addition, the governing design conditions (Fig. 2.12), drawings and photographs are presented. About 90% of the step heights are in the range of $0.2\,m \leq S_h \leq 0.3\,m$ and 50% of the steps have a width of $S_w = 1.0\,m$ or $1.5\,m$. Slope angles are mainly in the range of $1 \leq cot\alpha \leq 7.5$. Three of the structures have slopes of 1:10, while only one has a slope of 1:15. The analysis

---

[11]A gabion with a large width and depth but a small thickness. The mats are used as foundation and offer erosion protection.
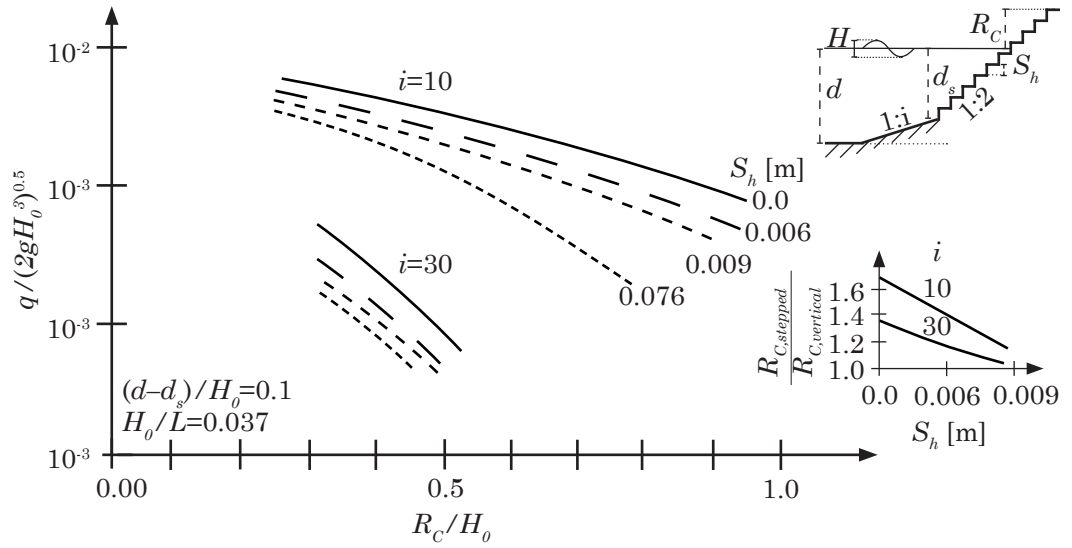
Figure 2.10: The influence of the foreshore inclination i on the dimensionless overtopping rate for stepped revetments. The comparison of the required freeboard height R_c between stepped revetments and vertical walls are also presented (modified after Goda and Kishira (1976)).
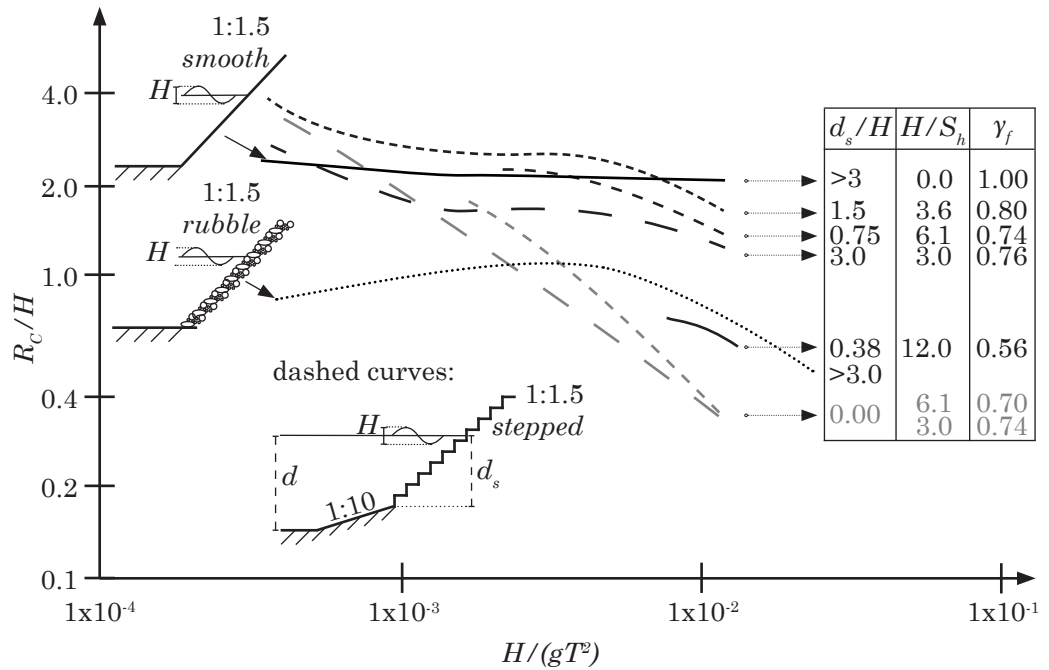
Figure 2.11: Comparison of the wave run-up with respect to the wave steepness at a 1:1.5 inclined plain-, rubble- and stepped slope with varying step height and toe depth (modified after Stoa (1978)).

of the step ratio H/S_h shows that the design wave height is always larger than the step height (in most cases between 5 and 20 times larger). Shibata et al. (1981) discussed the data set of Tabata et al. (1980) with respect to the general design methods and frequency distributions of relevant geometric parameter configurations (like Fig. 2.12, 2nd row).

USACE (1981) discusses the functional applications, limitations and the general design concepts of seawalls. A subsection focuses on 'Stepped Face Seawalls'. Within this section the potential of step-faced seawalls for dissipating wave energy, reducing wave reflection, wave run-up, wave overtopping and scour effects (toe armoring) are discussed. USACE (1981) also highlights the potential of stepped revetments to provide easy access to a beach exposed to moderate wave action.

Takayama et al. (1982) conducted physical model tests to determine the wave overtopping for low crest type sea walls. The tests include 135 tests where the run-up at stepped revetments are measured. The tests were performed in a $23\,m$ long and $5\,m$ wide wave flume (a $0.6\,m$ width flume-secton was separated for these experiments). Irregular waves were generated with a piston type wave generator. The wave overtopping was studied for two different step heights and three varying slopes ($n = 2, 3, 4$) for a range of hydraulic boundary conditions. In front of the stepped revetment a 1 in 30 inclined foreshore berm was installed. The data show that the reduction factor γ_f decreases with decreasing slope steepness for several dimensionless step heights H/S_h. A comparison of overtopping volumes for a stepped revetment to a vertical wall indicate that the volumes for stepped revetments are slightly higher. However, this increase is less dominant than as by Goda and Kishira (1976). With an increased dimensionless overtopping volume $q/\sqrt{2gH^3}$ the reduction coefficient γ_f becomes larger. A larger γ_f indicates a lower influence of the surface roughness on the stepped slope. Takayama et al. (1982) define the reduction factor for wave overtopping under given boundary conditions between $0.68 < \gamma_f < 0.9$. The authors conclude that the selected step height may be too small and for future tests larger step heights should be selected to avoid scale effects. Due to the relative large roughness coefficient the authors claim that a stepped revetment effectively reduces overtopping.

United Nations (1982) discussed the effectiveness of seawalls with 'stepped shapes' to prevent scour and reduce the wave run-up. It is suggested that stepped revetments are preferred coastal protection structures at beach resorts due to the accessibility these structures offer to the beach. Furthermore, the force of breaking waves is spread over several step surfaces. A potential for scour prevention with installation in the lower part of a sea-wall (below SWL) is mentioned.

The SPM (1984) gave a comprehensive summary of state of the art shore protection methods which includes some comments on 'stepped structures'. Stepped-face sea walls are designed for stability for cases with moderate waves. A combination of stepped- and curved-face seawall is built to resist high wave action and reduce scour (energy dissipation during wave run-down process). "For design calculations, forces on stepped structures may be computed as if the face were vertical, since the dynamic pressure is about the same as computed for vertical walls." SPM (1984) lists and refers findings by Saville (1955) and Saville (1956). Among other factors, the wave overtopping rate depends on the nature of
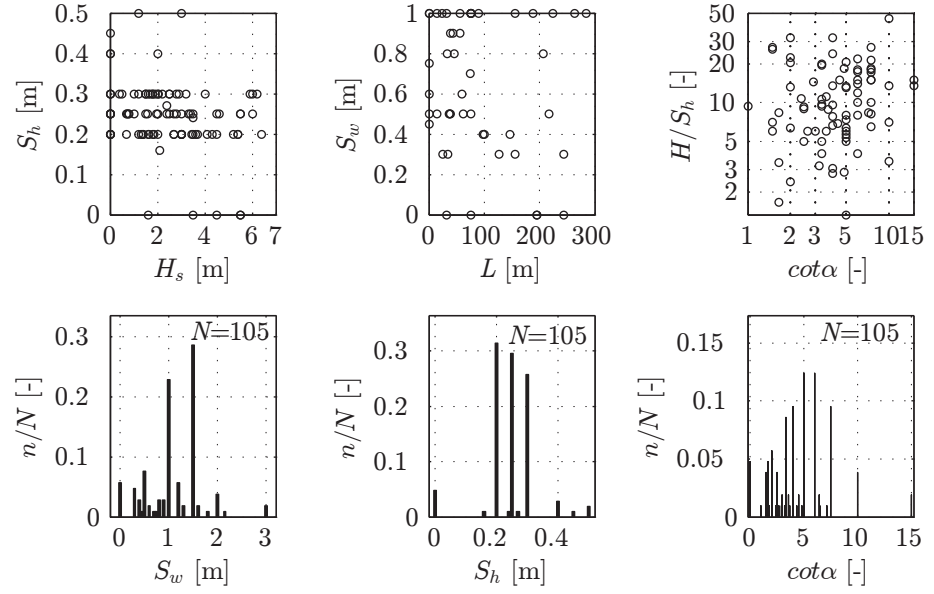
Figure 2.12: Visualization of data gathered by Tabata et al. (1980).

the slope face (smooth, stepped, or riprapped).

Hamilton (1988) confirms that stepped revetments offer a reduction in run-up heights and overtopping volumes. These findings are based on a documentation about the design and construction of a prototype structure at Sheerness. Furthermore, Hamilton (1988) confirms beach retention at the toe of a stepped face slope due to a reduced down-wash and indicates good locations for people to sit at the sea.

Heimbaugh (1988) conducted hydraulic model tests for a 'stepped seawall' in a $3.3\,m$ wide and $76\,m$ long wave flume following $Froude$ scale law (scale 1:19). The focusses of the tests were on the reduction of wave overtopping of stepped seawalls and to measure the wave-induced pressures on these steps. Heimbaugh (1988) aims to provide design guidance for stepped revetments which includes toe stability. For this study, the channel was divided in separate sections and the stepped seawall was tested in a $0.45\,m$ width section. A sloping structure ($n = 1.5, n = 2$) with step heights of $0.026\,m$ was analyzed. At the top of the revetment a curved seawall was added. The surface elevation in front of the model was measured with a wave gauge array of three wave gauges. Irregular waves (TMA spectra) generated by a hydraulically driven piston-type wave maker were tested. According to visual assessment, the rip-rap toe played a major role in the reduction of overtopping (compare the influence of composite walls at Eurotop (2016)). Overtopping volumes were less for more gentle slopes ($n = 2$). A design formula for wave overtopping prediction was derived. Due to seiche effects in the flume the overtopping data scatter.

$$Q[cfs/ft] = 7.78exp\left(-7.476\frac{R_c}{\sqrt[3]{H_{m0}^2 \cdot L_p}}\right) \tag{2.34}$$

With respect to the pressure distribution over the water depth at the structure, the maximum measured pressures at each sensor is given in Fig. 2.13 for an example test run with a wave steepness of $H_{m0}/L_p = 0.023$. The maximum pressure is recorded at the top of the re-curved seawall as expected. However, for the stepped revetment the maximum pressure occurs slightly above the still water level. The maximum pressure decreases with increasing water level. Fig. 2.13 indicates that short-duration ($< 0.02\,s$) pressure shocks followed by about $90\,\%$ smaller secondary pressure magnitudes ($2-3\,s$) were measured on the steps. The position of maximum pressure is dependent on the still water level.

Walton et al. (1989) provided a table with run-up reduction coefficients for various surfaces including stepped surfaces and stated that the results based on high end laboratory measurements as opposed to Stoa (1978) or SPM (1984) for instance. Walton et al. (1989) claim that due to labor-intensive on-site forming of cast-in-place concrete, precast components (e.g. stepped-face seawalls) are nowadays commonly used.

Asakawa et al. (1992) presented results of hydraulic model tests (*Froude* scale 1:20 and 1:30) of a so called 'terrace block'-revetment with a slope of 1:3 and 1:5. This type of revetment is installed at more than 100 locations in Japan. Single blocks were combined to form a stepped revetment. The revetment was designed by using interlocking units which were permeable and built on a filter layer. The measured wave run-up was lower for the milder slope (1:5). Furthermore, the results indicate that the permeable revetment offers a larger reduction in wave run-up when compared to an impermeable revetment. The stability of the impermeable stepped revetment could be improved by increasing the filter-layer thickness. For an offshore design wave height of $5.4\,m$ 'terrace-block'-units with a weight of $4.0\,t$ proved to be stable on an underlayer built by rocks with a thickness of $1.0\,m$. The scour development at the toe of the revetment could be reduced for permeable stepped revetments due to less wave run-down and lower reflection coefficients in comparison to the impermeable stepped revetment.

Ward and Ahrens (1992) reanalyzed tests by Heimbaugh (1988) and extended the data set by adding an additional test series for more wave heights and wave periods. Ward and Ahrens (1992) summarized that a stepped seawall is able to dissipate energy by evoking more turbulence and thereby reduces the wave overtopping volume. But in comparison to a large smooth revetment without steps it seems to be less effective in reducing overtopping volumes. Nevertheless, observations during the tests indicated that the steps might have been too small for an effective flow disruption ($9 < H/S_h < 10$). Ward and Ahrens (1992) presented the following equation to predict wave overtopping:

$$\frac{q}{\sqrt{gH_{m0}^3}} = exp\left(-11.174\frac{R_C}{\sqrt[3]{H_{m0}^2 L_0}} - 10.664\sqrt{\frac{H_{m0}}{L_0}}\right) (R^2 = 0.948) \qquad (2.35)$$

Pereira (1996) studied the formation of vortices at a single submerged step (negative freeboard heights) under non-breaking waves ($0.002 < H/L < 0.015$). This study focused on the kinematic processes induced by the interaction of waves and steps. Experiments with regular waves were conducted in a $19.4\,m$ long wave flume. Pereira (1996) assumed
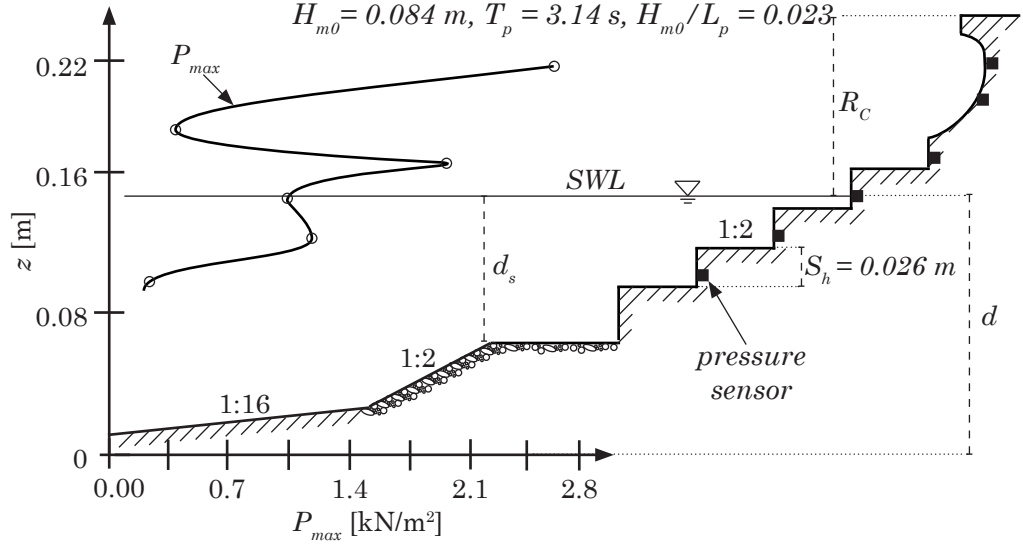
Figure 2.13: Example of the distribution of P_{max} with respect to the water depth in front of a stepped revetment with superimposed seawall (modified after Heimbaugh (1988)).

that vortex shedding at the edges of a step are decisive in the energy dissipation of waves over steps. A result of PIV measurements was that the vorticity is directly proportional to the velocity gradients at the step edge. The energy loss due to vortex shedding at a submerged step was calculated by an analytically derived approach (based on the vortex theory by Hamel (1916), Chapt. 5)

$$E_v = \frac{\pi^3 r_k^4}{T^2} \left[1 - 4ln \left(\frac{H}{2r_k} \right) \right]. \tag{2.36}$$

Ward (2003) conducted wave overtopping tests in a model scale of 1:35 of a stepped revetment for the city of Chicago, Illinois at Lake Michigan shoreline. Furthermore, the toe stability was tested. Wave conditions for a 10-year and 20-year return period storm event with related water levels were generated by a piston wave maker for irregular waves (*Jonswap* spectra). Parameters of interest were the number and size of the steps, the crest elevation R_c and the width of a promenade. The authors stated that the incident wave energy is increased by re-reflected waves at the wave board. They observed reasonably low overtopping rates for model configurations with high freeboard heights R_c, a large parapet on the promenade and an additional installed offshore breakwater. A prediction formula was developed:

$$\frac{75q + 1}{\sqrt{gH_{m0}^3}} = 1.1215exp \left(-7.743 \frac{R_p}{\sqrt[3]{H_{m0}^2 L_0}} - 10.501 \frac{R_C}{\sqrt[3]{H_{m0}^2 L_0}} - 14.222 \frac{d}{L_0} \right). \tag{2.37}$$

Krecic and Sayao (2003) conducted a reanalysis of the results by Ward (2003) because of lack of isolation of some key parameters including the revetment width and toe berm effects. According to the authors Ward (2003) did not measure the incident wave height at the toe of the structure, they estimated H_s by the shoaling equation defined by Goda

$(2010)^{12}$. The main part of the reanalysis of the data was a dimension analysis that yields to an adapted design formula for wave overtopping prediction at stepped revetments

$$\frac{q}{\sqrt{gH_s^3}} = 2.24 \cdot 10^{-5} exp\left(-2.5\frac{R_c + R_p}{H_s}\right)\left(\frac{d}{L_0}\right)^{-2.28}\left(\frac{B}{H_{m0}}\right)^{-1.23}\left(\frac{B_r}{H_s}\right)^{-0.25} \quad (2.38)$$

valid for $0.44 < R_c/H_s < 1.92$, $-0.18 < R_p/H_s < 0.42$, $0.01 < d/L_0 < 0.07$, $2.55 < B/H_s < 8.65$ and $1.0 < B_r/H_s < 8.7$ with a coefficient of determination of $R^2 = 0.92$.

Suzuki et al. (2003) conducted physical model tests with the focus on wave overtopping volume and velocity of overtopping water over the crest for smooth and stepped slopes ($n = 3$) in a $17\,m$ long wave flume. The flume has a width of $0.6\,m$ and the water level was between $0.3 < h_s < 0.53$. The simulated step height S_h was $0.01\,m$. Two freeboard heights R_c and two water depths at the toe of the seawall d $(0, 0.05\,m)$ were tested for four different sets of incident waves. The authors conclude a relative overtopping rate reduction and a smaller reflection coefficient at relatively large water depths in comparison with smooth seawalls.

Okayasu et al. (2005) compared wave overtopping volumes resulting from physical model tests conducted by Suzuki et al. (2003) over stepped and plain slope ($n = 3$) with results of numerical model tests (2D and 3D large eddy simulation). The 2D simulation model far overestimated the overtopping volume whereas the 3D simulation model fits the overtopping volume for a smooth surface but underestimated the overtopping by $50\,\%$ for the stepped surface. The authors mentioned that the step height in the simulation was equal to one grid size and therefore the model could not account for additional wave dissipation due to small eddies generated by the steps. The importance of an appropriate evaluation of shear stress and energy dissipation by the sea wall steps was mentioned.

Hughes (2005) estimated the influence of rough, impermeable slopes on the wave run-up identifying only slight differences of the run-up between waves that broke on the slope and non-breaking waves. Therefore, the formula is valid for breaking and non-breaking incident wave conditions. The implemented reduction factor $\gamma_f = 0.505$ which considers the effect of an impermeable rough surface on the wave run-up was derived from a best fit regression of data by Ahrens and Heimbaugh (1988) and Waal and van der Meer (1992) resulting in

$$\frac{R_{u,2\%}}{h} = 4.4(tan\alpha)^{0.7}\sqrt{0.639\left(\frac{H}{h}\right)^{2.026}\left(\frac{h}{gT^2}\right)^{-\left[0.18\left(\frac{H}{h}\right)^{-0.391}\right]}}\gamma_f \quad (2.39)$$

valid for $2.0 \le cot\alpha \le 4.0$.

Abdo (2007) presented an essay about the Bill Young reservoir in Florida, US. The reservoir is surrounded by a stepped revetment build from soil-cement. Abdo (2007) suggests an advantage of soil-cement revetments to be used in areas with a lack of available rock

---

[12]In previous edition: Goda Y. (2000). *Random Seas and Design of Maritime Structures (2nd Edition)*. World Scientific Publ., Singapore.

or rip-rap and a plenty supply of sand and confirms a reduction in the wave run-up at the reservoir.

A data set with high quality regarding the boundary conditions in the physical model tests (2nd order irregular waves, active reflection compensation, more than 1,000 waves/test, correction of data regarding scale effects) was presented by Van Steeg et al. (2012). The wave overtopping over stepped revetments with a step height of $S_h = 0.023\,m$ and $0.046\,m$ with varying freeboard heights ($0.12 < R_c < 0.26$) and two slopes ($n\{2,3\}$) was determined for varying wave heights $0.075 < H_{m0} < 0.155$, a single wave period $T_p = 1.58\,s$ and an adjusted water level ($0.72 < h < 0.927$). With these tests, reduction coefficients of $\gamma_{f,S_h=0.023} = 0.8 - 0.9$ and $\gamma_{f,S_h=0.046} = 0.6 - 0.7$ were derived. The tests also included wave overtopping measurements on stepped revetments with inclined step faces. The influence on the wave overtopping volumes was only marginal. Mean overtopping rates can be calculated with the derived reduction coefficient and the formulation according to Eurotop (2007) with the adapted regression coefficient for the smooth slope in this study:

$$\frac{q}{\sqrt{g \cdot H_{m0}^3}} = \frac{0.067}{\sqrt{tan\alpha}}\gamma_b \cdot \xi_{m-1,0} \cdot exp\left(-5.15\frac{R_c}{\xi_{m-1,0} \cdot H_{m0} \cdot \gamma_b \cdot \gamma_f \cdot \gamma_\beta \cdot \gamma_v}\right) \tag{2.40}$$

Xiaomin et al. (2013) conducted physical model tests ($Froude$ scale 1:10) in a $40.0\,m$ long wave flume with a width of $0.8\,m$ and a maximum water depth of $1.0\,m$. Regular waves were generated by a piston-type wave maker. Five different step heights and as reference a plain slope (all geometries with $n = 2.5$) were analyzed in order to evaluate the influence of the step height in relation to the wave height on the wave run-up (54 tests). It was found that the waves were absorbed well. Their data show a reduction factor for the wave run-up over stepped slopes between $0.35 < \gamma_f < 0.77$. Treuel (2013) reveals a minimum wave run-up height in the data set of Xiaomin et al. (2013) for a certain number of steps (not the minimum, not the maximum). According to the authors the run-up reduction coefficient can be derived by

$$\gamma_f = 1 - \frac{S_w}{S_w + 6H_s} \tag{2.41}$$

Physical model tests ($Froude$ scale 1:10) by Chuenchai et al. (2014) in a $16.0\,m$ long and $0.6\,m$ wide wave flume with flap type wave maker result in a design formula for wave run-up prediction for regular waves on 'stepped slopes'. The formula was based on 840 tests. Four different step heights ($S_h = 0.02\,m, 0.03\,m, 0.04\,m, 0.05\,m$) were tested with varying slope angles ($2.1 < n < 3.7$). The authors found that the wave run-up decreases with an increasing step height due to an increase in friction. They defined the reduction factor for wave run-up under given boundary conditions to $\gamma_f = 0.64$.

$$\frac{R_u}{H} = 0.98\xi^{0.94}\left[1 - 0.46\left(\frac{S_h}{H}\right)^{0.12}\right] (R^2 = 0.81, STD = 0.23) \tag{2.42}$$

Kerpen et al. (2014) refined and adapted an approach by Schüttrumpf (2001) for stepped revetments. The adaptation was based on physical model tests ($Froude$ scaling 1:5)

conducted in a laboratory wave flume. The flume has a width of $2.2\,m$, a length of $110\,m$ and a maximum water depth of $1.0\,m$. The model was placed on a horizontal bed at a distance of about $24.1\,m$ from the piston wave maker operating with 2nd order wave generation routines. At this position in the flume an observation window in the side flume wall allowed the study of processes beneath the water surface and permitted the thorough analysis of wave run-up and overtopping processes. Tests with regular waves for five gradually increasing different wave heights H, constant wave period $T = 2.0\,s$ and constant water level ($h = 0.995\,m$ at the toe of the structure) have been conducted for two specific but standard slope angles, i.e. 1:2 (30.0°) and 1:3 (19.7°). The water depth over the submerged foreshore berm at the toe of the stepped revetment $d = 0.5\,m$ was constant. The overtopping rates on a 1:2 sloped stepped revetment were 2.5 to 5 times larger compared to the 1:3 slope. Reduction coefficients in a range of $0.15 < \gamma_f < 0.5$ had been measured. A stepped revetment was described as aesthetically attractive and highly functional with the focus on flood protection. Formulae for prediction of the wave run-up and the mean overtopping discharge over stepped revetments were determined:

$$\begin{aligned}
\text{for } \xi < 3.75 : \quad & \frac{R_u}{H} = 0.6 \cdot \xi \\
\text{for } \xi \geq 3.75 : \quad & \frac{R_u}{H} = 2.36 \\
& (R^2 = 0.81, \ STD = 0.12)
\end{aligned}$$
(2.43)

and

$$\frac{q}{\sqrt{2gH^3}} = \left(0.163 - \frac{0.336}{\xi_d^3}\right) \left(1 - \frac{R_c}{2.25 \cdot tanh(0.5 \cdot \xi_b)H}\right)^{3.2} (R^2 = 0.98, \ STD = 0.0005).$$
(2.44)

A summary of the most important statements and conclusions from the literature review follows.

Summary

<u>Wave reflection:</u> The wave reflection at a stepped revetment is moderate and reduced in comparison to a smooth revetment (McCartney, 1976), (Suzuki et al., 2003).

<u>Wave run-up:</u> The wave run-up height is reduced by a stepped revetment in comparison to a smooth revetment due to increasing friction (all authors). The steps have to be placed above SWL to be efficient (Wassing, 1957). The wave run-up height at a stepped revetment increases with increasing wave height, increasing wave period or increasing Iribarren number (Saville, 1955), (Jachowski, 1964), (Nussbaum and Colley, 1971), (Asakawa et al., 1992). The wave run-up height decreases with increasing relative water depth d/H_{m0} at the toe of the structure (Jachowski, 1964), even with zero toe depth (Stoa, 1978). Offshore-inclined-face steps reduce the wave run-up slightly in comparison to vertical-faced steps (Jachowski, 1964). Nussbaum and Colley (1971) concluded that smaller step heights are more efficient than larger step heights in reducing the wave run-up. The wave run-up can be minimized by adapting the number of steps to the wave height (Treuel, 2013). A per-

meable stepped revetment reduces the wave run-up more effectively than an impermeable one (Asakawa et al., 1992).

Wave overtopping: The wave overtopping at a stepped revetment is decreased due to the wave-absorbing slope face (USACE, 1981), (Takayama et al., 1982), (SPM, 1984), (Hamilton, 1988). The wave overtopping volume at a stepped revetment increases with increasing wave height, increasing wave period or increasing Iribarren number (Saville, 1955). The wave overtopping decreases with decreasing slope angle and for several dimensionless step heights H_{m0}/S_h (Takayama et al., 1982). The reduction factor γ_f increases disproportionally to an increasing overtopping volume (Saville (1955) for $(2 < H_{m0}/S_h < 12)$. A stepped revetment requires 10-20% higher freeboard heights for $20 < H_{m0}/S_h < 30$ in comparison to a vertical wall (Goda and Kishira, 1976), lower required freeboard heights for a step ratio between $16 < H_{m0}/S_h < 40$ (Takayama et al., 1982). An impermeable stepped revetment $(9 < H_{m0}/S_h < 10)$ is less effective in reducing the wave overtopping in comparison to a large permeable revetment (Ward and Ahrens, 1992). A more gentle foreshore (1:30 vs. 1:10) decreases the wave overtopping at a stepped revetment (Goda and Kishira, 1976). The reduction factor γ_f is not significantly reduced for varying wave steepness values if the foreshore is flat (Stoa, 1978). A toe berm in front of a stepped revetment reduces the overtopping significantly (Heimbaugh, 1988). A combination of a stepped revetment with a topped re-curved seawall resists high wave action (SPM, 1984). The reduction coefficient γ_f is highly dependent on several wave and structure conditions (Stoa, 1978).

Pressures: A stepped revetment dissipates wave forces (USACE, 1981). Forces of breaking waves are spread over a number of steps (United Nations, 1982). Dynamic pressures at stepped revetments are in the same range as at vertical walls (SPM, 1984). The maximum pressure loads on a stepped revetment are measured slightly above the SWL (Heimbaugh, 1988).

Scour and erosion: A stepped revetment stabilizes the adjacent beach due to energy dissipation during the wave run-down compared to a smooth slope (O'Shaughnessy et al., 1924), (United Nations, 1982), (SPM, 1984), (Hamilton, 1988). Permeable stepped revetments offer an additional reduction of scour compared to impermeable stepped revetments (Asakawa et al., 1992). The scour development in front of a stepped revetment is in the same range as in front of a plain slope. The maximum scour depth is in a distance of L/3 from the structure toe and the maximum influence distance is one wave length from the toe (Sato et al., 1971).

Stability and construction: A failure of a stepped revetment begins slightly above SWL because incident wave breaking cause an upwards-directed force (Jachowski, 1964). To avoid sand losses of the core a properly designed underlying filter is of great importance (Jachowski, 1964). The stability of a permeable stepped revetment can be improved by an increased filter layer thickness (Asakawa et al., 1992). The use of pre-cast concrete elements is less labor-intensive in comparison to on-site casting of a stepped revetment and should therefore be favored (Walton et al., 1989).

Recreation and tourism: A stepped revetment provides an easy access to the beach (USACE, 1981) and is therefore preferably implemented at beach resorts (United Nations, 1982). Furthermore, a stepped revetment is beneficial and an attraction for tourists (Hamilton, 1988). A stepped revetment is an aesthetically attractive and highly functional flood protection system (Kerpen et al., 2014).

2.5   Evaluation and derivations

Until here, facts about stepped revetments, presented in the permanent literature, are presented. In the following, these facts are interpreted, evaluated and compared to each other. This discussion is required to identify functional and active principles governing the energy dissipation of the wave run-up and wave overtopping process at stepped revetments.

2.5.1   Evaluation of available data

Literature, discussed in section 2.4, contains a wide range of reduction factors γ_f which represent the proportion of a wave run-up or overtopping event on a stepped revetment in comparison to the same event on a revetment with a smooth surface. The boundary conditions of these tests differ in model scale, number of conducted tests, the wave characteristics (regular or irregular waves), number of waves within a single test, repeatability and variability of input parameters. These differences influence the post processing and the value of calculated reduction coefficient γ_f. Fig. 2.14 gives a value-range of reduction factors γ_f for stepped and other rough revetments.[13] The reduction coefficient varies from $0.35 < \gamma_f < 0.9$ and differs from case study to case study. The differences between factors for wave run-up and wave overtopping are indicated. This range of uncertainty indicates

---

[13]To evaluate the overall performance of a stepped revetment it has to be linked with the performance of other types of revetments. The performance is thereby not only related to an increased energy dissipation. Results of a multi-criteria analysis performed by Srivastava and Varming (2014) are summarized as an example. Srivastava and Varming (2014) analyzed 15 potential options for a revetment structure at lake Cathie Seawall, Port Macquarie, Australia. In a multi-criteria analysis the authors identified four major criteria (environmental impact, effectiveness of the solution, social value, economics – each item has numerous sub items) in an equally weighted mode. One of the four favorite solutions – besides a rock armoured revetment, irregular concrete blocks and a seabee coastal pavement – was a terraced concrete block seawall which resembles a stepped revetment. As advantage of a terraced sandstone seawall Srivastava and Varming (2014) identified a high degree of coastal protection and a high durability by low maintenance. Visual features could be incorporated to enhance aesthetics. Environmental features such as voids could be incorporated to encourage habitat growth. Stepped revetments require less construction material. The construction material is re-usable (concrete after processing). A stepped revetment is less reflective compared to a vertical wall due to the sloping geometry and can be designed for unrestricted beach access with lower risk for people to fall from the crest of a vertical wall construction. On the other hand, a stepped revetment is more expensive compared to a rock armoured revetment and more difficult to repair if damaged. The stability of a stepped revetment is sensitive to toe erosion. Some beach amenity may be loosen due to wave reflection. The main selection criterion of choosing different kinds of revetments indicates a potential increase of safety for men and assets due to stability enhancement and improvements in protective effects of dikes and embankments in the coastal protection scheme. Certainly, the availability of construction material nearby is a dominant factor, too.

the need for a deeper understanding of the dynamic processes over a stepped revetment for a range of geometry related and hydraulic boundary conditions. Only adequately chosen parameters enable a sufficient wave run-up and wave overtopping reduction at stepped revetments.

Only Saville (1955), Goda and Kishira (1976), Takayama et al. (1982), Heimbaugh (1988), Ward and Ahrens (1992), Van Steeg et al. (2012), Xiaomin et al. (2013) and Kerpen et al. (2014) provide data regarding wave run-up, wave overtopping, wave reflection and wave forces on stepped revetments. These data are re-analyzed in this section to allow a comparison of test results. For tests where regular waves (black labeling) were generated the mean wave height H and the mean wave run-up R_u are indicated whereas for tests with wave spectra (colored labeling) the spectral wave height H_{m0} and the wave run-up height $R_{u,2\%}$ exceeded by $2\,\%$ of all run-ups are shown.

First of all, the hydraulic boundary conditions are compared in terms of different wave steepnesses H/L versus the relative water depth h/L in Fig. 2.15. Direct or indirect information regarding the water depth h was given only by Saville (1955), Heimbaugh (1988), Van Steeg et al. (2012) and Xiaomin et al. (2013). Most tests were conducted for intermediate water depth. A relatively large data set (178 test runs) by Heimbaugh (1988) is close to shallow water conditions. Deep water conditions were tested in some cases by Saville (1955) and Xiaomin et al. (2013). Data by Takayama et al. (1982) seem to include extreme shallow water conditions with $0.012 < h/L < 0.03$. Since the report was written in Japanese and was not fully translated, these boundary conditions are based on an interpretation. Therefore these data are not given in Fig. 2.15 (a).

The hydraulic boundary conditions of the impacting waves are evaluated. Fig. 2.15 (b) indicate the wave steepness H/L against slope n. Data sets in regular waves are displayed in monochrome colors whereas data sets with wave spectra are displayed in color. For visual clarity, data by Goda and Kishira (1976) and Ward and Ahrens (1992) are slightly shifted horizontally next to $n = 2$, although a slope of $n = 2$ was tested. Saville (1955) provides data with a broad spectrum of wave steepness for a relatively steep slope angle. Data by Goda and Kishira (1976) are available for a moderate narrow variation of wave steepness and a particular slope. Data sets by Takayama et al. (1982) are based on tests with a single wave steepness but support a broad range of slope angles. Heimbaugh (1988) tested two relatively steep slope angles for average wave steepness. Data by Ward and Ahrens (1992) and Xiaomin et al. (2013) cover a wide range of wave steepnesses for more gentle slopes in comparison to Saville (1955). Van Steeg et al. (2012) tested an average range of wave steepness for two gentle slope angles. The ratio between the slope angle of a structure and wave steepness can be expressed by the Iribarren number $\xi = \frac{1/n}{\sqrt{H/L}}$ used further in the discussion.

Fig. 2.15 (c) gives an overview of data sets with respect to the relative step height S_h/H versus the Iribarren number ξ. Data sets in regular waves are displayed in monochrome colors, data sets with wave spectra are displayed in color. The Iribarren number ranges from $0.88 < \xi < 6.3$ and three particular tests up to $\xi = 13$ (not shown in the figure to assure visual clarity). Therefore, except for spilling wave breaking ($\xi < 0.2$), a broad
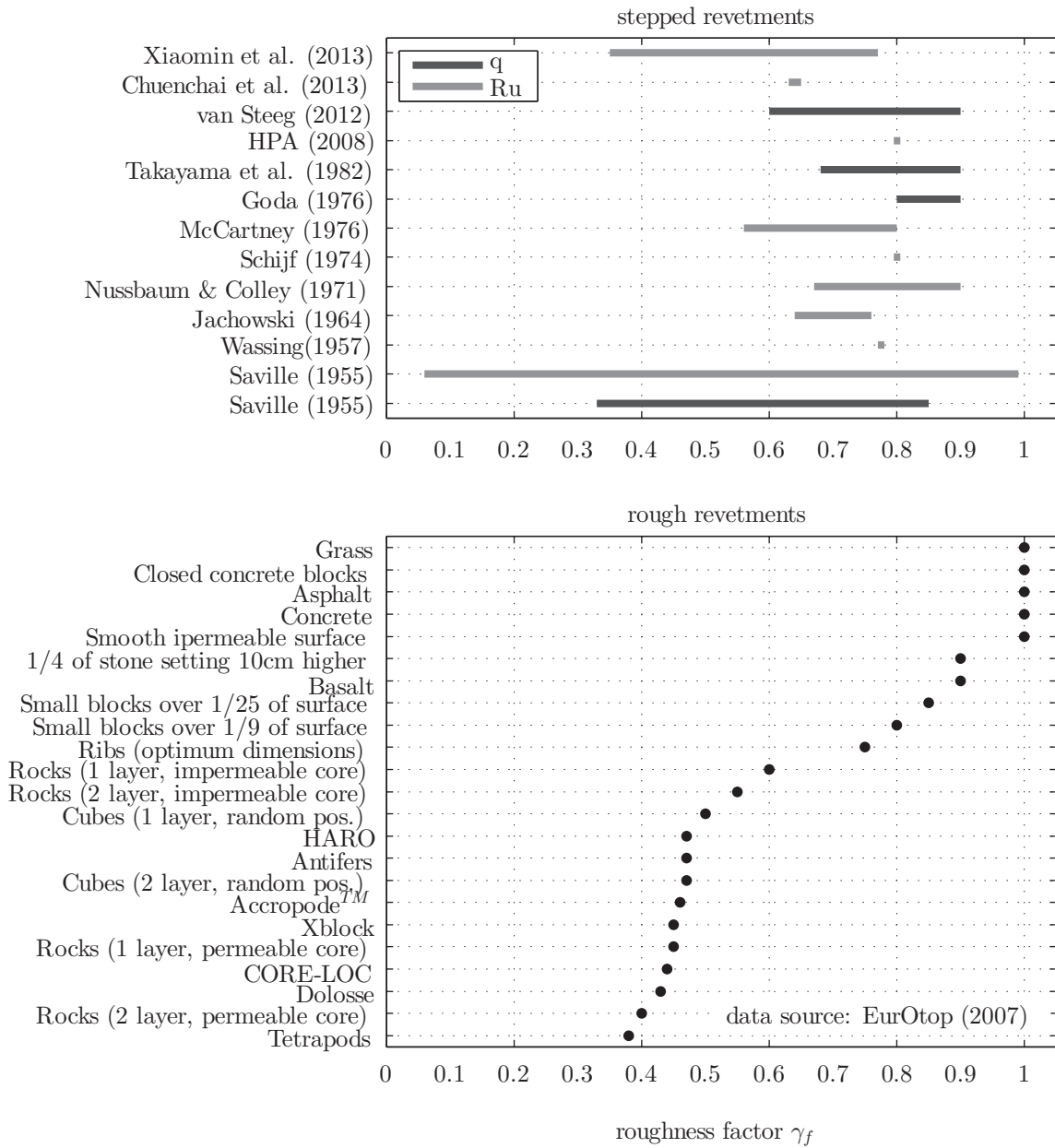
Figure 2.14: Value-overview of roughness factor γ_f for stepped revetments and other types of rough revetments.
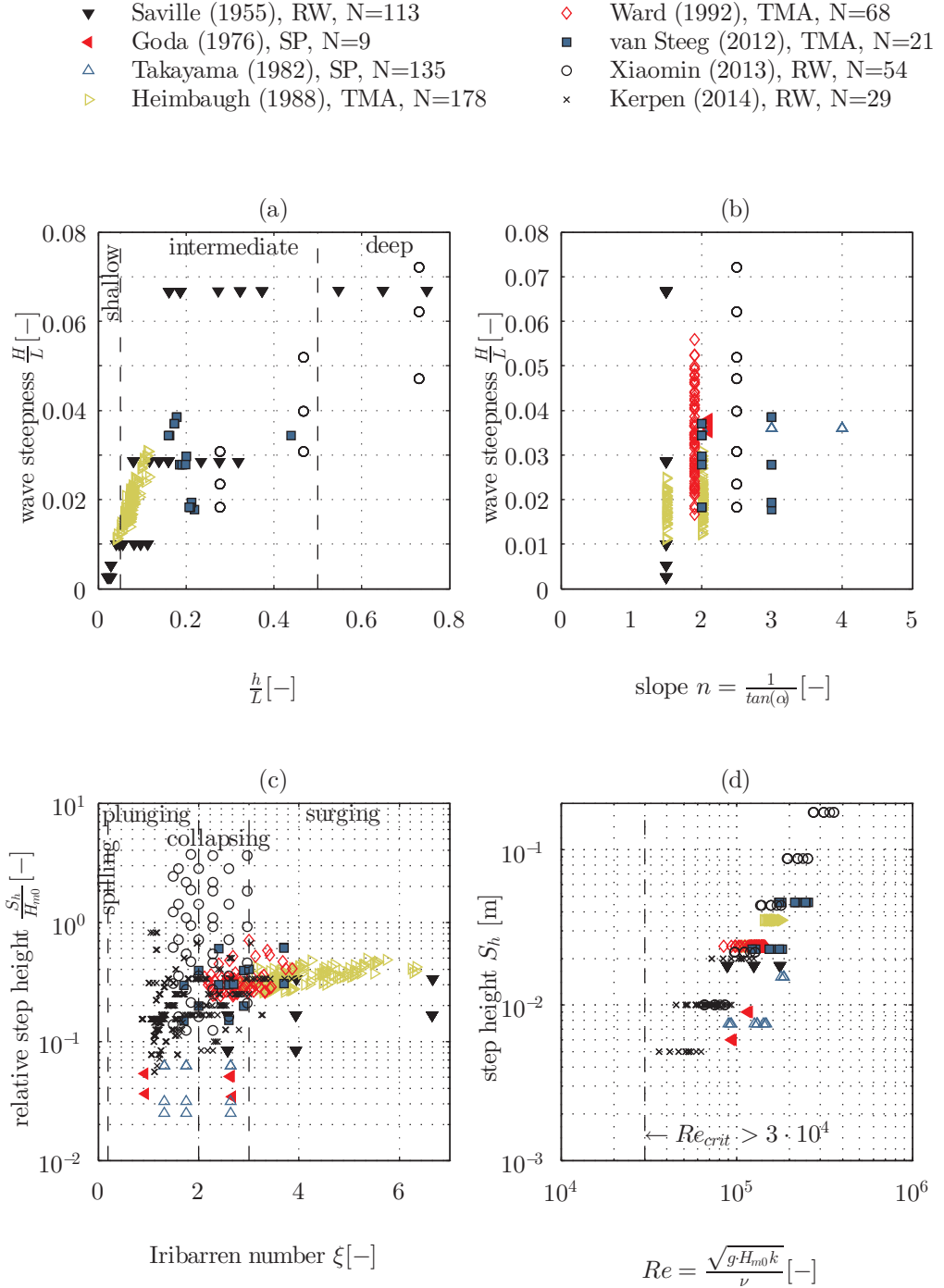
Figure 2.15: Overview of data sets obtained from literature: (a) wave steepness versus relative water depth with indication of shallow-, intermediate- and deep-water conditions, (b) wave steepness versus slope, (c) relative step height versus Iribarren number and (d) step height versus the critical Reynolds Number Re.

spectra of wave breaking is covered by literature with plunging ($0.2 < \xi < 2-3$), collapsing ($2 < \xi < 3$) and surging ($\xi > 2 - 3$) wave breaking. Relative step heights S_h/H are covered for a range of $0.025 < S_h/H < 3.6$. Most data are available for $1 < \xi < 6$ and $0.2 < S_h/H < 0.45$. Data by Goda and Kishira (1976) and Takayama et al. (1982) represent small relative step heights in comparison to the other test series. Xiaomin et al. (2013) provide the only data set for the case where the step heights S_h are larger than the wave height H. Nevertheless, all data sets cover a different range of parameter combination, causing differences in wave breaking over the revetment. Therefore it is difficult to compare the results from the various data sets.

The incorrect reproduction of turbulence in small scale models is well known (Frostick et al., 2011) and has a strong influence on the output of physical models. Therefore, Fig. 2.15 (d) allows a closer discussion of the range of Reynolds numbers (according to Eq. (3.5)) in the different data sets. The kinematic viscosity was assumed as $\nu_k = 1.004 \cdot 10^{-6}$ in all cases. Even the data sets with very small step height in model dimensions (Goda and Kishira (1976) and Takayama et al. (1982)) have roughness-related Reynolds numbers $Re > 3 \cdot 10^4$ (page 56) and can therefore be evaluated as valid.

Fig. 2.16 (a) gives an overview of the dimensionless wave run-up ($0.5 < R_u/H < 3.5$) versus Iribarren number ($0.9 < \xi < 3.6$ with additional four particular tests up to $\xi = 7.2$). The dimensionless wave run-up versus the Iribarren number has similar ranges for the compared data sets. Tests with regular waves (black) or wave spectra (colored) are indicated. The dimensionless wave run-up on stepped revetments tends to increase with an increasing Iribarren number, although the different data scatter significantly. The dimensionless overtopping discharges in the range of $2 \cdot 10^{-5} < \frac{q}{\sqrt{gH^3}} < 1$ are displayed in Fig. 2.16 (b) in a semi-logarithmic scale against the dimensionless freeboard height ($0.1 < R_u/H < 3$) for data provided by Saville (1955), Goda and Kishira (1976), Takayama et al. (1982), Heimbaugh (1988), Ward and Ahrens (1992) and Van Steeg et al. (2012). The measured overtopping rates for the same relative freeboard height differ in the order of the power two. But a grouping of data regarding the different authors can clearly be seen. When also considering the insights from Fig. 2.15 (c) the reason for the scatter, besides the geometry related differences may be due to the different wave breaking conditions within the model tests. As a result there are also differences in the energy dissipation.

In Fig. 2.16 (c) the data are compared in terms of the dimensionless overtopping versus the relative freeboard height normalized by the wave steepness. All data sets, except the ones by Takayama et al. (1982) and Goda and Kishira (1976), show roughly the same exponential decrease of the dimensionless overtopping rate with an increasing dimensionless freeboard height. In order to explain the significantly visible differences in the overtopping volumes, the range of step heights in the different test series were looked at closer. Goda and Kishira (1976) as well as Takayama et al. (1982) tested very small step heights in model scale ($S_{h,Takayama}\{0.008\,m, 0.015\,m\}, S_{h,Goda}\{0.006\,m, 0.009\,m\}$). This can be a first indication of the importance in distinguishing between boundary conditions with micro and macro roughness.

Xiaomin et al. (2013) tested a wide range of relative step heights ($0 < S_h/H_{m0} < 3.8$) for
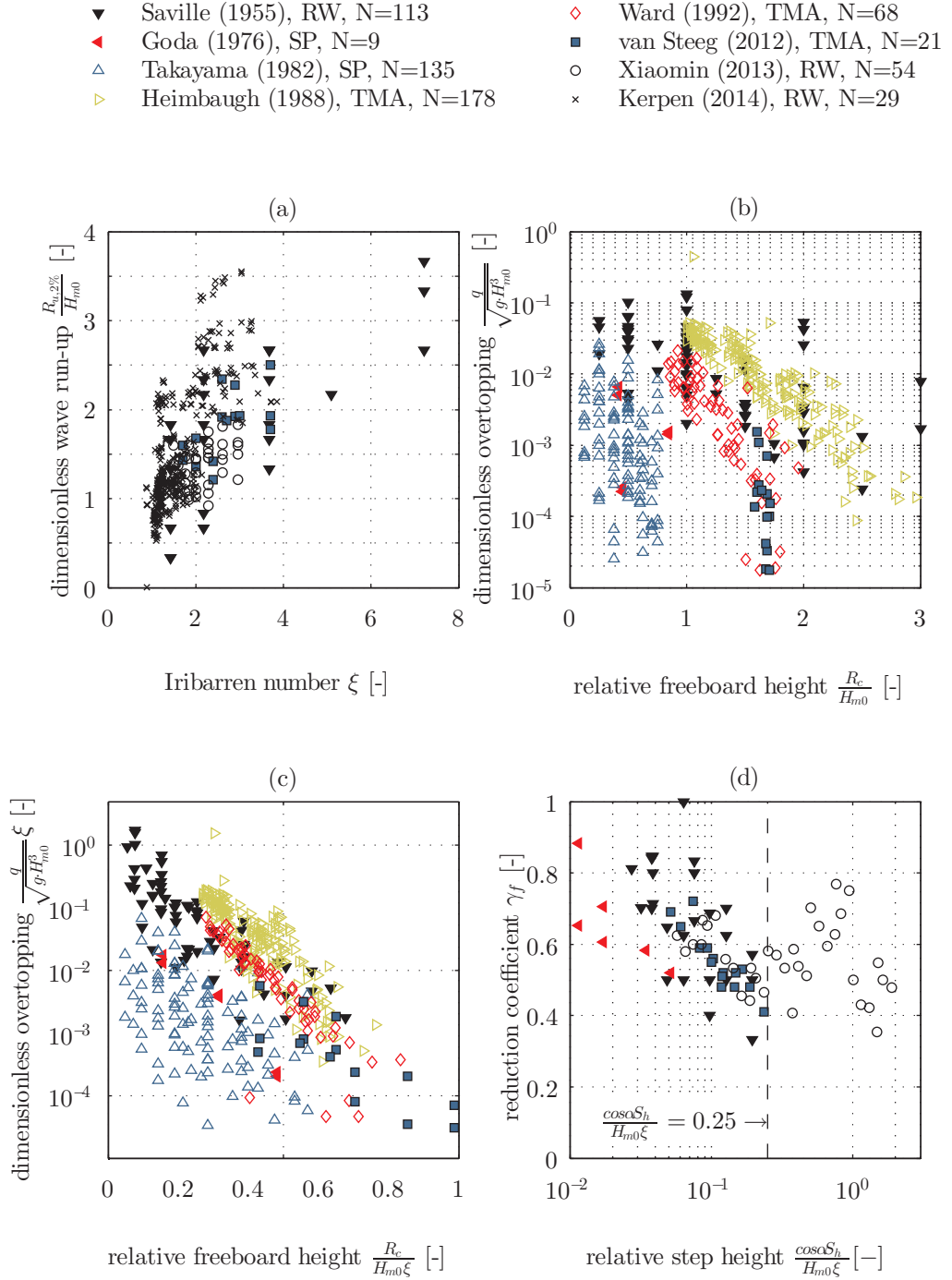
Figure 2.16: Overview of data sets obtained from literature: (a) dimensionless wave run-up versus Iribarren number, (b) dimensionless wave overtopping versus the relative freeboard height, (c) dimensionless wave overtopping versus the relative freeboard height normalized by ξ and (d) the dimensionless wave run-up versus the dimensionless step height.

regular waves. Treuel (2013) concluded that the data indicate an optimum step height leading to the lowest wave run-up due to the different kind of wave reflection and energy dissipation for varying H_{m0}/S_h-values. Fig. 2.16 (d) show a similar approach following Van Steeg et al. (2012) to consider the slope angle and the wave steepness additionally. The data by Treuel (2013) shows a minimum run-up for a relative step height of 0.25. However an optimum for $S_h/(H \cdot \xi) = 0.25$ cannot be proven yet since all other data have boundary conditions of $S_h/H < 0.5$. But the most valuable data set regarding the quality of the hydraulic model tests by Van Steeg et al. (2012) proves this finding for wave spectra in the range of $S_h/H < 0.5$. Data by Saville (1955) also confirm this claim. Data by Goda and Kishira (1976) however show lower reduction coefficients. Evidently, additional tests with $S_h/H > 0.5$ are not conducted yet and are required to confirm the optimum relative step height to reduce the wave overtopping.

Conclusion

Eight authors provide data related to wave interaction with stepped revetments. The existing reduction coefficients γ_f which describe the efficiency of wave run-up and overtopping reduction of stepped revetments, scatter significantly. The scatter can be explained by the variable hydraulic- and geometry-related boundary conditions of the tests from which the reduction factors are determined.

2.5.2 Evaluation of available prediction methods

Fig. 2.17 compares the existing approaches to predict the wave run-up height with respect to the Iribarren number. It was not possible to define boundary conditions which are valid for all existing approaches. Nevertheless an attempt was made to identify similar boundary conditions for all compared approaches. Therefore a step height of $S_h = 0.05\,m$, a water depth of $h_s = 1.0\,m$, a slope of $n = 3.5$ and a wave period of $T = 2.0\,s$ was selected. The wave height varied from $0.045\,m < H < 0.35\,m$. For approaches which are based on regular waves (black lines) mean values (H_m, T_m) were selected whereas for approaches with wave spectra (colored lines) spectral values (H_{m0}, $T_{m-1,0}$) were selected[14]. A reference is given to the Eurotop (2016) approach following Eq. (2.9) with appropriate friction coefficients $\gamma_{f,Eurotop}$. Approaches for regular waves by Chuenchai et al. (2014) with Eq. (2.42) and Kerpen et al. (2014) with Eq. (2.43) show comparable dimensionless run-up values between $1 < R_u/H < 1.5$ ($\approx 0.4 < \gamma_{f,Eurotop} < 0.5$). The approach by Wassing (1957) with Eq. (2.33) gives a value of 1.75 ($\gamma_{f,Eurotop} \approx 0.85$) for plunging waves. Following the approach by Hughes (2005) with Eq. (2.39) for wave spectra, dimensionless run-up values in the range of $1.8 < R_u/H_{m0} < 2.1$ ($0.6 < \gamma_{f,Eurotop} < 0.7$) for collapsing waves were determined. A general trend in all prediction approaches indicates that no clear trend exists and therefore it is not possible to conclude which approach offers the best prediction.

---

[14]Results of tests for regular and irregular waves have to be interpreted in a different way. It is assumed that the reader is aware of these principle differences for regular and irregular waves.
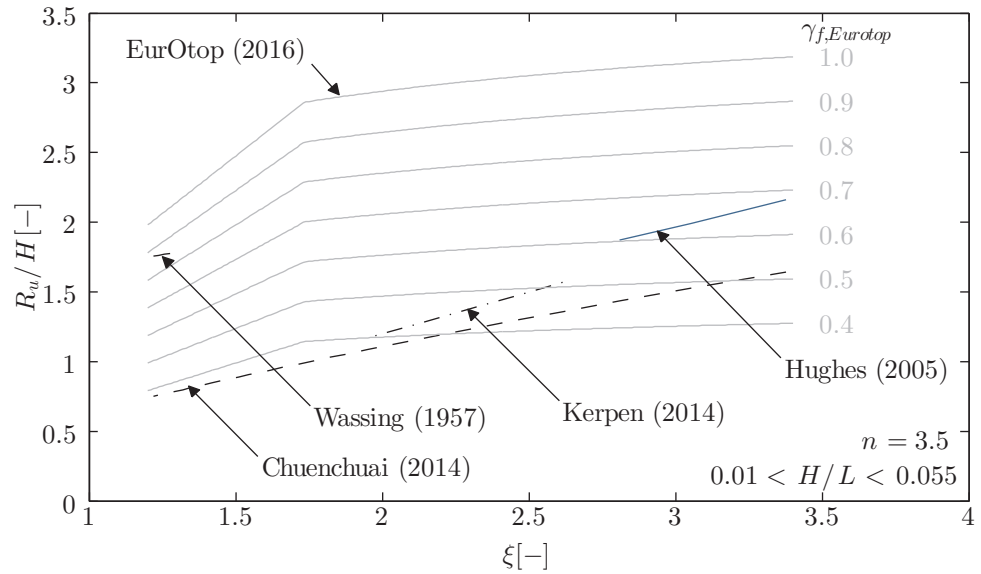
Figure 2.17: Comparison of available methods for the prediction of the wave run-up at stepped revetments with $S_h = 0.05\,m$, $h_s = 1.0\,m$, $n = 3.5$, $T = 2.0\,s$ and a varying wave height $0.045\,m < H < 0.35\,m$.

prediction for a step height of $0.05\,m$ also failed in this reference case.

Conclusion

A general trend is visible in most prediction approaches regarding the influence of the interaction of incident waves with a stepped revetment. However, a reliable assessment of the wave run-up height and wave overtopping volume is not possible as it is not clear which approach gives the best prediction.

2.5.3 Evaluation of the ratio of step height and wave height

The number of steps and as a consequence the relation of step height and wave height must significantly influence the energy dissipation at stepped revetments as the intensity of the turbulence is dependent on the roughness elements (shape and dimensions) and the flow velocity (Kármán, 1930). Xiaomin et al. (2013) presented results of hydraulic model tests (scale 1:10, *Froude* similitude) on the wave run-up at stepped revetments with varying step heights and a constant slope of 1:2.28. A re-analysis of this data set regarding the dependence of the wave run-up height and the step height at the revetment reveals an interesting finding discussed in the following.

The wave run-up height R_u, normalized with the wave height H, is defined as the relative wave run-up height (R_u/H). The relative step height S_h/H is a result of the step height S_h normalized by the wave height H. The theoretical correlation between the relative
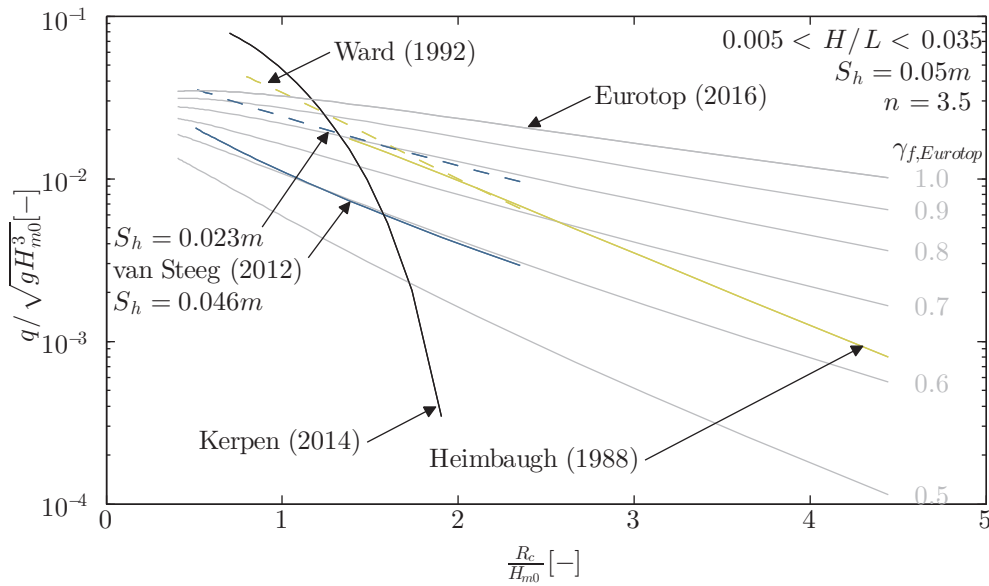
Figure 2.18: Comparison of available methods for the prediction of the wave overtopping at stepped revetments with $S_h = 0.05\,m$, $h_s = 1.0\,m$, $n = 3.5$, $T = 3.0\,s$, $R_c = 0.2\,m$ and a varying wave height $0.045\,m < H < 0.5\,m$.

wave run-up and relative step height is given in Fig. 2.19. The experimental results for the same parameters are given in Fig. 2.16 (d) (page 48).

Relative step heights equal to zero ($S_h = 0$) represent results of test runs with a smooth slope. Therefore, the highest relative wave run-up heights are measured for smooth slopes due to relatively low energy dissipation on the surface in comparison to the macro roughness surface of a stepped revetment. As a consequence the shear stresses on the smooth slope are also low and induce relatively low loads on the structure. Most of the kinetic wave energy converts to potential energy in the run-up process. With increasing step height, the roughness is increased continuously, the induced turbulence increases and as a consequence the wave run-up decreases. A minor part of the kinetic energy of the incident waves is converted to potential energy as some energy is dissipated by increasing turbulence.

For very small step heights ($H \gg S_h$) it is assumed that the step geometry has little influence on the energy dissipation. The flow direction of the wave run-up is still slope-parallel. Consequently, these small steps can be considered as micro roughness and are therefore comparable in terms of run-up reduction effectiveness to any other impermeable micro-rough surface.

With increasing step height ($H > S_h$), the slope-parallel wave run-up is further interrupted by the step edges. The flow processes at the single step becomes more important. Vortex shedding occurs at the step edges . Minor values of the kinetic energy of the incident wave convert to potential energy. More and more energy is dissipated by vortex induced turbulence and non-linear wave transformation processes over the steps.

global flow conditions:

$S_h = 0$	$S_h = 0.25H$	$S_h = 0.5H$	$S_h = 2H$	$S_h \to Inf$
plain slope	micro rough slope	macro rough slope	composite slope	vertical wall
slope-parallel flow	slope-parallel flow	almost slope-parallel flow	flow follows step shape	pure reflection

local flow conditions:

no pseudo-bottom	minor pseudo-bottom	major pseudo-bottom	indistinct pseudo-bottom	no pseudo-bottom
no roughness ind. turbulence	turbulence in step niches	major vortices in step niches	vortex shedding at step edges	re-direction of the flow
inner energy dissipation	minor energy dissipation	major energy dissipation	reduced energy dissiaption	low energy dissipation
moderate reflective	low reflective	moderate reflective	reflective	pure reflective
$S_h = 0$	$H \gg S_h$	$H > S_h$	$H < S_h$	$H \ll S_h$

qualitative run-up:

Figure 2.19: Analogy of the relative wave run-up on the relative step height in terms of plausible energy dissipation rates and reflection potential.

The re-analysis of experimental results by Xiaomin et al. (2013) suggest a minimum run-up at $S_h/H = 0.5$ and increase for $S_h/H > 0.5$.

Values of relative step heights larger than 0.5 tend to mimic run-up heights of a vertical wall. With increased relative step height ($H < S_h$) the influence of the offshore located steps decreases due to less energy dissipation in increasing water depth. The stepped revetment becomes more reflective. The wave breaking is still affected. Therefore, also the relative water depth over the step (d_{st}/S_h) influences the wave run-up. This system performance is comparable to composite walls ($2 \leq S_h/H$).

If the step height is much larger than the wave height ($H \ll S_h$) the wave run-up is comparable with a vertical wall. The kinetic energy of the incident wave is converted to potential energy. Due to the missing supportive slope the run-up height is lower. Most of the energy is reflected at the wall.

Conclusions

Hydraulic- and geometry-related functional and active principles governing the energy dissipation of the wave run-up at stepped revetments are derived. The presence of an optimum in the ratio of step height and wave height is meaningful in a physical point of view. Since Xiaomin et al. (2013) conducted tests with regular waves it has to be proven if also tests with wave spectra confirm this finding.

2.6 Consequences

A comprehensive literature review focused on the wave interaction with stepped revetments and similar coastal protection structures with a stepped face (e.g. sea walls). The literature review has described research of more than 60 years in more than 30 publications and reports (section 2.4). All relevant hydraulic- and geometry-related parameters for the design and dimensioning of a stepped revetment such as wave run-up and overtopping, wave loads and pressure shocks, wave reflection, scour development at the toe of stepped revetments and the stability analysis of prefabricated units forming a stepped revetment have been analyzed by permanent literature. Many of these reports present empirically derived design formulae which are only valid for a specific case. Recent guide lines do not provide a reliable prediction method for stepped revetments.

In addition, it has been shown in section 2.5.1 that the reduction factor γ_f which presents the reduction of wave run-up and wave-overtopping at stepped revetments in comparison to a smooth slope, spreads significantly ($0.4 < \gamma_f < 0.9$). Nearly all conducted model tests have different hydraulic- and geometry-related boundary conditions and cover different ranges in a dimensionless scale ($\xi_{m-1,0}$, R_c/H_{m0}, S_h/H_{m0}). Every approach is valid for specific cases only. However, presently there is no single approach that is valid for a broad range of hydraulic- and geometry-related boundary conditions.

As an example, the contradictorily findings of Nussbaum and Colley (1971) versus Goda and Kishira (1976), related to the influence of the step height S_h on the reduction coeffi-

cient γ_f, are quoted. Nussbaum and Colley (1971) derived, that smaller step heights are more effective in the run-up reduction compared to large step heights (Fig. 2.8, page 32, no specification about the quantity of 'small' is given by the authors). Goda and Kishira (1976) derived the contradictory correlation between step height and reduction coefficient (Fig. 2.10, page 34). By current knowledge, it is not possible to verify the reasons for this contradictory findings. It is assumed, that differences in the step ratio (H/S_h) between both data sets cause this phenomenon.

As discussed beforehand, reasons for scatter can be explained by the differences in data. Some of the tests were conducted with outdated hydraulic boundary conditions which are invalid nowadays (possible influence of the surface tension at $H < 0.03\,m$ by Jachowski (1964), laminar flow in the steps for very small step heights S_h by Goda and Kishira (1976), only tests with regular waves important to understand the hydraulic phenomena but not representative for the hydraulic design by Saville (1955), Jachowski (1964), Nussbaum and Colley (1971), Sato et al. (1971), Xiaomin et al. (2013) and Chuenchai et al. (2014)). Many authors are varying only a few hydraulic parameters within the test on a more or less unique-shaped geometry not comparable to others.

The importance of the ratio of step height and wave height could be discussed. Hydraulic- and geometry-related functional and active principles governing the energy dissipation of the wave run-up at stepped revetments could be derived based on a re-analysis of data by Xiaomin et al. (2013). According to this, the presence of an optimum in the ratio of step height and wave height is meaningful. The validity for wave spectra including dependencies of the wave steepness and the slope are unknown. Since it is rarely possible to compare the existing data and no data set combines a wide range of geometry-related and hydraulic boundary conditions (enabling the identification and description of universal processes) it is evident that there is still a need for additional research.

2.6.1 Required novelty

A novel approach is required, which covers and helps understanding the energy dissipation in a more holistic manner. The required approach should consider hydraulic- and geometry-related boundary conditions at the interaction of waves with stepped revetments, namely:

- the influence of the slope,

- the influence of the wave steepness and

- the influence of the wave height with respect to the step height.

With these parameters, also the effects of wave breaking (plunging and surging), considered with a variation of Iribarren numbers, are covered. Furthermore, it should be ensured that wide ranges of slopes, wave steepnesses and step ratios are investigated. Then, the new approach enables a more general applicability and is set apart from existing approaches.

3 Hydraulic model tests

3.1 Theoretical background

3.1.1 Froude similitude

"A Physical Model is a physical system reproduced (usually at a reduced size) so that the major dominant forces acting on the system are represented in the model in a correct proportion to the actual physical system" (Hughes, 1993). To be able to reproduce wave conditions and structural parameters realistically, the scale of a model has to be selected carefully. It is well known that the results of hydraulic model tests (prototype dimensions often scaled with the *Froude* law) are subjected to scale effects due to processes that cannot be fully represented in the model. Ideally, geometric, dynamic and kinematic similarity in the model has to be ensured. Since this is not possible, the results of the hydraulic model test includes scale effects. Geometric similarity entails a constant relation between a length in the prototype and in the model. Kinematic similarity is given in a constant time relation between processes in nature and in the model. Dynamic similarity says that the forces in nature and model have a constant relation (with requirement of geometric and kinematic similarity) (Frostick et al., 2011).

With *Froude* (Fr), *Reynolds* (Re), *Weber* (We), *Mach* (Ma), *Cauchy* (Ca), *Richardson* (Ri), *Euler* (Eu) and *Strouhal* (St), several scaling numbers have been introduced. Frostick et al. (2011) name Fr, Re, We and Ca numbers as most important for hydraulic model tests on breakwaters. The geometry of stepped revetments with sloping and vertical parts is similar to breakwaters. Thus, the named scaling numbers have to be applied in the context of this work. The following overview is based on summaries by Hughes (1993) and Frostick et al. (2011).

The relative influence of inertial and gravity forces in hydraulic flows is defined as the *Froude* Number

$$Fr = \frac{inertial\ force}{gravity\ force} = \sqrt{\frac{\rho L^2 v^2}{\rho L^3 g}} = \frac{v}{\sqrt{gL}} \tag{3.1}$$

Nearly all free surface models are *Froude*-scaled with a requirement of identical *Froude* Numbers in nature and model ($Fr_N = Fr_M$) since this is the most important criterion to consider in the design process of a coastal scale model.

When a fluid interacts with the surface of an object or structure (laminar boundary layer on the surface), viscous forces dominate in the hydraulic flow and the ratio between inertial and viscous forces defined in the *Reynolds* Number become important. The *Reynolds* Number is defined as:

$$Re = \frac{inertial\ force}{viscous\ force} = \frac{\rho L^2 v^2}{\mu v L} = \frac{\rho L v}{\mu} \tag{3.2}$$

Reynolds similitude is achieved for identical *Reynolds* Numbers in nature and in the model ($Re_N = Re_M$). "If the modeler uses a *Froude* model law (since the wave field is dominated by the influences of gravity and inertia) and insures that the model *Reynolds* Number is in the same range as the prototype, then the *Reynolds* number need not be exactly the same. This argument holds for the *Weber* Number as well." (Frostick et al., 2011). Whereas the *Weber* and *Cauchy* Numbers are relevant for the aeration, water turbulence and water compressibility, a model scale should not be chosen too small.

Hudson et al. (1957) conducted model tests on slopes with 1:3 and 1:6 slope in scales of 1:17 and 1:30. The study concluded that no measurable scale effects were observed for the run-up for both scales. However, scale effects possibly have an influence on the results of the 1:30 scale tests since results present some scatter. Dai and Kamel (1969) conducted hydraulic model tests on rubble mound breakwaters and established an important boundary condition for hydraulic model tests: a sufficiently turbulent flow on the surface of and inside a revetment is ensured if a *Reynolds* number is larger than $Re > 3 \cdot 10^4$. SPM (1984) provides a run-up correction factor to compensate scale effects in hydraulic model tests. This factor is dependent on the slope of the structure. Frostick et al. (2011) presents state-of-the-art guidelines for physical model tests.

Dai and Kamel (1969) defined the *Reynolds* number as

$$Re = \frac{V_R \, \delta}{\nu} \tag{3.3}$$

with a critical *Reynolds* number of $Re > 3 \cdot 10^{-3}$. V_R is the value of water particle velocity parallel to the side slope of breakwater at a distance R equal to half the characteristic diameter of the cover-layer unit. δ is the characteristic diameter of unit of the primary layer and ν the kinematic viscosity of water at 15.5 °C water temperature. If the water particle velocity is calculated with the shallow water conditions for the case where the water depth is equal to the wave height and is substituted in Eq. (3.3) the equation as presented by Stoa (1978) is achieved with the characteristic diameter k_r to:

$$Re = \frac{\sqrt{gH_{D=0}} \, k_r}{\nu} \tag{3.4}$$

This approach is stated by Frostick et al. (2011) with the characteristic diameter D_n under the fraction bar

$$Re = \frac{\sqrt{gH_s \cdot D_n}}{\nu_k} \tag{3.5}$$

and a critical roughness-related *Reynolds* number of $Re > 3 \cdot 10^{-4}$.

With respect to stepped revetments a characteristic surface roughness length has to be defined. Required parameters are defined in Fig. 3.1. The pseudo-bottom, step height S_h

and step width S_w form a triangle. The characteristic step diameter or roughness length k_h is defined as the orthogonal distance of the pseudo-bottom to the step niche corner.

If air entrainment or the flow of thin layers of liquid plays a major role (e.g. interaction of breaking waves with objects or structures), surface tension becomes important. The ratio of inertial forces to surface tension forces is defined by the *Weber* Number

$$We = \frac{inertial\ force}{surface\ tension\ force} = \frac{\rho L^2 V^2}{\sigma V L} = \frac{\rho L^2 V}{\nu}. \tag{3.6}$$

Weber similitude is achieved for identical *Weber* Numbers in nature and model ($We_N = We_M$).

Model and scale effects can be minimized by considering the similitude laws and adjusting the model set-up and test program accordingly. As an example, the step height in relation to the wave height should be chosen in a way to enable turbulent flow conditions in the step niches (critical *Reynolds* number).

3.1.2   Dimensional analysis

Yalin (1971) states that 'the progress of science means the birth of new ideas: the introduction of new concepts'. The theoretically unlimited number of concepts can be defined by only three independent entities – length (L), time (T) and mass (M) – defined as fundamental entities. Furthermore, an entity is defined as a quantity of numbers if it can be measured. According to Hughes (1993) the dimension of any physical quantity a or property with a special unit $[a]$ (definitions by Yalin (1971)) can be represented in terms of the three fundamental dimensions of length (L), time (T) and mass (M) by the expression

$$[a] = L^\alpha T^\beta M^\gamma \tag{3.7}$$

where the nature of the physical quantity a is reflected by the numerical values of the exponents α, β and γ. Hence,
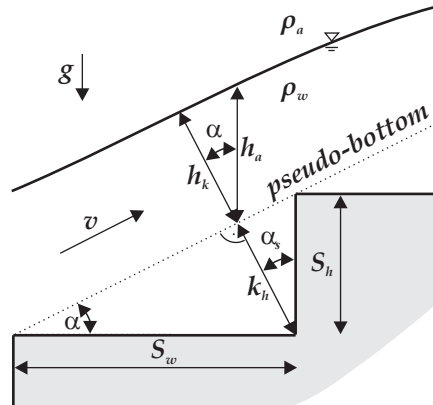
Figure 3.1: Definition of the characteristic diameter k_h at stepped revetments.

$$\alpha \neq 0, \beta = 0, \gamma = 0 \text{ constrains } \textbf{Geometric} \text{ quantity}$$
$$\alpha \neq 0, \beta \neq 0, \gamma = 0 \text{ constrains } \textbf{Kinematic} \text{ quantity}$$
$$\alpha \neq 0, \beta \neq 0, \gamma \neq 0 \text{ constrains } \textbf{Dynamic} \text{ quantity}$$

If all exponents (α, β, γ) in Eq. (3.7) are zero, the unit of the quantity a cannot depend on the fundamental units. Now it is required to describe a number of physical quantities of a number of n different kinds by the value of any one in the relation and the ratios of the others to this one to define the complete physical equation

$$f(Q_1, Q_2, \cdots Q_n) = 0 \qquad (3.8)$$

and follow the approach by Buckingham (1914). 'If none of the quantities involved in the relation has been overlooked, the equation will give a complete description of the relation subsisting among the quantities represented in it, and will be a complete equation'. Coefficients in the equation represent dimensionless numbers. The n physical quantities Q can be written in a dimensional matrix of order k including independent arguments $\Pi_1, \cdots \Pi_k$ and Eq. (3.8) may be more simply written as

$$F(\Pi_1, \Pi_2, \cdots \Pi_{n-k}) = 0. \qquad (3.9)$$

If k is defined as 'the number of arbitrary fundamental units needed as a basis for the absolute system $[Q_1], \cdots [Q_n]$ by which the $Q's$ are measured [...] there is always, among the n units $[Q]$, at least one set of k which may be used as fundamental units, the remaining $(n-k)$ being derived from them' (Buckingham, 1914).

To describe the wave run-up and wave overtopping process over stepped revetments, four related parameter groups – wave motion, geometry, substance properties, kinematic and dynamic – can be identified. These parameters are drawn in Fig. 3.1 and Fig. 3.2 and categorized in Tab. 3.1 – 3.4.
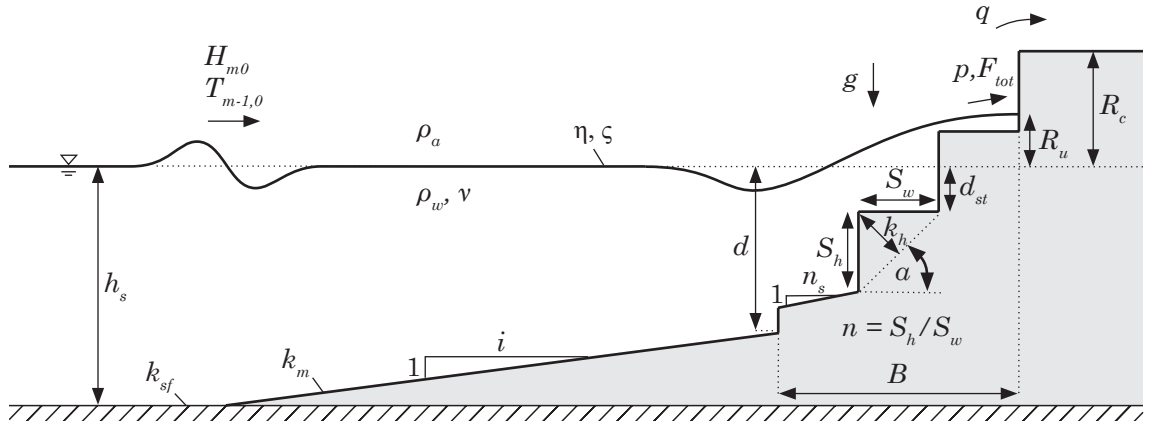
Figure 3.2: Schematic model set-up with definition of geometric and hydraulic parameters.

Table 3.1: Variables of wave motion used in the dimensional analysis.

Description	Symbol	Dimension	Unit
Wave height	H_{m0}	$[L^1 T^0 M^0]$	$[m]$
Wave period	T	$[L^0 T^1 M^0]$	$[s]$
Wave steepness	s	$[L^0 T^0 M^0]$	$[-]$
Wave run-up height	R_u	$[L^1 T^0 M^0]$	$[m]$
Wave overtopping volume	q	$[L^2 T^1 M^0]$	$[m^3/(sm)]$
Wave slamming force	F_{tot}	$[L^1 T^{-2} M^1]$	$[N]$
Pressure	p	$[L^1 T^{-2} M^{-1}]$	$[N/m^2]$
Wave run-up velocity	v_{R_u}	$[L^1 T^{-1} M^0]$	$[m/s]$
Thickness of run-up layer	h_k	$[L^1 T^0 M^0]$	$[m]$

Table 3.2: Fluid-related variables of water and air relevant for the wave run-up and overtopping process over stepped revetments.

Description	Symbol	Dimension	Unit
Density water/air	ρ_w, ρ_a	$[L^{-3} T^0 M^1]$	$[kg/m^3]$
Surface tension	σ	$[L^{-1} T^{-2} M^1]$	$[kg/(s^2 m)]$

Table 3.3: Kinematic and dynamic variables relevant for the wave run-up and overtopping process over stepped revetments.

Description	Symbol	Dimension	Unit
Kinematic viscosity	ν	$[L^2 T^{-1} M^0]$	$[m^2/s]$
Gravitational acceleration	g	$[L^1 T^{-2} M^0]$	$[m/s^2]$

Table 3.4: Geometry-related variables relevant for the wave run-up and overtopping process over stepped revetments.

Description	Symbol	Dimension	Unit
Topography			
Beach profile			
Surface roughness (flume)	k_{sf}	$[L^1 T^0 M^0]$	$[m]$
Surface roughness (model)	k_m	$[L^1 T^0 M^0]$	$[m]$
Water depth (deep water)	h_s	$[L^1 T^0 M^0]$	$[m]$
Foreshore slope	i	$[L^1 T^0 M^0]$	$[m]$
Water depth (structure toe)	d	$[L^1 T^0 M^0]$	$[m]$
Step height	S_h	$[L^1 T^0 M^0]$	$[m]$
Step width	S_w	$[L^1 T^0 M^0]$	$[m]$
Slope	n	$[L^1 T^0 M^0]$	$[m]$
Step freeboard above SWL	d_{st}	$[L^1 T^0 M^0]$	$[m]$
Freeboard height	R_c	$[L^1 T^0 M^0]$	$[m]$
Characteristic step diameter	k_h	$[L^1 T^0 M^0]$	$[m]$

The physical model tests conducted in this research reflect idealized boundary conditions. Not all parameters listed in Tab. 3.1 – 3.4 have been varied during the parameter study or can be represented by other parameters. Surface tension σ plays a role in context with the hydraulic model tests but is discussed in context with scale effects and is excluded from further analysis. The kinematic viscosity of water is temperature related. The temperature is kept constant $(20 - 21.5\,^\circ\mathrm{C})$ during the tests. As a result the kinematic viscosity ν remains almost constant throughout the test campaign and the changes in kinematic viscosity are negligible. Topography and bathymetry are constant values or described by other parameters. The surface roughness of the flume (k_{sf}) and the model (k_m) is assumed to be sufficiently smooth to be negligible. A foreshore slope is not implemented in the model set-up $(i = 0)$ since the study aims to investigate the undistributed hydraulic processes on the stepped revetment slope. Therefore the water depth h_s in the far-field of the model is equal to the water depth d at the toe of the structure.

After taking the mentioned assumptions into account, the key variables which describe the interaction of incoming waves with stepped revetments can be described with Eq. (3.8) as

$$f \left(\underbrace{H_{m0}, T_{m-1,0}, s, R_u, q, F_{tot}, p, v_{r_u}, h_k,}_{Wave} \underbrace{\rho_w, \rho_a,}_{Fluid} \underbrace{g}_{\substack{Kinematic,\\Dynamic}} , \underbrace{h_s, S_h, n, d_{st}, R_c, k_h}_{Geometry} \right) = 0$$

(3.10)

According to Buckingham (1914) the transformation of a non-dimensional notation (Eq. (3.8)) to a dimensionless notation (Eq. (3.9)) can be applied to Eq. (3.10). Thereby the following equations separated for wave run-up and wave overtopping are obtained:

wave run-up:

$$F \left(\frac{h_s}{L}, \frac{S_h}{H_{m0}}, n, \frac{R_u}{H_{m0}}, \xi_{m-1,0}, \frac{k_h}{H_{m0}}, \frac{d_{st}}{H_{m0}}, \underbrace{\frac{c}{\sqrt{gH_{m0}}}}_{Fr} \right) = 0$$

(3.11)

wave overtopping:

$$F \left(\frac{h_s}{L}, \frac{S_h}{H_{m0}}, n, \frac{R_c}{H_{m0}}, \xi_{m-1,0}, \frac{k_h}{H_{m0}}, \frac{d_{st}}{H_{m0}}, \frac{q}{\sqrt{gH_{m0}^3}}, \underbrace{\frac{c}{\sqrt{gH_{m0}}}}_{Fr} \right) = 0$$

These dimensionless notations have to be taken into account to describe the wave interaction with a stepped revetment. This interaction includes wave reflection, non-linear wave transformation processes, energy dissipation, wave run-up, wave splash-up, wave run-down, wave transmission and wave overtopping.

Knowing the dimensionless notations and relevant processes for the wave interaction with a stepped revetment allows the development of a consistent test program.

3.2   Wave flume

Hydraulic model tests which focus on the wave interaction with stepped revetments were conducted in the so-called wave flume 'Schneiderberg' (WKS). The flume is constructed from reinforced concrete and has a length of $110\,m$, a width of $2.2\,m$ and an overall depth of 2.0 m. The water depth can be varied from $0.0\,m$ to $1.2\,m$. The WKS is equipped with a hydraulic driven piston type wave maker and wet-back area built by *Kempf & Remmers*. Waves can be generated with a total stroke of $0.6\,m$ and a maximum velocity of $1.2\,m/s$. Hence, dependent on the water depth, wave heights up to $H_s = 0.32\,m$ and wave periods larger than $T \geq 0.9\,s$ can be generated. At a distance of $20.0\,m$ from the wave board a glass observation window of a width of $5.0\,m$ is located. A 1:10 inclined rubble mound slope is located at the end of the flume to serve as a passive wave absorber.

3.3   Experimental set-up

Hydraulic model tests were performed with two different set-ups. The first set-up focused on the measurement of real loadings of the stepped revetment with target values wave reflection, wave run-up, wave overtopping and induced pressures on the steps (configuration 1). The second configuration focused on the video-recording of turbulence over the stepped revetment and therefore the hydrodynamics of the wave interaction with stepped revetments (configuration 2).

3.3.1   Model set-ups

Configuration 1. At a distance of $75\,m$ from the wave board composite lumber sheets divide the flume in three parallel sub-sections. Each sub-section has a width of about $0.7\,m$ and is $11\,m$ long (Fig. 3.3, further details are given in the appendix Fig. D.1, page 145). At the end of each of the sub-sections the structure to be tested is implemented with a slope of 1:1 (left, view from the wave maker), 1:2 (right) and 1:3 (center). The idealized shape of different stepped revetments with step heights of $S_h = 0.3\,m$ and $0.05\,m$ is constructed from composite lumber sheets on the horizontal flume bed. As reference case a smooth slope was tested. A side and top view of the different slope variations is given in Fig. 3.4.

Configuration 2. The same model as described in 'Configuration 1' is placed at a distance of $28.9\,m$ from the wave board. At this position the flume has an observation section (glass walls) which enables the observer to study processes under the water surface. The division of the flume in three parallel sub-sections is built up only for a length of $3.0\,m$ as only tests with about 20 regular waves are conducted. It is assumed that the interference between the three sections in this case is negligible.
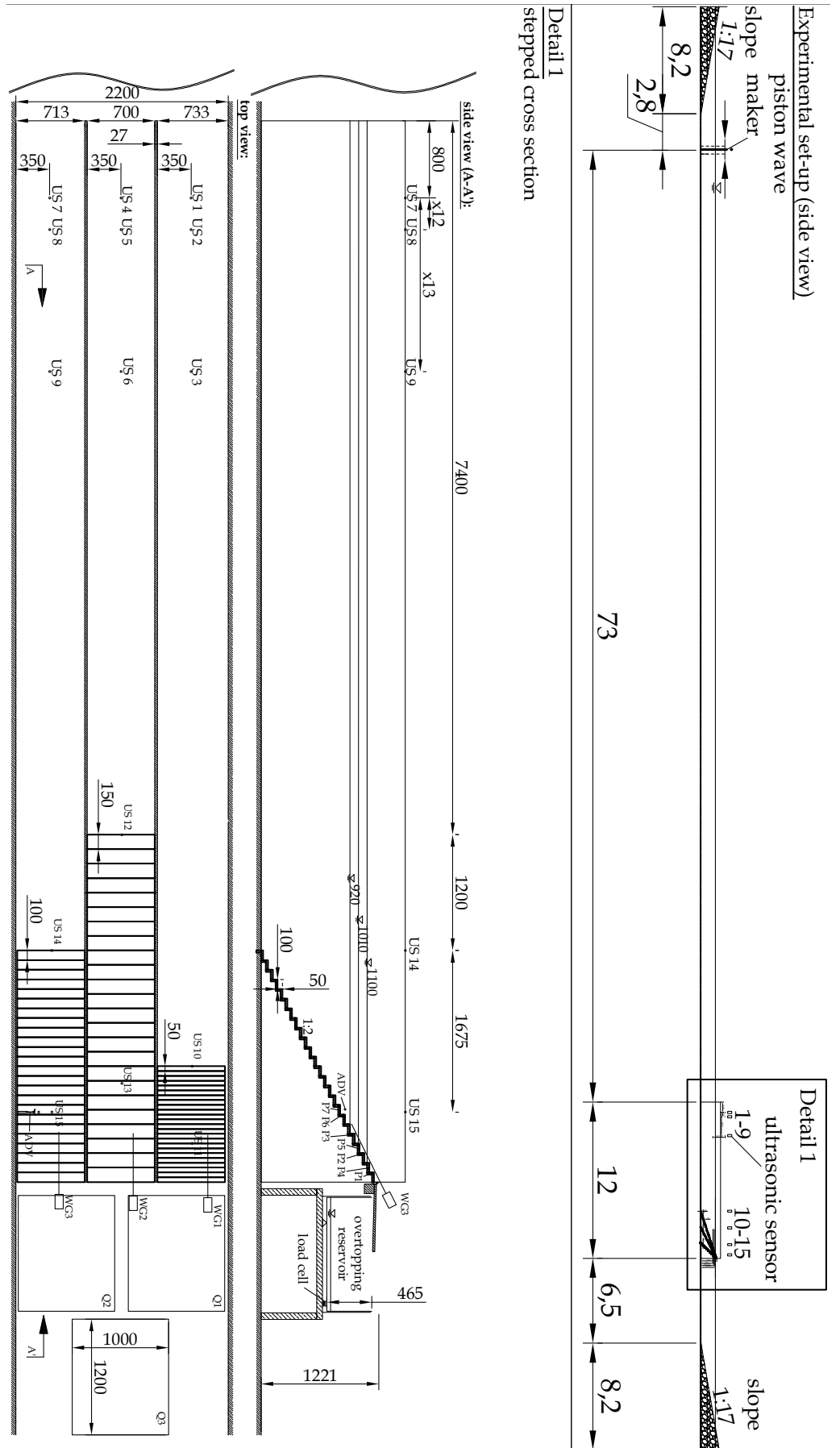
Figure 3.3.: Side and top view of the stepped revetment with 0.05 m step height in the wave flume.
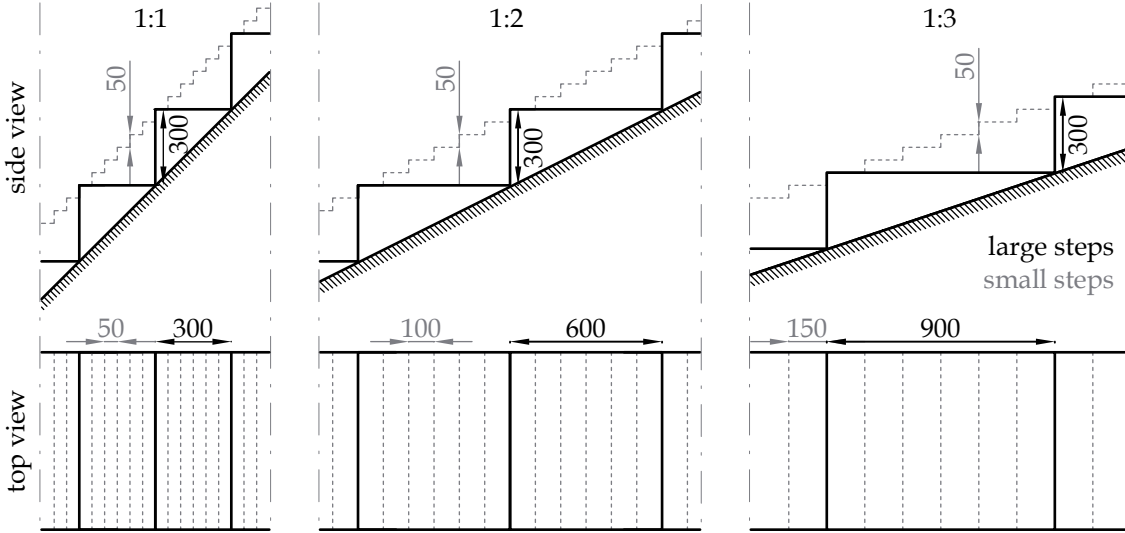
Figure 3.4: Side and top view of slope variation and tested step dimensions.

3.3.2 Instrumentation

The overall instrumentation set-up is given in Fig. 3.3 (further details are given in appendix D). All sensors are denoted with abbreviations and are consecutively numbered. A complete list is given in appendix E.

The **surface elevation** is measured by 15 ultrasonic sensors (US) fabricated by *General Acoustics*. Sensor category $USS10$ with a measuring range of 200 to 1200 mm, a superior resolution of 0.36 mm and a measuring rate of 50 Hz is used in combination with a *UltraLab ULS HF58* controller. The sensors are calibrated in real-time by a reference track. For all sensors the linear calibration constant is $-0.1\,m/V$. Data is sent to the DAQ by analog outputs that underlay a systemic delay of 720 ms in the signal transfer captured in the post processing. Three sensors are positioned at the start of each sub-section at a distance larger than two wave lengths from the toe of the revetment (Fig. 3.5). One sensor is placed at the toe of the stepped revetment and another one in the shallow water region of the still water level (Fig. 3.6).

The **flow velocity** is measured in three dimensions at a single point over the 1:2 inclined revetment by an acoustic Doppler velocimeter (ADV). The employed ADV is a 3D water velocity sensor by *Nortek AS* (labeled *Vectrino+* in the lab probe configuration) and is a down-looking cable probe. The measurement technology is based on the coherent Doppler processing. The probe ensures an accuracy of $\pm 0.5\,\%$ with respect to the measured value $\pm 1\,mm$. The measuring range can be selected between 0.01 to 4 m/s and was set constant to 1.0 m/s during all tests. The sampling volume is located at a distance of 0.05 m from the actuator with a diameter of 6 mm and a height of 7 mm. The probe is connected by a serial interface connection (RS232) with the control computer and controlled by the *Vectrino Plus* firmware. The analog outputs are set to a 100 Hz sampling rate. As calibration function $1V = 0.4\,m/s - 1$ is set.

Wave induced **pressures** are measured at the 1:2 inclined revetment by seven pressure

transducers (*ATM.1ST/N* fabricated by *sts-sensors*) with a range from 0 to 150 *mbar* and a non-conformity of $\pm 0.1\%$ from full scale. The probes are connected by a serial interface connection (RS232) and provide an output signal from 0 to 10 V. The configuration of the probes allows a local (over a single step) and a more global interpretation (for the whole revetment). Calibration functions for each sensor including the corresponding coefficients of determination are given in Table 3.5.

Table 3.5: Calibration for pressure sensors.

sensor	function	R^2
P1	$1V = 7076.9\,mbar - 2.60$	1.0
P2	$1V = 7043.1\,mbar - 3.94$	1.0
P3	$1V = 7100.2\,mbar - 1.78$	1.0
P4	$1V = 7063.7\,mbar - 4.53$	1.0
P5	$1V = 7089.2\,mbar - 2.16$	1.0
P6	$1V = 7128.1\,mbar - 2.28$	1.0
P7	$1V = 7114.6\,mbar - 2.17$	1.0

The **wave run-up** was recorded in each of the three sub-sections by a 1.0 m long wave gauge (*GHM* by *Delft Hydraulics*): The gauges are placed in all three sub-sections inclined above the upper edges of the stepped revetment. The wave gauges consist of two parallel stainless steel rods that function on the measuring principle of electrodes of an electric conduction meter. The analog output of the device is linearly proportional to the liquid level between the sensor rods. The probes are connected to a control unit that supplies an analog output signal of 0 to 10V by an *BNC*-connector. An accuracy of up to 0.5 % from the measuring range can be achieved. Calibration functions for each sensor including the corresponding coefficients of determination are given in Table 3.6.

Table 3.6: Calibration for wave run-up gauges ($S_h = 0.3\,m$).

sensor	function	R^2
WP1	$1V = -28.73\,m + 5.18$	1.00
WP2	$1V = -27.42\,m + 4.89$	0.99
WP3	$1V = -24,78\,m + 4.50$	0.99

The **wave overtopping volumes** are measured indirectly for each sub-section by collecting the overtopped water in a reservoir. The reservoir is mounted on a floating bearing and a load cell (*HBM, C9C*) with a range of 2 kN and an accuracy of 0.2 % from the measuring range (Fig. 3.7). Furthermore the sensor has an IP67 protection. The floating bearing and the load cell are arranged in such a way that the reservoir is supported at two positions above the floating bearing and in one position over the load cell. The distances are calculated in such a way that the sensor is able to measure a total weight equivalent to 0.4 m^3 storage capacity of the reservoir. Calibration functions for each sensor including the corresponding coefficients of determination are given in Table 3.7.

In some cases overtopping volumes larger than 0.4 m^3 are expected. For these cases a

Table 3.7: Calibration for pressure sensors in overtopping reservoirs.

sensor	function	R^2
Q1	$1\,mV/V = 707.11\,l - 74.7$	0.99
Q2	$1\,mV/V = 650.03\,l - 77.2$	0.99
Q3	$1\,mV/V = 681.83\,l - 86,6$	0.99

pump is implemented in the overtopping reservoir in order to reduce the water volume in the reservoir when needed. The pump is triggered and a $9\,V$-signal is recorded when the pump is active. During a calibration of the pumps a linear performance was measured for emptying the whole reservoirs ($400\,l$). Pump capacities are listed in Tab. 3.8.

Table 3.8: Pump capacities with respect to the three overtopping reservoirs.

reservoir	pump capacity $\left[\frac{l}{s}\right]$
1	2.196
2	1.471
3	1.668

All tests were recorded by **video** camera (*Logitech C930e*) to allow the identification of physical phenomena. The camera with a ZEISS® lens certification has a resolution of 1920x1080 px.

3.3.3   Wave generation

The principle idea of the generation of a predefined wave spectrum is given in Fig. 3.8. The wave spectra are generated as cyclic files by $Delft_{AUKE}$ wave generation routines for 2nd order wave generation. Cyclic means that the wave board moves continuously from the last motion in the pre-calculated time series to the first motion of the same time series. About 1,500 wave board motions have been generated in each single test. Only waves unaffected by the ramp-up and ramp-down of the wave generator are considered. Therefore 1,000 waves in the middle of the wave time series are selected for post processing[15]. As waves with a high frequency travel slower than waves with low frequencies, every frequency domain reaches a wave gauge in a distance to the wave maker in a different time. Hence, the propagation time of the highest frequency (usually $3\,f_p$) has to be taken into account before starting with the analysis of the data.

3.3.4   Data acquisition

A data acquisition system by *Hottinger Baldwin Messtechnik GmbH (HBM)* is used. Two hardware units *QuantumX MX840A* (with eight channels) and one unit *QuantumX MX1601B* (with 16 channels) enable a synchronized recording of 32 data channels with

---

[15]This influence is discussed in section 3.6.
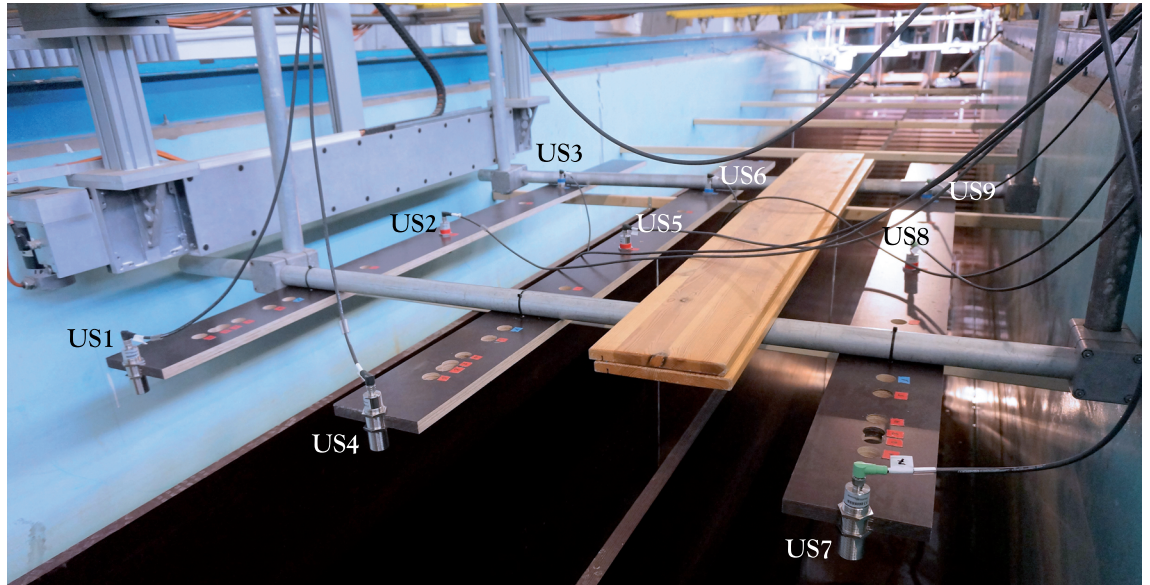
Figure 3.5: Ultrasonic sensor arrays for reflection analysis in the front-end of the subsections with perspective towards the model.
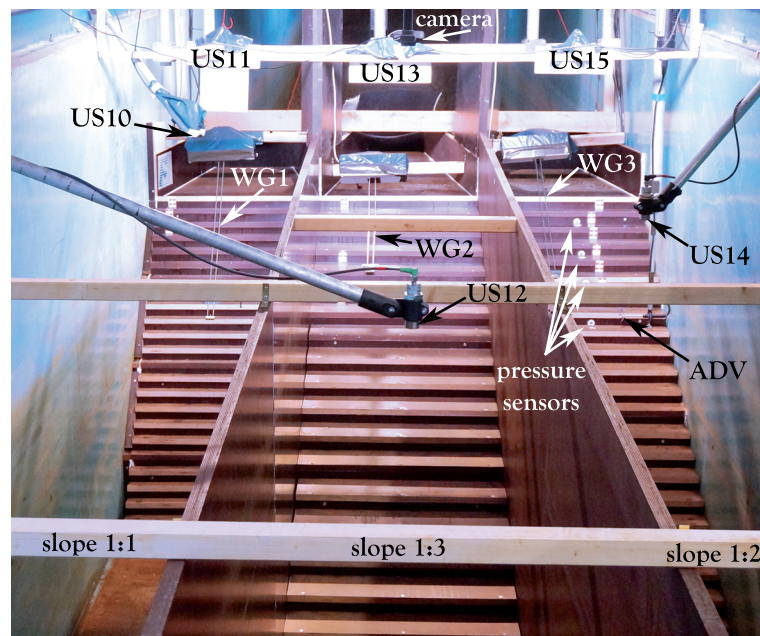
Figure 3.6: Instrumentation over the stepped revetment with a step height of $0.05\,m$.
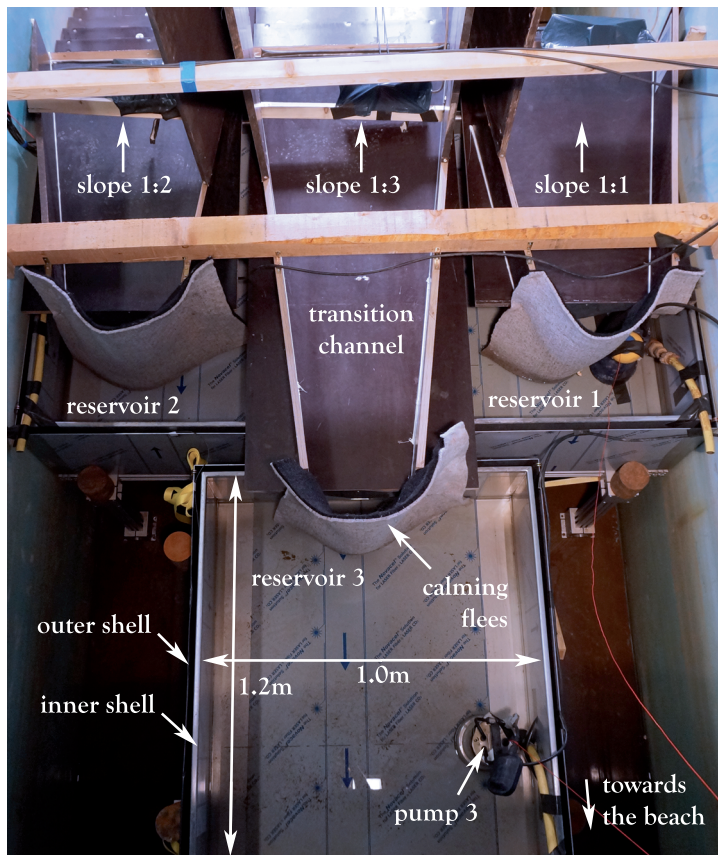
Figure 3.7: Overtopping reservoirs with pumps and connected transition channel.
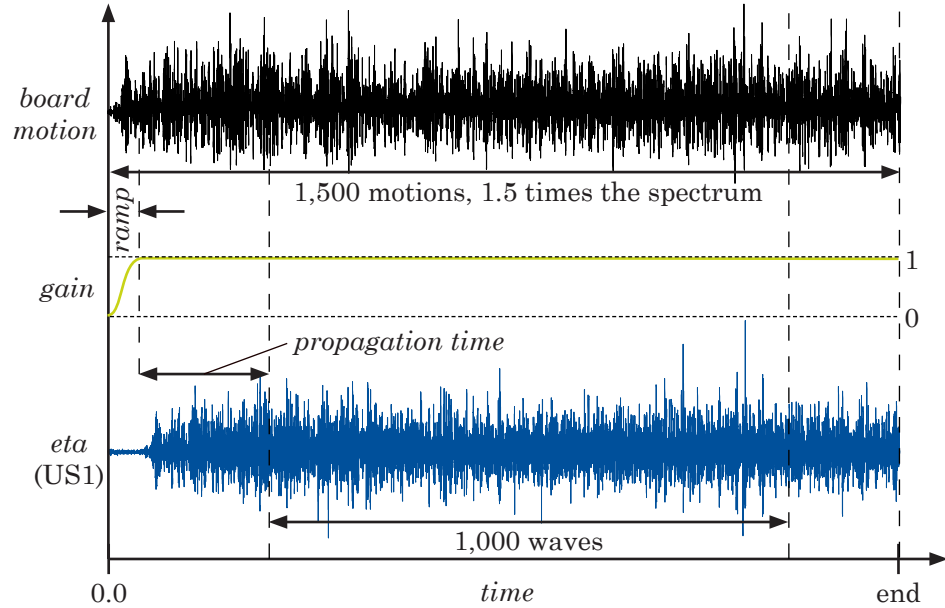
Figure 3.8: Definition of the time interval within a time series selected for further post processing.

different sampling rates. Two universal amplifier *QuantumX MX840A* are used to control and record data from sensors with different requirements for power supply and sampling rate (pressure sensors with half bridge and $5\,V$ DC-supply-voltage, force transducers with full bridge and $5\,V$ DC-supply-voltage, analog wave gauge signal 0 to $10\,V$, analog ADV signal $\pm2.5\,V$, pump trigger 0 to $9\,V$). The universal amplifier MX1601B is used to measure inputs based on normalized voltage $\pm10\,V$ by 16 electrically isolated channels recording data from the analog outputs of the two *UltraLab ULS HF58*. A working standard calibration certificate is stored in each DAQ-instrument and guarantees quality and traceability.

The data from the 15 ultrasonic sensors are transferred by BNC connections to the MX1601 and sampled within *catmanEasy* with $100\,Hz$. Signals for *x*-, *y*- and *z*-orientation are sampled with $100\,Hz$ from the ADV probe by a BNC connection to the MX1601 and MX840A. Pressure transducers are connected via a serial interface connection (RS232) to the MX840A_2 and recorded with $2,400\,Hz$, transducers in strongly exposed regions close to the still water level with $19,200\,Hz$ to ensure an accurate recording of the peak pressures with more than four data points in the peak. Data from the run-up probes are connected by the amplifier unit by BNC connections and sampled with $100\,Hz$ by the MX840A_1. The load cells mounted in the overtopping-units are connected via a serial interface connection (RS232) with the MX840_1 and recorded with $100\,Hz$. Videos are recorded with a resolution of $640x480\,px$ and a sampling rate of $20\,Hz$ in the *AVI*-file format encoded by the H.264 video encoder.

The data acquisition is controlled by the software *catmanEasy* (version 4.1, *HBM*). Within the software the video data can be recorded synchronously. Results are stored channel-wise in *Matlab*-files with the file extension **.mat*.
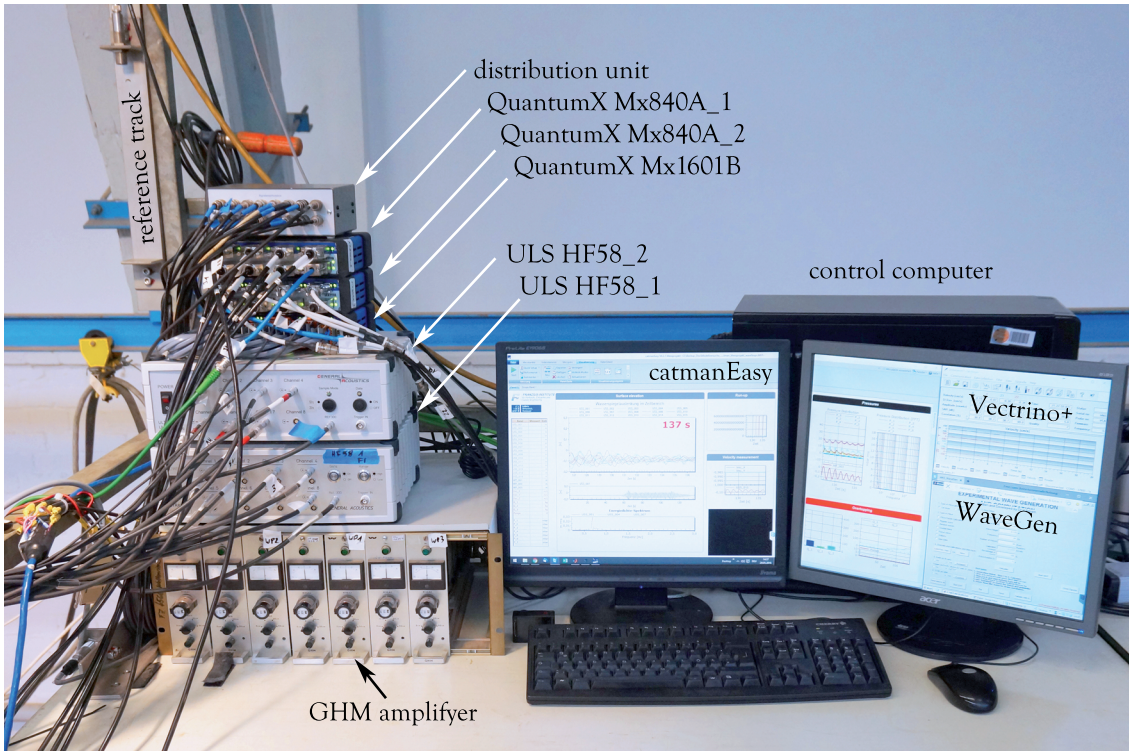
Figure 3.9: Data acquisition set-up.
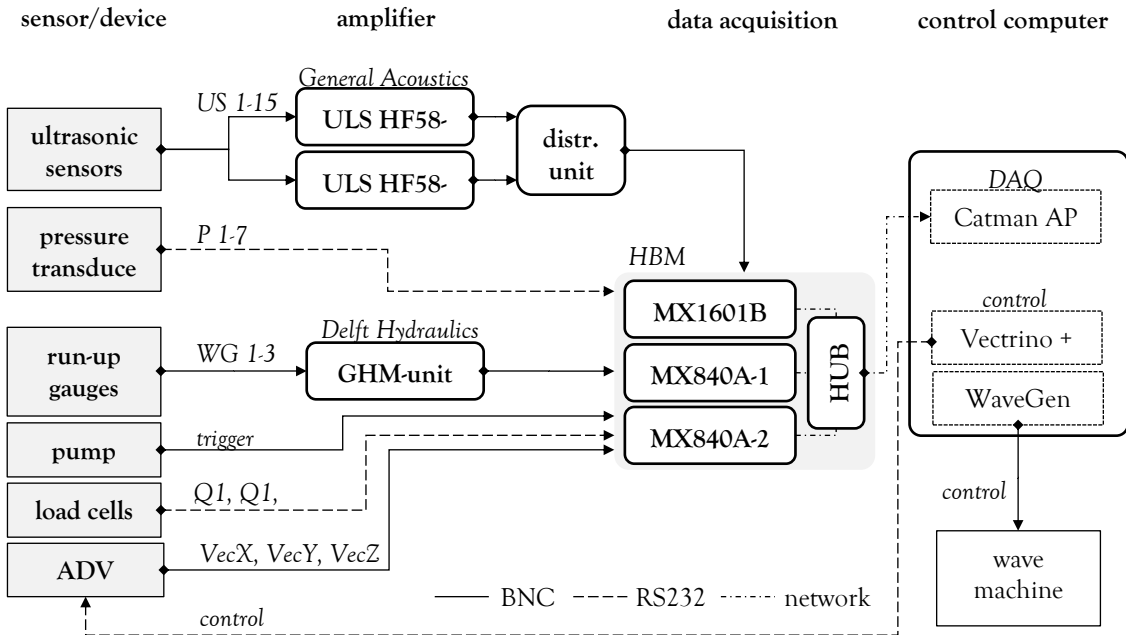
Figure 3.10: Data acquisition circuit flow chart.

3.4 Test program

The test program was drawn up based on the findings of the dimensional analysis (section 3.1.2) and the derived boundary conditions. The generated wave spectra follow the characteristic of a standard Jonswap spectrum with a peak enhancement factor of 3.3 and a relative peak width of $\sigma = 0.07$ and 0.09 for frequencies below and above the peak frequency respectively. The spectrum was selected to represent North Sea wave conditions. The hydraulic related parameters wave height H_{m0}, wave period T_p and water level h_s are varied. The geometry related parameters slope angle $cot\alpha = n$ and the height of the steps of the revetment S_h are varied. By changing these five input parameters all other relevant parameters in the dimension analysis can be derived as follows:

$$
\begin{aligned}
R_c =& \text{crest height} - h_s \\
k_h =& cos\alpha \cdot S_h \\
d_{st} =& \begin{cases} \text{for } d_{st} > S_h/2: & round_{up}\left(\frac{R_c}{S_h}\right) \cdot S_h - R_c \\ \text{for } d_{st} < S_h/2: & d_{st} - S_h \end{cases} \\
xi =& \frac{tan\alpha}{\sqrt{\frac{H}{L}}}
\end{aligned}
\tag{3.12}
$$

The test program is designed to cover a wide range of dimensionless parameters. The test runs given in Tab. 3.9 cover the following dimensionless ranges:

$$
\begin{aligned}
0.17 <& \frac{h_s}{L} < 0.58 \\
0.02 <& \frac{H}{L} < 0.07 \\
1.6 <& \xi < 7.7 \\
0.22 <& \frac{H}{S_h} < 4.0
\end{aligned}
\tag{3.13}
$$

Every test in the test program is conducted once. The repeatability of tests for exactly the same geometry and hydraulic related boundary conditions, which include the same phase shifting of all energy components with respect to their frequency, is shown with tests # $014 - 017$ and are discussed in Chapter 3.6.

3.5 Data processing

Within the data acquisition the calibration of the respective sensors is directly applied and all channels are stored in SI-units. Nevertheless, the raw-data of each channel has to be individually post-processed to assure a correct evaluation of the data. Applied editing tools are briefly described afterwards to allow an estimation of the influence of the post-processing on the individual results.

Table 3.9: Test data of hydraulic model tests.

#	S_h [m]	R_c [m]	H_{m0} [m]	T_p [s]	h_s [m]	d_{st} [m]	$\frac{H_{m0}}{S_h}$ [-]	$n=1$ $\xi_{m-1,0}$ [-]	$n=2$ $\xi_{m-1,0}$ [-]	$n=3$ $\xi_{m-1,0}$ [-]
001	0.0	0.121	0.067	1.47	1.100	0.0	Inf	7.3	3.5	2.2
002	0.0	0.121	0.100	1.39	1.100	0.0	Inf	5.8	2.7	1.8
003	0.0	0.121	0.100	2.07	1.100	0.0	Inf	6.8	3.6	2.3
004	0.0	0.211	0.067	1.47	1.010	0.0	Inf	7.4	3.6	2.2
005	0.0	0.211	0.100	1.39	1.010	0.0	Inf	6.0	2.8	1.8
006	0.0	0.211	0.100	2.07	1.010	0.0	Inf	7.1	3.7	2.4
007	0.0	0.211	0.100	2.07	1.010	0.0	Inf	7.1	3.7	2.4
008	0.0	0.211	0.100	2.07	1.010	0.0	Inf	7.2	3.7	2.4
009	0.0	0.300	0.067	1.47	0.921	0.0	Inf	7.3	3.4	2.2
010	0.0	0.300	0.100	1.39	0.921	0.0	Inf	5.9	2.8	1.9
011	0.0	0.300	0.200	2.07	0.921	0.0	Inf	5.0	2.5	1.7
012	0.05	0.121	0.067	1.47	1.100	0.029	1.34	7.7	3.8	2.4
013	0.05	0.121	0.100	1.10	1.100	0.029	2.00	5.9	3.0	1.9
014	0.05	0.121	0.100	1.39	1.100	0.029	2.00	6.0	3.0	1.9
015	0.05	0.121	0.100	1.39	1.100	0.029	2.00	6.0	3.0	1.9
016	0.05	0.121	0.100	1.39	1.100	0.029	2.00	6.0	3.0	1.9
017	0.05	0.121	0.100	1.39	1.100	0.029	2.00	6.0	3.0	1.9
018	0.05	0.121	0.100	2.07	1.100	0.029	2.00	7.6	3.8	2.5
019	0.05	0.121	0.150	2.07	1.100	0.029	3.00	6.6	3.4	2.3
020	0.05	0.121	0.150	2.57	1.100	0.029	3.00	6.7	3.6	2.4
021	0.05	0.121	0.200	2.07	1.100	0.029	4.00	5.9	3.0	2.0
022	0.05	0.211	0.100	2.07	1.010	0.039	2.00	7.6	3.8	2.5
023	0.05	0.211	0.100	2.07	1.010	0.039	2.00	7.6	3.8	2.5
024	0.05	0.211	0.100	2.07	1.010	0.039	2.00	7.6	3.8	2.5
025	0.3	0.121	0.067	1.47	1.100	0.179	0.22	4.9	2.6	1.6
026	0.3	0.121	0.100	1.39	1.100	0.179	0.33	5.5	2.5	1.7
027	0.3	0.121	0.150	3.10	1.100	0.179	0.50	7.2	3.5	2.3
028	0.3	0.121	0.200	2.07	1.100	0.179	0.67	5.5	2.8	1.9
029	0.3	0.211	0.067	1.47	1.010	0.089	0.22	7.2	3.5	2.5
030	0.3	0.211	0.100	1.39	1.010	0.089	0.33	5.8	2.8	1.9
031	0.3	0.211	0.200	2.07	1.010	0.089	0.67	5.4	2.7	1.8
032	0.3	0.300	0.067	1.47	0.921	0.0	0.22	7.1	3.3	2.2
033	0.3	0.300	0.100	1.39	0.921	0.0	0.33	5.9	2.8	1.8
034	0.3	0.300	0.200	2.07	0.921	0.0	0.67	5.2	2.6	1.8

3.5.1 Surface elevation

The surface elevation is recorded by ultrasonic sensors. In a first step the offset of the recorded data is eliminated by a subtraction of the mean value of the first $n = 1,000$ values from all values i.

$$data = data - \frac{\sum\limits_{i=1}^{n} data_i}{n}.$$

(3.14)

In a second step the data is de-noised with a $M = 4^{th}$ order weighted moving average filter with two loops

$$dataFiltered_i = \frac{1}{M} \sum_{j=0}^{M-1} data_{i+j}.$$

(3.15)

Finally spikes are eliminated by a second order polynomial *Savitzky-Golay* smoothing filter. Required polynomial coefficients a_i and a standardization factor h over $np = 41$ time samples are applied.

$$dataFiltered_i = \frac{1}{h} \sum_{i=-\frac{np-1}{2}}^{\frac{np-1}{2}} a_i data_{t+i}.$$

(3.16)

Based on the data of the filtered surface elevation, a spectral analysis is conducted at US1, 4 and 7. The peak period is also calculated for each sub-section.

The incident and reflected wave heights (H_{inc}, H_{ref}) and therefore also the reflection coefficient C_r have to be determined. The method of Baldock and Simmonds (1999), which is an improvement of the method by Frigaard and Brorsen (1995) following linear theory, was applied for the reflection analysis. The algorithm is based on a two sensor water surface measurement. The two sensors have to be arranged at a distance $\Delta x < L/4$ from each other in order to avoid singularities in a frequency range where the wave spectrum is without significant energy. Since three sensors are implemented at the front of each sub-section, the algorithm is applied on two pairs of sensors and the incident and reflected wave heights are weighted as a mean of both calculations.

The spectral wave period $T_{m-1,0}$ is calculated by the 'dat2spec2'-routine within the 'WAFO toolbox' developed by Brodtkorb et al. (2002).

3.5.2 Wave run-up

Raw-data from the wave gauges, used to measure the wave run-up, have to be thoroughly post-processed since the highly turbulent flow and air entrainment over the stepped revetment lead to spikes in the signals that have to be filtered.

The raw-data have several outliers in the order of magnitude of $\pm E^{15}$. These spikes are single data points that are corrected with the simple approach to set every absolute value larger than $|R_u| > 2\,m$ to zero. After this step minor spikes are deleted by a

second order polynomial *Savitzky-Golay* smoothing filter. The run-up height with a certain percentage of exceedance is also calculated. For example, the 2 % exceedance for the run-up is determined by calculating the run-up height exceeded by 2 % of all incident waves.

3.5.3   Wave overtopping

The wave overtopping volume is recorded in two dependent ways – the load cell under the reservoir and the pump in the reservoir. Loads increase if water overtops the revetment crest. Loads decrease if the pump is activated and water is pumped from the reservoir. The mean overtopping volume can be calculated by the mass balance.[16]

Raw-data from the pump-channel are filtered with a 2nd order low-pass Butterworth filter to allow the analysis of activity of the pump in the reservoir. The pump is activated if the gradient is positive and disabled if the gradient is negative. With the time-interval in-between activation and de-activation of the pump and the pump capacity (Tab. 3.8) the first part of the overtopping volume can be calculated. The second part is calculated by the difference between the loadings at the end of the time series (1,000 waves). The sum of part 1 and part 2 has to be normalized with the duration of this time span and the width of the revetment crest to compute the mean overtopping discharge $q\,[m^3/(sm)]$.

3.5.4   Pressures

Raw-data from the pressure sensors are offset-corrected by means of the first five seconds of the data. Then the time and amplitude of the peaks are calculated with the boundary condition that the minimum peak height is $10\,mbar$ and that the minimum distance between two peaks is at least 0.8 times the wave period. The pressure with a certain percentage of exceedance is calculated finally by a descend sorting of all recorded pressure peaks within a single test run. Then the mean of a certain number of events is averaged. Further discussions on the pressure data are given in Chapt. 4.

3.6   Data quality

Every test in the test program is conducted once. Nevertheless, the meaning of such a single measurement has to be evaluated with respect to the statistic uncertainty of a single data point. The repeatability of tests for exactly the same hydraulic- and geometry-related boundary conditions including the same phase shifting of all energy components with respect to their frequency is shown with tests # 014–017. The mean measured and predicted values are listed in Tab. G.1 (page 155) for the following: run-up height,

---

[16]It was originally planned to analyze the probability distribution of individual wave overtopping volumes at the stepped revetments (according to Victor et al. (2012)). However, this was not possible since the transition channel between the crest of the revetment and reservoir (compare Fig. 3.7) was too long with too gentle slope. This led to a blurred and time-delayed recording of the overtopping event. Although, large single overtopping volumes were clearly recorded, it was not possible to filter the data to identify all individual overtopping events.

mean overtopping volume, reflection coefficient and reduction coefficient for run-up and overtopping.

The relative error ($\epsilon = 1 - $ value/mean value) is for most measured parameters in the range of $\pm 1\%$. The measured overtopping volumes scatter slightly more ($-11\% < \epsilon_{q,max} < 6.6\%$, $\epsilon_{q,mean} \approx \pm 5\%$). This range is however acceptable for the measurement of mean overtopping discharges in wave spectra. A significant relative error is recorded for test run 017. This test was stopped after four minutes due to technical problems. As the wave spectra could not be fully recorded, some energy content of the spectrum is missing and therefore the distribution of the wave heights in the recorded data series is not representative to the desired Jonswap spectrum (compare Fig. 3.8). Therefore, the post processing considers only test runs with 1,000 waves.

The ratio of the input wave parameters to the measured wave parameters are presented in Fig. 3.11. The measured wave height, wave period and Iribarren number are given normalized by the origin input value over the wave steepness. It can be seen that the wave height is in principle about 5 % too low whereas the wave period matches quite well. As the Iribarren number is directly proportional to the wave height both trends are symmetrical. The reason for the scatter is that the transfer function of the wave maker was not optimally selected. The transfer function had been adapted for the overall wave conditions without separating the incident and reflected waves. An example of a detailed analysis of the post-processed surface elevation measured by $US5$ in the far field of a 1:3 inclined stepped revetment with a step height of $H_{m0}/S_h = 2$ is given in Fig. I.1 (page 161) for test run # 3014. Here it can clearly be seen that the spectral wave height H_{m0} matches the input value. Furthermore the spectral density distributions as well as the distribution of the wave heights and wave periods in the spectrum present reliable data. Nevertheless, as the main focus of these model tests is to analyze the interaction of varying wave conditions with stepped revetments, these slight differences in wave heights are not a major problem. The incident wave conditions are recorded in the near-field of the stepped revetment and the post-processing is based on these calculated values. The absence of an active absorption system in this flume leads to further problems with re-reflections at the wave board for long wave trains as tested in this study. These re-reflected waves change the spectral density of the input spectrum. Indications on this effect can be read out of the spectral density distribution given in the appendix (Fig. I.1, page 161).

3.7 Conclusions

In order to gain knowledge in the field of wave interaction with stepped revetments, comprehensive model tests are conducted in a wave flume. Nine set-ups with slopes $n\{1, 2, 3\}$ and step height $S_h\{0.0\,m, 0.05\,m, 0.3\,m\}$) are analyzed in a wave flume. The focus of the tests is on the wave reflection, wave run-up, wave overtopping and wave loading. In an additional set-up the vorticity under the water surface has been analyzed at a 1:2 slope for the three different step heights. A systematic test program was selected based on a carefully derived dimension analysis. The focus of this new set of data was to fill knowledge
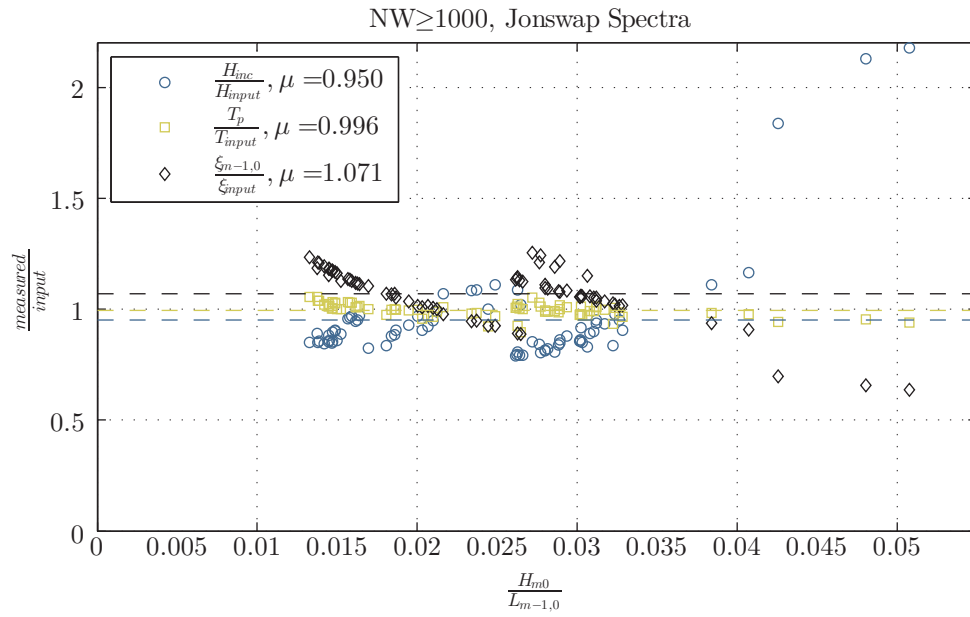
Figure 3.11: Comparison of generated and measured wave parameters including mean value.

gaps for hydraulic processes at stepped revetments in the range of $0.5 \leq H_{m0}/S_h \leq 2$ as identified in section 2.4. The essential instrumentation to measure the surface elevation, velocities, the wave run-up, wave overtopping and pressure loads on the revetment has been described. The reason for the installation of each instrument where to place each instrument has been discussed. Resolutions, sampling rates and measuring ranges were discussed. The synchronized data acquisition was described. The most relevant steps in the data post processing for each sensor were described in order to enable an assessment of the results given in the following. Consequently, the data quality was discussed.

4   Results of physical model tests

The objective of the present study is to identify and describe the hydraulic processes which occur when waves interact with a stepped revetment. In the data-analysis, mean values of parameters will be presented to allow a discussion on the principle performance of the processes. The standard deviation (STD) is also given, which allows the quantification of error margins between two dimensionless values. It will be explicitly mentioned when a presented prediction or design guideline is based on the envelope of a correlation. All measured and calculated values discussed in this chapter are listed in appendix F.

The hydraulic model tests are analyzed to determine the wave reflection, wave run-up, wave overtopping and wave forces on the stepped revetment. Firstly, to get an overall idea of the wave interaction with the tested slopes (varying slopes $1 \leq n \leq 3$ and step heights $0.0\,m \leq S_h \leq 0.3\,m$) the principle type of wave breaking given in Fig. 4.1 is discussed. The evolution of the breaking process is displayed for characteristic time steps t of the wave period T (t/T). In the first row $((a), (b), (c))$ the wave run-up processes over a plain slope is shown, in the middle row $((d), (e), (f))$ a stepped revetment with a step height of 0.05m ($H/S_h = 2$) and in the bottom row $((g), (h), (i))$ a revetment with 0.3m step height ($H/S_h = 0.33$). The figure presents the wave run-up for revetments with slopes of 1:1 $((a), (d), (g))$, 1:2 $((b), (e), (h))$ and 1:3 $((c), (f), (i))$.

In all the tested cases the incident wave is deflected upwards at the steps of the revetment close to the SWL due to its energy and the slope orientation. In dependence of the wave steepness H/L and the slope of the revetment n, the wave exhibits its typical type of breaking as surging (steep slopes) or plunging (more gentle slopes). The wave breaking characteristics are defined by the Iribarren number ξ. In the case of surging breakers, most of the energy is reflected off the structure as shown in figure (a). More energy is dissipated in the case of plunging breakers due to the wave breaking (impact on the plain slope) and induced turbulence in the run-up flow (air intrusion) (c).

With a small relative water depth (d/L) close to the SWL followed by a vertical section more energy is dissipated over a stepped revetment independent of the slope of the revetment. The process is explained in sub-figure (h). As a wave reaches a step shoaling of the wave takes place. At the time of shoaling, some wave energy is reflected at the submerged steps below SWL (1). After an inundation of the horizontal part of a single step the wave slams against the vertical step face (2) and is deflected upwards (3). Depending on the wave characteristics, the impact and therefore also the shape of the wave changes. As a result, a standing wave can arise in front of the vertical step face or an up-rushing jet of water is formed that is often accompanied with spray. For (h) the water volume is deflected upwards and overturns after reaching the highest elevation. In the case of (g) the water is not deflected in the air and is simply pulled down by gravity.

The largest tested step configuration (i) exhibits a different behavior. After passing step 1-4 explained for (h) the reflected wave is superimposed with the next incoming wave (5). As a result a standing wave is formed on the wide horizontal face of the step and a water cushion on the step. The standing wave leads to a slightly higher water level in front
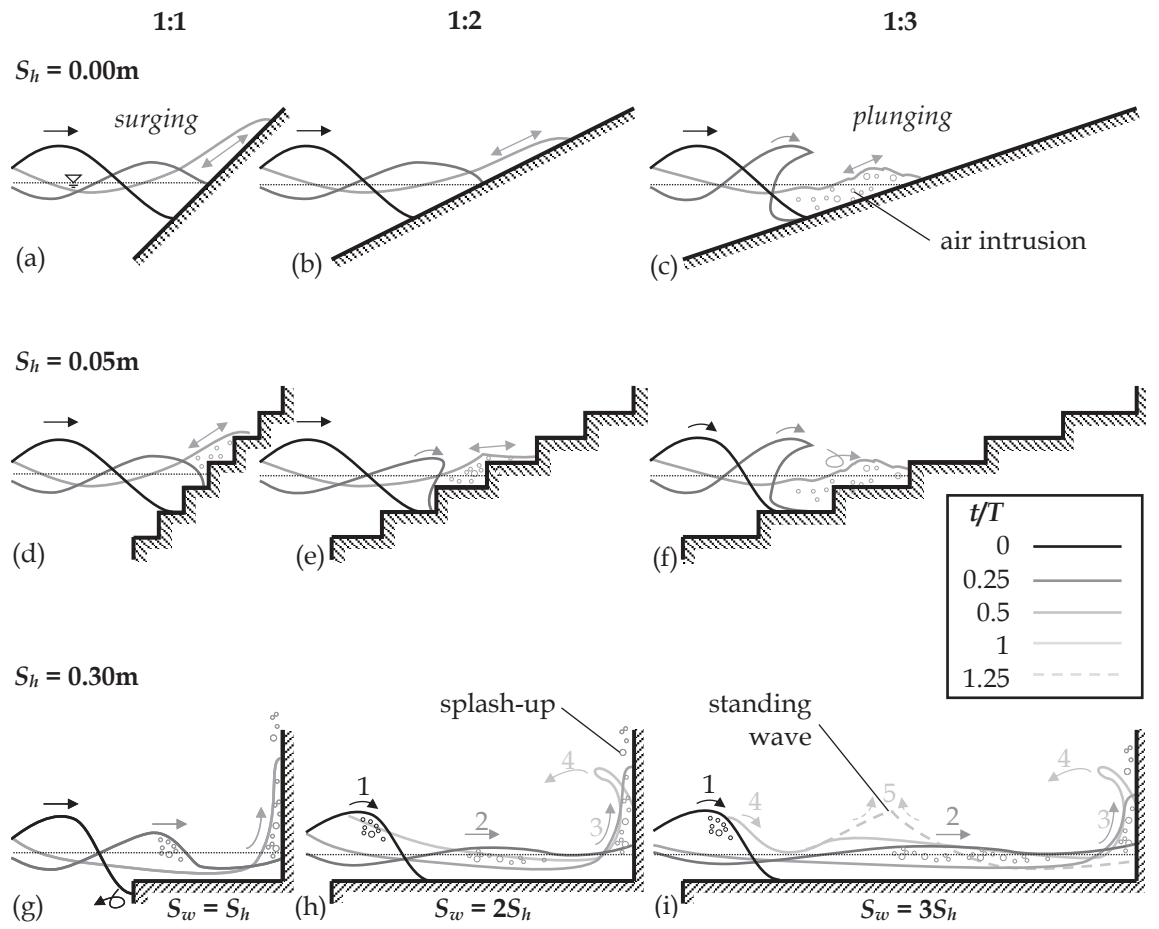
Figure 4.1: Qualitative type of wave breaking ($H \approx 0.1\,m$, $H/L \approx 0.04$) with respect to slope and step height.

of the step face. This special case of revetment geometry is very similar to the system performance of large berms located in front of a vertical wall (e.g. Chen et al. (2016)). Among other factors, the higher energy loss during the wave run-up is caused by the air intrusion for all types of waves.

In the following analysis the relative step height S_h/H is often given inverse as step ratio H/S_h in order to emphasize the depiction of processes with wave heights larger than the step height:

$$
\begin{aligned}
S_h/H : &\quad \text{relative step height} \\
H/S_h : &\quad \text{step ratio}
\end{aligned}
\tag{4.1}
$$

4.1   Wave reflection

The analysis of wave reflection indirectly quantifies the energy dissipation of a coastal protection structure. It is assumed that the energy of an incident wave E_{inc} is partly reduced by the energy dissipation from the interaction with the structure (turbulence due to the run-up, overtopping). The remaining energy is reflected by the structure and can be measured as a reflected wave. Separating the incident (H_{inc}) and reflected wave height (H_{ref}) from the measured wave field in front of the structure allows the quantification of dissipated energy E_{dis} from the interaction of the wave with the structure by

$$
E_{dis} = E_{inc}\left(1 - \frac{H_{ref}}{H_{inc}}\right)\left[\frac{J}{m}\right].
\tag{4.2}
$$

The total energy per meter wave-crest width E_{tot} can be expressed as the sum of kinetic energy E_{kin} (orbital velocity) and potential energy E_{pot} (related to wave length and wave height) by

$$
\begin{aligned}
E_{tot} &= E_{kin} + E_{pot} \\
&= \frac{1}{16}\rho g H^2 L + \frac{1}{16}\rho g H^2 L \\
&= \frac{1}{8}\rho g H^2 L \left[\frac{J}{m^2}\right]
\end{aligned}
\tag{4.3}
$$

where ρ is the fluid density, g the gravitational constant, H the wave height and L the wave .

The wave reflection itself is strongly dependent on the wave breaking. The different type of wave breaking over smooth and stepped revetments with varying slope angle is qualitatively shown in Fig. 4.1. The reference case is a smooth slope (Fig. 4.1 (a)–(c)).

To analyze the wave reflection, the reflection coefficient C_r versus the Iribarren number $\xi_{m-1,0}$ of the investigated model tests is presented in Fig. 4.2. As a comparison the figure also gives empirical predictions for sloping structures with plain and rough surfaces. For all predictions (including the measured data for stepped revetments) the amount of reflected wave energy decreases for decreasing Iribarren numbers. A decreasing Iribarren

number implies a gentler slope and/or steeper waves. Furthermore, a wide spreading can be observed in the existing empirical approaches to calculate the reflection coefficient for smooth and rough impermeable slopes. Battjes (1974b) presents an approach for plunging waves which depicts a steep gradient of increasing reflection coefficient for increasing Iribarren numbers. Stepped revetments with relative large step heights (exemplarily step ratios of $H_{m0}/S_h < 0.5$) show a comparable trend to that of Battjes (1974b). However, for Iribarren numbers larger than 5 the measurements deviate from Battjes' prediction and have a more or less constant reflection coefficient. The reflection coefficient for stepped revetments with step ratios larger than 0.5 ($H_{m0}/S_h \geq 0.5$) seem to follow the empirical approach by Postama (1989) for impermeable rock revetments. Data for a stepped revetment provided by Goda and Kishira (1976) confirm this trend. It is deduced that large step ratios H_{m0}/S_h behave more or less like a vertical wall. Small step ratios H_{m0}/S_h can be interpreted as a 'real' surface roughness. Therefore small step ratios show comparable reflection coefficients as rough impermeable rock slopes.

Since it was proven that the step ratio significantly influences the energy dissipation, the common approach which describes the reflection coefficient C_r as a function of only the Iribarren number $\xi_{m-1,0}$ is not sufficient. Therefore, the reflection coefficient C_r is given in Fig. 4.3 as a function of the slope $tan\alpha$, the wave height H_{m0} and the step geometry represented by $\sqrt{S_h^2 + S_w^2}$. The data are categorized with respect to the step ratio $H_{m0}/S_h \geq 0.5$ and $H_{m0}/S_h < 0.5$. The data is evidently sorted in two groups. The first group ($H_{m0}/S_h \geq 0.5$) indicates a decreasing reflection coefficient for increasing dimensionless step heights $\left(tan\alpha H_{m0}/\sqrt{S_h^2 + S_w^2}\right)$ for step ratios lower 0.5. However, the second group ($H_{m0}/S_h < 0.5$) shows an increasing reflection coefficient for increasing dimensionless step heights $\left(tan\alpha H_{m0}/\sqrt{S_h^2 + S_w^2}\right)$. These observations lead to the empirically derived equations

$$\text{for } \frac{H_{m0}}{S_h} < 0.5:$$
$$C_r = 0.47 + 1.18\frac{tan\alpha H_{m0}}{\sqrt{S_h^2 + S_w^2}}$$
$$\text{for } \frac{H_{m0}}{S_h} \geq 0.5:$$
$$C_r = 0.16 + 0.54 \cdot exp\left(11.55\frac{tan\alpha H_{m0}}{\sqrt{S_h^2 + S_w^2}}\right)^{-0.04}.$$

$$(4.4)$$

Outliers can be identified for $H/L < 0.015$. Underpredicted outliers correspond to Iribarren numbers $\xi > 8$. Fig. 4.4 gives an indication of the regression quality of Eq. (4.4) where the calculated reflection coefficient $C_{r,calc.}$ is plotted against the measured reflection coefficient $C_{r,meas.}$. The derived formula yields a coefficient of determination of $R^2 = 0.8$ with a corresponding standard deviation of $STD = 0.033$ and is valid for $0.015 < H_{m0}/L_{m-1,0} < 0.05$, $1 < \xi_{m-1,0} < 8$, $1 \leq cot\alpha \leq 3$ and $0.2 < H_{m0}/S_h < 30$. Hence, an acceptable prediction of the reflection coefficient can be achieved by the derived formula.
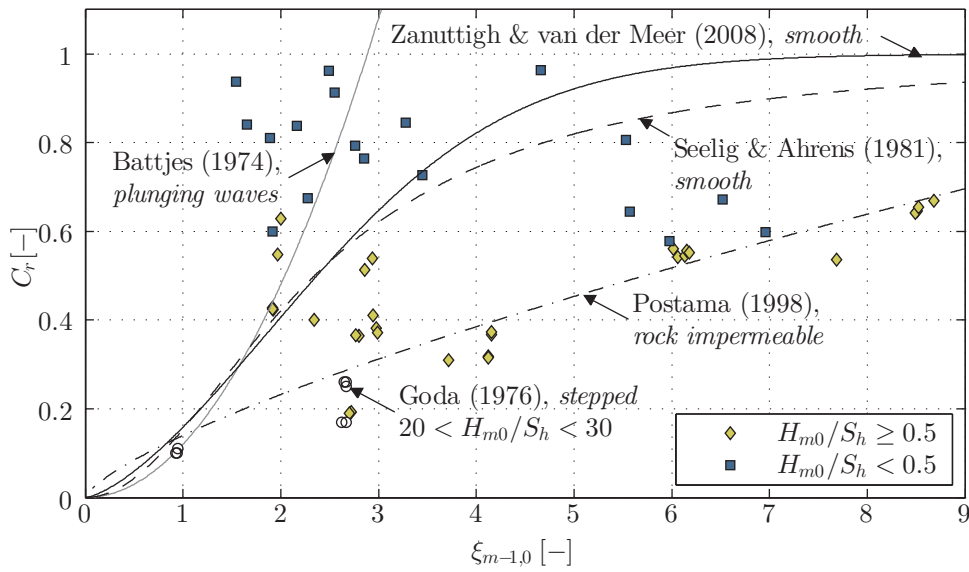
Figure 4.2: Wave reflection coefficients C_r with respect to the Iribarren number $\xi_{m-1,0}$ in comparison to theoretical approaches for smooth and rough surfaces.
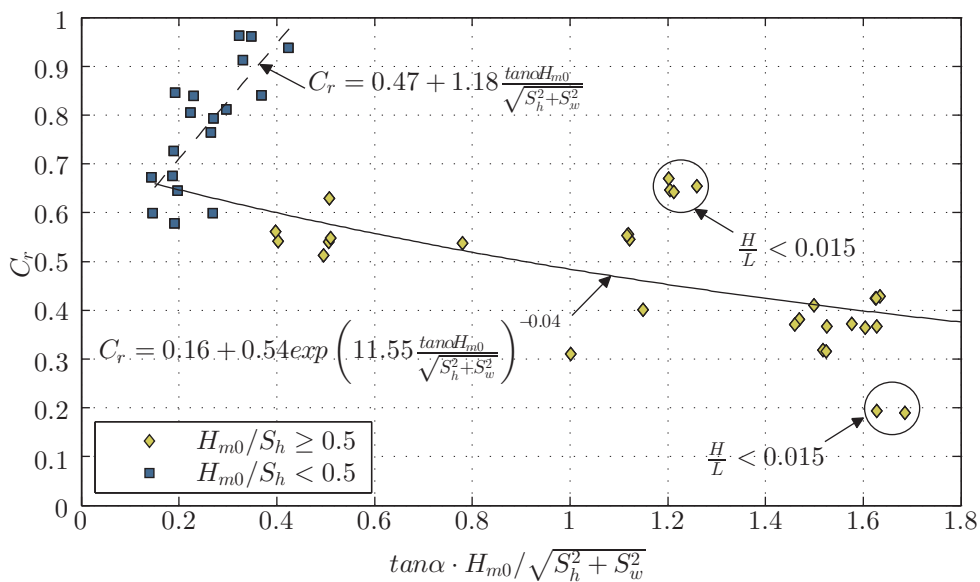
Figure 4.3: Wave reflection coefficients with respect to the step ratio.
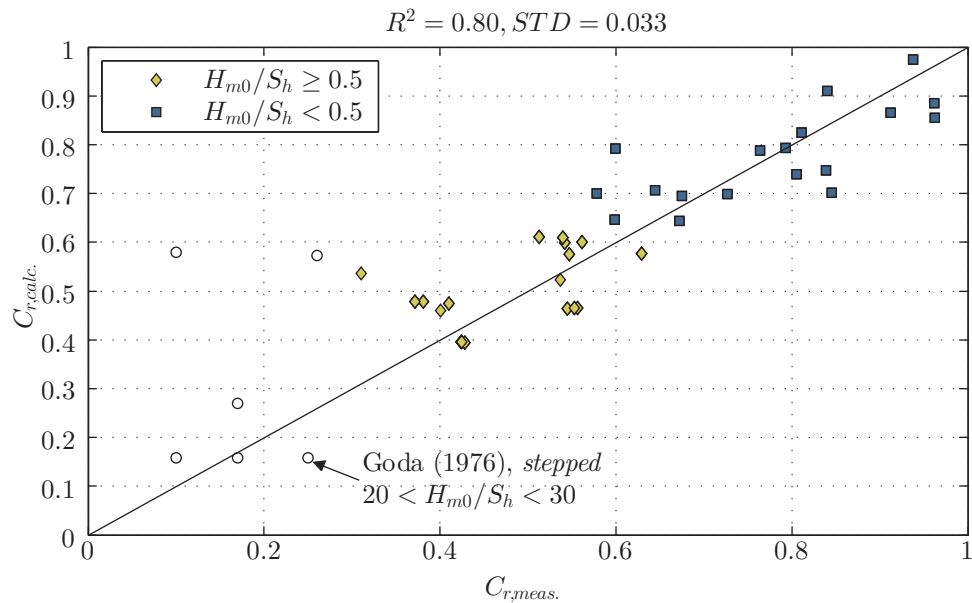
Figure 4.4: Regression quality.

Conclusion

The reflection for smooth and impermeable rock slopes given in literature clearly decreases with decreasing Iribarren number. The reflection at stepped revetments however deviate from this trend. Large step heights ($H_{m0}/S_h < 0.5$) show a comparable reflection to plain or composite vertical walls and can consequently be classified as highly reflective. Smaller step heights ($H_{m0}/S_h \geq 0.5$) in contrast tend to reflect like rough impermeable surfaces and are therefore moderately reflective.

4.2   Wave run-up

The wave run-up defined in Chapt. 2 is measured by run-up gauges (Chapt. 3).

All hydraulic- and geometry-related boundary conditions have a different influence on the wave run-up. Fig. 4.5 shows the exemplary influence of single parameters (H_{m0}, L_p and S_h) on the wave run-up height. The run-up $R_{u,2\%}$ increases linearly with increasing wave height H_{m0} (left), increasing wave length L_p (center) and decreasing slope n. A qualitative trend indication shows that the step height S_h has a nonlinear influence on the wave run-up (right). From the smallest step height (defined as zero, representing a plain slope) the run-up decreases for all slopes with increasing step height of the revetment. If the step height is larger than the wave height, the run-up becomes even higher than for a plain slope. This behavior can be explained if one considers that a step with infinite height represents a vertical wall. Consequently, the run-up is then equal to almost twice the wave height.

Fig. 4.6 displays the data dimensionless with the relative wave run-up $\frac{R_{u,2\%}}{H_{m0}}$ as a function
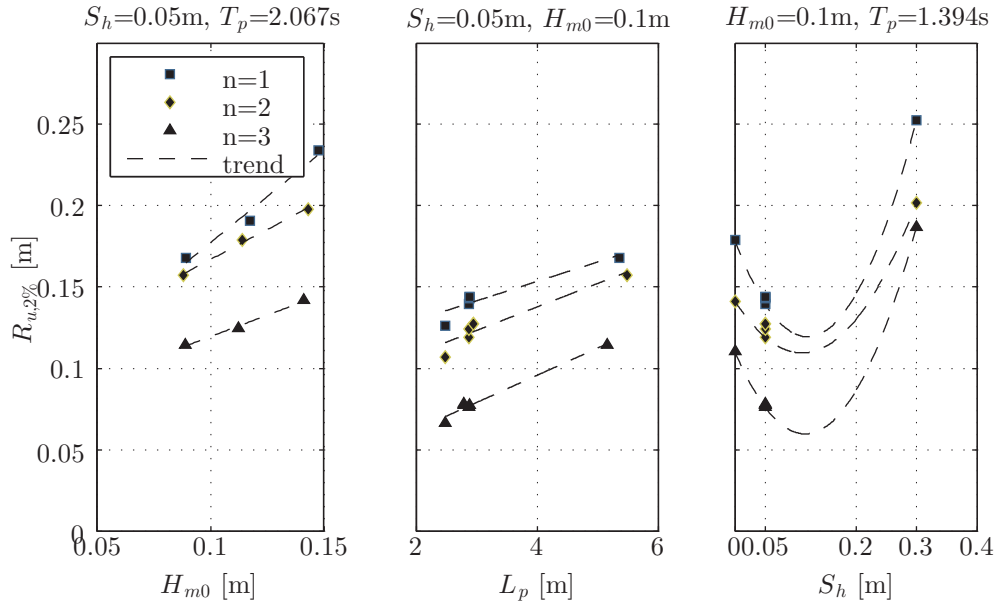
Figure 4.5: Exemplary development of run-up height $R_{u,2\%}$ for variation of wave height H_{m0} (left), wave length L_p (center) and step height S_h (right).

of the Iribarren number $\xi_{m-1,0}$. To assure representative data sets, only results for run-up tests at stepped revetments with more than 1,000 waves, a reflection coefficient smaller than 0.9 and a wave steepness larger than 0.015 are taken into account. Empirical formulations for run-up prediction at smooth slopes by Van der Meer and Janssen (1994), Schüttrumpf (2001) and Eurotop (2016) are given as reference. Generally, the dimensionless wave run-up height increases with an increasing Iribarren number for smooth and rough surfaces. Both tested step heights ($S_h = 0.05\,m$ and $0.3\,m$) – presented in the figure as two data sets with $H_{m0}/S_h \geq 1$ and $H_{m0}/S_h < 1$ – reveal a reduction of the relative wave run-up in comparison to a smooth slope[17]. In cases, where the wave height is larger than the step height ($H_{m0}/S_h \geq 1$) the run-up reduction is more effective. For plain slopes the breaker type plays a major role since the relative run-up increases more dominantly for plunging breakers than for surging breakers. On the contrary, this effect is less dominant for stepped revetments. The reason for this is a high turbulence in the wave run-up for all kinds of waves (breaking and non-breaking) over stepped revetments and therefore more similar energy dissipation performance. A regression with a hyperbolic tangent function (following the approach by Schüttrumpf (2001)) leads to the empirical derived formula to calculate the wave run-up at stepped revetments:

---

[17]Data sets for smooth slopes are available in the present study. Within the post processing it became apparent that the run-up for smooth slopes was not measured correctly as the distance between the run-up gauge and the smooth slope ($\approx 0.01\,m$) was too far to detect the real wave run-up height. Since the run-up gauges measured lower run-up values as present ($20-40\,\%$ deviation based on visual sample comprarision), it was decided to rather compare the results from the run-up measurements for stepped revetments to the empirical approaches for smooth slopes from literature.

$$\frac{R_{u,2\%}}{H_{m0}} = a \cdot tanh\left(b \cdot \xi_{m-1,0}\right).$$

$$\text{with: } a = 3.0, b = 0.65 \, for \, \frac{H_{m0}}{S_h} = \infty \text{ (Schüttrumpf, 2001)}$$

$$a = 2.6, b = 0.38 \, for \, \frac{H_{m0}}{S_h} \geq 1 \tag{4.5}$$

$$a = 2.0, b = 0.28 \, for \, \frac{H_{m0}}{S_h} < 1$$

The run-up reduction coefficient $\gamma_{f,R_{u,2\%}}$ is defined as the relation of the run-up at a stepped revetment to the run-up over a plain slope. Following the approach of Schüttrumpf (2001), Fig. 4.7 gives the run-up reduction factor as a function of the dimensionless step height $k_h/(H_{m0} \cdot \xi_{m-1,0})$. The data digitized from Saville (1955), Van Steeg et al. (2012) and Xiaomin et al. (2013) are presented since these studies contribute data for additional ranges of step ratios. The reduction coefficient decreases with an increasing dimensionless step height. The magnitude of influence is dominantly driven by the step ratio H_{m0}/S_h. The larger the wave height becomes with respect to the step height, the more energy is dissipated. With a regression analysis of the data, a correlation of the run-up reduction to the dimensionless step height can be derived as presented in the following equation:

$$\frac{R_{u,2\%}}{H_{m0}} = 3.0 \cdot tanh\left(0.65 \cdot \xi_{m-1,0}\right) \cdot \gamma_{f,R_{u2\%}}.$$

$$\text{with: } \gamma_{f,R_{u2\%}} = \left[1 - a \cdot atan\left(\frac{k_h \cdot b}{H_{m0} \cdot \xi_{m-1,0}}\right)\right] \cdot c$$

$$a = 1 - 0.97 \cdot atan\left(8.1\frac{H_{m0}}{S_h}\right) \tag{4.6}$$

$$b = 1 - \frac{1}{0.075} \cdot atan\left(0.6\frac{H_{m0}}{S_h}\right)$$

$$c = \begin{cases} \text{for } H_{m0}/S_h < 0.5: & 0.75 \\ \text{for } H_{m0}/S_h \geq 0.5: & 1 \end{cases}$$

By juxtaposition to Eq. (4.6) in Fig. 4.7 with the measured data, it is evident that trends are represented well (quantification defined later). [18] However, large deviations can be detected for the case where the wave height is equal to the step height. In this case, the relative distance to the SWL to the closest step edge becomes important as it significantly influences the transformation of the incident waves (wave reflection vs. wave breaking). This relationship is denoted by d_{st} hereafter. The parameter d_{st} is defined as positive for $d_{st} \leq S_h/2$ and as negative for $d_{st} > S_h/2$. The influence is discussed in Fig. 4.9.

The reduction coefficient is related to the dimensionless step height $(|d_{st}| \cdot \gamma_{f_{R_{u,2\%}},general}/k_h)$

---

[18]The missing data coverage for reduction coefficients smaller than $\gamma_f < 0.4$ is discussed at the end of this section.
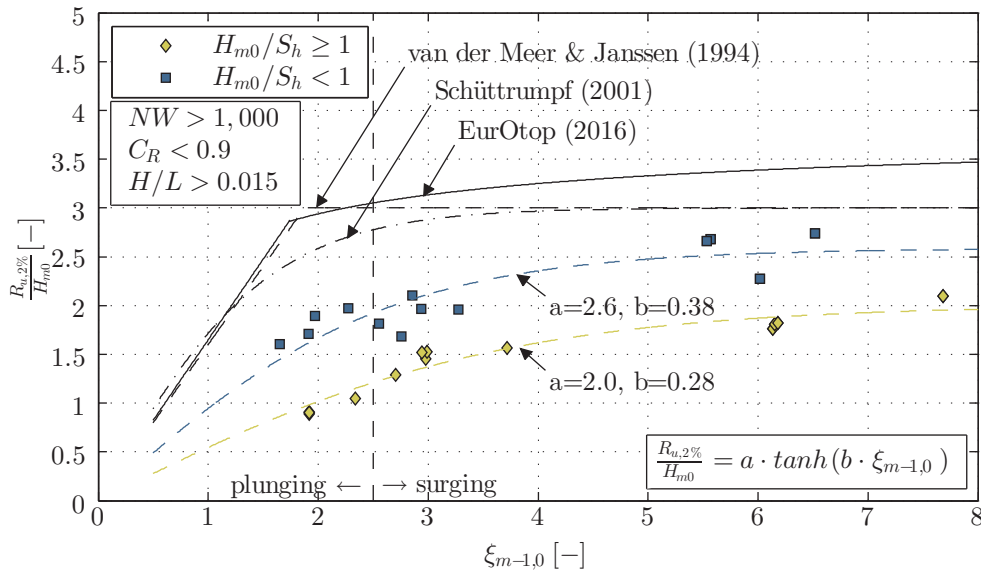
Figure 4.6: Relative wave run-up $\frac{R_{u,2\%}}{H_{m0}}$ over Iribarren number $\xi_{m-1,0}$ for stepped revetments in comparison to empirical formulae for smooth slopes by Van der Meer and Janssen (1994), Schüttrumpf (2001) and Eurotop (2016).
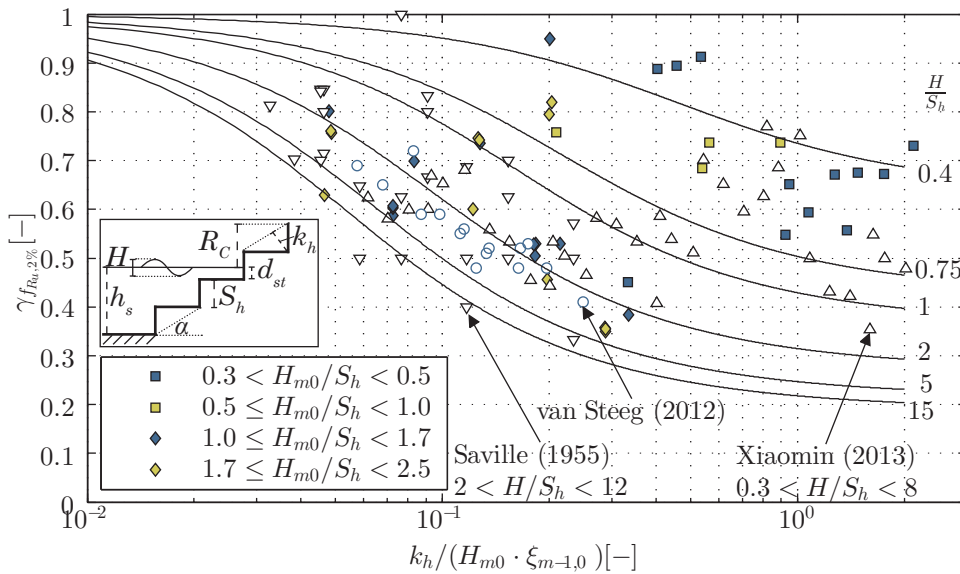
Figure 4.7: Run-up reduction coefficient $\gamma_{f,R_{u,2\%}}$ based on wave run-up over smooth slopes according to Schüttrumpf (2001) over step ratio.

where $\gamma_{f_{R_{u,2\%}},general}$ is equal to the reduction factor in Eq. (4.6) ($\gamma_{f_{R_{u,2\%}},\text{Eq.}(4.6)}$). Available data for $1 < H_{m0}/S_h < 2$ are given. Separate trends for surging and plunging wave breaking are identified. The physical processes are illustrated in Fig. 4.8. For surging waves $\gamma_{f_{R_{u,2\%}}}$ decreases with increasing distance between the SWL and the step edge. This behavior is due to the increasing vortex shedding on the step edge close to the SWL, which results in an increasing $|d_{st}| \cdot \gamma_{f_{R_{u,2\%}},general}/k_h$. For plunging waves, a large part of the wave energy is reflected at the step faces.

$$\text{for } 1 < H_{m0}/S_h < 2: \qquad \gamma_{f_{R_{u,2\%}}} = 0.65 + (1.4 \cdot B_r)\left(\frac{|d_{st}| \cdot \gamma_{f_{R_{u,2\%}},general}}{k_h} - 0.5\right)^2$$

$$\text{with: } \gamma_{f_{R_{u,2\%}},general} = \gamma_{f_{R_{u,2\%}},\text{Eq.}(4.6)}$$

$$\text{for: } \frac{H_{m0}}{L_{m-1,0}} \geq 0.015: \quad B_r = 1$$

$$\text{for: } \frac{H_{m0}}{L_{m-1,0}} < 0.015: \quad B_r = 1.4$$

(4.7)

Fig. 4.10 shows the regression quality of the wave run-up prediction at stepped revetments for Eq. (4.6)-(4.7) with respect to the measured values. The derived formula gives a coefficient of determination of $R^2 = 0.70$ with a corresponding standard deviation of $STD = 0.051$ and is valid for $0.01 < H_{m0}/L_{m-1,0} < 0.05$, $1.5 < \xi_{m-1,0} < 7.5$, $1 cot\alpha 3$ and $0.2 < H_{m0}/S_h < 15$. Fig. 4.10 does not include the data by Saville (1955) and Xiaomin et al. (2013) since these studies are based on tests with regular waves. If one also takes the regular wave data sets into account, the coefficient of determination would reduce to $R^2 = 0.42$. However, the standard deviation remains $STD = 0.048$. Therefore, a prediction for regular waves is possible with the derived equations but is not taken into account for the final evaluation of the results. It can be concluded that an acceptable prediction of the dimensionless wave run-up height can be achieved by the derived formula.

Conclusion

Stepped revetments can reduce the wave run-up in a range of $10 - 60\%$ in comparison to a plain slope. The reduction coefficient $\gamma_{f_{R_{u,2\%}}}$ decreases for an increasing dimensionless step height ($k_h/(H_{m0} \cdot \xi_{m-1,0})$). The run-up reduction of a stepped revetment is more effective if the step height is smaller than the wave height ($30 - 60\%$ for $H_{m0}/S_h \geq 1$ and $10 - 40\%$ for $H_{m0}/S_h < 1$).

$H/L = 0.016$
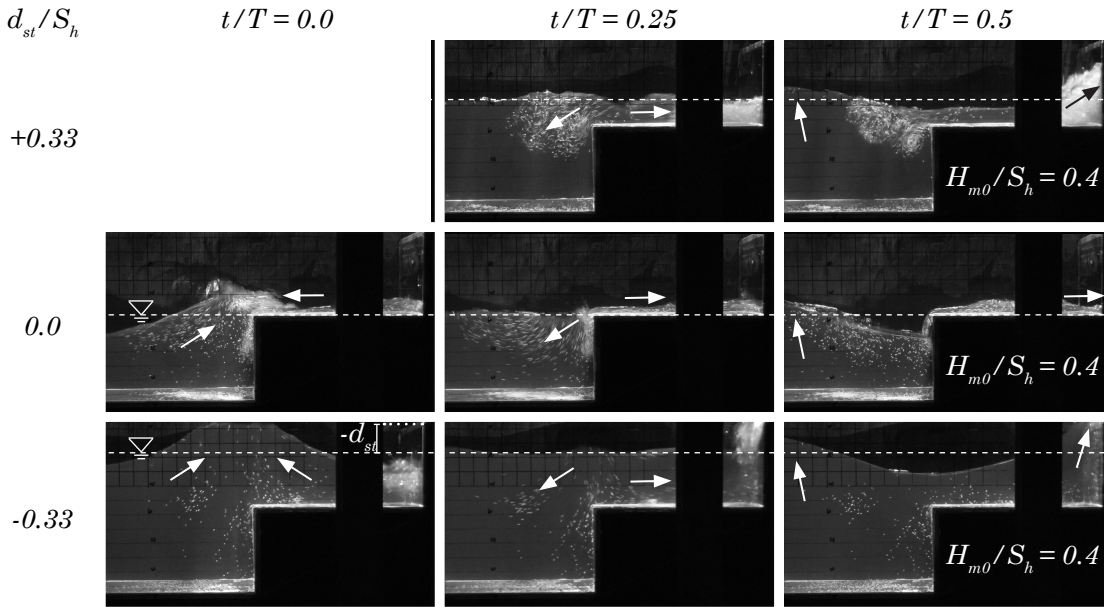
$H/L = 0.065$
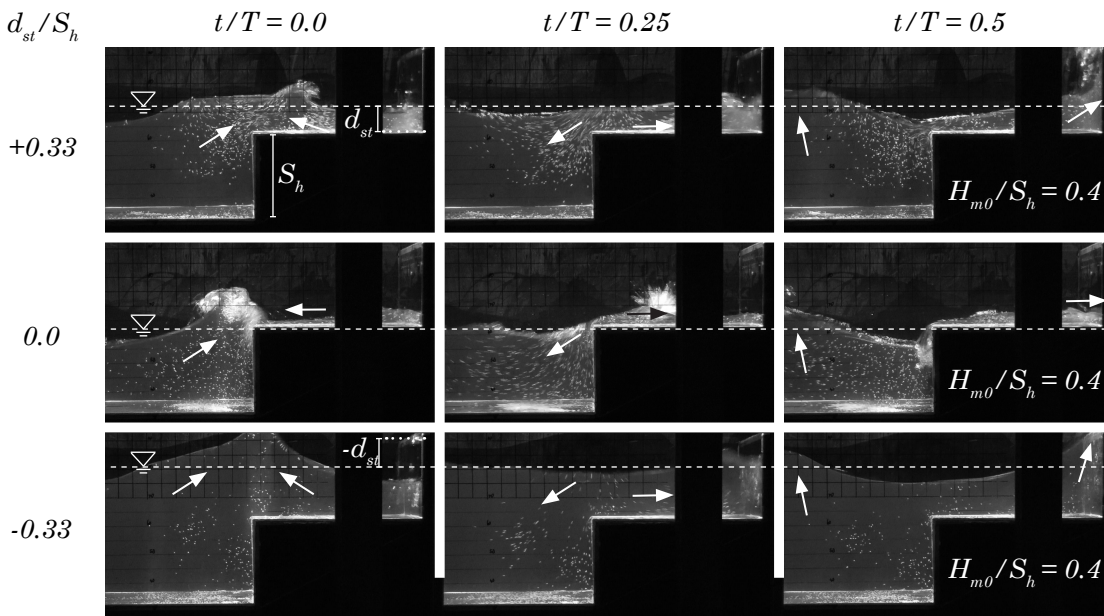
Figure 4.8: Flow processes over a step with $H_{m0}/S_h = 0.4$ for three different positions of the still water level.
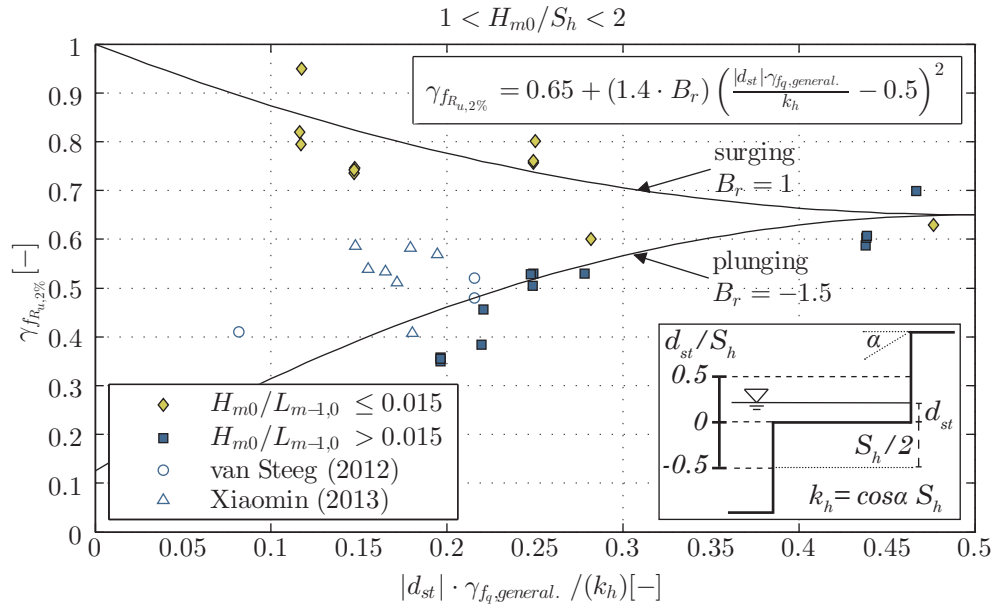
Figure 4.9: Run-up reduction coefficient $\gamma_{f_{R_{u,2\%}}}$ based on wave run-up over smooth slopes according to Schüttrumpf (2001) over step ratio.
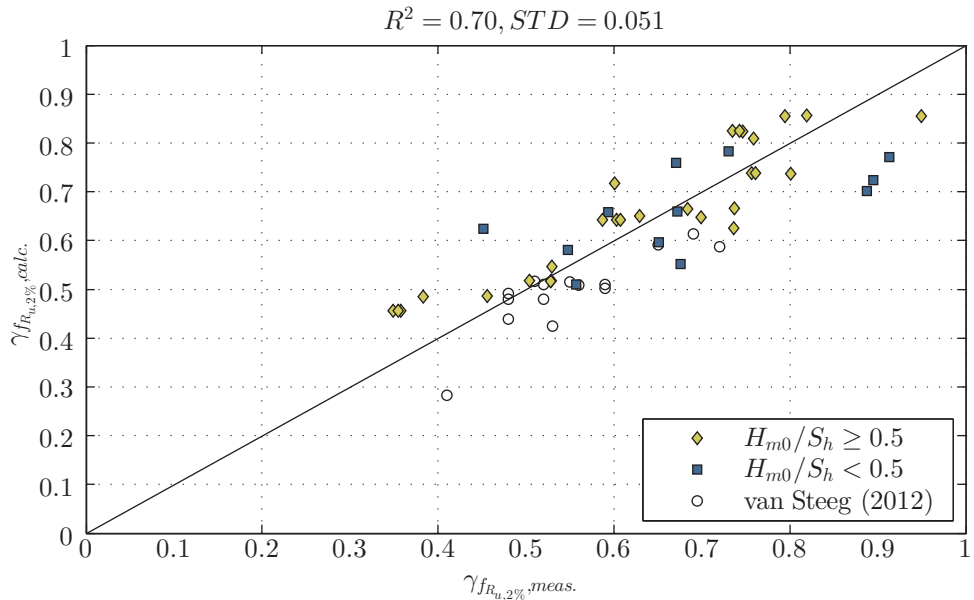
Figure 4.10: Regression quality of the wave run-up prediction at stepped revetments.

4.2.1 Asymptotic analysis

Xiaomin et al. (2013) and Treuel (2013) supposed an optimum in the run-up reduction for a specific relation of wave height and step height. A re-analysis of the data provided by Xiaomin et al. (2013) and Treuel (2013) (section 2.5.1, (Kerpen et al., 2014)) leads to an optimum for $H_{m0}/S_h \approx 2$. Fig. 4.7 (and Fig. 2.16(d), page 48) indicates the presence of such a minimal turning point of the reduction coefficient $\gamma_{f_{R_{u,2\%}}}$ for the dimensionless step height $k_h/(H_{m0} \cdot \xi_{m-1,0}) \approx 0.25$. In the following, it is discussed why an optimum in the run-up reduction occurs.

The reduction coefficient $\gamma_{f_{R_{u,2\%}}}$, calculated with Eq. (4.6), decreases for a constant step ratio H_{m0}/S_h with increasing dimensionless step height $k_h/(H_{m0} \cdot \xi_{m-1,0})$. The dimensionless step height is equivalent to:

$$\frac{k_h}{H_{m0} \cdot \xi_{m-1,0}} \; \hat{=} \; \frac{cos\alpha \cdot S_h}{H_{m0} \cdot \frac{tan\alpha}{\sqrt{\frac{H_{m0}}{L_{m-1,0}}}}} \; \hat{=} \; \frac{cos\alpha \cdot n \cdot \sqrt{\frac{H_{m0}}{L_{m-1,0}}}}{\frac{H_{m0}}{S_h}}. \tag{4.8}$$

If the step ratio H_{m0}/S_h is kept constant (as for the given curves in Fig. 4.7) the run-up reduction coefficient $\gamma_{f_{R_{u,2\%}}}$ is only dependent on the Iribarren number. It can be concluded that the reduction coefficient decreases with increasing Iribarren number. The decrease is more dominant for larger step ratios (H_{m0}/S_h).

If the slope n of the revetment is kept constant, the run-up reduction coefficient $\gamma_{f_{R_{u,2\%}}}$ is dependent on the step ratio (H_{m0}/S_h) and the wave steepness ($H_{m0}/L_{m-1,0}$). The influence of the slope n on the run-up reduction coefficient is discussed in Fig. 4.11. Beside curves for constant relative wave heights, seven curves for constant slopes ($1 \leq n \leq 30$) and a constant Iribarren number ($\xi_{m-1,0} = 2$) are given. It can be concluded that the run-up reduction coefficient $\gamma_{f_{R_{u,2\%}}}$ decreases with increasing slope n due to increased energy dissipation on the extended slope length. Furthermore, a relative minimum is present for a step ratio of $H_{m0}/S_h = 2$ for all slopes. Slopes gentler than $n \geq 3$ have no additional effect on the run-up reduction. This is caused by shallower wave steepnesses ($H_{m0}/L_{m-1,0} \leq 0.027$).

If the Iribarren number – considering the differences in the wave breaking due to incorporation of slope and wave steepness – is kept constant, the run-up reduction coefficient $\gamma_{f_{R_{u,2\%}}}$ is dependent on the step ratio (H_{m0}/S_h) and the slope (n). The influence of the Iribarren number $\xi_{m-1,0}$ on the run-up reduction coefficient is discussed in Fig. 4.12. Beside curves for constant relative wave heights, seven curves for constant Iribarren numbers ($1 \leq \xi_{m-1,0} \leq 10$) and a constant slope ($n = 3$) are given. The run-up reduction coefficient $\gamma_{f_{R_{u,2\%}}}$ decreases with decreasing Iribarren number. This trend is plausible, as plunging waves ($\xi_{m-1,0} < 2.5$) are much more turbulent then surging waves ($\xi_{m-1,0} > 2.5$). For large Iribarren numbers ($\xi_{m-1,0} = 10$) the run-up reduction coefficient is low (0.8-0.9). A minimal turning point is present for a step ratio of $H_{m0}/S_h = 2$ for all Iribarren numbers. The finite maximum value of the wave steepness (theoretically: $s_{max} = 1/7$, (Miche,
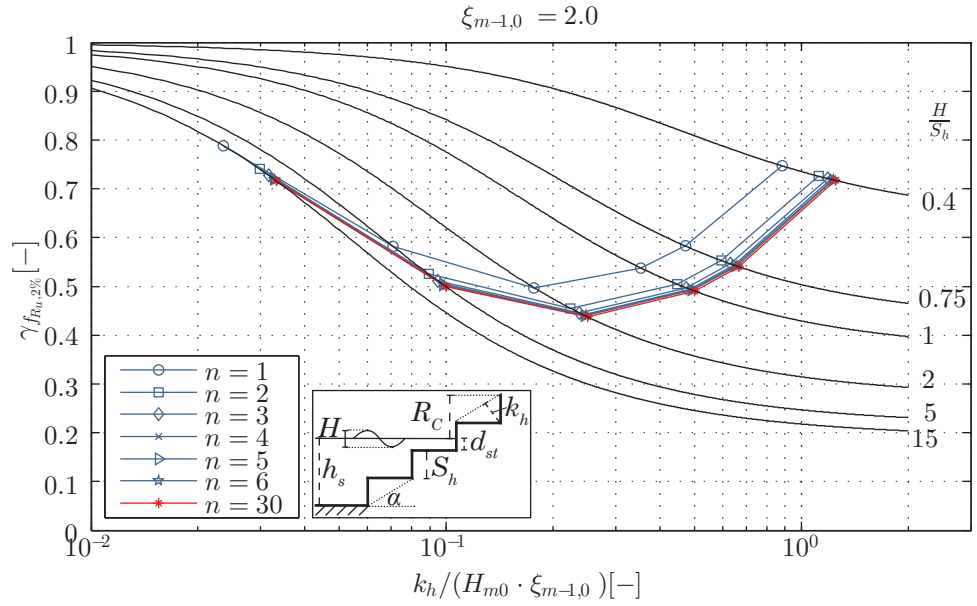
Figure 4.11: Influence of the slope n for $\xi_{m-1,0} = 2.0$ on the run-up reduction coefficient $\gamma_{f_{R_{u,2\%}}}$ (data for further Iribarren numbers in appendix H).

1944)) has to be considered. Therefore, the calculated wave steepnesses given on the right hand side of the red dotted line are invalid for the given slope ($n = 3$).

In a final step, the present findings are proven on the available data (Fig. 4.13). The data confirm the steepness limitation in the run-up reduction. In this way of presentations ($\gamma_{f_{R_{u,2\%}}}$ versus $k_h/(H_{m0} \cdot \xi_{m-1,0})$) a dimensionless step height with values larger than one is only meaningful for $H_{m0}/S_h < 1$ (due to the steepness limitation). The minimal value of the reduction coefficient $\gamma_{f_{R_{u,2\%}},min}$ was supposed to correspond with a dimensionless step height of $k_h/(H_{m0} \cdot \xi_{m-1,0}) = 0.25$. The new findings show that this value represents only the result of present available data. The discussed correlations clearly feature the minimum run-up reduction coefficient for a step ratio of $H_{m0}/S_h = 2$.

Conclusion

The optimum correlation between wave height and step height to reduce the wave run-up most effectively is derived to $H_{m0}/S_h = 2$. The run-up reduction coefficient $\gamma_{f_{R_{u,2\%}}}$ decreases with gentler slopes and shows no further significant decrease for ($n > 3$). The run-up reduction coefficient $\gamma_{f_{R_{u,2\%}}}$ decreases for steeper waves ($H/L \to 1/7$) and for larger step ratios ($H_{m0}/S_h \to 15$).
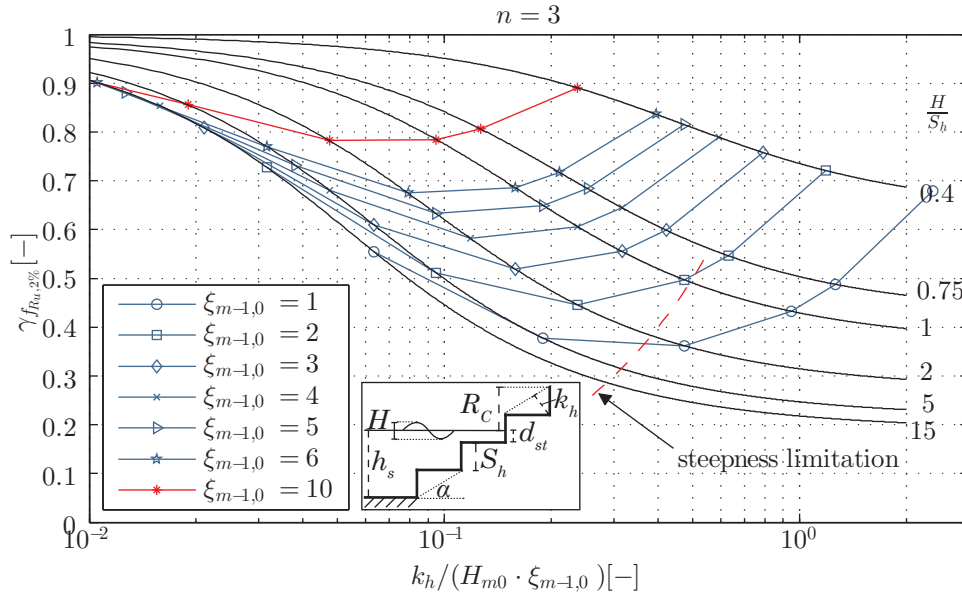
Figure 4.12: Influence of the Iribarren number $\xi_{m-1,0}$ for $n = 3$ on the run-up reduction coefficient $\gamma_{f_{R_{u,2\%}}}$ (data for further slopes in appendix H).
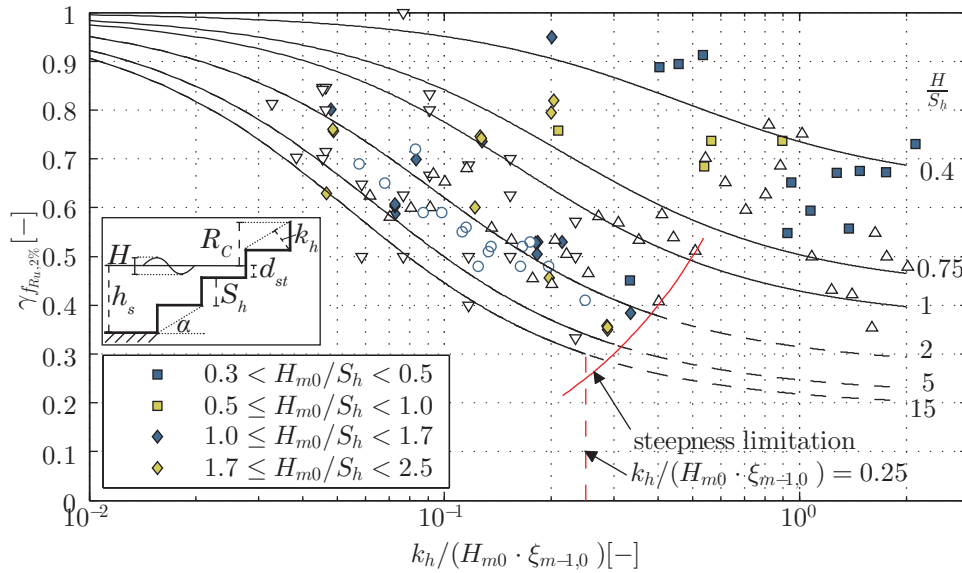
Figure 4.13: Limitation of the minimum reduction coefficient $\gamma_{f_{R_{u,2\%}}}$ due to finite maximum values for the wave steepness.

4.3 Wave overtopping

All hydraulic- and geometry-related boundary conditions have a different influence on the wave overtopping. Generally, all results from tests with zero overtopping have been eliminated in the data analysis. Firstly, the overtopping discharge per meter crest length ($q\left[\frac{l}{sm}\right]$) is displayed in Fig. 4.14 as a function of the relative freeboard height (R_c/H_{m0}). The graph displays data for a smooth surface and stepped revetments with two different step heights ($S_h = 0.05\,m$ and $S_h = 0.3m$). For all geometries the discharge decreases with increasing dimensionless freeboard height or more directly expressed with increasing freeboard height R_c or decreasing wave height H_{m0}. Furthermore, the single data sets present some scatter. To assure data quality, only results of test runs with more than 1,000 waves and a minimum wave height of $H_{m0} = 0.04\,m$ are taken into account.

To sufficiently compare the measured data from previous studies, the overtopping data are displayed dimensionless in Fig. 4.15. The dimensionless wave overtopping volume $q/(gH_{m0}^3)^{0.5}$ is given in a semi-logarithmic scale versus the dimensionless freeboard height R_c/H_{m0}. The dimensionless overtopping volume decreases with increasing dimensionless freeboard height for smooth and stepped slopes. As expected, the dimensionless overtopping volumes for smooth slopes are always larger than for stepped slopes with the same relative freeboard height. No clear trend for different step geometries can be seen in this graph. The black line represents the best fit regression of the measured overtopping volumes with a smooth slope leading to

$$\frac{q}{\sqrt{gH_{m0}^3}} = 0.04exp\left[\left(-1.1\frac{R_c}{H_{m0}}\right)^{1.4}\right] \tag{4.9}$$

valid in a range of $1.0 < \frac{R_C}{H_{m0}} < 3.5$.

In a comparison to the best fit of Van der Meer and Bruce (2014), it can be seen that the measured overtopping rates for smooth slopes are slightly larger. Therefore, the reduction coefficient $\gamma_{f,q}$ is derived according to Eq. (2.19) to guarantee a valid prediction of the reduction coefficient, thereby considering boundary conditions of the present tests. It is known that wave breaking significantly affects wave overtopping. Therefore, the calculated $\gamma_{f,q}$–values are given in Fig. 4.16 with respect to the Iribarren number $\xi_{m-1,0}$. Data are separated for cases with small step heights ($H_{m0}/S_h \geq 0.5$) and large step heights ($H_{m0}/S_h \geq 0.5$). Results by Van Steeg et al. (2012) ($1.5 < H_{m0}/S_h < 6.5$) and Goda and Kishira (1976) ($20 < H_{m0}/S_h < 30$) extend the database.

For all tests the reduction coefficient γ_{f_q} decreases with decreasing Iribarren number. All tests with values $H_{m0}/S_h \geq 0.5$ follow roughly the same trend. The reduction factors for step heights much larger than the wave height are however in a constant range of $0.88 < \gamma_{f_q} < 0.98$. Hence, a first simplified approach to predict the reduction coefficient for a stepped revetment with step ratios $H_{m0}/S_h \geq 0.5$ can be given with

$$\begin{aligned} \gamma_{f_q} &= 0.1 \cdot \xi_{m-1,0} + 0.3 \text{ (probabilistic)} \\ \gamma_{f_q} &= 0.07 \cdot \xi_{m-1,0} + 0.5 \text{ (deterministic)} \end{aligned} \tag{4.10}$$
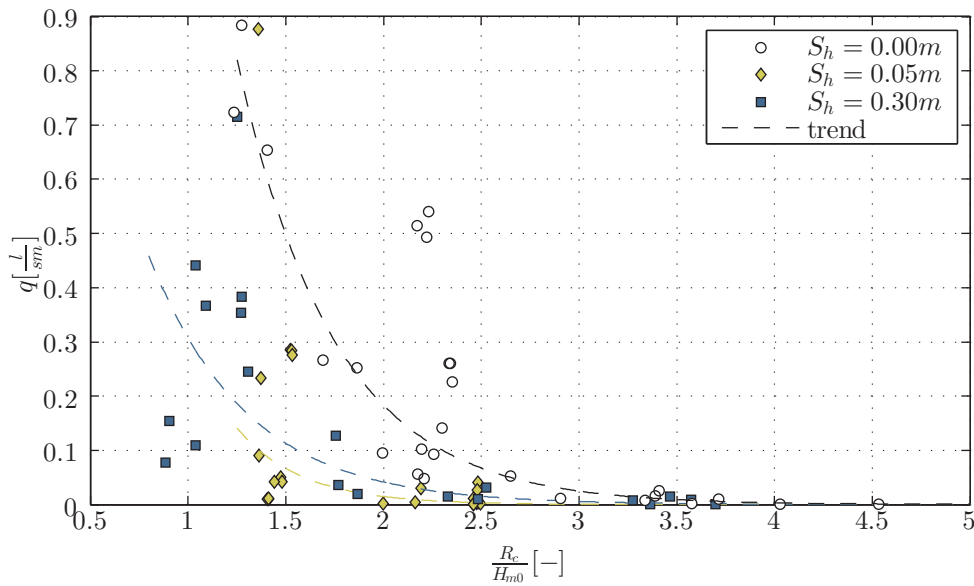
Figure 4.14: Overtopping discharge per meter crest length and second over relative freeboard height.
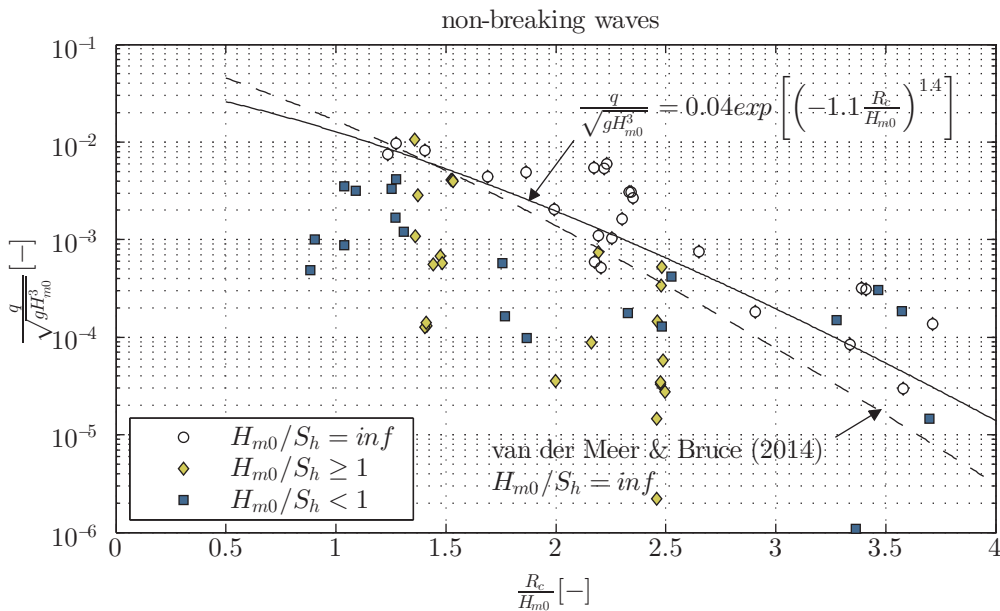
Figure 4.15: Relative overtopping discharge over relative freeboard height.
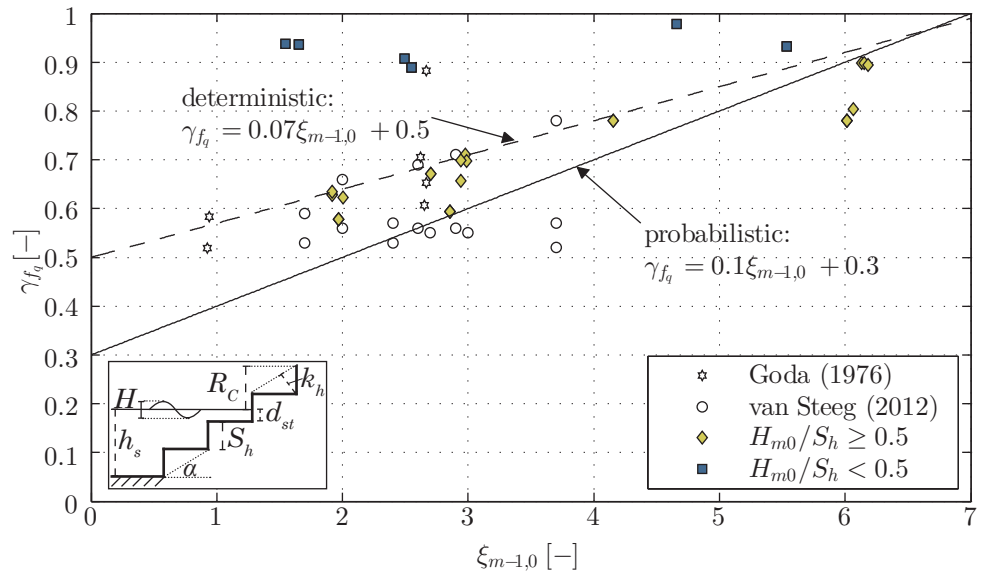
Figure 4.16: Influence of the Iribarren number $\xi_{m-1,0}$ on the reduction coefficient γ_{f_q}.

Nevertheless, data scatter by $\pm 30\,\%$ for this prediction. A more thorough analysis of variables (geometry and hydraulic boundary related) will clarify the reason for the scatter of this simple prediction.

As the ratio of wave height H_{m0} to step height S_h differs in many tests the influence of the dimensionless step height will be analyzed next. To take the slope of the revetment into account a characteristic step diameter is defined as

$$k_h = cos\alpha \cdot S_h. \tag{4.11}$$

The characteristic step diameter (k_h) is defined as the shortest distance between an imaginary straight line between two step edges and the step niche in-between (Fig. 4.16). Since the Iribarren number has a strong influence on the processes, it also is included. Fig. 4.17 gives the reduction coefficient γ_{f_q} versus the dimensionless step height $k_h/(H_{m0}\xi_{m-1,0})$. Due to the wide range of dimensionless step heights and an accumulation of data points for relative low values, the abscissa is given in a logarithmic scale from 0.01 to 2. For a better orientation in the diagram, regression lines according to Eq. (4.12) are given for a range of step ratios H_{m0}/S_h. The reduction coefficient decreases for increasing dimensionless step heights for the given correlation. The decay of the reduction coefficient is more dominant for decreasing dimensionless step heights. The minimal value for the reduction coefficient is dependent on the dimensionless step height and tends to $\gamma_{f_q} \approx 0.4$. The dependencies of the reduction coefficient and the dimensionless step height can be described in a hyperbolic tangent correlation as
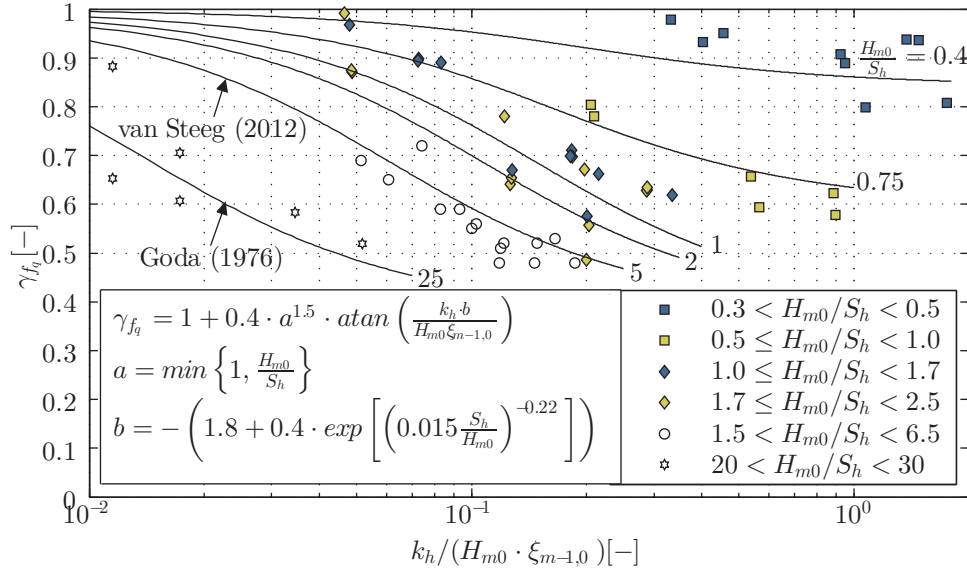
Figure 4.17: Overtopping reduction coefficient $\gamma_{f,q}$ over dimensionless step height.

$$\gamma_{f_q} = 1 + 0.4 \cdot a^{1.5} \cdot atan\left(\frac{k_h \cdot b}{H_{m0}\xi_{m-1,0}}\right)$$

$$a = min\left\{1, \frac{H_{m0}}{S_h}\right\} \tag{4.12}$$

$$b = -\left(1.8 + 0.4 \cdot exp\left[\left(0.015\frac{S_h}{H_{m0}}\right)^{-0.22}\right]\right)$$

where the factors a and b express the additional influence of the step ratio on the process. The applicability of Eq. (4.12) can be confirmed in Fig. 4.17 for $1.0 > H_{m0}/S_h > 2.5$.

Clear deviations are identified for $1.0 < H_{m0}/S_h < 2.5$. In this range an additional parameter plays an important role. This parameter can be identified as the relative position of the still water level to the nearest step edge denoted by d_{st} hereafter. If wave height and step height are almost equal, the hydrodynamic processes (wave breaking, run-up, run-down) differ for varying water levels. The different processes are given in Fig. 4.8 as an example. The parameter d_{st} is defined as positive for $d_{st} \leq S_h/2$ and as negative for $d_{st} > S_h/2$. For positive values the incident wave interacts with the reflected wave on the highest submerged step. Hence, high turbulence significantly reduces the energy of the incident wave. For values equal to zero or slightly negative, a larger part of the energy of the incident wave is reflected and a limited amount of water is running up the slope. For values close to $d_{st} = -0.5$, most of the energy of the incident wave is reflected and a small amount of energy dissipates by vortex shedding at the submerged step edge. To take these effects into account the reduction coefficient is related to the dimensionless step height $|d_{st}| \cdot \gamma_{f_q,general}/k_h$ where $\gamma_{f_q,general}$ equals $\gamma_{f_q,Eq.(4.12)}$ in Fig. 4.18. Available data for $0.5 < H_{m0}/S_h < 2.5$ are given. The lowest value of γ_{f_q} is measured for dimension-

less step heights between 0.2 and 0.3. The reduction factor γ_{f_q} increases for increasing dimensionless step heights.

$$\text{for } 0.5 < H_{m0}/S_h < 2.5: \qquad \gamma_{f_q} = 0.6 + 2.3 \left(\frac{|d_{st}| \cdot \gamma_{f_q,general}}{k_h} \right)^2 \tag{4.13}$$

$$\text{with: } \gamma_{f_q,general} = \gamma_{f_q,\text{Eq.(4.12)}}$$

The quality of Eq. (4.12) and Eq. (4.13) is discussed in Fig. 4.19. Measured values $\gamma_{f_q,meas.}$ are correlated with calculated reduction coefficients $\gamma_{f_q,calc.}$. A coefficient of determination of $R^2 = 0.82$ is evidence of a good correlation. The standard deviation of the method is $STD = 0.046$. The formula is valid for $0.01 < H_{m0}/L_{m-1,0} < 0.05$, $1 < \xi_{m-1,0} < 6.5$, $1 \leq cot\alpha \leq 3$, $1 < R_c/H_{m0} < 3.5$ and $0.2 < H_{m0}/S_h < 30$. The derived reduction coefficient is substituted in the prediction of the wave overtopping in Eq. (4.9) describing the wave overtopping on a smooth slope by

$$\frac{q}{\sqrt{gH_{m0}^3}} = 0.04 exp \left[- \left(1.1 \frac{R_c}{H_{m0}\gamma_{f,q}} \right)^{1.4} \right] . \tag{4.14}$$

If differences between Eq. (4.9) for the measured overtopping rates at the smooth slope form this study and the predicted values according to Eq. (2.16) provided by Van der Meer and Bruce (2014) are admitted Eq. (4.12) is also valid for the generic Van der Meer and Bruce (2014) formula.

Conclusion

Stepped revetments can reduce the wave overtopping volume in comparison to a smooth slope. The effectiveness mainly depends on the step ratio H_{m0}/S_h and the Iribarren number. If the step height is two times larger than the incident wave height, the revetment is reflective and the wave overtopping cannot be reduced significantly $(2 - 10\%)$. Due to the macro roughness of a stepped revetment the overtopping volume of plunging breakers can be reduced most effectively $(40 - 60\%)$ since most of the energy is dissipated by the wave breaking. The wave run-up, and as a consequence the wave overtopping, is reduced significantly since the wave run-up with a relatively low energy content is disturbed by the stepped surface. Thus, the effectiveness of reducing the wave overtopping volume for collapsing and surging wave breaking decreases $(10 - 30\%)$ for a more gentle wave steepness and increasing Iribarren number. The position of the SWL with respect to the step edge becomes important if step height and wave height are in the same range $(0.5 < H_{m0}/S_h < 2.)$. In this case the highest energy dissipation can be achieved if the SWL is close to the step edge.
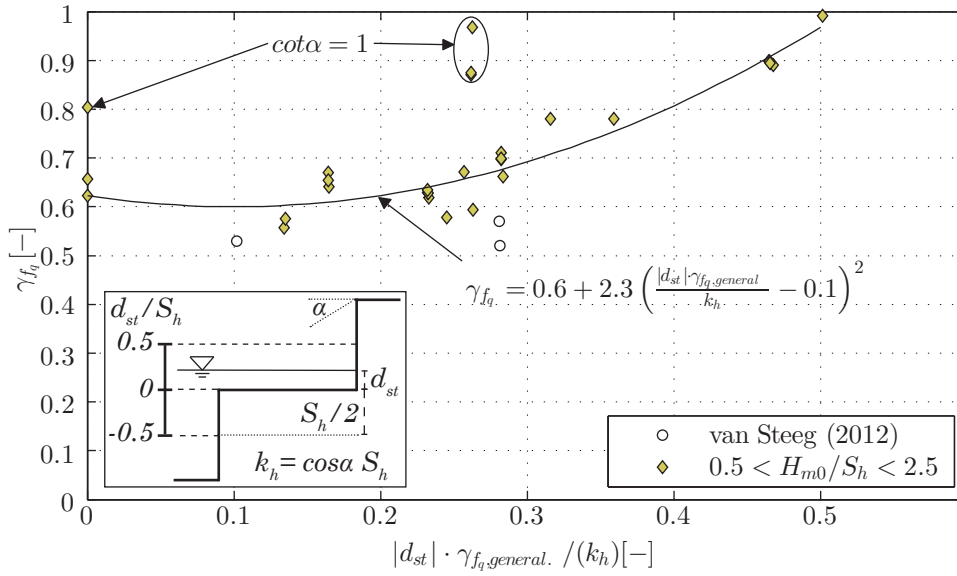
Figure 4.18: Influence of the relative position to the still water level on the reduction coefficient γ_{f_q} for step ratios in a range of $0.5 < H_{m0}/S_h < 2.5$.
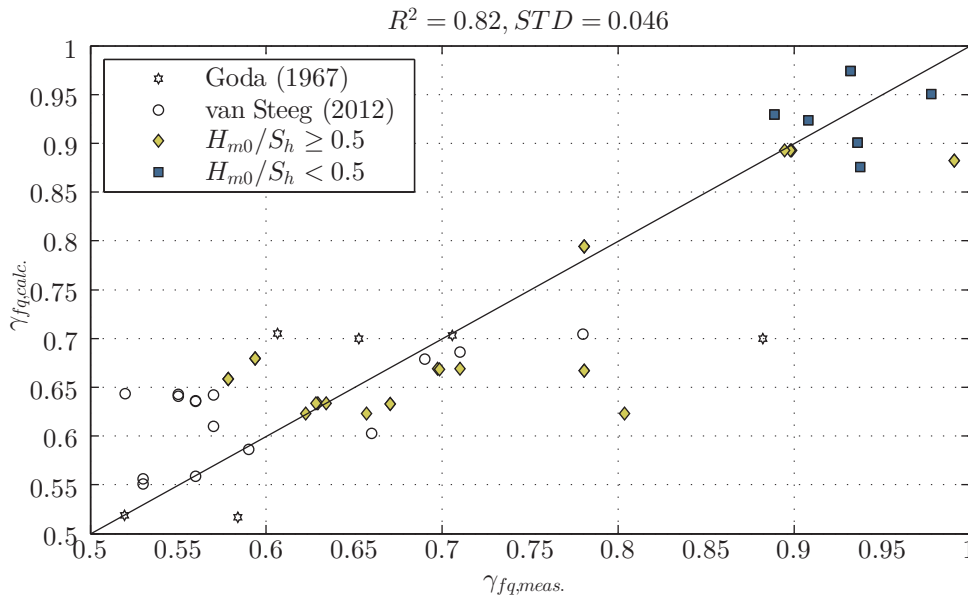
Figure 4.19: Correlation between measured and calculated reduction coefficients γ_{f_q} according to Eq. (4.12) and Eq. (4.13).

4.4 Wave loads

Wave loads have been measured on the 1:2 inclined stepped revetment. The measurements were taken by pressure sensors which were placed along the horizontally and vertically orientated step faces. This section derives the horizontal impact forces by waves.

Every single wave in a wave spectrum generates an individual impact on the structure. The magnitude of the impact depends on its individual wave kinematics and the influence of the previous wave (remaining water layer over a pressure sensor and amount of aeration in the wave). The analysis of wave loads can include a number of parameters such as maximum pressure or a mean pressure. The maximum induced pressure P_{max} is very important for the design of a structure. But, a comparison between single tests is less convincing since the maximum values scatter significantly from test to test. Therefore, the pressures will rather be described with a probability of exceedance (e.g. 2% of all waves $p_{2\%}$). This approach is more representative.

In order to compare the measured data to data from previous investigations, the pressure values as an average of the 4 highest waves out of a 1,000-wave test should be calculated. Hence, $p_{0.4\%}$ is calculated. In Fig. 4.20 the normalized pressure impact $p_{0.4\%}/(\rho g H_{m0})$ is given on the abscissa and the relative position to the SWL (z/H_{m0}) on the ordinate. For both step heights ($S_h\{0.05\,m, 0.3\,m\}$) the maximum pressure impact is close to the SWL. The maximum pressure decreases significantly within a range of $\pm H_{m0}$, mainly in the range of $\pm 2H_{m0}$. For comparison, a reference line for the horizontal impact forces (mean of the four highest measurements out of 1,000 waves) as described by Cuomo et al. (2010) (Eq. (2.32)) is drawn. Corresponding single data points – not given in this figure – scatter significantly along the abscissa. The $p_{2\%}$ wave loads measured over a stepped revetment tend to be about 50% smaller than those measured at a vertical wall. On the contrary the steps at the SWL show pressures comparable to those measured on a vertical wall.

Two functions are fitted to the data ($R^2 = 0.62$, $STD = 0.189$) to describe the correlation of the pressure evolution and the vertical position of the wave loads along the water depth in a range of $0.01 < p_{0.4\%}/(\rho g H_{m0}) \le 3.6$ with

$$
\begin{aligned}
&\text{above } SWL: \\
&\frac{p_{0.4\%}}{\rho g H_{m0}} = min\left\{ 2831.66 + tan\left(\frac{\frac{z}{H_{m0}} + 1171.64}{74572}\right), 3.6 \right\} \\
&\text{below } SWL: \\
&\frac{p_{0.4\%}}{\rho g H_{m0}} = min\left\{ 6.15 + tan\left(-\frac{\frac{z}{H_{m0}} - 4.97}{2.87}\right), 3.6 \right\}.
\end{aligned}
\tag{4.15}
$$

Single wave load events (Fig. 4.21) can be separated into three phases. At the beginning of the impact ($0 \le t/T <\approx 0.005$) the pressure rises rapidly to a peak. The peak is followed by a decay phase ($\approx 0.005 < t/T <\approx 0.1$) which is dependent on the stiffness of the structure.
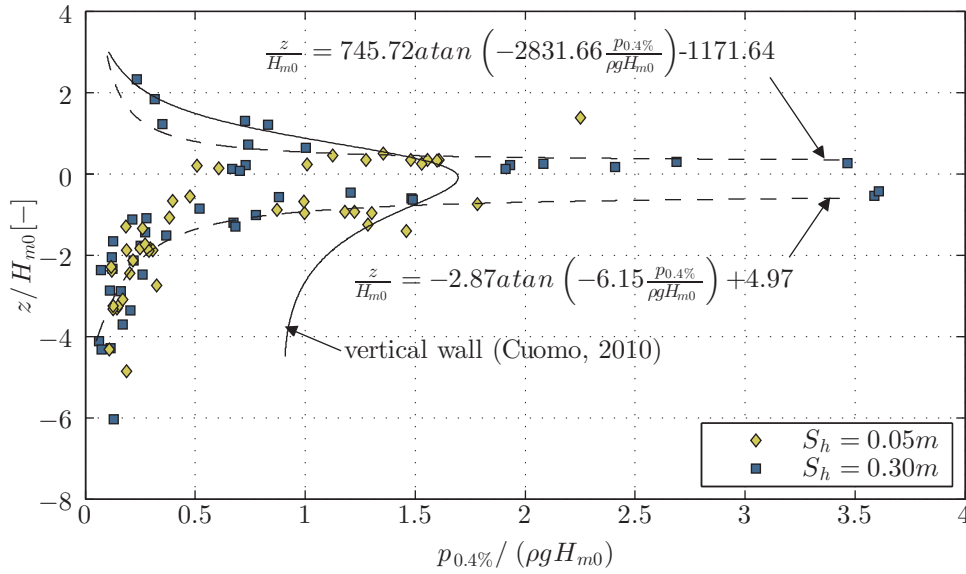
Figure 4.20: Normalized pressure impact as a function of the relative position around the still water level $(z/H_{m0} = 0)$ for a stepped revetment.

The third phase is the pressure plateau $(t/T \approx 0.1 - 1)$ which is mainly caused by the hydro-static pressure of the wave run-up on the structure. These findings are comparable with the ones by Heimbaugh (1988) (short-duration pressure shock $< 0.02\,s$ followed by an about 90% smaller secondary pressure magnitude with a duration of $2-3\,s$). The pressure evolution is very similar to impacts of pluning waves on vertical walls, classified by Oumeraci et al. (1993) with *Load case 3* (Fig. 2.1, page 22). The negative pressure values result from the high-frequent response of the model set-up.

The pressure sensors P1, P2 and P3 show differences in the pressure evolution that can be explained by their position relative to the *SWL*. An example of the impacting wave on a 1:2 sloped stepped revetment $(S_h = 0.3\,m, H_{m0} = 0.2\,m, T_p = 2\,s, h_s = 0.7\,m)$ is given for three time steps $(dt = 0.02\,s)$ and qualitative position of the pressure sensors P1, P2 and P3 in Fig. 4.22. P1 is located above the *SWL*, P2 close to the *SWL* and P3 under the *SWL*. Shortly before the impact (left) P1 and P2 are emerged while P3 is submerged by the incoming wave. At the moment of the impact by the strong aerated wave (center), P2 is fully exposed to the impact whereas P3 is still submerged. As a result the pressure shock is damped. P1 is still emerged at the moment of the impact. Shortly after the impact (right), the up-rushing jet of water reaches P1. Consequently the pressure increases at P1, P2 and P3. From the time the wave rushes down the step and P1 to P2 emerge again, the pressure decreases within one wave period.

The measurements of the wave impacts are different for each impact event. To identify general definitions for a wave spectrum, a mean impact parameter $P_{2\%}$ is calculated as the mean of the 20 highest impacts within a time series of 1,000 waves. Fig. 4.23 shows the superimposition of the highest 20 impact events measured by pressure sensor P2.
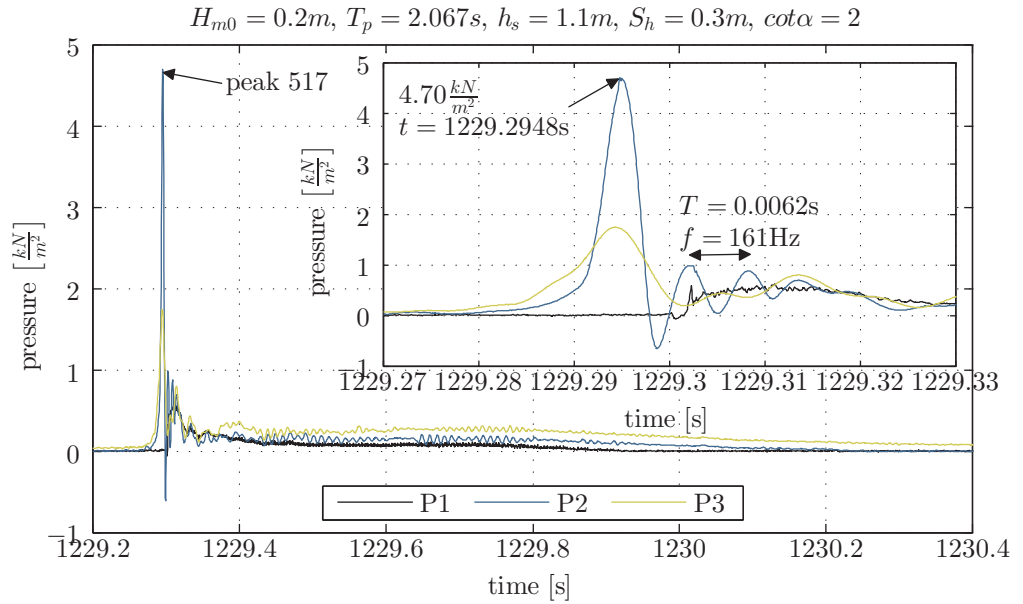
Figure 4.21: Evolution of the wave impact at the pressure sensors P1, P2 and P3.
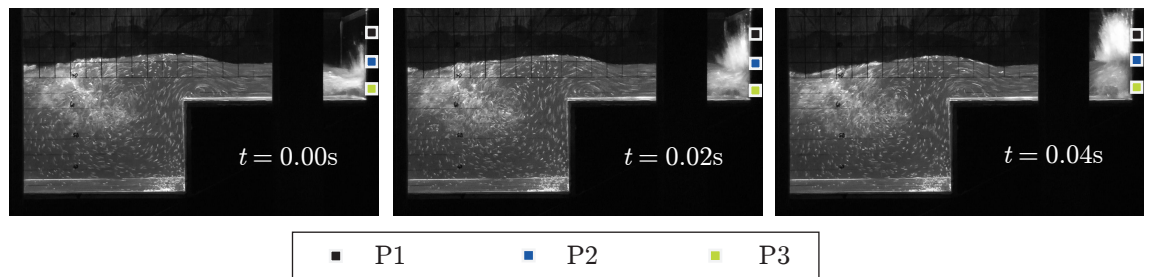
Figure 4.22: Impacting wave on a 1:2 sloped stepped revetment with $S_h = 0.3\,m$, $H_{m0} = 0.2\,m$, $T_p = 2\,s$, $h_s = 0.7\,m$ at three time steps $dt = 0.02\,s$ and qualitative position of the pressure sensors P1, P2 and P3.

The test conditions were a Jonswap spectrum on a 1:2 sloped stepped revetment ($S_h = 0.3\,m$, $H_{m0} = 0.2\,m$, $T_p = 2.067\,s$, $h_s = 1.1\,m$). The mean impact curve $P2_{2\%}$ and corresponding box plots present maximum values, interquantile ranges (IQR) and the bandwidth of the averaged pressure impacts. In this particular case the mean impact force is $P2_{2\%} = 2.77\,kN/m^2$, the maximum impact $P2_{max} = 4.7\,kN/m^2$ and the total bandwidth is $P2_{bandwidth} = 2.1\,kN/m^2$ with an IQR of $P2_{IQR} = 0.8\,kN/m^2$. The mean decay frequency is $119\,Hz$. This is $25\,\%$ less than for $P2_{max}$ but confirms a stiff structure. The decay of the mean amplitudes follows an exponential trend.

The correlation of the relative mean pressure $P2_{2\%}/(\rho g H_{m0})$ with the normalized maximum pressure $P2_{max}/P2_{2\%}$, normalized IQR $P2_{IQR}/P2_{2\%}$ and normalized bandwidth $P2_{range}/P2_{2\%}$ of all conducted tests is given in Fig. 4.24. Data are separated with respect to the two tested step heights. For the maximum pressure no clear trend can be identified. The maximum pressure scatters in a range of $0.4 < P2_{max}/P2_{2\%} < 2.5$, with a little more scatter for the larger step heights. This behavior would be expected since the maximum wave height in a spectrum scatters significantly. For the IQR a clear trend can be identified as the normalized IQR increases with increasing normalized mean pressure in a range of $0.1 < P2_{IQR}/P2_{2\%} < 0.6$. The trend can be described by linear regression as

$$P2_{IQR} = \frac{1}{7}\frac{P2_{2\%}^2}{\rho g H_{m0}}. \tag{4.16}$$

The normalized bandwidth is in a range of $0.3 < P2_{range}/P2_{2\%} < 1.0$ and tends to decrease with increasing normalized mean pressure. Data for small step heights follow the trend better than data for the large step heights. This effect is due to the fact that smaller step heights cause a more steady run-up process which results in relatively small extreme values. The trend can be described by linear regression as

$$P2_{2\%} = 0.31\frac{P2_{2\%}^2}{\rho g H_{m0}}. \tag{4.17}$$

Conclusion

The maximum pressures are measured at the SWL. Pressures decrease significantly when the distance to the SWL increases. Below $z/H_{m0} \leq -2$ the dynamic loading on a stepped revetment can be neglected. Above SWL the vertical pressure distribution at a stepped revetment is comparable to conditions at a vertical wall whereas the pressure distribution below SWL is reduced by $70\,\%$ compared to that of a vertical wall. Therefore, the statement by SPM (1984) that pressures at a stepped revetment can be calculated by vertical wall conditions is valid above the SWL only. However, below the SWL the stepped revetment is subjected to pressures which are about three times lower.
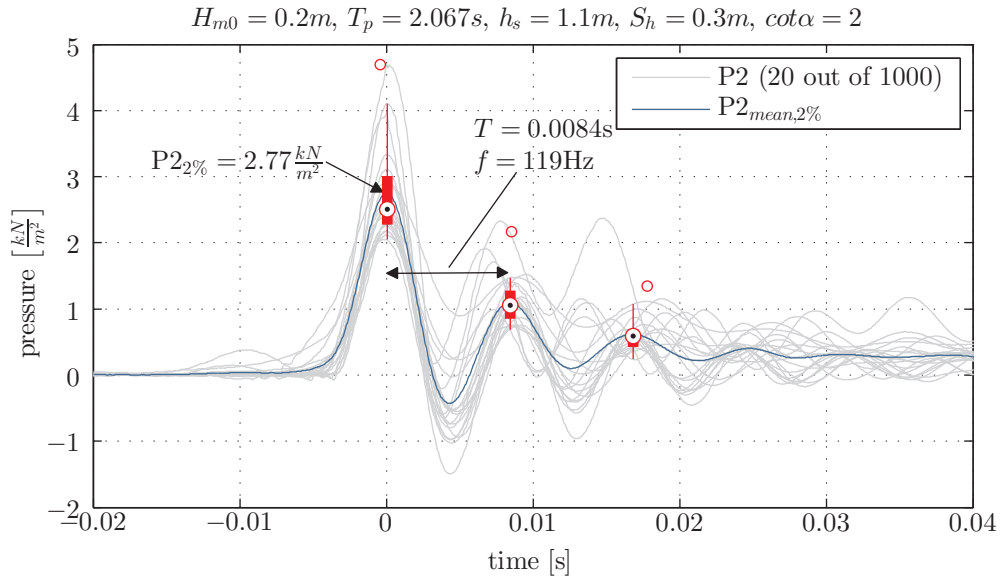
Figure 4.23: Definition of the $P_{2\%}$ pressure including maximum values, interquantile ranges (IQR) and the bandwidth of the results.
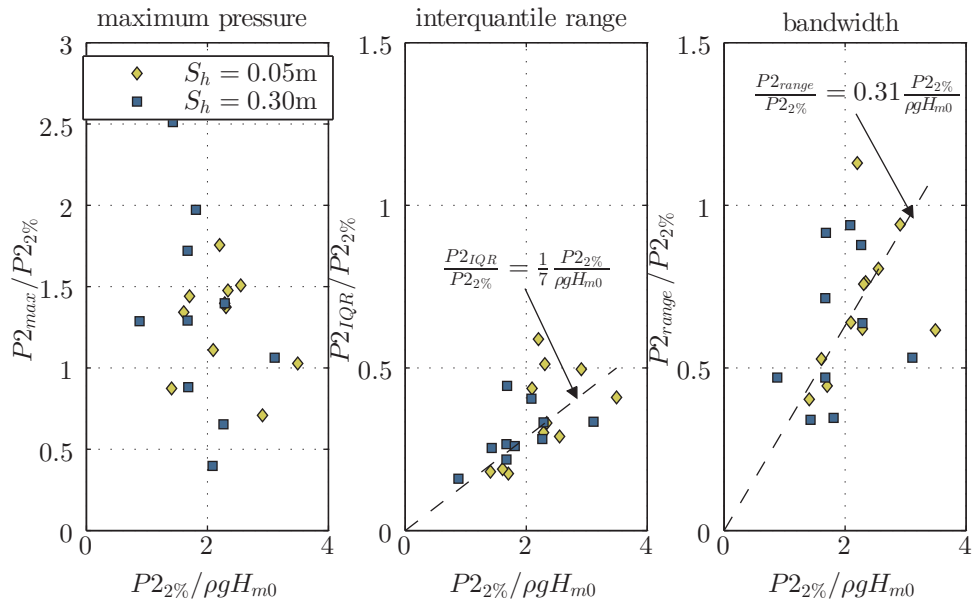
Figure 4.24: Correlation of the $P_{2\%}$ pressure with the normalized maximum pressure (left), normalized IQR (center) and normalized bandwidth (left).

4.5   Model- and scale effects

Model effects occur due to the idealized repetition of prototype geometries, limiting space in a test facility or the test procedure. Scale effects occur due to the selected scaling law that is based on idealizations. Thus, all relevant forces acting within the prototype condition cannot be correctly reproduced in the model.

4.5.1   Model effects

The uncertainties of the measuring instruments and details about the data acquisition and post-processing are described in section 3.3. Most of the positions of the individual sensors are selected according to best practice recommendations from Hughes (1993) and Frostick et al. (2011). Well-established routines have been used to filter and post-process the raw-data to calculate the target values. The measured target values (reflection coefficient, run-up height, overtopping volume, pressure loads) are subjected to statistical uncertainties. These uncertainties are caused by the irregular nature of the incoming waves and the performance of the measuring instruments (range, resolution and accuracy of each measuring device).

To ensure high quality results, tests are conducted with more than 1,000 single waves (section 3.3.3). Nevertheless, fully-developed waves are always represented insufficiently and lead to idealized surface elevations. As the tests are conducted in a two-dimensional wave flume long-shore processes cannot be considered. Since the wave flume *Schneiderberg* is not equipped with active absorption control, re-reflections can affect the results and may lead to more wave energy in front of the tested revetments and slopes (compare section 3.6). Incident wave conditions are calculated in front of the structure in order to capture these influences on the data.

Over a distance of $12\,m$ seawards from the revetment crest the wave flume was separated in three equally spaced test sections with a width of $\approx 0.7\,m$ (Fig. 3.3). In every section a revetment with a different slope was installed and therefore the reflection differs for each section. Due to diffraction at the beginning of the separation sheets, some of the reflected wave energy can proceed towards the adjacent sections. To estimate the influence of this effect, waves were generated manually in the middle flume section and their propagation was observed. With still water conditions minor motions of the water surface in the adjacent wave flumes were visible. According to Daemrich and Kohlhase (1979), who followed an approach by Sommerfeld (1896), the diffracted wave height in this case can be estimated to be in the range of $10 - 15\,\%$ of the reflected wave height. As the calculated incident wave conditions in every section of the flume were equally and in the range of the target wave conditions the mutual affection between the sections was estimated to be negligible.

Reduction coefficients are calculated with respect to tests with smooth slopes conducted under the same boundary conditions (except for the wave run-up). Therefore it is assumed, that these calculated reduction factors are meaningful. The target values are expressed

by maxima. Most of the data analysis is undertaken with mean values ($C_R\,[-]$, $R_{u,2\%}\,[m]$, $q\,[m^3/(sm)]$, $P_{2\%}\,[N/m^2]$) in order to reduce the scatter of single events and thereby follow best practice solutions.

4.5.2   Scale effects

When tests are not conducted under prototype conditions, the *Froude*-scaling law is applied to scale the hydraulic- and geometry-related boundary conditions. Therefore, predominantly inertial forces and gravity are considered whereas viscosity, elasticity, and surface tension are incorrectly represented (compare Fig. 4.25). In the *EC Mast III Opticrest* research project results obtained from scaled model tests were compared to prototype tests in oder to identify scale effects. As an example, Troch et al. (1998) found about 50 % higher run-up heights for a rubble mound breakwater in prototype conditions than predicted based by calculation methods based on physical model tests.

For the present study, all friction effects – especially on the boundary layer – are overestimated since these effects can be better expressed with the *Reynolds*-law which considers viscosity. With wave breaking the *Weber*, *Reynolds* and *Cauchy*-law should be apply. Therefore, by applying the *Froude*-law, the effects of wave breaking are only idealized. Furthermore, to the wave run-up process *Reynold*'s and *Weber*'s law are important.

The surface roughness of the tested revetments can be described as very smooth as it is constructed by wooden planks with a special smooth surface which is comparable to glass. For the smooth slopes – used as a reference – this means that the surface is not ideally smooth and therefore the run-up is slightly reduced due to surface friction. For the stepped slopes a slightly higher run-up is expected in the model tests as the surface is much smoother than e.g. concrete and therefore less friction is expected in the interface of step and water. Nevertheless, calculated reduction coefficients are on the safe side, as both boundaries lead to conservative reductions coefficients. Overall, the effect of the surface roughness is of minor importance.

Force	Model Law	Scale		
		1:1	1:10	1:100
Gravity	FROUDE	1	1	1
Friction	REYNOLDS	1	1:31.6	1:1000
Elasticity	CAUCHY	1	1:10	1:100
Surface Tension	WEBER	1	1:100	1:10000
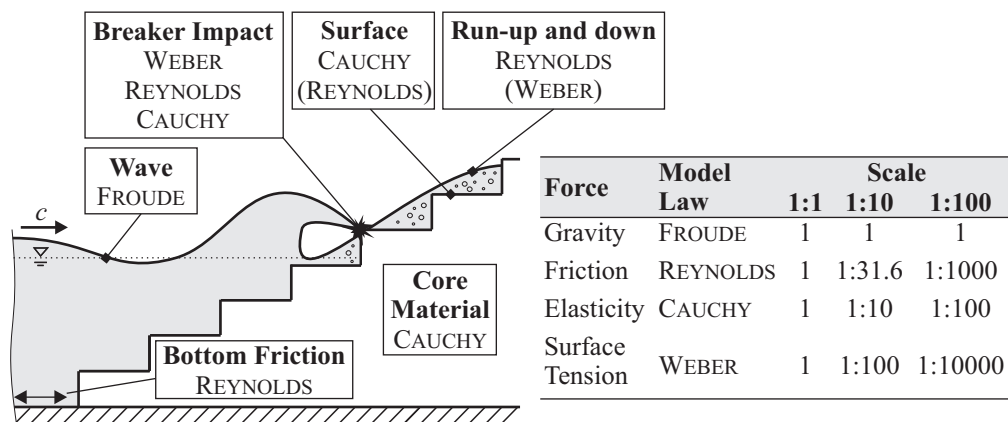
Figure 4.25: The influence of model law and model scale on the measured target values (modified after Führböter).

It is expected that the inability to scale the air entrainment will have a more significant effect. The importance of the air entrainment for the energy dissipation is discussed in Führböter (1971). The influence of scale effects affecting the air entrainment with *Froude* similitude was derived by Chanson and Murzyn (2008) for hydraulic jumps. It is assumed that the described principle processes are comparable with the process of the wave run-up over stepped revetments. Chanson and Murzyn (2008) conclude that the aeration is significantly lower in smaller scales and cannot be achieved under *Froude* similitude. Consequently, full scale tests are required. The intensity of aeration will have an influence on the turbulence. Less aeration will lead to slightly less turbulence. Furthermore, pressure shocks are damped by air entrainment. Hence, the conducted model tests provide conservative results with respect to wave run-up heights and wave overtopping volumes as well as wave loads on stepped revetments.

4.6   Conclusions

Hydraulic model tests were conducted to increase knowledge about the hydraulic- and geometry-related energy dissipation at stepped revetments. The discussed results can be concluded as follows:

- The <u>wave reflection</u> for smooth slopes and impermeable rock slopes clearly decreases with decreasing Iribarren number. Stepped revetments show different behavior. Large step heights ($H_{m0}/S_h < 0.5$) show a comparable reflection to plain or composite vertical walls. They can be classified as highly reflective. Smaller step heights ($H_{m0}/S_h \geq 0.5$) tend to show the same reflection behavior as rough impermeable surfaces and are therefore classified as moderately reflective.

- A stepped revetment can reduce the <u>wave run-up</u> in a range of $10 - 60\,\%$ in comparison to a plain slope. The reduction coefficient $\gamma_{f_{R_{u,2\%}}}$ decreases for an increasing dimensionless step height ($k_h/(H_{m0} \cdot \xi_{m-1,0})$). The run-up reduction of a stepped revetment is more effective for the case where the step height is smaller than the wave height ($30 - 60\,\%$ reduction for $H_{m0}/S_h \geq 1$ and $10 - 40\,\%$ for $H_{m0}/S_h < 1$). The minimal reduction coefficient $\gamma_{f_{R_{u,2\%}}}$ can be achieved independent of the wave steepness for a step ratio of $H_{m0}/S_h = 2$. The run-up reduction becomes more effective with a decreasing Iribarren number. The run-up reduction is more effective with shallower slopes $1 \leq n \leq 3$. No further significant decrease of $\gamma_{f_{R_{u,2\%}}}$ was predicted for gentler slopes ($n > 3$).

- A stepped revetment decreases the <u>wave overtopping</u> volume in comparison to a smooth slope. The effectiveness of wave overtopping reduction is mainly dependent on the step ratio H_{m0}/S_h and the Iribarren number. If the step height is two times larger than the incident wave height, the revetment is reflective and the wave overtopping cannot be reduced significantly (by $2 - 10\,\%$). For plunging breakers the overtopping volume can be reduced most effectively ($40 - 60\,\%$) due to the macro roughness of a stepped revetment. Most of the energy is dissipated by the wave

breaking. The wave run-up, and as a consequence also the wave overtopping, is reduced significantly as the wave run-up with a relatively low energy content is disturbed by the stepped surface. Thus, the efficiency in reducing the wave overtopping volume for collapsing and surging wave breaking decreases $(10 - 30\,\%)$ with more gentle wave steepnesses and increasing Iribarren numbers. The position of the SWL with respect to the step edge becomes important if the step height and wave height are in the same range $(0.5 < H_{m0}/S_h < 2.)$. In this case the highest energy dissipation can be achieved if the SWL is close to the step edge.

- The reduction coefficients, considering a reduced wave run-up $(\gamma_{f_{R_{u,2\%}}})$ and wave overtopping (γ_{f_q}) at stepped revetments compared to smooth slopes, are not equal for equivalent hydraulic- and geometry-related boundary conditions. The run-up reduction coefficients show lower values compared to the overtopping reduction coefficients. This is an expectable result, as all the kinetic energy of a incident wave changes to potential energy during the run-up process. In the case of wave overtopping the highest run-up is never reached and therefore less energy dissipated compared to a wave run-up at a infinite stepped slope.

- The maximum <u>pressures</u> are measured at the SWL. Pressures decrease significantly with an increasing distance to the SWL. Below $z/H_{m0} \leq -2$ the dynamic loading on a stepped revetment can be neglected. Above SWL, the vertical pressure distribution at a stepped revetment is comparable to conditions at a vertical wall. The pressure distribution below the SWL is reduced by $70\,\%$ compared to a vertical wall. Therefore, the statement by SPM (1984) that pressures at a stepped revetment can be calculated for vertical wall conditions is valid above SWL only. Below the SWL mean pressures for a stepped revetment are three times lower than for a vertical wall.

- In all tests significant <u>air intrusion</u> was observed. It is therefore expected that most findings of this study are subjected to scale effects. According to Chanson and Murzyn (2008) the aeration is significantly lower in smaller scales and cannot be achieved under $Froude$ similitude. The level of aeration will have an influence on the turbulence. Less aeration will lead to less turbulence. Hence, from a design point of view the results from the performed model tests are conservative.

With the novel prediction approaches the apparently contradictory findings of Nussbaum and Colley (1971) and Goda and Kishira (1976) can be resolved. Nussbaum and Colley (1971) detected lower run-up values with decreasing step height whereas Goda and Kishira (1976) detected the opposite system performance. Obviously, Goda and Kishira (1976) conducted model tests where the wave height was much larger than the step height $(20 < H/S_h < 30)$. An increase of the step height leads to a decrease in the energy dissipation for this range of step ratios (Fig. 4.11 and 4.12) as the surface roughness is increased and more turbulence is induced by the steps. The tests conducted by Nussbaum and Colley (1971) can be estimated[19] to be in a range of $1 < H/S_h < 4$. Fig. H.2 and 4.12 prove that

---

[19]Nussbaum and Colley (1971) provide the hydraulic boundary conditions dimensionless. The step

the energy dissipation decreases for step ratios larger $H/S_h > 2$. Therefore, both findings – formerly contradictory – can be verified with the novel approach.

A design example application of the derived formulae is presented for an example case in appendix B (page 139).

---

height is given in dimensions with $S_h = 0.025\,m$ and $0.05\,m$. With respect to the flume dimensions given in Nussbaum and Colley (1971) it seems obvious that they tested waves with a height of $0.05\,m < H < 0.1\,m$. This would lead to relative wave heights in a range of $1 < H/S_h < 4$.

5 Theoretical approach to energy dissipation

In Chapt. 4 empirical formulae have been derived in order to predict the target parameters (reflection coefficient, run-up height, overtopping volume, pressure load). Even though these results are sufficient, the physical processes involved in the energy dissipation are not highlighted in detail. Therefore, in this chapter an analytic approach is derived to calculate the energy dissipation in the wave interaction with a stepped revetment. The overall objective is to estimate the energy losses E_v for waves that interact with a stepped revetment. The reduced energy content will be derived for

$$\gamma_E = \frac{E_{ref}}{E_{inc}} = \frac{E_{inc} - E_v}{E_{inc}}. \tag{5.1}$$

The energy of the incident wave E_{inc} can be calculated with Eq. (4.3) (page 79).

The analytical approach is based on investigations by Pereira (1996) on the energy dissipation at a single submerged step with infinite length. This approach will be expanded for a finite number of submerged steps with varying water depth.

5.1 Relevant wave and vortex theory

The analytic approach is based on linear wave theory. Therefore, a sinusoidal wave profile with small amplitudes ($H \ll L$ and $H \ll h_s$) over a plain seabed is assumed. A discussion of the integral boundary conditions of the linear wave and vortex theory assured for this approach can be read in Pereira (1996). A comprehensive discussion of the wave motion in liquids with free surface is presented in Stoker (1992). Boundary layer theories are essentially discussed in Schlichting et al. (2013). The most important assumptions and derivations are given in this section.

Generally, fluid particles under waves are assumed to move in an orbit. The angular or orbital velocity ω of the fluid particle depends on the wave period T:

$$\omega = \frac{2\pi}{T}. \tag{5.2}$$

The vorticity Ω can be expressed by the velocity ω of each fluid particle as

$$\Omega = 2\omega. \tag{5.3}$$

An idealized vortex system describing the outflow current in a cylindrical tank is given in Fig. 5.1. The angular velocity is calculated with the principle of fluid mechanics. The inner circumferential velocity $v_{\phi,i}$ of an ideal vortex – known as a roller – with radius r can be calculated by

$$v_{\phi,i} = r\omega. \tag{5.4}$$
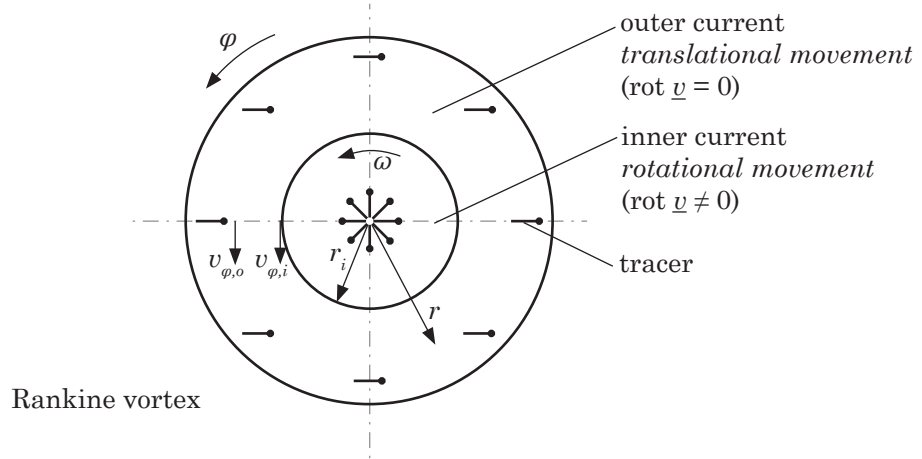
Figure 5.1: Plan view of a vortex system (redrawn according to Siekmann and Thamsen (2013))

The outer circumferential velocity $v_{\phi,o}$ is a potential flow ($\underline{\Omega} = \mathrm{rot}\,\underline{v} = 0$) and can be calculated by considering the circulation or flow of vorticity Γ with respect to the radius r:

$$v_{\phi,o} = \frac{\Gamma}{2\pi r}. \tag{5.5}$$

It is assumed that the circulation is constant over time (Thomson-Theorem[20]) and space (Helmholtz-Theorem[21]).

Compared to the Rankine-vortex with a fixed radius, the Hamel-Oseen-vortex (or Lamb-Oseen-vortex) combines the solid body rotation ω present in the center of a large vortex with the potential vortex rotation Ω at a larger radius of the vortex. Thereby, the vorticity of a vortex can be calculated for every time step and location in the vortex whereas the approach by Rankine uses only representative constant rotation velocities in the outer current. According to Hamel (1916) the flow velocity in a circumferential direction that decreases due to viscosity ν can be calculated with respect to time t and radius r by

$$v_{\phi}(r,t) = \frac{\Gamma_0}{2\pi r}\left[1 - exp\left(-\frac{r^2}{4\nu t}\right)\right]. \tag{5.6}$$

The circulation or flow of vorticity Γ is the sum of all local vortex intensities ω^* along the vortex steam line with cross section A and can therefore be described with

$$\Gamma = \int \underline{\omega}^* dA. \tag{5.7}$$

---

[20]The circulation of a fluid is constant if the driving forces are energy conserving and the fluid is incompressible and inviscid.

[21]1st: The strength of a vortex filament is consistent along its length. 2nd: A vortex filament cannot end in a fluid; it must extend to the boundaries of the fluid or from a closed path. 3rd: In the absence of external rotational forces, a fluid that is initially irrotational remains irrotational. (Busse and Bestehorn, 2006)

The formation of a vortex is a boundary layer phenomenon depicted in Fig. 5.2. Close to a wall, a flow velocity u is reduced by the shear stresses induced by surface roughness (k_{sf}). Idealized, the thickness δ of the boundary layer is dependent on the surface roughness and the fluid viscosity η. At the bottom of the boundary layer ($z = 0$) the flow velocity is equal to zero $u_{z=0} \approx 0$. At the top of the boundary layer ($z = \delta$) the flow velocity $u_{z=\delta}$ is unaffected by the rough surface. If the velocity in the velocity profile in the boundary layer reaches exactly zero ($u_{z=0} = 0$) and a vertical tangent to the adjacent surface occurs, the flow is able to move away from the surface and a vortex can emerge. This effect also occurs on flat bottoms, but is significantly evoked by a step edge. A rotation is induced by the gradient in the flow which is partly affected by the boundary layer. At a step edge, pressure differences between the horizontal flow above the step and the inactive fluid below the step increase the driving forces of the rotation.

With the hypothesis that for shallow water wave conditions ($h_s/L < 0.05$) the following conditions apply

- the circulation Γ is proportional to the product of the length of the boundary layer I_G and the maximum tangential velocity $u_{\Theta,max}$ in the boundary layer ($\Gamma \sim I_G \cdot u_{\Theta,max}$),

- the length of the boundary layer I_G over the step is equivalent to the orbit of the fluid particle over the step and therefore proportional to the wave length L ($I_G \sim L$),

- the maximum tangential velocity $u_{\Theta,max}$ in the boundary layer with the height δ over the step is proportional to the step height S_h ($u_{\Theta,max} \sim S_h$)

the vorticity Γ can be expressed in the proportional relation

$$\Gamma \sim \frac{L S_h}{T}. \tag{5.8}$$
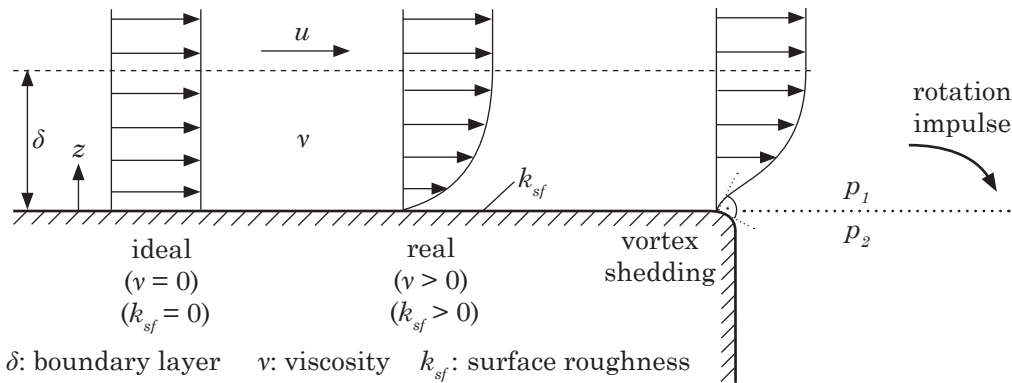
Figure 5.2: Idealized phenomena of ideal and real flow velocity profiles in the boundary layer over a step with beginning of vortex shedding at the step edge (modified after Schlichting et al. (2013)).

5.2 Vortex based energy dissipation at a single step

To describe and understand the energy dissipation that takes place as a wave interacts with a stepped revetment, it is important to look more closely at the vortex shedding. However, since so many processes are present, it is necessary to make some assumptions and simplifications. It is assumed that the flow follows a circular path. The aim of the analytical description of the energy dissipation of the wave interaction is to extend the approach by Pereira (1996) for a sequence of steps. Pereira (1996) followed the analytical description of spiral-shape motions in viscous fluids derived by Hamel (1916) for the interaction of regular waves with a single submerged step. The energy loss induced by a single submerged step can be calculated according to Pereira (1996) with

$$E_v = \frac{1}{16}\pi\rho\Omega^2 r_k^4 \left[1 + 4ln\left(\frac{\eta_c}{r_k}\right)\right].$$

$$
\begin{aligned}
\text{with } E_v : \quad & \text{Energy loss due to vorticity } [N/m] \\
\rho : \quad & \text{fluid density } [kg/m^3] \\
\Omega : \quad & \text{vorticity } [1/s] \\
r_k : \quad & \text{radius of the center vortex } [N/m] \\
\eta_c : \quad & \text{wave crest amplitude } [m]
\end{aligned}
$$

(5.9)

The mean radius of the center vortex r_m – which represents the radius of the center vortex r_k – can be theoretically derived by Squire (1965) with

$$r_m = r_k = \sqrt{1.25 \cdot 4\nu t}.$$

(5.10)

Within Eq. (5.9) the energy dissipation due to wave reflection and wave transmission of a single submerged step is represented. Since Pereira (1996) systematically analyzed a range of wave steepnesses of $0.002 < H/L < 0.015$ (section 2.4), energy dissipation due to wave breaking is not considered. Furthermore, Pereira (1996) stated that his measurements indicated that Eq. (5.10) only applies for large values of t since the time for the formation of a vortex in front of and behind a step is only half a wave period T. Therefore, this derived theoretical approach is only valid for very long waves.

When substituting Eq. (5.3) – Eq. (5.8) into Eq. (5.9) and assuming the shallow water wave length $L = T\sqrt{gh_s}$, the energy dissipation with respect to the water depth h_s, step height S_h and wave height H can be determined by

$$E_v = \frac{1}{16\pi}\rho g h_s S_h^2 \left[1 + 4ln\left(\frac{H}{2\sqrt{5\nu t}}\right)\right].$$

(5.11)

5.3   Energy dissipation for multiple steps

The extended approach is based on some assumptions that will be discussed below. The process is described in Fig. 5.3. Fig. 5.3(a) gives the process and phase angle definition for vortex induced energy dissipation of a single wave propagating over a single submerged step (idealized according to Pereira (1996)). $Wave\,1$ with energy E_1 propagates from deeper water (d_1) over a step edge to a shallower water depth (d_2). Due to shallow water conditions a certain volume of fluid is transported by the wave and a flow over the step edge is induced $(0 \leq t/T \leq 0.5)$. The flow results in vortex shedding at the step edge and induces $vortex\,A$ with circulation Γ_A. The energy content over the step E_2 is reduced due to turbulence in $vortex\,A$ and can therefore be expressed by $E_2 = E_1 - E_v$. After half a wave period an opposing flow (backwash) is forced over the step $(0.5 < t/T \leq 1)$ inducing $vortex\,B$ with circulation Γ_B. A further interaction of $vortex\,B$ with a new vortex $(t/T > 1)$ induced by $wave\,2$ is neglected. Fig. 5.3(b) describes the assumed global system. The energy dissipation is calculated step-wise for two areas. $Area\,1$ covers the energy dissipation below the SWL, $area\,2$ the energy dissipation above the SWL.

5.3.1   Energy dissipation below the SWL

Definitions for $area\,1$ are given in Fig. 5.3(c). It is assumed that the velocity components below the shallow water condition $(h_s/L \leq 0.05)$ are less dominant for the energy dissipation and can therefore be neglected. The number of steps i under the SWL that have to be taken into account can be calculated with

$$i \geq \frac{0.05L - d_{st}}{S_h}.$$ (5.12)

The water depth over each step d_j is calculated for each time step t with

$$d(n,t) = \int_{j=1}^{i} \int_{t=0}^{T} j \cdot S_h + d_{st} + \frac{H}{2} \cdot cos(\omega t) \mathrm{d}j \mathrm{d}t.$$ (5.13)

The time step Δt of the calculation is based on the Courant-criteria (Courant et al., 1928). When the spacial resolution is related to the step width $(\Delta x = cot\alpha \cdot S_h)$ and the wave velocity is calculated with respect to shallow water conditions $\left(c = \sqrt{g \cdot h_s}\right)$, the time resolution gives

$$\Delta t \leq \frac{\Delta x}{c} = \frac{cot\alpha \cdot S_h}{\sqrt{g \cdot h_s}}.$$ (5.14)

Finally, the energy dissipation of a single wave with the wave period T and the wave height H is calculated with Eq. (5.11) for j submerged steps at the particular water depth over each step d by

$$E_v(j,t) = \int_{j=1}^{i} \int_{t=0}^{T} \frac{1}{16\pi} \rho g d_j S_h^2 \left[1 + 4ln\left(\frac{H}{2\sqrt{5\nu t}}\right)\right] \mathrm{d}j \mathrm{d}t.$$ (5.15)
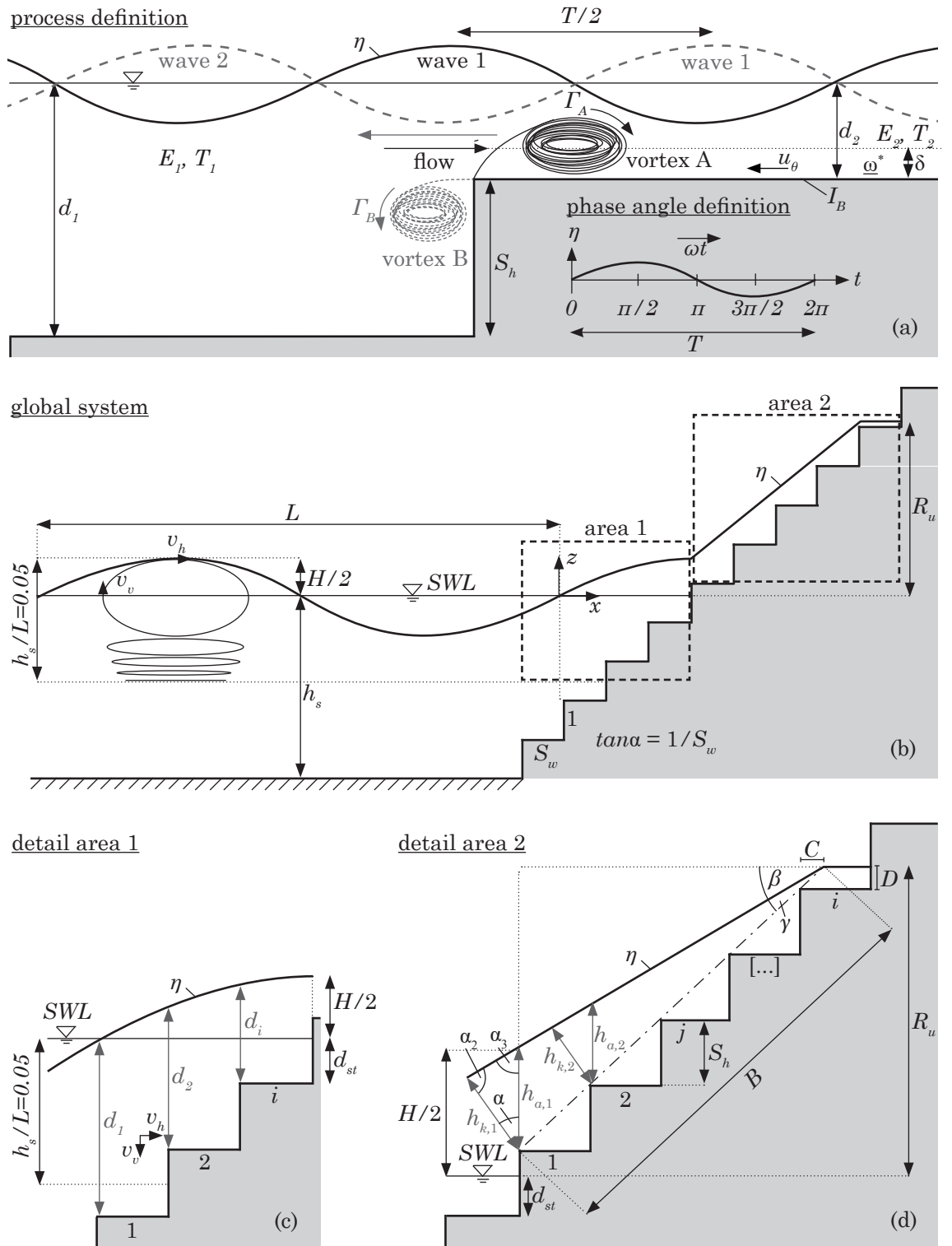
Figure 5.3: Definition of boundary conditions for the analytic approach of the energy dissipation within the run-up process

5.3.2   Energy dissipation above the SWL

Definitions for $area\,2$ describing the energy dissipation above the SWL are given in Fig. 5.3(d). It is assumed that the wave run-up can be idealized by a triangle that spans between the step edge at the SWL, the wave amplitude $H/2$ above the SWL and the run-up elevation R_u. The water depth $h_{a,j}$ over each step can then be calculated by

$$
\begin{aligned}
h_{a,j} &= h_{k,1}/sin\alpha_3. \\
\text{with: } h_{k,j} &= B_j \cdot tan\gamma \\
B_j &= \frac{(N_{steps} - j) \cdot S_w + C}{cos\alpha} \\
C &= D/\tan\alpha \\
D &= R_u - S_h - d_{st} - (N_{steps} - 1) \cdot S_h \\
N_{steps} &= (R_u/S_h)_{round_{up}} \\
d_{st} &= \left[(R_c/S_h)_{round_{up}} - (R_c/S_h)\right] \cdot S_h \\
tan\alpha &= S_h/S_w \\
\alpha_2 &= 90° - \gamma \\
\alpha_3 &= 180° - \alpha - \alpha_2 \\
tan\beta &= \frac{R_c - H/2}{(N_{steps} - 1) \cdot S_w + C} \\
\gamma &= \alpha - \beta
\end{aligned}
\tag{5.16}
$$

It is assumed that the model approach for the wave propagation over the submerged step is valid. As a result, the energy dissipation due to run-up and run-down at a step edge is already considered for each wave of period T and thus no distinction is made between energy dissipation during wave run-up and run-down. This assumption can only be drawn because the whole approach is based on long waves with low wave steepness.

Thus, the energy dissipation E_v for j emerged steps above the SWL of a single wave with the wave period T and the wave height H, can be calculated with Eq. (5.15) for particular water depth $h_{a,j}$ over each step as calculated with Eq. (5.16).

5.4   Comparison with results of physical model tests

Now, the range of applicability for the analytically derived approach for the calculation of the energy dissipation over stepped revetments is discussed. The energy dissipation is calculated by spectral wave parameters $(H_{m0}, T_{m-1,0})$ to obtain values representative for a wave spectrum. Therefore, the energy reduction coefficient γ_E (analytic.) and the reduction factor of the wave run-up $\gamma_{f_{R_u,2\%}}$ (meas.) are given in Fig. 5.4 with respect to the dimensionless step height. The reduction factor $\gamma_{f_{R_u,2\%}}$ decreases with increasing dimensionless step height (compare also Fig. 4.7, page 85). The derived energy reduction

coefficient γ_E is in a comparable range for $H_{m0}/S_h > 1$. The energy dissipation for step heights larger than the wave height is significantly over-predicted. This leads to negative γ_E-values for these cases. To identify the driving processes leading to this over-prediction, the analytically derived reduction coefficient is given normalized with the empirically derived reduction coefficient over the wave steepness $H_{m0}/L_{m-1,0}$ in Fig. 5.5. The values scatter significantly for waves steeper than 0.015 while only minor deviations ($\pm 10\,\%$) are present for wave steepnesses smaller than 0.015. This result is meaningful as the approach by Pereira (1996) is only valid for waves with a gentle steepness. Pereira (1996) also observed more scatter for steeper waves. The reduction factor for a slope of 1:3 is $20 - 25\,\%$ over-predicted in comparison to the 1:1 and 1:2 slope. This is an indication that additional energy dissipation (e.g. due to non-linear transformation processes in shallow water, wave breaking, wave transmission, friction) are not correctly considered in the approach.

To underline the evolution of the energy dissipation over steps, the calculated reduction of the normalized incident wave energy (right ordinate) is given with respect to the local water depth (left ordinate) over the steps in Fig. 5.6. Repeated tests with a wave steepness of $s_{input} \leq 0.015$ (#022 − 024) are given. For an estimate of the applied hydraulic boundary conditions, the surface elevation η is given in its mean maximum and minimum displacement from the SWL. To evaluate the quality of the calculated energy reduction the related $\gamma_{f,R_{u,2\%}}$ is given. The energy dissipation is given for the three tested slopes (1:1 in (a), 1:2 in (b) and 1:3 in (c)). For all slopes a distinct energy reduction starts with shallow water conditions. The gradient of the energy dissipation increases with decreasing water depth over the steps. The largest part of energy is dissipated at the step slightly below the SWL. The amount of energy reduced by the steps above the SWL is negligible. This is reasonable since only a minor part of the wave reaches this area. The energy dissipation follows the schematic description of the energy dissipation of surging waves over a dike given by Führböter (1991). For slopes of 1:1 and 1:2, the energy dissipation follows the curve of the $\gamma_{f,R_{u,2\%}}$-values and has only minor deviations. Consequently, the approach gives a good prediction for the above mentioned cases. For the slope 1:3 the energy dissipation is over-predicted. This over-prediction was already associated to the incorrect application of the non-linear transformation processes in the approach.

Conclusion: The analytically derived approach is valid for a gentle wave steepness ($s_{m-1,0} \leq 0.015$) and wave heights larger than the step height ($H_{m0}/S_h > 1$) for 1:1 and 1:2 sloped stepped revetments ($\pm 10\,\%$ accuracy). For more gentle slopes (1:3) the energy dissipation is over-predicted ($20 - 25\,\%$). The energy dissipation increases nonlinearly with decreasing water depth.
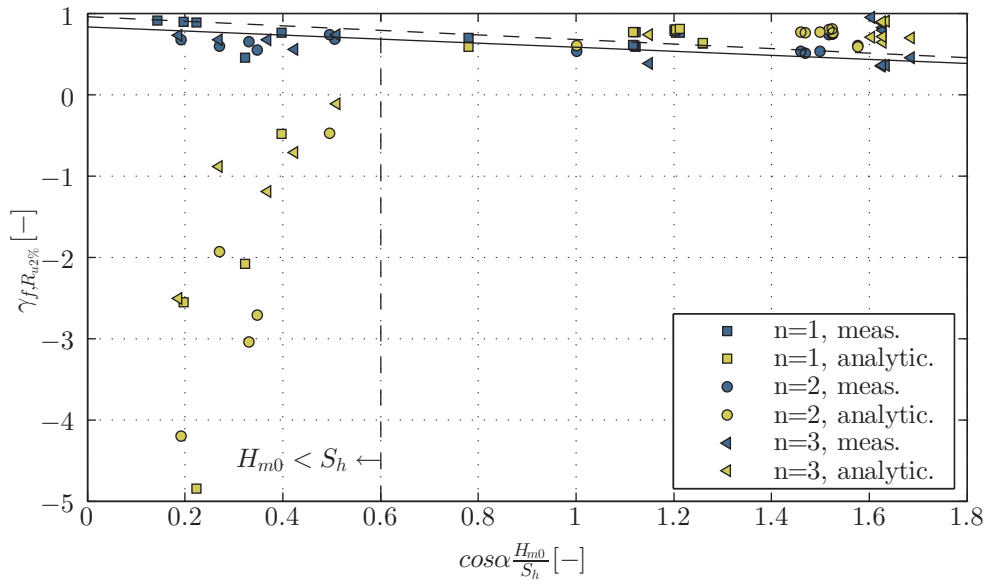
Figure 5.4: Comparison of empirically and analytically derived reduction coefficients $\gamma_{f,R_{u,2\%}}$ for stepped revetments.
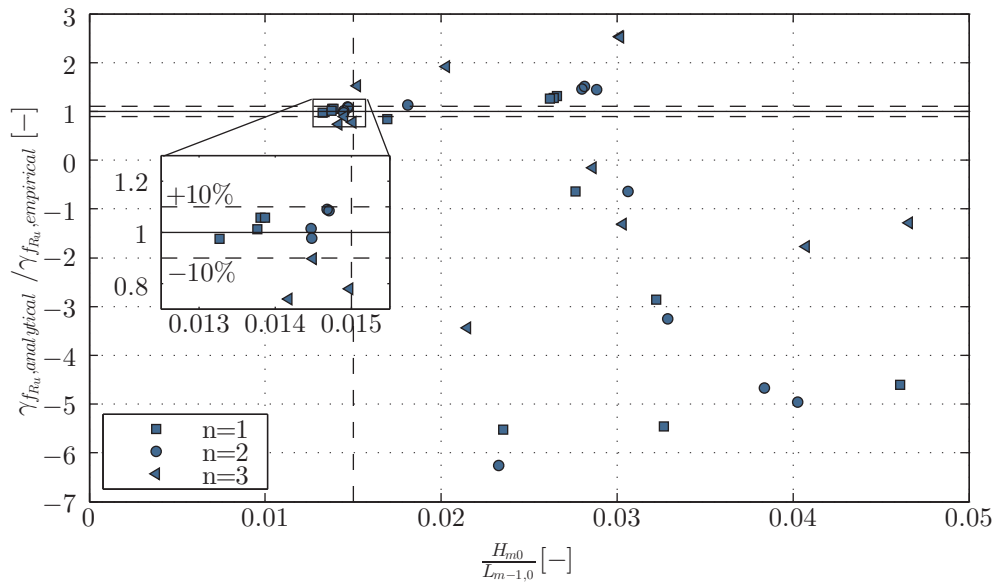
Figure 5.5: Relative reduction coefficient $\gamma_{f,R_{u,2\%},analytical}/\gamma_{f,R_{u,2\%},empirical}$ for stepped revetments for varying wave steepness.
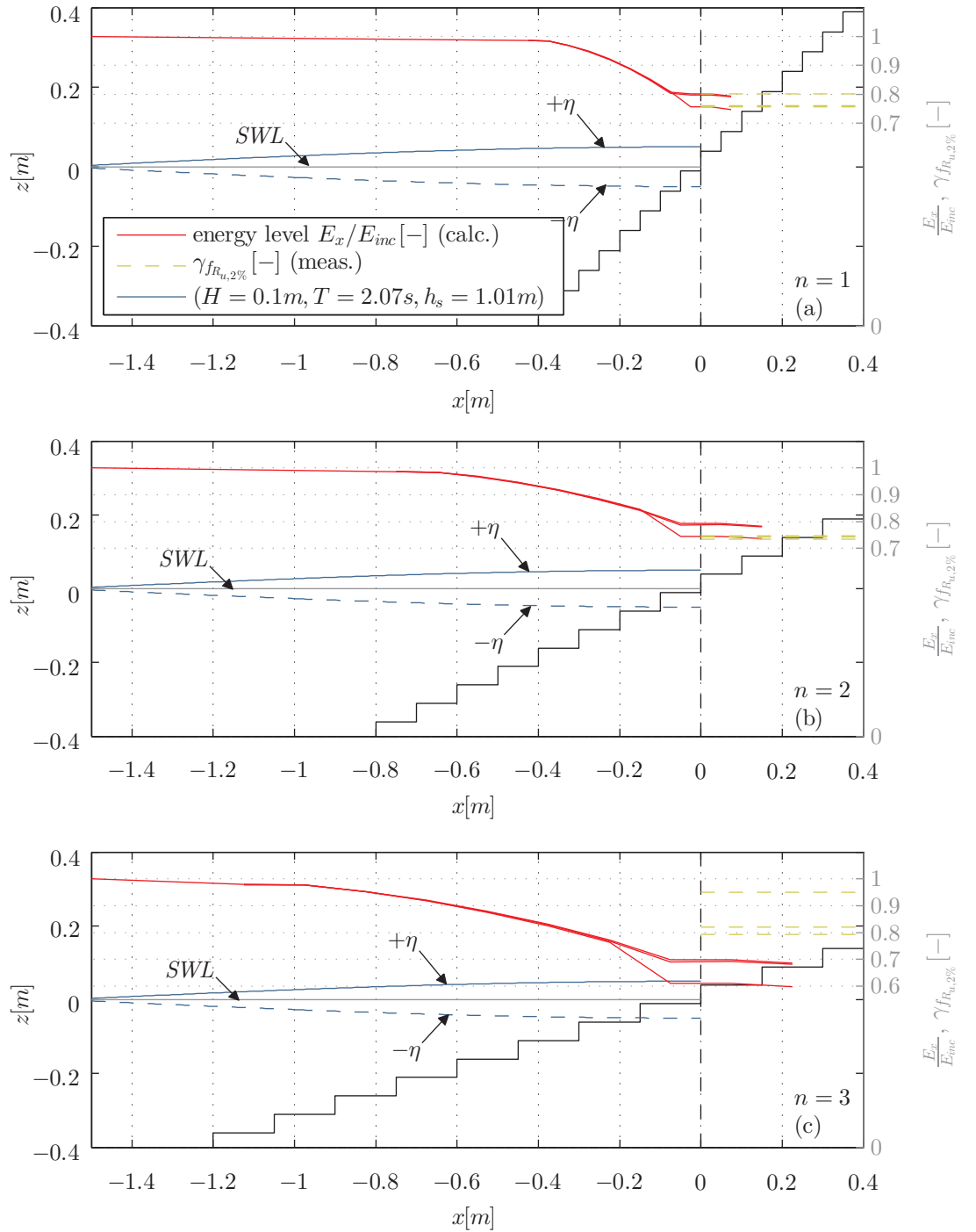
Figure 5.6: Comparison of empirically derived reduction coefficients $\gamma_{f,R_{u,2\%}}$ with the analytically derived energy dissipation E_v/E_{inc} for stepped revetments. Results from repetition of test $\#022 - 024$ with $H_{m0} = 0.1\,m$, $T_p = 2.07\,s$, $h_s = 1.01\,m$ for slopes $n = 1 - 3$.

5.5 Application of the new approach

The objective of this study is to systematically describe the hydraulic processes that take place when waves interact with a stepped revetment. With a better understanding of the hydraulic processes, an optimized and reliable design for stepped revetments can be developed. The analytically derived approach is applied to show the influence of the step ratio H_{m0}/S_h on the energy dissipation. A higher energy dissipation of the revetment leads to reduced wave reflection, wave run-up heights and wave overtopping volumes but to an increased loading on the revetment (Chapt. 4). The analytic approach is only valid for cases with a gentle wave steepness at a 1:1 and 1:2 inclined slope. Based on the principles of the analytical approach, conclusions can be drawn with respect to the energy dissipation of surging waves at stepped revetments.

Fig. 5.7 shows the application of the analytically derived approach to predict the run-up reduction factor $\gamma_{f,R_{u,2\%}}$ at a slope of 1:1 and 1:2 for a range of dimensionless step heights $1 < H_{m0}/S_h < 20$. It can be seen that the reduction is most efficient if the step height is equal to the wave height $1 < H_{m0}/S_h < 3$. If the wave height becomes larger than three times the step height the reduction is only 10%. If the wave height is 20 times larger than the step height, the derived reduction of $\approx 2\,\%$ is negligible.

As most of the wave energy for this type of wave ($H/L < 0.015$) is reduced below the SWL (compare Fig. 5.6), the turbulence induced by larger steps is higher. The wave run-up for waves with gentle steepness ($H/L < 0.015$) over a steep stepped revetment (1:1, 1:2) is highly turbulent due to the the air intrusion and the interaction with the run-down of the previous wave (Fig. 5.8). The run-down of the previous wave fills the step pockets and forms a kind of water cushion overflown by the run-up. Therefore, the roughness is artificially reduced for the actual wave and the energy reduction is smaller in comparison to a smooth slope.

It has to be clearly stated that the low reduction coefficient for relative wave heights $H_{m0}/S_h > 2$ (given in Fig. 5.7) is only valid for surging waves with $H/L < 0.015$ and relatively steep slope (1:1 and 1:2). For these boundary conditions the structure reacts strongly reflective and has no significant wave run-up reduction as already explained. The energy dissipation for plunging waves on a stepped slope relative to a smooth slope is much more effective ($\gamma_{f,R_{u,2\%}} \approx 0.5 - 0.7$): a lot of the energy of the incident wave is dissipated due to the plunging wave breaking. The remaining energy for the wave run-up is then significantly reduced due to the presence of steps.

5.6 Conclusions

Based on the findings in Chapt. 2 - 4 an analytic approach for the prediction of the energy dissipation by a stepped revetment was derived. The principle idea of the approach was to describe the energy dissipation by the vorticity induced by vortex shedding under waves at the step edges. An approach valid for the transmission of long waves ($H/L < 0.015$) over a single submerged step was extended to calculate the energy dissipation over a
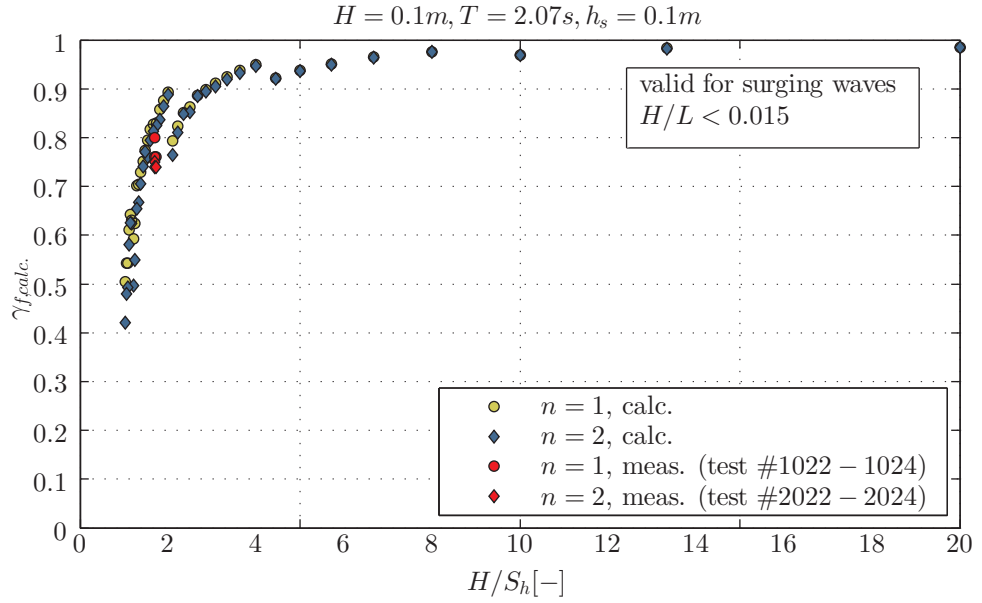
Figure 5.7: Application of the analytically derived approach to predict $\gamma_{f,R_{u,2\%}}$ at a slope of 1:1 and 1:2 for a range of dimensionless step heights $1 < H_{m0}/S_h < 20$.
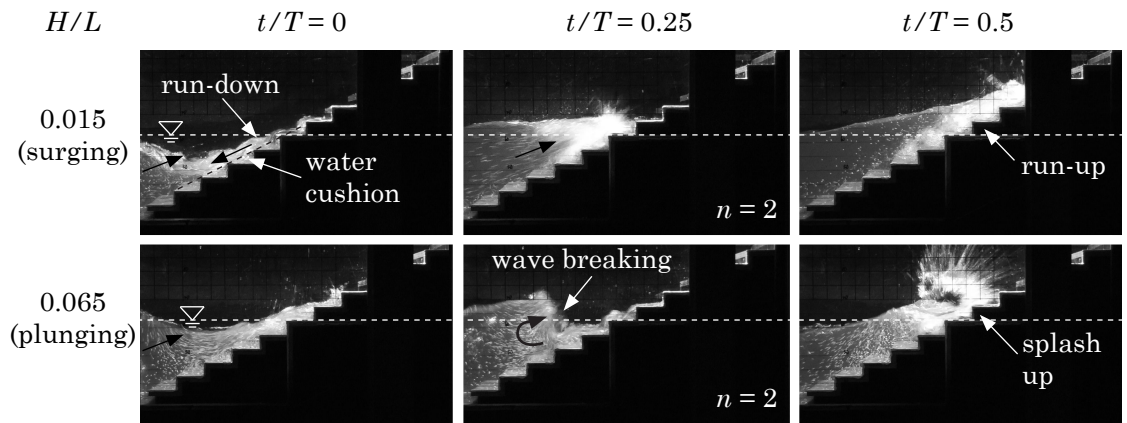
Figure 5.8: Principle wave run-up at a stepped revetment with $S_h = 0.05\,m$ for spilling ($H/L = 0.015$) and plunging waves ($H/L = 0.065$).

finite number of consecutive steps in shallow waters and emerged stepped slopes. The newly derived approach was discussed with respect to its applicability. The approach is valid for 1:1 and 1:2 sloped stepped revetments ($\pm 10\,\%$ precision), which are subjected to a gentle wave steepness ($s_{m-1,0} \leq 0.015$) and wave heights larger than the step height ($H_{m0}/S_h > 1$). For gentler slopes (1:3), the energy dissipation is over-predicted ($20-25\,\%$). By implementation of the new approach the reduction of the incident wave energy could be assessed. The result of this approach was that most energy is dissipated close to the SWL. Under certain boundary conditions, the energy dissipation above the SWL had only a minor influence on the energy dissipation. The energy dissipation over a stepped revetment was comparable to a schematic description of the energy dissipation for surging waves over a dike as given by Führböter (1991). By comparing the results from the analytic approach for gentle wave steepnesses ($H/L < 0.015$) to the results from the empirically derived energy dissipation for steeper waves ($0.015 < H/L < 0.05$), the principle difference of the wave interaction of surging and plunging waves with a stepped revetment was discussed. It could be concluded that stepped revetments are more effective ($20-30\,\%$) in reducing the wave run-up for plunging waves in comparison to surging waves.

6 Summary and Outlook

6.1 Summary

It was the objective of this study to gain knowledge on the energy dissipation of waves interacting with stepped revetments. The main benefit of stepped revetments is an increased energy dissipation in comparison to smooth revetments. The increased energy dissipation is a result of higher turbulence on the slope. Additionally, stepped revetments can offer easy and save access, e.g. from a promenade to the beach. In contrast, rough revetment surfaces, e.g. made of rocks or concrete armor units, are generally difficult to walk on. Revetments with rock or concrete armor units are therefore unsuitable in areas which require high levels of safety from large wave impacts but are simultaneously important for tourism. These requirements are the driver behind understanding the mechanisms that occur when incident waves interact with stepped coastal protection systems. Eventually, this knowledge will allow for a save and optimal design for such a type of revetment previously not available in a comprehensive manner.

To evaluate the performance and applicability of stepped revetments as coastal protection, a comprehensive literature review has been conducted. In more than 60 years of research, numerous studies have published results on the wave run-up, wave overtopping, scour development, and wave loading on coastal protection structures with a stepped face. Yet, each of these studies individually covers a limited range of application – while often being project-related or very site-specific. The main findings from comparing all individual studies are:

- The relation of the wave height to the step height influences the energy dissipation significantly but knowledge about the driving processes was still constrained. A more universal approach towards understanding the interaction of waves and stepped revetments was missing.

- Prediction methods for stepped revetment design contained large uncertainties as the parameter space was segmented.

Based on these findings, a new set of hydraulic model tests was conducted and subsequently analyzed. The set-up and test program was specifically developed to supplement the present knowledge gaps. The tests included 102 individual test-runs with irregular waves covering slope angles of $1 \leq cot\alpha \leq 3$, wave steepnesses of $0.015 < H_{m0}/L_{m-1,0} < 0.045$, Iribarren numbers of $1.5 < \xi_{m-1,0} < 8.5$ and step ratios of $0.5 < H_{m0}/S_h < 2.5$. An analysis of the new data set enabled conclusions about the energy dissipation of stepped revetments applicable for a wide range of hydraulic- and geometry-related boundary conditions which allow for more holistic conclusions. The main findings of the current study are:

- Stepped revetments have reflection coefficients comparable to plain or composite walls ($0.6 < C_r < 0.95$) in cases where the step ratios are large ($H_{m0}/S_h < 0.5$).

Moderate reflection coefficients are present $(0.35 < C_r < 0.6)$ for small step heights $(H_{m0}/S_h \geq 0.5)$ and are comparable to impermeable rock revetments.

- Wave run-up can be reduced by a stepped revetment by $10 - 60\%$ in comparison to plain slopes. The reduction coefficient $\gamma_{f_{R_{u,2\%}}}$ decreases for increasing dimensionless step heights $(k_h/(H_{m0} \cdot \xi_{m-1,0}))$. Step heights smaller than the wave height are more effective in the run-up reduction ($30 - 60\%$ for $H_{m0}/S_h \geq 1$ and $10 - 40\%$ for $H_{m0}/S_h < 1$). The minimal reduction coefficient $\gamma_{f_{R_{u,2\%}}}$ can be achieved for a step ratio of $H_{m0}/S_h = 2$. The run-up reduction becomes more effective with decreasing Iribarren number. The run-up reduction is more effective with larger slopes $(1 \leq n \leq 3)$. No further significant decrease of $\gamma_{f_{R_{u,2\%}}}$ was predicted for gentler slopes $(n > 3)$.

- The run-up reduction coefficients show lower values compared to the overtopping reduction coefficients as all the kinetic energy of an incident wave changes to potential energy during the run-up. In the case of wave overtopping the highest possible run-up is never reached and therefore less energy dissipated compared to a wave run-up at an infinite stepped slope.

- The effectiveness of the wave overtopping reduction at stepped revetments mainly depends on the step ratio H_{m0}/S_h and the Iribarren number. For step heights two times larger than the incident wave height, a slight reduction of $2 - 10\%$ compared to a smooth slope was observed. Within plunging waves, the overtopping could be reduced most effectively ($40 - 60\%$). Most of the energy is dissipated by wave breaking. The wave run-up is significantly reduced in cases where the wave run-up with a relatively low energy content is interrupted by the stepped surface; this consequentially affects wave overtopping as well. The effectiveness in reducing the wave overtopping for collapsing and surging wave breaking decreases ($10 - 30\%$).

- The position of the still water level (SWL) with respect to the step edge becomes important ($\pm 20\%$ reduction) if the step height and wave height are in the same range ($0.5 < H_{m0}/S_h < 2$). In this case the highest energy dissipation was achieved if the SWL was close to the step edge.

- The maximum wave loads acting on individual steps of stepped revetments were determined to occur close to the SWL. The wave loads decreased significantly with increasing distance to the SWL. Above the SWL the loads at a stepped revetment were comparable to conditions at a vertical wall whereas the loads below SWL were about 70% lower.

- A clarificiation about apparently contradictory findings of Nussbaum and Colley (1971) and Goda and Kishira (1976) (decreasing versus increasing energy dissipation with decreasing step ratio (H/S_h)) was achieved by the novel derivation of the minimal turning point in the energy dissipation at stepped revetments for $H/S_h = 2$.

Based on the individual findings, outlined prediction formulae have been derived empirically (summary on page 126). These prediction formulae are attributed to wave reflection,

wave run-up, wave overtopping and wave loads on stepped revetments and are summed up in the table in the following along with the corresponding range of applicability, the coefficient of determination and the standard deviation. The application of these formulae was demonstrated as a practical use case in appendix B.

An analytic approach for the calculation of the energy dissipation of waves with low steepness ($H/L < 0.015$) at a stepped revetment with steep slopes ($1 \leq n \leq 2$) was derived. The nonlinearity of the energy dissipation process over stepped revetments (increase of the energy dissipation with decreasing water depth) was emphasized.

For the first time, prediction formulae for reduction coefficients correlated to wave run-up and wave overtopping at stepped revetments consider the wave steepness, the slope and the step ratio coincidently. Due to the wide range of key parameters considered in the regression of data (at least $0.01 < H/L < 0.05$, $1.5 < \xi < 6.5$, $1 \leq cot\alpha \leq 3$, $0.2 < H/S_h < 15$), the formulae provide a wide range of applicability. Therefore, the formulae provide a novel and holistic design approach for stepped revetments.

6.2   Outlook

While the current research contributed to reducing existing deficiencies in the understanding of wave-structure interaction on stepped revetments, further research needs were identified in the process of analysis. Based on the findings of the present study, future research questions can be addressed:

- The influence of the model scale on the test results was only qualitatively addressed for those test groups researched in hydraulic model tests. It was discussed how the intensity of aeration mainly influenced the turbulence levels on the revetment. As the aeration is significantly lower in smaller scales, less turbulence is induced and finally the target values wave run-up and wave overtopping are predicted more conservatively. It is anticipated that by conducting larger scale model tests (or in-situ-measurements as Troch et al. (1998)) transfer functions can be derived to correct the provided prediction formulae for apparent scale effects. These large scale tests are already proposed to be conducted in the research project "waveSTEPS", supported by the *Federal Ministry of Education and Research* (BMBF) until 2019 in the large wave flume (GWK) in Hannover.

- The structural stability of the lateral interfaces of a section covered by a stepped revetment towards a next section that might be covered with an erodible surface (e.g. grass) requires particular attention; no guidance was given in this study how the interface might respond to external loads such as wave loads. Due to the increased turbulence over the revetment it is assumed that the wave- and current-induced loadings are increased in this interface. The vulnerability of such interfaces has been proven with the run-up simulator (Van der Meer, 2011) and is depicted for in-situ tests at a stair case in Eurotop (2016).

target value	valid for	R^2	STD
wave reflection for $\frac{H_{m0}}{S_h} < 0.5$: $\quad C_r = 0.47 + 1.18 \frac{tan\alpha H_{m0}}{\sqrt{S_h^2+S_w^2}}$ for $\frac{H_{m0}}{S_h} \geq 0.5$: $\quad C_r = 0.16 + 0.54 \cdot exp\left(11.55\frac{tan\alpha H_{m0}}{\sqrt{S_h^2+S_w^2}}\right)^{-0.04}$	$0.015 < \frac{H}{L} < 0.05$ $1 < \xi < 8$ $1 \leq cot\alpha \leq 3$ $0.2 < \frac{H}{S_h} < 30$	0.80	0.033
wave run-up $\frac{R_{u,2\%}}{H_{m0}} = 3.0 \cdot tanh\left(0.65 \cdot \xi_{m-1,0}\right) \cdot \gamma_{f,R_{u2\%}}$ for $1 > H_{m0}/S_h > 2$: $\quad \gamma_{f,R_{u2\%}} = \left[1 - a \cdot atan\left(\frac{k_h \cdot b}{H_{m0}\cdot\xi_{m-1,0}}\right)\right] \cdot c$ $\quad a = 1 - 0.97 \cdot atan\left(8.1\frac{H_{m0}}{S_h}\right)$ $\quad b = 1 - \frac{1}{0.075} \cdot atan\left(0.6\frac{H_{m0}}{S_h}\right)$ $\quad c = 0.75$ for: $H_{m0}/S_h < 0.5$ $\quad c = 1.0$ for: $H_{m0}/S_h \geq 0.5$ for $1 < H_{m0}/S_h < 2$: $\quad \gamma_{f_{R_{u,2\%}}} = 0.65 + (1.4 \cdot B_r)\left(\frac{|d_{st}|\cdot\gamma_{f_{R_{u,2\%}},general}}{k_h} - 0.5\right)^2$ $\quad$ with: $\gamma_{f_{R_{u,2\%}},general} = \gamma_{f_{R_{u,2\%}},(1>H_{m0}/S_h>2)}$ $\quad$ for: $\frac{H_{m0}}{L_{m-1,0}} \geq 0.015$: $\quad B_r = 1$ $\quad$ for: $\frac{H_{m0}}{L_{m-1,0}} < 0.015$: $\quad B_r = 1.4$	$0.01 < \frac{H}{L} < 0.05$ $1.5 < \xi < 7.5$ $1 \leq cot\alpha \leq 3$ $0.2 < \frac{H}{S_h} < 15$	0.70	0.051
wave overtopping $\frac{q}{\sqrt{gH_{m0}^3}} = 0.04exp\left[-\left(1.1\frac{R_c}{H_{m0}\gamma_{f,q}}\right)^{1.4}\right]$ for $0.5 > H_{m0}/S_h > 2.5$: $\quad \gamma_{f_q} = 1 + 0.4 \cdot a^{1.5} \cdot atan\left(\frac{k_h \cdot b}{H_{m0}\xi_{m-1,0}}\right)$ $\quad a = min\left\{1, \frac{H_{m0}}{S_h}\right\}$ $\quad b = -\left(1.8 + 0.4 \cdot exp\left[\left(0.015\frac{S_h}{H_{m0}}\right)^{-0.22}\right]\right)$ for $0.5 < H_{m0}/S_h < 2.5$: $\quad \gamma_{f_q} = 0.6 + 2.3\left(\frac{|d_{st}|\cdot\gamma_{f_q,general}}{k_h}\right)^2$ $\quad$ with: $\gamma_{f_q,general} = \gamma_{f_q,(0.5>H_{m0}/S_h>2.5)}$	$0.01 < \frac{H}{L} < 0.05$ $1 < \xi < 6.5$ $1 \leq cot\alpha \leq 3$ $1 < \frac{R_c}{H} < 3.5$ $0.2 < \frac{H}{S_h} < 30$	0.82	0.046
wave loads above SWL: $\quad \frac{p_{0.4\%}}{\rho g H_{m0}} = min\left\{2831.66 + tan\left(\frac{\frac{z}{H_{m0}}+1171.64}{74572}\right), 3.6\right\}$ below SWL: $\quad \frac{p_{0.4\%}}{\rho g H_{m0}} = min\left\{6.15 + tan\left(-\frac{\frac{z}{H_{m0}}-4.97}{2.87}\right), 3.6\right\}$	$0.01 < \frac{H}{L} < 0.05$ $1 < \xi < 8$ $1 \leq cot\alpha \leq 3$ $0.2 < \frac{H}{S_h} < 2.5$ $-6 < \frac{z}{H} < 2$	0.62	0.189

- This study focused on impermeable stepped revetments while the effect of permeability is intentionally neglected. Examples from literature indicated improvements with respect to the run-up reduction and toe scouring for permeable stepped revetments. It is still unknown how effective a permeable stepped revetment with respect to wave run-up reduction would be and if improvements in terms of the construction of a porous stepped revetment could be achieved (wave loading, material requirements, weight, filter layer design). As an addition to the popular "building-with-nature" approach, currently introduced to the coastal engineering discipline (de Vriend et al., 2014), the systematic planting with vegetation could be possible. This would increase the turbulence over the revetment and could lead to improvements in amenity and ecology. Typical problems in the predictability of the stability due to failures of the planting could be counteracted by a porous step-system.

Bibliography

Abdo, F. Y. (2007). Armoring tampa bay reservoir with soil-cement: Soil-cement protects upstream embankment of reservoir against erosive wave attack. *Government Engineering*, pages 52–54.

Ahrens, J. P. and Heimbaugh, M. S. (1988). *Approximate upper limit of irregular wave runup on riprap*, volume CERC-88-5 of *Technical Report*. Vicksburg, Miss.

Ahrens, J. P. and Titus, M. F. (1985). Wave runup formulas for smooth slopes. *Journal of Waterway, Port, Coastal, and Ocean Engineering*, 111(1):128–133.

Allsop, N. W. H. and Calabrese, M. (1999). *Forces on vertical breakwaters: Effects of oblique or short-crested waves.*, volume 465 of *Report*. HW Wallingford, Wallingford.

Allsop, N. W. H. and Vicinanza, D. (1996). Wave impact loadings on vertical breakwaters: development of new prediction formulae. *Proc. of the 11th International Harbour Congress, Antwerpen, Belgium*, pages 275–284.

Asakawa, T., Hasegawa, M., Sato, H., and Hamaguchi, N. (1992). Recent developments on shore protection in japan. In Institution of Civil Engineers, editor, *Coastal Structures and Breakwaters: Proceedings of the Conference Organized by the Institution of Civil Engineers, and Held in London on 6-8 November 1991*, pages 409–422. Telford.

ASCE (1995). *Wave forces on inclined and vertical wall structures.* American Society of Civil Engineers, New York.

Bagnold, R. A. (1939). *Interim report on wave-pressure research*, volume 12 of *Excerpt Journal of The Institution of Civil Engineers*. The Institution, London.

Baldock, T. E. and Simmonds, D. J. (1999). Separation of incident and reflected waves over sloping bathymetry. *Coastal Engineering*, 38(3):167–176.

Battjes, J. A. (1974a). *Computation of set-up, longshore currents, run-up and overtopping due to wind-generated waves: Techn. Hogeschool, Proefschr.–Delft, 1974.* Delft Univ. of Technology, Delft.

Battjes, J. A. (1974b). Surf similarity. *Proc. 14TH ASCE Coastal Eng. Conf. (Copenhagen, Denmark)*, (1):446–480.

Besley, P. (1999). *Overtopping of seawalls - design and assessment manual: R and D Technical Report W178.* Bristol, UK.

Bradbury, A., Rogers, J., and Thomas, D. (2012). *Toe structures management manual*, volume SC070056/R. Environment Agency, Bristol.

Brodtkorb, P. A., Johannesson, P., Lindgren, G., Rychlik, I., Rydén, J., and Sjö, E. (2002). Wafo - a matlab toolbox for the analysis of random waves and loads. In *Proc. 10'th ISOPE 2000*, volume 3, pages 343–350.

Bruun, P. and Günbak, A. R. (1977). Stability of sloping structures in relation to the iribarren number risk criteria in design. *Coastal Engineering*, (1 (1977)):287–322.

Buckingham, E. (1914). On physically similar systems; illustrations of the use of dimensional equations. *Phys. Rev.*, 4(4):345–376.

Busse, F. H. and Bestehorn, M. (2006). *Hydrodynamik und Strukturbildung: Mit einer kurzen Einführung in die Kontinuumsmechanik.* Springer-Lehrbuch. Springer Berlin Heidelberg.

Capel, A. (2014). Wave run-up and overtopping reduction by block revetments with enhanced roughness. *Coastal Engineering*, (34):76–92.

CEM (2002). *Coastal engineering manual.* Veri-Tech, Vicksburg, Miss., version 2.02, professional ed. edition.

Chanson, H. and Murzyn, F. (May 12-16, 2008). Froude similitude and scale effects affecting air entrainment in hydraulic jumps. In Babcock, Jr.,Roger W and Walton, R., editors, *World Environmental and Water Resources Congress 2008*, pages 1–10.

Chen, X., Hofland, B., and Uijttewaal, W. (2016). Maximum overtopping forces on a dike-mounted wall with a shallow foreshore. *Coastal Engineering*, 116:89–102.

Chuenchai, W., Pholyeam, N., Phetchawang, S., and Rasmeemasmuang, T. (2014). Wave run-up on stepped slopes. *KMUTT Research & Development Journal*, 36(3):329–340.

Courant, R., Friedrichs, K. O., and Lewy, H. (1928). *Uber die partiellen Differenzengleichungen der mathematischen Physik*, volume Heft 1/2 of *Mathematische Annalen, Sonderabdruck aus Band 100*. J. Springer, Berlin.

Cuomo, G., Allsop, N. W. H., Bruce, T. P., and Pearson, J. (2010). Breaking wave loads at vertical seawalls and breakwaters. *Coastal Engineering*, 57(4):424–439.

Daemrich, K.-F. and Kohlhase, S. (1979). Einfluß des Reflexionsgrades eines Wellenbrechers auf die Wellenhöhen im Diffraktionsbereich. *Die Küste*, (34):187–197.

Dai, Y. B. and Kamel, A. M. (1969). Scale effect tests for rubble-mound breakwaters: Hydraulic model investigation. *U S Waterways Experiment Station-Research Report H-69-2*, (69-2).

de Vriend, H., van Koningsveld, M., and Aarninkhof, S. (2014). 'building with nature': The new dutch approach to coastal and river works. *Proceedings of the Institution of Civil Engineers - Civil Engineering*, (167):18–24.

EAK (2007). *Empfehlungen für die Ausführung von Küstenschutzwerken*, volume 65 of *Die Küste*. Westholsteinische Verl.-Anst. Boyens, Heide.

Eurotop (2007). *Wave overtopping of sea defences and related structures: Assessment manual: Pullen, Tim; Allsop, N. William H.; Bruce, Tom; Kortenhaus, Andreas; Schüttrumpf, Holger; Van der Meer, Jentsje W.*, volume 73 of *Die Küste*. Boyens, Heide i. Holstein.

Eurotop (2016). *Manual on wave overtopping of sea defences and related structures: An overtopping manual largely based on European research, but for worldwide application: Pullen, Tim; Allsop, N. William H.; Bruce, Tom; Kortenhaus, Andreas; Schüttrumpf, Holger; Van der Meer, Jentsje W.; Troch, Peter; Zanuttigh, B.; De Rouck, J.* www.overtopping-manual.com, 2nd edition.

Franzius, L. (1965). Wirkung und Wirtschaftlichkeit von Rauhdeckwerken im Hinblick auf den Wellenauflauf: Techn. Hochsch., Diss. Hannover. *Mitteilungen des Franzius-Instituts für Grund- und Wasserbau der Technischen Hochschule Hannnover*, (25):149–268.

Frigaard, P. and Brorsen, M. (1995). A time-domain method for separating incident and reflected irregular waves. *Coastal Engineering*, 24(3-4):205–215.

Frostick, L. E., McLelland, S. J., and Mercer, T. G. (2011). *Users guide to physical modelling and experimentation: Experience of the HYDRALAB network.* CRC Press/Balkema, Leiden, The Netherlands, 1st ed. edition.

Führböter, A. (1971). *Über die Bedeutung des Lufteinschlages für die Energieumwandlung in Brandungszonen*, volume 36 of *Mitteilungen des Franzius-Instituts*. Franzius-Institut.

Führböter, A. (1991). Wellenbelastung von Deich– und Deckwerksböschungen. *Jahrbuch der Hafenbautechnischen Gesellschaft (HTG)*, (46):225–282.

Goda, Y. (2010). *Random seas and design of maritime structures*, volume 33 of *Advanced series on ocean engineering*. World Scientific Publ, Singapore, 3. ed. edition.

Goda, Y. and Kishira, X. (1976). Experiments on irregular wave overtopping charakteristics of seawall of low crest types. *Technical Note of PARI*, (242):1–29.

Grilli, S. T., Losada, M. A., and Martin, F. (1993). Wave impact forces on mixed breakwaters. In *Proceedings of the Coastal Engineering Conference*, volume 1, pages 1161–1174.

Grüne, J. and Bergmann, H. (1994). Wave loads on seadikes with composite slopes and berms. *Proc. 24th Int. Conf. on Coastal Eingineering, Kobe, Japan*, pages 1175–1089.

Hamel, G. (1916). Spiralförmige Bewegung zäher Flüssigkeiten. *Jahresbereich der Deutschen Mathematiker-Vereinigung*, (25):34–60.

Hamilton, W. A. H. (1988). Communication on the design and construction of sea defences at Sheerness by J. E. Robinson. *Water and Environment Journal*, 2(2):181–182.

Heimbaugh, M. S. (1988). *Coastal engineering studies in support of Virginia Beach, Virginia, Beach Erosion Control and Hurricane Protection Project: Report 1, Physical model tests of irregular wave overtopping and pressure measurements*, volume 88-1 of *CERC*. available from National Technical Information Service, Springfield, Va.

Hudson, R. Y. (1959). *Laboratory investigation of rubble-mound breakwaters*, volume no. 2-224 of *Miscellaneous Paper*. Waterways Experiment Station, Vicksburg, Miss.

Hudson, R. Y., Jackson, R. A., and Cuckler, R. E. (1957). *Wave Run-Up and Overtopping Levee Sections, Lake Okeechobee, Florida, Hydraulic Model Investigation*. Defense Technical Information Center, Ft. Belvoir.

Hughes, S. A. (1993). *Physical models and laboratory techniques in coastal engineering*, volume 7 of *Advanced series on ocean engineering*. World Scientific, Singapore.

Hughes, S. A. (2005). *Estimating Irregular Wave Runup on Rough, Impermeable Slopes*, volume CHETN-III-70. Defense Technical Information Center, Ft. Belvoir.

Hunt, A. (2003). *Extreme Waves, Overtopping and Flooding at Sea Defences*. University of Oxford, Oxford.

Hunt, Jr., I. A. (1959). Design of seawalls and breakwaters. *Journal of the Waterways and Harbors Division*, 85(3):123–152.

Jachowski, R. A. (1964). Interlocking precast concrete block seawall. *Proc. of the 9th Int. Conf. on Coastal Engineering, Lisbon, Portugal*, (9):504–517.

Kamel, A. M. (1968). *Water wave pressures on seawalls and breakwaters*, volume 2-10 of *Research report / U.S. Army Engineer Waterways Experiment Station*. U.S. Army Engineer Waterways Experiment Station, Vicksburg, Miss.

Kármán, T. v. (1930). Mechanical similitude and turbulence. *Nachrichten von der Gesellschaft der Wissenschaften zu Göttingen*, (5):58–76.

Kerpen, N. B., Goseberg, N., and Schlurmann, T. (2014). Experimental investigations on wave overtopping on stepped embankments. *Proceedings of the 5th International Conference on Application of physical modelling to port and coastal protection*, (2):262–269.

Kirkgöz, M. S. (1983). Secondary pressures of waves breaking on seawall. *Journal of Waterway, Port, Coastal, and Ocean Engineering*, 109(4):487–490.

Krecic, M. R. and Sayao, O. J. (2003). Wave overtopping on chicago shoreline revetment. *Coastal Structures 2013, ASCE*, pages 542–554.

Mansard, E. and Funke, E. (1980). *The Measurement of Incident and Reflected Spectra Using a Least squares Method*. Coastal Engineering. ASCE - Texas Digital Library, Sydney, Australia.

Mase, H. (1989). Random wave runup height on gentle slope. *Journal of Waterway, Port, Coastal, and Ocean Engineering*, 115(5):649–661.

McCartney, B. L. (1976). *Survey of coastal revetment types*, volume 76-7 of *Miscellaneous Report*. Coastal Engineering Research Center, Fort Belvoir, Va.

Miche, R. (1944). *Mouvements ondulatoires de la mer en profondeur constante ou décroissante: Forme limite de la houle lors de son déferlement, application aux digues maritimes*, volume 114 of *Annales des Ponts et Chaussees*. Paris.

Minikin, R. R. (1963). *Winds, waves and maritime structures: Studies in harbour making and in the protection of coasts*. Griffin, London.

Neelamani, S. and Sandhya, N. (2005). Surface roughness effect of vertical and sloped seawalls in incident random wave fields. *Ocean Engineering*, 32(3-4):395–416.

Nussbaum, P. J. and Colley, B. E. (1971). *Dam construction and facing with soil-cement.* Research and Development Bulletin. Portland Cement Association, Chicago, Ill.

Okayasu, A., Suzuki, T., and Matsubayashi, Y. (2005). Laboratory experiment and three-dimensional large eddy simulation of wave overtopping on gentle slope seawalls. *Coastal Engineering Journal*, 47(2-3):71–89.

O'Shaughnessy, M. M., Perry, L., Haupt, L. M., Leeds, C. T., and Fowler, C. E. (1924). *Ocean Beach Esplanade, San Francisco, California.* American Society of Civil Engineers, New York.

Oumeraci, H., Klammer, P., and Partenscky, H. W. (1993). Classification of breaking wave loads on vertical structures. *Journal of Waterway, Port, Coastal and Ocean Engineering*, 119(4):381–397.

Pereira, I. M. (1996). *Wirbelablösungen, die Oberflächenwellen beim Passieren einer Stufe erzeugen*, volume 132 of *Mitteilung des Instituts für Wasserbau und Wasserwirtschaft, Technische Universität Berlin.* Berlin.

Postama, G. M. (1989). *Wave reflection from rock slopes under random wave attack.* TU Delft, Faculty of Civil Engineering and Geosciences, Hydraulic Engineering, Delft.

Rowe, S. (2012a). Appendix f concrete stepped revetment examples: Report to the cabinet to be held on 14th febuary 2012: http://shortlinks.de/2gww.

Rowe, S. (2012b). Scarborough coastal defence strategy - the Scarborough Spa, rock revetmant and stepped concrete revetment comparison: Report to the cabinet to be held on 14th febuary 2012: http://shortlinks.de/8rhm.

Sainflou, G. (1928). *Essai sur les digues maritimes verticales.* École nationale des Ponts et Chaussées, Paris.

Sato, S., Irie, I., and Katsuhiro, S. (1971). Experimantal study on the scour prevention works at the foot of sea walls. *Technical Note of the Port and Harbour Research Institute, Ministry of Transport*, (117):3–38.

Saville, T. (1955). *Laboratory data on wave run-up and overtopping on shore structures*, volume no. 64 of *Technical memorandum - Beach Erosion Board.* U.S. Beach Erosion Board, Washington, D.C.

Saville, T. (1956). Wave run-up on shore structures. *Proceedings of the American Society of Civil Engineering*, (952-WW2):1–14.

Saville, T. (1957). Wave run-up on composite slopes. *Proceedings of 6th Conference on Coastal Engineering, Gainesville, Florida*, (6):691–699.

Schlichting, H., Krause, E., Oertel, H. J., and Gersten, K. (2013). *Grenzschicht-Theorie.* Springer, Berlin Heidelberg.

Schüttrumpf, H. F. (2001). *Wellenüberlaufströmung bei Seedeichen: Experimentelle und theoretische Untersuchungen*, volume 149 of *Mitteilungen aus dem Leichtweiß Institut für Wasserbau.* Braunschweig.

Seelig, W. N. and Ahrens, J. P. (1981). *Estimation of wave reflection and energy dissipation coefficients for beaches, revetments, and breakwaters*, volume No. 81-1 of *USA. Army. Coastal Engineering Research Center. Technical paper.* USA Army. Coastal Engin. Res. Center, Fort Belvoir, Va.

Selivanov, L. V. (1972). Determination of wave loads on sloping structures: Discussion of construction norms: Translated from gidrotekhnicheskoie stroitel'stvo, no. 5, pp. 49-50, may, 1972. *Hydrotechnical Construction*, 6(5):487–489.

Shibata, K., Yagyu, T., and Murata, T. (1981). Design method of stepped face seawall. *Technical Note of the Port and Harbour Research Institute, Ministry of Transport*, (380).

Siekmann, H. E. and Thamsen, P. U. (2013). *Strömungslehre.* Springer-Lehrbuch. Springer Verlag, Berlin Heidelberg.

Sommerfeld, A. (1896). Mathematische Theorie der Diffraction: Mit einer Tafel. *Mathematische Annalen*, 47(2):317–374.

SPM (1984). *Shore protection manual.* U.S. Army Corps of Engineers, Washington, 4th ed. edition.

Squire, H. B. (1965). The growth of a vortex in turbulent flow. *Aeronautical Quarterly*, 16(3):302–306.

Srivastava, H. and Varming, C. (2014). *Option Assessment and Preliminary Design Report: Project: Lake Cathie Revetment Wall Investigation and Design.* Reference: 237746. Aurecon Australia Pty Ltd, Neutral Bay, Australia.

Stoa, P. N. (1978). *Reanalysis of wave runup on structures and beaches*, volume CERC-TP-78-2. Coastal Engineering Research Center, Fort Belvoir.

Stoker, J. J. (1992). *Water Waves: The Mathematical Theory with Applications.* Pure and applied mathematics. John Wiley & Sons, New York.

Suzuki, T., Tanaka, M., and Okayasu, A. (2003). Laboratory experiments on wave overtopping over smooth and stepped gentle slope seawalls. *Asian and Pacific Coasts*, pages CD–ROM.

Szmytkiewicz, M., Kolodko, J., and Zeidler, R. B. (1994). *Irregular wave run-up on various slopes and optimization guidelines.* Report Polish Academy of Sciences. Institute of Hydro-engineering, Polen.

Tabata, T., Shibata, K., and Yagyu, T. (1980). Compilation of existing design data of stepped face seawall. *Technical Note of the Port and Harbour Research Institute, Ministry of Transport*, (346).

Takayama, T., Nagai, T., and Nishida, K. (1982). Decrease of wave overtopping amound due to seawalls of low crest types. *Reoport of The Port and Harbour Research Institute*, (21(2) (in Japanese)):151–206.

TAW (2002). *Technisch rapport golfoploop en golfoverslag bij dijken.* TAW, Delft, Netherlands.

Treuel, F. M. (2013). Physikalische Modellierung von Wellenauflauf an gestuften Böschungen (TP 1.3): Klimzug-Nord: Projekt des Monats März 2013.

Troch, P., De Rouck, J., and Van Damme, L. (1998). Instrumentation and prototype measurements at the zeebrugge rubble mound breakwater. *Coastal Engineering*, 35(1–2):141–166.

United Nations (1982). Technologies for coastal erosion control. *Department of Natural Resources and Energy, Department of Technical Co-operation for Development.*

USACE (1981). *Seawalls - Their applications and limitations.* Coastal Engineering Technical Note. U.S. Army Corps of Engineering, Fort Belvoir.

USACE (1995). *Design of Coastal Revetments, Seawalls and Bulkheads*, volume EM 1110-2-1614 of *Engineer Manual.* Department of the Army, Washington, D.C.

Van der Meer, J. W. (1998). *Wave run-up and overtopping: Chapter 8 in: Seawalls, dikes and revetments.* Pilarczyk, K. W., Balkema, Rotterdam.

Van der Meer, J. W. (2011). *The wave run-up simulator: Idea, necessity, theoretical background and design.* Van der Meer Consulting, Heerenveen, the Netherlands.

Van der Meer, J. W. and Bruce, T. P. (2014). New physical insights and design formulas on wave overtopping at sloping and vertical structures. *Journal of Waterway, Port, Coastal and Ocean Engineering*, 140(6).

Van der Meer, J. W. and Janssen, J. P. (1994). *Wave run-up and wave overtopping at dikes and revetments*, volume no. 485 of *Publication.* Delft Hydraulics, Delft, Netherlands.

Van der Meer, J. W. and Stam, C. J. (1992). Wave runup on smooth and rock slopes of coastal structures. *Journal of Waterway, Port, Coastal and Ocean Engineering*, 118(5):534–550.

Van Steeg, P., KIein Breteler, M., and Provoost, Y. (2016). Large-scale physical model tests to determine influence factor of roughness for wave run-up of channel shaped block revetments. *Proceedings of the 6th International Conference on the Application of Physical Modelling in Coastal and Port Engineering and Science, Ottawa, Canada.*

Van Steeg, P., Wolters, G., and van Gent, M. (2012). *Invloedsfactor voor ruwheid van een getrapt talud bij golfoverslag bij dijken: Verslag fysieke modeltesten en analyse*, volume 1206984-000-HYE-0006 of *Project Report.* Delft, The Netherlands.

Victor, L., van der Meer, J., and Troch, P. (2012). Probability distribution of individual wave overtopping volumes for smooth impermeable steep slopes with low crest freeboards. *Coastal Engineering*, 64:87–101.

Waal, J. d. and van der Meer, J. W. (1992). Wave runup and overtopping on coastal structures. *Coastal Engineering Proceedings*, 1(23).

Walton, Jr., T. L., Ahrens, J. P., Truitt, C. L., and Dean, R. G. (1989). *Criteria for Evaluating Coastal Flood-Protection Structures.* Defense Technical Information Center, Ft. Belvoir.

Ward, D. L. (2003). *Overtopping Studies of a Stepped Revetment for City of Chicago, Illinois.* Defense Technical Information Center, Ft. Belvoir.

Ward, D. L. and Ahrens, J. P. (1992). *Overtopping Rates for Seawalls*, volume CERC-92-3 of *Miscellaneous Paper.* U.S. Army Corps of Engineers, Washington, D.C.

Wassing, F. (1957). *Model Investigation on Wave Run-Up Carried out in the Netherlands during the Past Twenty Years*, volume 6 of *Proceedings of 6th Conference on Coastal Engineering.* Coastal Engineering Research Council, Gainesville, Florida.

West, I. M. (2016). Hurst spit - barrier beach of the west solent: Geology of the wessex coast of southern england: http://www.southampton.ac.uk/˜imw/hurst-castle-spit.htm.

Xiaomin, W., Liehong, J., and Treuel, F. M. (2013). The study on wave run-up roughness and permeability coefficient of stepped slope dike. *Proceedings of the 7th International Conference on Asian and Pacific Coasts (APAC 2013)*, pages 295–299.

Yalin, M. S. (1971). *Theory of hydraulic models.* Macmillan civil engineering hydraulics. Macmillan, London.

Zanuttigh, B. and Van der Meer, J. W. (2008). Wave reflection from coastal structures in design conditions. *Coastal Engineering*, 55(10):771–779.

A Appendices

B Design example application

An example application of the design of a stepped revetment with the new derived formulae is given in the following. It is assumed that the coastal protection at the north-western end of the North Frisian Island Baltrum is to be renewed. The chosen site is frequently visited by tourists throughout the year. As a consequence, an easy access to the beach has to be guaranteed. As a second constraint, the city center of Baltrum requires protection to storm surges by a coastal protection system with specified crest height of $+7.9\,mNN$. In the planning process, the installation of a stepped revetment is considered in viable option by planners and designers. The required dimensions of such a stepped revetment are therefore given.

Hydraulic boundary conditions
A storm event with wind speeds of $20\,m/s$ from north-north-east at a storm surge water level of $+5.0\,mNN$ is considered and the following hydraulic boundary conditions can be estimated at this location:

$$
\begin{aligned}
h_s &= 5.1\,m \\
H_s &= 2.4\,m \\
T_m &= 8.0\,s
\end{aligned}
\tag{B.1}
$$

The mean wave length L_m is then calculated according to intermediate conditions. The relative water level in front of the stepped revetment is in a range of $0.05 < h_s/L < 0.5$. Wave length and Iribarren number yield:

$$
\begin{aligned}
L_m &= \frac{gT_m^2}{2\pi} \cdot tanh\left(\frac{2\pi \cdot h_s}{L_m}\right) \\
&= \frac{g(8\,s)^2}{2\pi} \cdot tanh\left(\frac{2\pi \cdot 5.1\,m}{L_m}\right) \\
&= 53.8\,m \\
\xi_m &= \frac{tan\alpha}{\sqrt{\frac{H_s}{L_m}}} = \frac{1}{3\sqrt{\frac{2.4\,m}{53.8\,m}}} = 1.58\,[-]
\end{aligned}
\tag{B.2}
$$

In a next step, the run-up height is calculated according to Eq. 4.6. The reduction coefficient for the run-up is calculated with respect to the required step heights (here exemplary

with $S_h = 0.15\,m$ to

$$
\begin{aligned}
\gamma_{f,R_{u2\%}} &= 1 - \left[1 - 0.97 \cdot atan\left(8.1\frac{H_s}{S_h}\right)\right] \cdot atan\left(\frac{k \cdot \left[1 - \frac{1}{0.075} \cdot atan\left(0.6\frac{H_s}{S_h}\right)\right]}{H_s \cdot \xi_m}\right) \\
&= 1 - \left[1 - 0.97 \cdot atan\left(8.1\frac{2.4\,m}{0.15\,m}\right)\right] \cdot atan\left(\frac{k \cdot \left[1 - \frac{1}{0.075} \cdot atan\left(0.6\frac{2.4\,m}{0.15\,m}\right)\right]}{2.4\,m \cdot 1.58}\right) \\
&= 0.686\,[-].
\end{aligned}
\tag{B.3}
$$

With the reduction coefficient the wave run-up at the stepped revetment under given hydraulic- and geometry-related boundary conditions can be calculated to

$$
\begin{aligned}
R_{u,2\%} &= 3.0 \cdot tanh\left(0.65 \cdot \xi_m\right) \cdot \gamma_{f,R_{u2\%}} \cdot H_m \\
&= 3.0 \cdot tanh\left(0.65 \cdot 1.58\right) \cdot 0.686 \cdot 2.4\,m \\
&= 3.81\,m.
\end{aligned}
\tag{B.4}
$$

As the calculated wave run-up is larger than the remaining freeboard height under the given storm conditions

$$
R_{u,2\%} = 3.81\,m > 2.8\,m = R_c
\tag{B.5}
$$

wave overtopping has to be considered. The reduction coefficient for a stepped surface is calculated with Eq. (4.12) to

$$
\begin{aligned}
\gamma_{f_q} &= 1 + 0.4 \cdot \left(min\left\{1, \frac{H_m}{S_h}\right\}\right)^{1.5} \cdot atan\left(\frac{k_h \cdot \left[-\left(1.8 + 0.4 \cdot exp\left[\left(0.015\frac{S_h}{H_m}\right)^{-0.22}\right]\right)\right]}{H_m \cdot \xi_m}\right) \\
&= 1 + 0.4 \cdot \left(min\left\{1, \frac{2.4\,m}{0.15\,m}\right\}\right)^{1.5} \cdot atan\left(\frac{0.142\,m \cdot \left[-\left(1.8 + 0.4 \cdot exp\left[\left(0.015\frac{0.15\,m}{2.4\,m}\right)^{-0.22}\right]\right)\right]}{2.4\,m \cdot 1.58}\right) \\
&= 0.593\,[-].
\end{aligned}
\tag{B.6}
$$

To predict the wave-overtopping at a stepped revetment Eq. (2.15) is used. Therefore, the mean overtopping volume is estimated to

$$
\begin{aligned}
q &= 0.09 \cdot exp\left[-\left(1.5\frac{R_c}{H_m \cdot \gamma_f \cdot \gamma_\beta \cdot \gamma^*}\right)^{1.3}\right] \cdot \sqrt{g \cdot H_m^3} \\
&= 0.09 \cdot exp\left[-\left(1.5\frac{2.8\,m}{2.4\,m \cdot 0.593 \cdot 1 \cdot 1}\right)^{1.3}\right] \cdot \sqrt{g \cdot (2.4\,m)^3} \\
&= 11.1\,[l/(sm)].
\end{aligned}
\tag{B.7}
$$

If one exercises the calculation for a number of step heights the correlation according to

Fig. B.1 is achieved. The figure gives quantities of predicted wave run-up heights, mean overtopping volumes and corresponding reflection coefficients following Eq. (4.4). The quantities are given for two slopes (1:2 and 1:3) in order to estimate the slope influence.

For this design example, the highest run-up is predicted for step heights of $0.1\,m$. With increasing step heights the run-up height decreases. The same trend can be seen for the mean wave overtopping volume. Steps with a height up to $0.5\,m$ are most effective in the run-up reduction. If the step height is increased further, the run-up decreases only slightly. The optimum run-up reduction would be achieved for $H_s/S_h = 2$. But, the corresponding step height of $S_h = H_s/2 = 2.4\,m/2 = 1.2\,m$ would result in a dangerous edge to fall down. The predicted mean wave overtopping volume also decreases with increasing step height. As overtopping volumes of $11.1\,l/(sm)$ are predicted for a step height of $0.15\,m$, the design has to be evaluated as insufficient for the chosen boundary conditions. The mean overtopping volume would cause major damage on the inner slope. A step height of $0.5\,m$ reduces the overtopping volumes more effectively. Values of $7.5\,l/(sm)$ are assessed as acceptable at this specific site. A slope of 1:2 gives $\approx 10\,\%$ higher mean overtopping volumes for this step height.

The designed stepped revetment is visualized in Fig. B.2 and it is outlined for what purposes the two different step heights could be used for. While the smaller step height is a feasible option for walking or gaining height, the second, larger step height allows for resting and contemplation. Both described revetments ($S_h = 0.15\,m$ and $S_h = 0.5\,m$) increase touristic value. Whereas the large step height provides some type of panorama terrace, the small step height enables the easy access to the beach front. A combination of both revetments is possible. An example is given in Fig. B.3. Although the figure shows the inner slope of a revetment, the principle of a possible use is obvious.
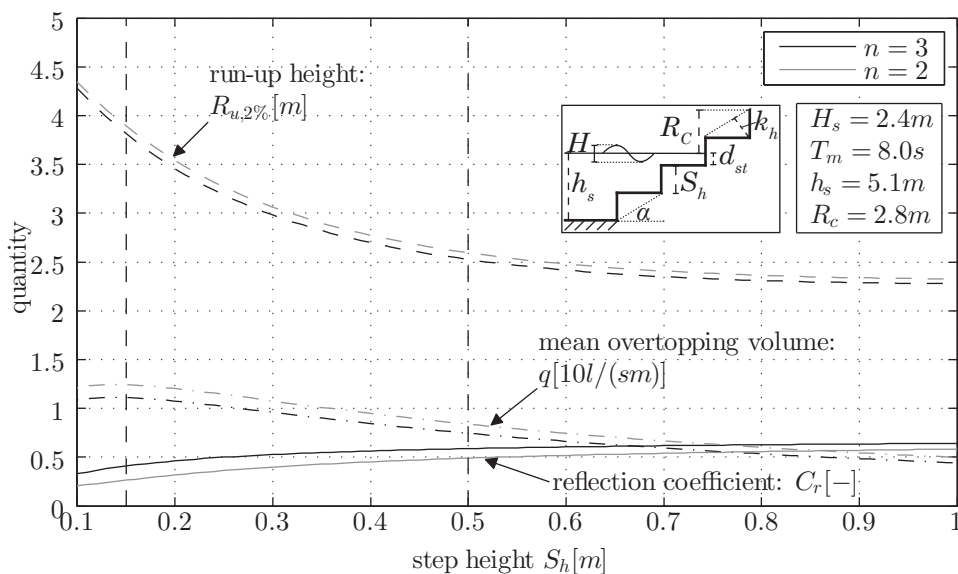
Figure B.1: Decision diagram for the application study.
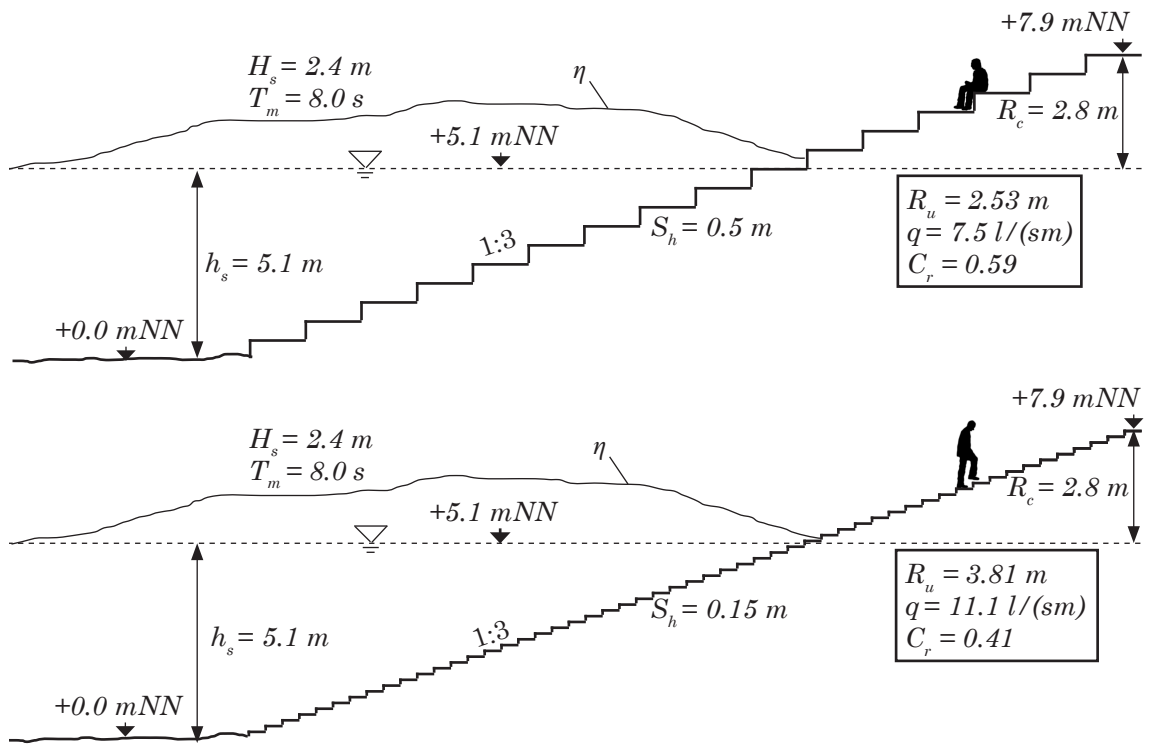
Figure B.2: Visualized result of the application study.
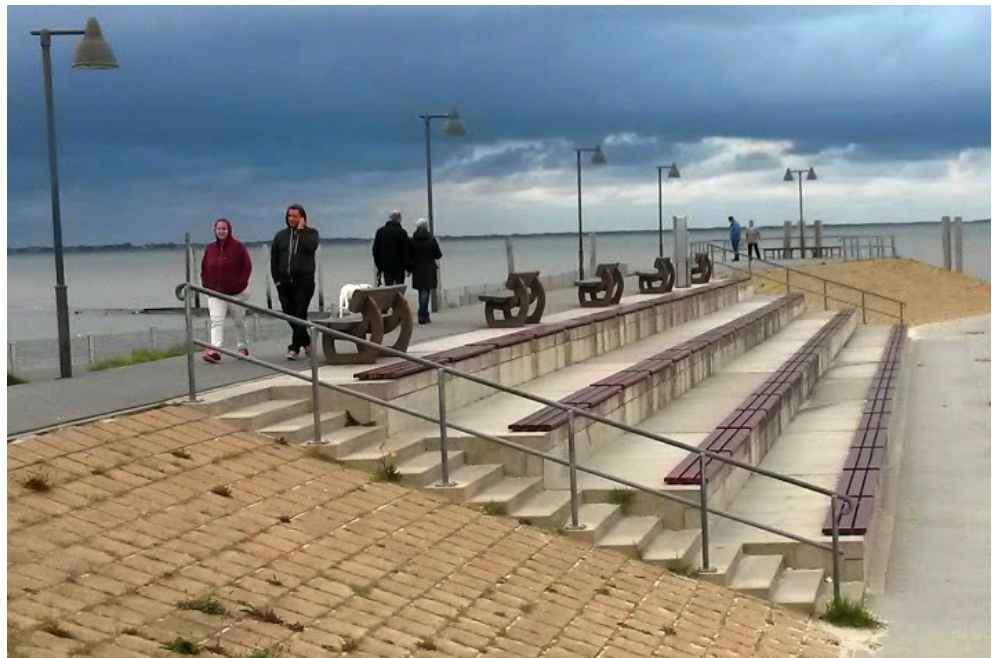
Figure B.3: Stepped slope in Nessmersiel, Germany, as example for a combination of slopes with more than one step height.

C   Overview to parameters for stepped revetments given in literature

	Boundary conditions					Hydraulic parameter				Geometry parameter					Output / Measurements					
author	key parameter	number of tests	scale	state of sea	wave maker	H [m]	T [s]	d [m]	h [m]	Rc [m]	n [m]	Sh [m]	Step type	i [m]	Ru [m]	q [l/(sm)]	Rc/H [-]	H/Sh [-]	ξ [-]	γf [-]
Saville (1955)	Ru, q	25 (Ru), 88 (q)	1:17	regular	plunger	0.054 - 0.215	0.717 - 3.63	0 - 0.161	0.34 - 0.50	0.05 - 0.43	1.5	0.018	vertical	10	0.018 - 0.466	0 - 18.44	0.25 - 5.0	2 - 12	1.4 - 13.1	0.33 - 0.85 (Ru), 0.06 - 0.099 (q)
Wassing (1957)	Ru	-	-	regular	equilibrium piston + wind	-	-	0.32	0.32	-	3.5	0.14, 0.35	vertical	-	-	-	-	-	1.08 - 1.27	0.77 - 0.78 (Ru)
Jachowski (1964)	Ru, Ns	-	1:10 (Ns), 1:16 (Rn)	regular	-	0.008 - 0.358	0.73 - 4.7	0 - 0.38	0.38	0.05 - 0.43	2.3	0.016	vertical, inclined	50	-	-	0.04 - 1.88	-	-	-
Nussbaum & Colley (1971)	Ru	110	-	regular	piston	<0.17	-	0.53	0.53	-	2.3	0.025, 0.051	vertical, round	-	-	-	0.80 - 2.30	-	-	0.62 - 0.72 (sharp), 0.86 (round)
Sato, Irie & Sasaki (1971)	scour depth	-	1:10	regular	flap	0.06, 0.12	1.52	0	0.47	0.1	3	0.05	vertical	10	-	-	-	1.2, 2.4	1.83, 2.55	1.11 (scour)
Goda & Kishira (1976)	q	9	1:33	irregular	-	0.164 - 0.178	1.74	-	-	0.073, 0.148	2	0.006, 0.009	vertical	10, 30	-	0.048 - 1.73	0.40, 0.83	19.4, 29.1	0.9 - 2.67	0.8 - 0.9 (q)
Takajama et al. (1982)	q	135	1:33	irregular	piston	0.12 - 0.3	1.46 - 2.32	0 - 0.12	-	0.03 - 0.21	2, 3, 4	0.008, 0.015	vertical	30	-	0.006 - 3.4	0.15 - 0.40	16 - 40	1.3 - 2.6	0.68 - 0.9 (q)
Heimbaugh (1988)	q, p	178	1:13 (q), 1:19 (q, p)	irregular (TMA)	piston	0.217 - 0.253	2.27 - 6.32	0.09 - 0.2	0.26 - 0.37	0.09 - 0.24	1.5, 2	0.02 - 0.035	vertical	16	-	0.003 - 36	0.26 - 0.80	9.04 - 10.54	2.8 - 6.3	-
Asakawa (1992)	-	-	1:20, 1:30	irregular	-	-	-	-	-	-	3, 5	-	-	-	-	-	-	-	-	-
Ward (1992)	q	68	1:19	irregular (TMA)	piston	0.034 - 0.1	1.1 - 3.37	0.098 - 0.14	-	0.082 - 0.124	2	0.024	vertical	16	-	0.001 - 1.9	-	-	2.1 - 3.8	-
Pereira (1996)	vorticity	22	-	regular	piston	0.014 - 0.048	0.5 - 2.2	0.375	0.375	-0.15/-0.03	-	0.15	vertical	-	-	-	-	-	-	-
Ward (2003)	q, Ns, toe	-	1:35	irregular	piston	0.066 - 0.113	1.37 - 1.61	0.41	-	0.08 -	3	0.01	vertical	20	-	-	-	-	-	-
Suzuki (2003)	q	12	-	regular (ARC)	-	0.113	1.61	0 - 0.05	0.3 - 0.35	0.08 - 0.11	3	0.01	vertical	20	-	-	-	-	-	-
van Steeg (2012)	q	21	1:10	irregular (2nd order)	piston (ARC)	0.075 - 0.155	1.58	0.72 - 0.927	0.72 - 0.927	0.12 - 0.26	2, 3	0.023, 0.046	vertical, inclined	-	-	0.002 - 0.26	1.67 - 1.7	1.6 - 6.74	1.7 - 3.7	0.8 - 0.9 (q, <Sh), 0.6 - 0.7 (q, >Sh)
Chuenchai et al. (2013)	Ru	-	1:10	regular	flap	0.03 - 0.13	0.6 - 1.2	0.35	0.35	0.35	2.1 - 3.7	0.02 - 0.05	vertical	-	0 - 0.16	0.013 - 0.192	v	0.6 - 6.5	0.5 - 3.0	~0.64 (Ru)
Xiamoin et al. (2013)	Ru	54	1:10	regular	piston	0.048 - 0.08	0.8 - 1.3	0.73	0.73	0.16	2.5	0 - 0.176	vertical	-	0 - 0.16	-	2.0 - 3.4	0.27 - 8.0	1.48 - 2.96	0.35 - 0.77 (Ru)
Kerpen et al. (2014)	q	29	1:5	regular (2nd order)	piston	0.113 - 0.164	2.0	0.5	0.995	0.202	2.3	0.04, 0.08	vertical	-	0 - 0.16	0.001 - 3.7	1.1 - 1.7	0.38 - 1.22	2.0 - 3.6	0.14 - 0.5 (q)

D Model set-up
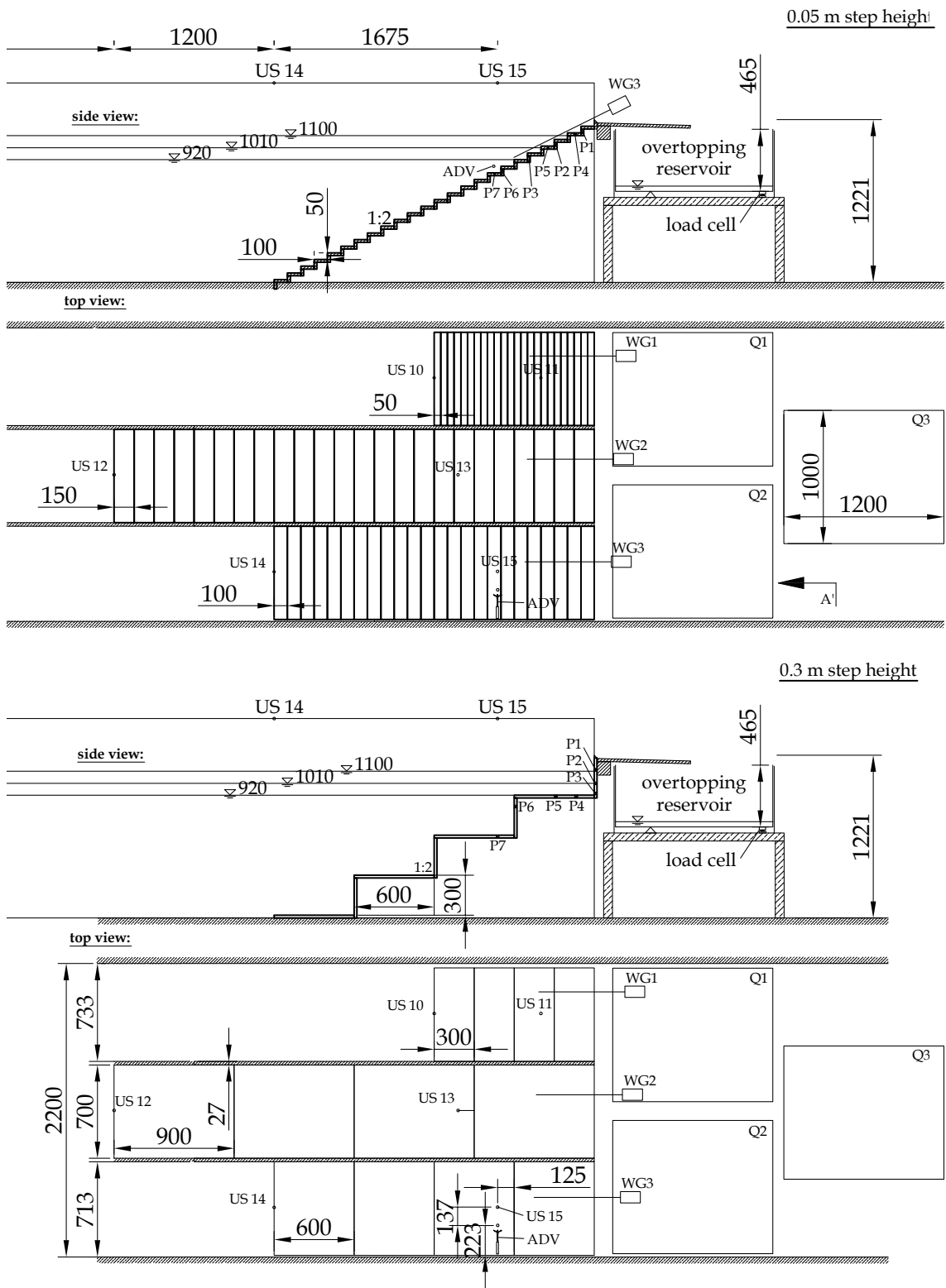
Figure D.1: Side and top view of the tested stepped revetments with 0.05 m and 0.3 m step height including instrumentation in the wave flume

E   Channel specification

amplifier		DAQ (HBM)		sensor			catman AP				sampling freq.
cable-ID	designation	designation	channel	manufacturer	designation	serial_ID	channel-ID	name	unit	file extension	
-	-	MX1601B	-	-	-	-	1	time	s		
1	ULS HF58_1	MX1601B	1	General Acoustics	USS10	121	2	USS1	m	...100Hz.MAT	100 Hz
2	ULS HF58_1	MX1601B	2	General Acoustics	USS10	117	3	USS2	m	...100Hz.MAT	100 Hz
3	ULS HF58_1	MX1601B	3	General Acoustics	USS10	116	4	USS3	m	...100Hz.MAT	100 Hz
4	ULS HF58_1	MX1601B	4	General Acoustics	USS10	115	5	USS4	m	...100Hz.MAT	100 Hz
5	ULS HF58_1	MX1601B	5	General Acoustics	USS10	112	6	USS5	m	...100Hz.MAT	100 Hz
6	ULS HF58_1	MX1601B	6	General Acoustics	USS10	113	7	USS6	m	...100Hz.MAT	100 Hz
7	ULS HF58_1	MX1601B	7	General Acoustics	USS10	114	8	USS7	m	...100Hz.MAT	100 Hz
8	ULS HF58_1	MX1601B	8	General Acoustics	USS10	98	9	USS8	m	...100Hz.MAT	100 Hz
9	ULS HF58_2	MX1601B	9	General Acoustics	USS10	99	10	USS9	m	...100Hz.MAT	100 Hz
10	ULS HF58_2	MX1601B	10	General Acoustics	USS10	118	11	USS10	m	...100Hz.MAT	100 Hz
11	ULS HF58_2	MX1601B	11	General Acoustics	USS10	124	12	USS11	m	...100Hz.MAT	100 Hz
12	ULS HF58_2	MX1601B	12	General Acoustics	USS10	121	13	USS12	m	...100Hz.MAT	100 Hz
13	ULS HF58_2	MX1601B	13	General Acoustics	USS10	127	14	USS13	m	...100Hz.MAT	100 Hz
14	ULS HF58_2	MX1601B	14	General Acoustics	USS10	122	15	USS14	m	...100Hz.MAT	100 Hz
15	ULS HF58_2	MX1601B	15	General Acoustics	USS10	133	16	USS15	m	...100Hz.MAT	100 Hz
16	-	MX1601B	16	Nortek As	Vectrino +	21399	17	Vec_Z	m/s	...100Hz.MAT	100 Hz
19	GHM unit	MX840A_1	1	Delft Hydraulics	GHM	-	19	WP1	m	...100Hz.MAT	100 Hz
20	GHM unit	MX840A_1	2	Delft Hydraulics	GHM	-	20	WP2	m	...100Hz.MAT	100 Hz
21	GHM unit	MX840A_1	3	Delft Hydraulics	GHM	-	21	WP3	m	...100Hz.MAT	100 Hz
22	-	MX840A_1	4	Nortek As	Vectrino +	21399	22	Vec_X	m/s	...100Hz.MAT	100 Hz
23	-	MX840A_1	5	Nortek As	Vectrino +	21399	23	Vec_Y	m/s	...100Hz.MAT	100 Hz
24	-	MX840A_1	6	HBM	C9C-2kN	194910608	24	Q1	kg	...100Hz.MAT	100 Hz
25	-	MX840A_1	7	HBM	C9C-2kN	194910606	25	Q2	kg	...100Hz.MAT	100 Hz
26	-	MX840A_1	8	HBM	C9C-2kN	194910605	26	Q3	kg	...100Hz.MAT	100 Hz
27	-	MX840A_2	1	GE	ATM 1ST./N	910510	2	P1	mbar	...19200Hz.MAT	19200 Hz
28	-	MX840A_2	2	STS	ATM 1ST./N	910507	3	P2	mbar	...19200Hz.MAT	19200 Hz
29	-	MX840A_2	3	STS	ATM 1ST./N	910508	4	P3	mbar	...19200Hz.MAT	19200 Hz
30	-	MX840A_2	4	STS	ATM 1ST./N	910509	2 / 5	P4	mbar	...19200Hz.MAT	19200 Hz
31	-	MX840A_2	5	STS	ATM 1ST./N	910511	3 / 2	P5	mbar	...2400Hz.MAT	2400 Hz
32	-	MX840A_2	6	STS	ATM 1ST./N	910512	4 / 3	P6	mbar	...2400Hz.MAT	2400 Hz
33	-	MX840A_2	7	STS	ATM 1ST./N	910513	5 / 4	P7	mbar	...2400Hz.MAT	2400 Hz
34	-	MX840A_2	8	Achme	9V adapter	-	28	Pumps	V	...100Hz.MAT	100 Hz

F   Test program

Table F.1: Test program and results for slope $n = 1$.

#	n	S_h	R_c	H_{m0}	$T_{m-1,0}$	h_s	d_{st}	NW	$\xi_{m-1,0}$	R_u	q	C_r	$\gamma_{f_{R_u,2\%}}$	γ_{f_q}
	[-]	[m]	[m]	[m]	[s]	[m]	[m]	[-]	[-]	[m]	[l/(sm)]	[-]	[-]	[-]
1001	1	0.00	0.121	0.061	1.46	1.100	0.000	1342	7.3	0.147	0.095	0.81	1.00	1.00
1002	1	0.00	0.121	0.086	1.39	1.100	0.000	1270	5.9	0.179	0.654	0.78	1.00	1.00
1003	1	0.00	0.121	0.110	2.14	1.100	0.000	85	7.5	0.220	0.934	0.79	1.00	1.00
1004	1	0.00	0.211	0.059	1.46	1.010	0.000	1363	7.4	0.158	0.001	0.85	1.00	1.00
1005	1	0.00	0.211	0.080	1.41	1.010	0.000	1280	6.2	0.218	0.053	0.84	1.00	1.00
1006	1	0.00	0.211	0.096	2.13	1.010	0.000	1481	8.0	0.226	0.048	0.79	1.00	1.00
1007	1	0.00	0.211	0.096	2.13	1.010	0.000	1484	8.0	0.236	0.103	0.82	1.00	1.00
1008	1	0.00	0.211	0.097	2.13	1.010	0.000	1495	7.9	0.227	0.056	0.83	1.00	1.00
1009	1	0.00	0.300	0.059	1.47	0.921	0.000	1297	7.3	0.156	0.000	0.86	1.00	1.00
1010	1	0.00	0.300	0.081	1.43	0.921	0.000	1297	6.2	0.231	0.010	0.85	1.00	1.00
1011	1	0.00	0.300	0.186	2.27	0.921	0.000	439	6.1	0.384	0.739	0.85	1.00	1.00
1012	1	0.05	0.121	0.055	1.46	1.100	0.029	1298	7.7	0.116	0.030	0.54	0.70	0.89
1013	1	0.05	0.121	0.064	1.22	1.100	0.029	427	6.0	0.126	0.164	0.69	0.66	0.90
1014	1	0.05	0.121	0.079	1.40	1.100	0.029	1261	6.2	0.144	0.276	0.55	0.61	0.89
1015	1	0.05	0.121	0.079	1.40	1.100	0.029	1256	6.2	0.143	0.284	0.56	0.60	0.90
1016	1	0.05	0.121	0.079	1.39	1.100	0.029	1261	6.1	0.140	0.286	0.54	0.59	0.90
1017	1	0.05	0.121	0.085	1.40	1.100	0.029	167	5.9	0.162	0.293	0.61	0.63	0.90
1018	1	0.05	0.121	0.089	2.18	1.100	0.029	1422	8.5	0.168	0.877	0.65	0.63	0.99
1019	1	0.05	0.121	0.117	2.25	1.100	0.029	171	7.7	0.191	1.346	0.71	0.54	0.75

Table F.1: Test program and results for slope $n = 1$.

#	n	S_h	R_c	H_{m0}	$T_{m-1,0}$	h_s	d_{st}	NW	$\xi_{m-1,0}$	R_u	q	C_r	$\gamma_{f_{R_{u,2\%}}}$	γ_{f_q}
	[-]	[m]	[m]	[m]	[s]	[m]	[m]	[-]	[-]	[m]	[l/(sm)]	[-]	[-]	[-]
1020	1	0.05	0.121	0.132	2.73	1.100	0.029	179	8.5	0.199	1.929	0.69	0.50	0.74
1021	1	0.05	0.121	0.147	2.28	1.100	0.029	162	6.9	0.233	0.685	0.68	0.53	0.59
1022	1	0.05	0.211	0.085	2.18	1.010	0.039	1410	8.7	0.204	0.041	0.67	0.80	0.97
1023	1	0.05	0.211	0.085	2.14	1.010	0.039	1434	8.5	0.193	0.026	0.65	0.76	0.87
1024	1	0.05	0.211	0.086	2.15	1.010	0.039	1371	8.5	0.196	0.011	0.64	0.76	0.87
1025	1	0.30	0.121	0.095	1.38	1.100	0.179	1413	5.5	0.252	0.383	0.81	0.89	0.93
1026	1	0.30	0.121	0.123	3.39	1.100	0.179	307	10.8	0.300	1.848	0.57	0.81	0.76
1027	1	0.30	0.121	0.137	1.40	1.100	0.179	1428	4.7	0.184	0.077	0.96	0.45	0.98
1028	1	0.30	0.121	0.171	2.15	1.100	0.179	278	6.1	0.365	1.431	0.58	0.71	0.61
1029	1	0.30	0.211	0.061	1.31	1.010	0.089	1586	6.5	0.167	0.014	0.67	0.91	1.21
1030	1	0.30	0.211	0.084	1.30	1.010	0.089	1390	5.6	0.224	0.032	0.64	0.89	0.95
1031	1	0.30	0.211	0.168	2.13	1.010	0.089	1515	6.0	0.383	0.715	0.56	0.76	0.78
1032	1	0.30	0.300	0.062	1.42	0.921	0.000	1339	7.0	0.000	0.000	0.60	0.00	0.00
1033	1	0.30	0.300	0.081	1.38	0.921	0.000	1294	6.0	0.000	0.001	0.58	0.00	0.84
1034	1	0.30	0.300	0.171	2.18	0.921	0.000	1468	6.1	0.000	0.127	0.54	0.00	0.80

Table F.2: Test program and results for slope $n = 2$.

#	n	S_h	R_c	H_{m0}	$T_{m-1,0}$	h_s	d_{st}	NW	$\xi_{m-1,0}$	R_u	q	C_r	$\gamma_{f_{R_{u,2\%}}}$	γ_{f_q}
	[-]	[m]	[m]	[m]	[s]	[m]	[m]	[-]	[-]	[m]	[l/(sm)]	[-]	[-]	[-]
2001	2	0.00	0.121	0.065	1.46	1.100	0.000	1342	3.5	0.132	0.252	0.68	1.00	1.00
2002	2	0.00	0.121	0.095	1.41	1.100	0.000	1270	2.8	0.141	0.884	0.65	1.00	1.00
2003	2	0.00	0.121	0.097	2.17	1.100	0.000	85	4.1	0.284	1.463	0.58	1.00	1.00
2004	2	0.00	0.211	0.062	1.46	1.010	0.000	1363	3.6	0.262	0.016	0.67	1.00	1.00
2005	2	0.00	0.211	0.092	1.41	1.010	0.000	1280	2.9	0.315	0.141	0.62	1.00	1.00
2006	2	0.00	0.211	0.090	2.13	1.010	0.000	1481	4.1	0.359	0.226	0.63	1.00	1.00
2007	2	0.00	0.211	0.090	2.13	1.010	0.000	1484	4.1	0.363	0.260	0.63	1.00	1.00
2008	2	0.00	0.211	0.090	2.12	1.010	0.000	1495	4.1	0.363	0.261	0.64	1.00	1.00
2009	2	0.00	0.300	0.066	1.45	0.921	0.000	1297	3.4	0.225	0.001	0.66	1.00	1.00
2010	2	0.00	0.300	0.088	1.41	0.921	0.000	1297	2.9	0.331	0.025	0.56	1.00	1.00
2011	2	0.00	0.300	0.184	2.24	0.921	0.000	439	3.0	0.383	1.196	0.53	1.00	1.00
2012	2	0.05	0.121	0.056	1.43	1.100	0.029	1298	3.7	0.088	0.004	0.31	0.53	0.66
2013	2	0.05	0.121	0.063	1.20	1.100	0.029	427	3.0	0.107	0.016	0.54	0.59	0.58
2014	2	0.05	0.121	0.084	1.38	1.100	0.029	1261	2.9	0.127	0.042	0.41	0.53	0.70
2015	2	0.05	0.121	0.082	1.38	1.100	0.029	1256	3.0	0.124	0.042	0.37	0.53	0.70
2016	2	0.05	0.121	0.082	1.38	1.100	0.029	1261	3.0	0.119	0.050	0.38	0.50	0.71
2017	2	0.05	0.121	0.084	1.37	1.100	0.029	167	2.9	0.144	0.039	0.41	0.60	0.69
2018	2	0.05	0.121	0.088	2.11	1.100	0.029	1422	4.2	0.157	0.234	0.37	0.60	0.78
2019	2	0.05	0.121	0.114	2.20	1.100	0.029	171	3.8	0.179	1.338	0.38	0.53	0.64
2020	2	0.05	0.121	0.119	2.81	1.100	0.029	179	4.6	0.197	1.799	0.41	0.55	0.65
2021	2	0.05	0.121	0.143	2.26	1.100	0.029	162	3.5	0.190	1.907	0.40	0.45	0.60
2022	2	0.05	0.211	0.085	2.09	1.010	0.039	1410	4.2	0.189	0.003	0.37	0.75	0.64

Table F.2: Test program and results for slope $n = 2$.

#	n	S_h	R_c	H_{m0}	$T_{m-1,0}$	h_s	d_{st}	NW	$\xi_{m-1,0}$	R_u	q	C_r	$\gamma_{f_{R_{u,2\%}}}$	γ_{f_q}
	[-]	[m]	[m]	[m]	[s]	[m]	[m]	[-]	[-]	[m]	[l/(sm)]	[-]	[-]	[-]
2023	2	0.05	0.211	0.085	2.07	1.010	0.039	1434	4.1	0.185	0.004	0.32	0.74	0.67
2024	2	0.05	0.211	0.085	2.08	1.010	0.039	1371	4.1	0.188	0.003	0.32	0.74	0.65
2025	2	0.30	0.121	0.111	1.37	1.100	0.179	1413	2.6	0.202	0.367	0.91	0.65	0.89
2026	2	0.30	0.121	0.129	3.18	1.100	0.179	307	4.9	0.353	1.163	0.50	0.92	0.59
2027	2	0.30	0.121	0.116	1.38	1.100	0.179	1428	2.5	0.177	0.109	0.96	0.55	0.91
2028	2	0.30	0.121	0.167	2.08	1.100	0.179	278	3.0	0.342	1.190	0.59	0.71	0.52
2029	2	0.30	0.211	0.064	1.36	1.010	0.089	1586	3.3	0.126	0.008	0.85	0.67	0.94
2030	2	0.30	0.211	0.091	1.34	1.010	0.089	1390	2.8	0.153	0.015	0.79	0.59	0.80
2031	2	0.30	0.211	0.166	2.01	1.010	0.089	1515	2.9	0.350	0.354	0.51	0.74	0.59
2032	2	0.30	0.300	0.064	1.41	0.921	0.000	1339	3.4	0.000	0.000	0.73	0.00	0.00
2033	2	0.30	0.300	0.089	1.38	0.921	0.000	1294	2.8	0.000	0.000	0.76	0.00	0.65
2034	2	0.30	0.300	0.170	2.11	0.921	0.000	1468	2.9	0.333	0.036	0.54	0.68	0.66

Table F.3: Test program and results for slope $n = 3$.

#	n	S_h	R_c	H_{m0}	$T_{m-1,0}$	h_s	d_{st}	NW	$\xi_{m-1,0}$	R_u	q	C_r	$\gamma_{f_{R_{u,2\%}}}$	γ_{f_q}
	[-]	[m]	[m]	[m]	[s]	[m]	[m]	[-]	[-]	[m]	[l/(sm)]	[-]	[-]	[-]
3001	3	0.00	0.121	0.072	1.48	1.100	0.000	1342	2.3	0.096	0.266	0.57	1.00	1.00
3002	3	0.00	0.121	0.098	1.40	1.100	0.000	1270	1.9	0.110	0.723	0.54	1.00	1.00
3003	3	0.00	0.121	0.106	2.15	1.100	0.000	85	2.6	0.159	1.934	0.56	1.00	1.00
3004	3	0.00	0.211	0.073	1.44	1.010	0.000	1363	2.2	0.085	0.011	0.53	1.00	1.00
3005	3	0.00	0.211	0.094	1.39	1.010	0.000	1280	1.9	0.101	0.092	0.51	1.00	1.00
3006	3	0.00	0.211	0.097	2.10	1.010	0.000	1481	2.6	0.167	0.514	0.44	1.00	1.00
3007	3	0.00	0.211	0.095	2.09	1.010	0.000	1484	2.6	0.177	0.540	0.40	1.00	1.00
3008	3	0.00	0.211	0.095	2.08	1.010	0.000	1495	2.6	0.173	0.493	0.38	1.00	1.00
3009	3	0.00	0.300	0.074	1.42	0.921	0.000	1297	2.1	0.020	0.000	0.53	1.00	1.00
3010	3	0.00	0.300	0.090	1.38	0.921	0.000	1297	1.9	0.075	0.007	0.47	1.00	1.00
3011	3	0.00	0.300	0.183	2.26	0.921	0.000	439	2.0	0.188	1.185	0.35	1.00	1.00
3012	3	0.05	0.121	0.061	1.40	1.100	0.029	1298	2.3	0.063	0.002	0.40	0.38	0.62
3013	3	0.05	0.121	0.062	1.19	1.100	0.029	427	2.0	0.066	0.005	0.52	0.41	0.53
3014	3	0.05	0.121	0.086	1.36	1.100	0.029	1261	1.9	0.077	0.011	0.42	0.35	0.63
3015	3	0.05	0.121	0.086	1.36	1.100	0.029	1256	1.9	0.078	0.010	0.43	0.36	0.63
3016	3	0.05	0.121	0.086	1.36	1.100	0.029	1261	1.9	0.076	0.010	0.42	0.35	0.63
3017	3	0.05	0.121	0.094	1.36	1.100	0.029	167	1.8	0.090	0.010	0.49	0.38	0.63
3018	3	0.05	0.121	0.089	2.07	1.100	0.029	1422	2.7	0.115	0.090	0.19	0.46	0.67
3019	3	0.05	0.121	0.112	2.17	1.100	0.029	171	2.5	0.124	0.692	0.25	0.40	0.59
3020	3	0.05	0.121	0.120	2.79	1.100	0.029	179	3.0	0.137	1.007	0.18	0.39	0.60
3021	3	0.05	0.121	0.141	2.22	1.100	0.029	162	2.3	0.140	1.973	0.28	0.37	0.61
3022	3	0.05	0.211	0.086	2.07	1.010	0.039	1410	2.7	0.199	0.001	0.19	0.82	0.56

Table F.3: Test program and results for slope $n = 3$.

#	n	S_h	R_c	H_{m0}	$T_{m-1,0}$	h_s	d_{st}	NW	$\xi_{m-1,0}$	R_u	q	C_r	$\gamma_{f_{R_{u,2\%}}}$	γ_{f_q}
	[-]	[m]	[m]	[m]	[s]	[m]	[m]	[-]	[-]	[m]	[l/(sm)]	[-]	[-]	[-]
3023	3	0.05	0.211	0.085	2.11	1.010	0.039	1434	2.8	0.229	0.002	0.36	0.95	0.58
3024	3	0.05	0.211	0.086	2.10	1.010	0.039	1371	2.8	0.193	0.000	0.37	0.79	0.49
3025	3	0.30	0.121	0.116	1.36	1.100	0.179	1413	1.7	0.187	0.441	0.84	0.68	0.94
3026	3	0.30	0.121	0.138	3.09	1.100	0.179	307	3.1	0.315	1.096	0.41	0.79	0.56
3027	3	0.30	0.121	0.134	1.38	1.100	0.179	1428	1.5	0.171	0.154	0.94	0.56	0.94
3028	3	0.30	0.121	0.161	2.09	1.100	0.179	278	2.0	0.274	0.690	0.53	0.66	0.49
3029	3	0.30	0.211	0.059	1.35	1.010	0.089	1586	2.3	0.117	0.008	0.68	0.73	0.98
3030	3	0.30	0.211	0.085	1.36	1.010	0.089	1390	1.9	0.145	0.010	0.60	0.67	0.81
3031	3	0.30	0.211	0.161	2.05	1.010	0.089	1515	2.0	0.305	0.245	0.55	0.74	0.58
3032	3	0.30	0.300	0.073	1.44	0.921	0.000	1339	2.2	0.000	0.000	0.84	0.00	0.00
3033	3	0.30	0.300	0.094	1.41	0.921	0.000	1294	1.9	0.000	0.000	0.81	0.00	0.00
3034	3	0.30	0.300	0.161	2.09	0.921	0.000	1468	2.0	0.000	0.020	0.63	0.00	0.62

G Quantification of test repeatability

Table G.1: Quantification of deviations in the resulting target values for repetitions of test 014 (referenced by test 015, 016 and 017).

| | | R_u | q | C_r | $\gamma_{f_{R_{u,2\%}}}$ | γ_{f_q} |
		[m]	[l/(sm)]	[-]	[-]	[-]
$\mu_{1014-1016}$		0.142	0.282	0.551	0.599	0.897
$\mu_{2014-2016}$		0.124	0.045	0.387	0.520	0.702
$\mu_{3014-3016}$		0.077	0.010	0.426	0.354	0.631
#	NW	rel. error	rel. error	rel. error	rel. error	rel. error
1014	1261	-0.011	0.021	-0.003	-0.014	0.003
1015	1256	-0.007	-0.008	-0.009	-0.007	-0.001
1016	1261	0.018	-0.013	0.012	0.021	-0.002
1017	167	-0.139	-0.040	-0.113	-0.055	-0.005
2014	1261	-0.030	0.053	-0.058	-0.015	0.005
2015	1256	-0.006	0.066	0.042	-0.016	0.006
2016	1261	0.036	-0.119	0.016	0.031	-0.012
2017	167	-0.163	0.122	-0.058	-0.149	0.013
3014	1261	-0.001	-0.065	0.002	-0.003	-0.006
3015	1256	-0.013	0.041	-0.006	-0.010	0.004
3016	1261	0.015	0.024	0.004	0.013	0.002
3017	167	-0.164	0.009	-0.151	-0.083	0.001

H Influence of the slope and the Iribarren number on the run-up reduction coefficient
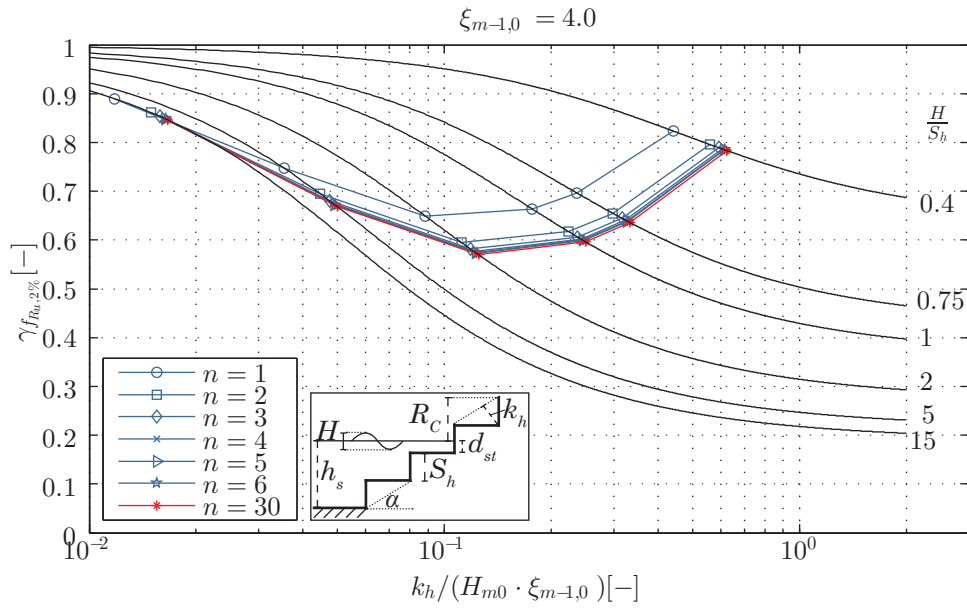

Figure H.1: Influence of the slope n on the run-up reduction coefficient $\gamma_{f_{R_{u,2\%}}}$ for Iribarren number $\xi_{m-1,0} = 4$.
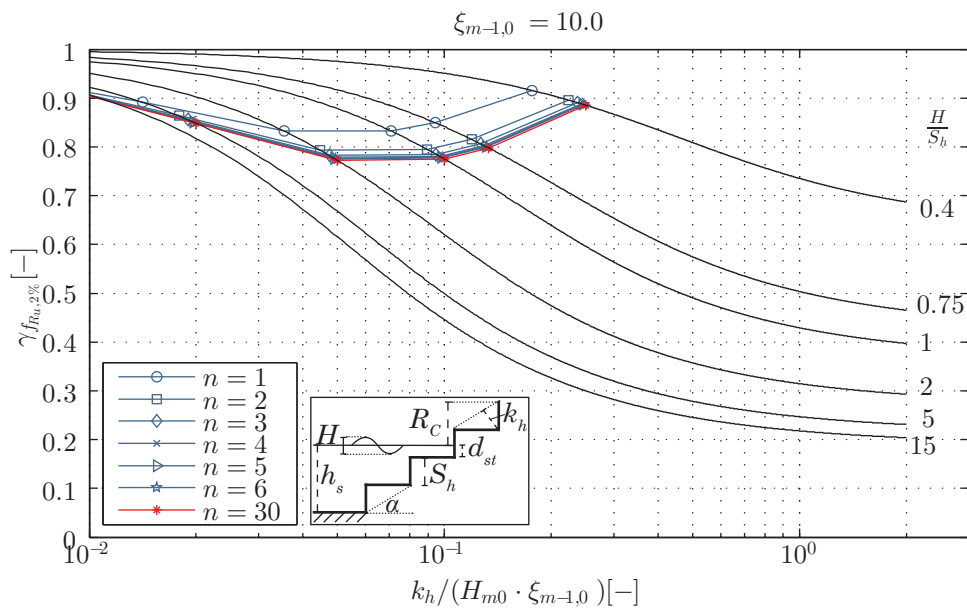

Figure H.2: Influence of the slope n on the run-up reduction coefficient $\gamma_{f_{R_{u,2\%}}}$ for Iribarren number $\xi_{m-1,0} = 10$.
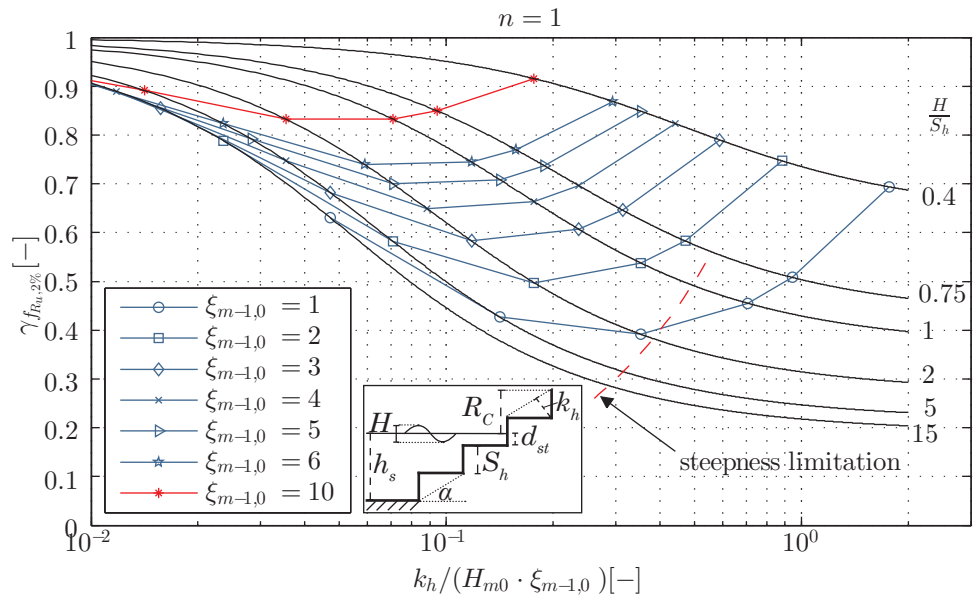
Figure H.3: Influence of the Iribarren number $\xi_{m-1,0}$ on the run-up reduction coefficient $\gamma_{f_{R_{u,2\%}}}$ for slope $n = 1$.
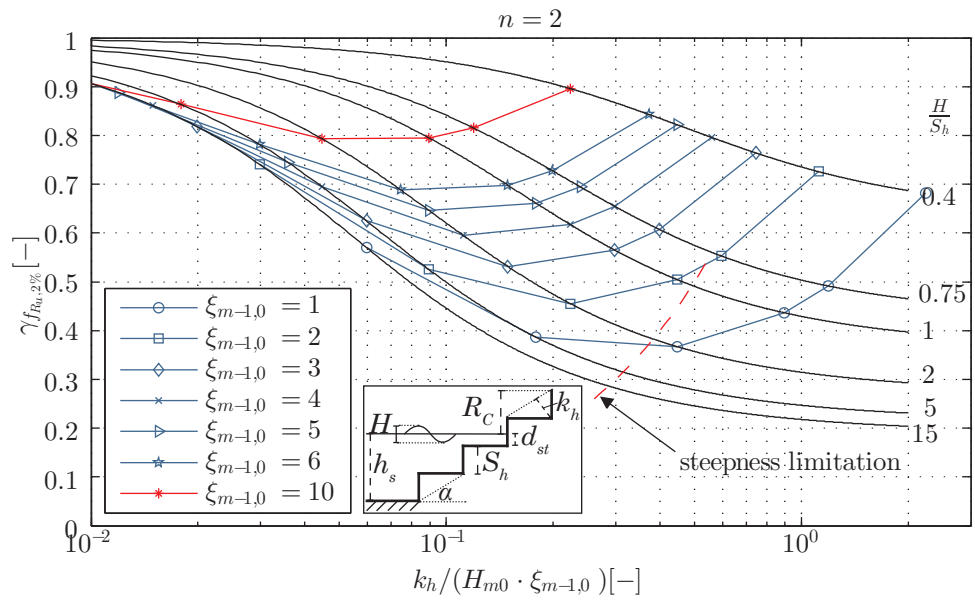

Figure H.4: Influence of the Iribarren number $\xi_{m-1,0}$ on the run-up reduction coefficient $\gamma_{f_{R_{u,2\%}}}$ for slope $n = 2$.
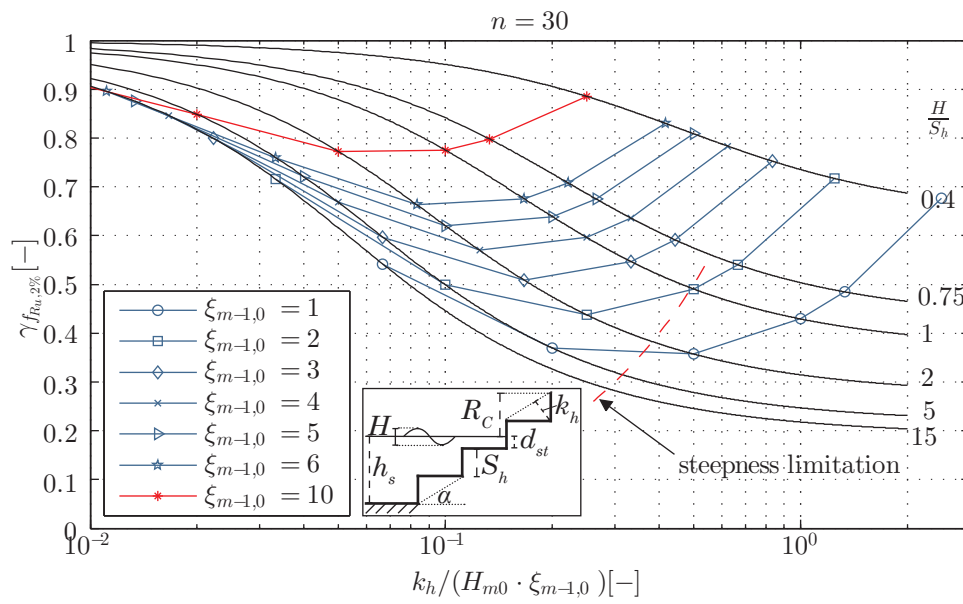
Figure H.5: Influence of the Iribarren number $\xi_{m-1,0}$ on the run-up reduction coefficient $\gamma_{f_{R_{u,2\%}}}$ for slope $n = 30$.
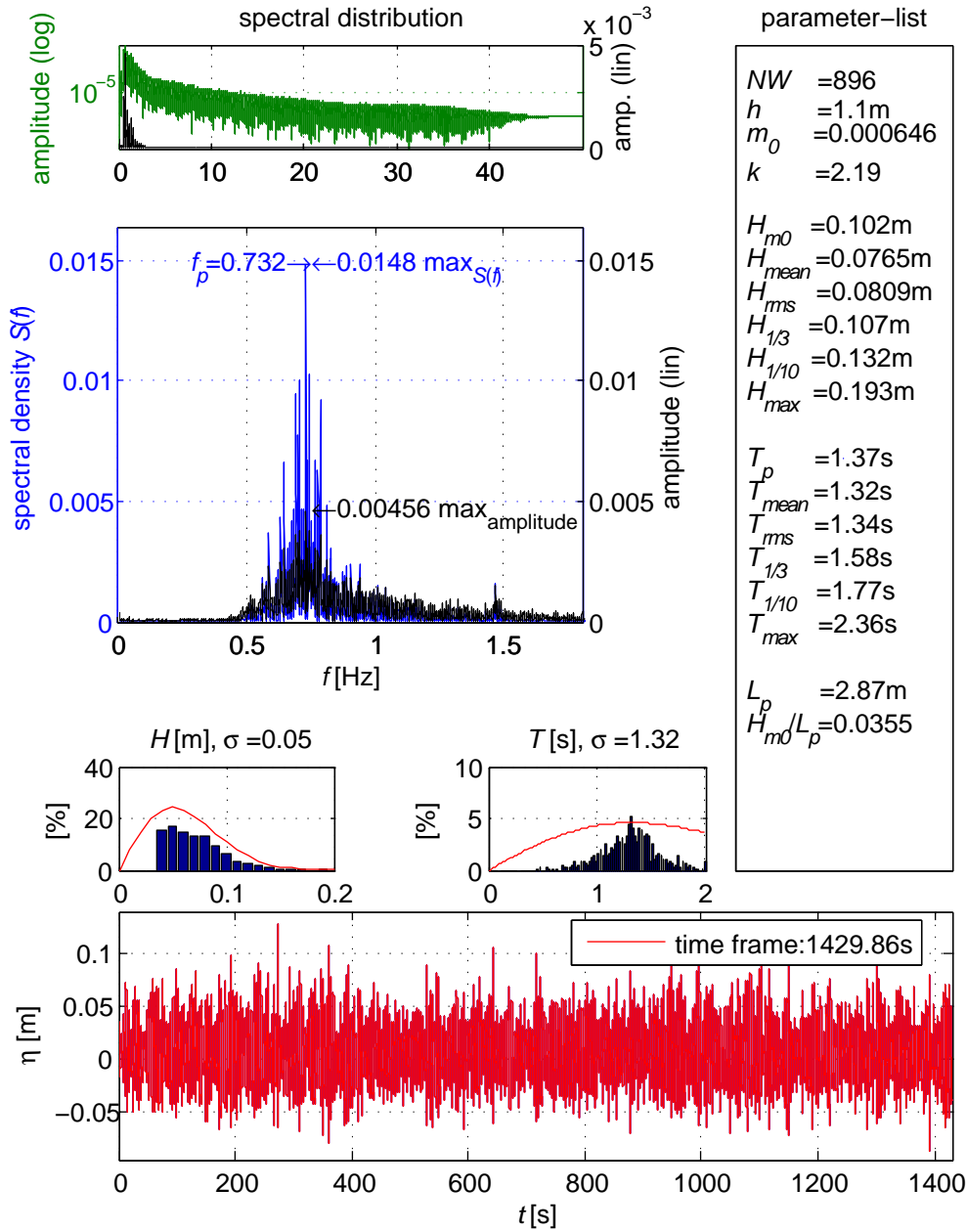
I Exemplary wave spectrum

Figure I.1: Post-processed surface elevation measured by ultrasonic sensor $US\,5$ in the far field of the 1:3 inclined stepped revetment with a step height of $H_{m0}/S_h = 2$ including derived hydraulic boundary conditions.

J   Curriculum Vitae

Personal Details

Name	Nils Bernhard Kerpen
Date/place of birth	August 23, 1983 in Gronau (Westf.)
Personal status	married, two children

Work Experience

Mar. 2012 – current	Laboratory Engineer at Ludwig-Franzius-Institute for Hydraulic, Estuarine and Coastal Engineering, Leibniz Universität Hannover *Breakwater stability tests in DAAD-Programm "A New Passage to India" at Indian Institute of Technology in Chennai, India. (Okt. – Dez. 2013)*
Oct. 2009 – Feb. 2012	Research Associate at Franzius-Institute for Hydraulic, Waterways and Coastal Engineering, Leibniz Universität Hannover

Education

Oct. 2004 – Sep. 2009	University education in Civil Engineering with specification Water and Environment, at Leibniz Universität Hannover Degree: Diplomingenieur (equivalent to Master Degree)
Oct. 2007 – Sep. 2009	Student assistant at Franzius-Institute for Hydraulic, Waterways and Coastal Engineering, Leibniz Universität Hannover

Alternative Service

Aug. 2003 – Jun. 2004	Carer at Bethesda retirement home in Gronau (Westf.)

School Education

Aug. 1994 – Jun. 2003	Missionsgymnasium St. Antonius Bardel – International College of Science and the Arts, Bad Bentheim Graduated with German Abitur (equivalent to A-levels)

Awards

2016	Best Paper Award for Youth Scholar, 8th Chinese-German Joint Symposium on Hydraulic and Ocean Engineering, Ocean University of China, Qingdao, China
2009	Winner of ideas competition "Inventions contra waterweed" awarded by UFZ Leipzig and Ruhrverband Essen

Memberships

since Feb. 2008	Gesellschaft der Förderer des Ludwig-Franzius-Instituts e.V.
since Feb. 2008	Hafentechnische Gesellschaft e.V.

Hannover, 4th January 2017

Nils B. Kerpen